



HAL
open science

Synthesis of poly(ionic liquid)-type nanogels by cobalt-mediated radical cross-linking copolymerization, for coating applications

Mathilde Weiss-Maurin

► **To cite this version:**

Mathilde Weiss-Maurin. Synthesis of poly(ionic liquid)-type nanogels by cobalt-mediated radical cross-linking copolymerization, for coating applications. *Polymers*. Université de Bordeaux; Université de Liège, 2016. English. NNT : 2016BORD0152 . tel-01591165

HAL Id: tel-01591165

<https://theses.hal.science/tel-01591165>

Submitted on 21 Sep 2017

HAL is a multi-disciplinary open access archive for the deposit and dissemination of scientific research documents, whether they are published or not. The documents may come from teaching and research institutions in France or abroad, or from public or private research centers.

L'archive ouverte pluridisciplinaire **HAL**, est destinée au dépôt et à la diffusion de documents scientifiques de niveau recherche, publiés ou non, émanant des établissements d'enseignement et de recherche français ou étrangers, des laboratoires publics ou privés.



THÈSE EN COTUTELLE PRÉSENTÉE

POUR OBTENIR LE GRADE DE

DOCTEUR DE

L'UNIVERSITÉ DE BORDEAUX

ET DE L'UNIVERSITÉ DE LIEGE

ÉCOLE DOCTORALE DES SCIENCES CHIMIQUES (UBX)

ÉCOLE DOCTORALE DE CHIMIE (ULg)

SPÉCIALITÉ POLYMERES

Par Mathilde WEISS-MAURIN

**SYNTHESE DE NANOGELS A BASE DE POLY(IONIQUES
LIQUIDES) PAR COPOLYMERISATION RADICALAIRE
RETICULANTE CONTRÔLÉE PAR LE COBALT, POUR DES
APPLICATIONS DE REVÊTEMENT**

Sous la direction de Daniel TATON
et de Christophe DETREMBLEUR

Soutenue le 20 septembre 2016 à Liège

Membres du jury :

Mme DUWEZ Anne-Sophie Professeur ULg
M. BILLON Laurent Professeur UPPA
M. JUNKERS Thomas Professeur Hasselt
M. CARLOTTI Stéphane Professeur IPB
M. GROGNA Mathurin Docteur CRM
M. TATON Daniel Professeur UBx
M. DETREMBLEUR Christophe Docteur ULg
M. DEBUIGNE Antoine Docteur ULg

Présidente
Rapporteur
Rapporteur
Secrétaire
Examineur
Examineur
Examineur
Invité

Titre : Synthèse de Nanogels à base de Poly(liquides ioniques), par Copolymérisation Radicalaire Réticulante Contrôlée par le Cobalt, pour des Applications de Revêtement

Résumé : La synthèse de nanogels par voie directe est étudiée par la copolymérisation radicalaire réticulante contrôlée par le cobalt (CMRCcP) d'un monomère monovinyle et d'un réticulant divinyle. La synthèse de nanogels globulaires a été réalisée en utilisant un système de co-monomères soit neutres (acétate de vinyle et adiate de divinyle) soit liquides ioniques. Le contrôle de la polymérisation est vérifié dans tous les cas, les liaisons C-Co situées aux extrémités des chaînes polymères ont été réactivées, afin de former des nanogels de « seconde-génération ». Dans le cas de monomères liquides ioniques, différents contre-anions ont été utilisés afin de jouer sur l'hydrophilie des co-monomères : la CMRCcP du bromure de *N*-vinyl-3-ethyl imidazolium (VEtImBr) et du bromure de 1,13-divinyl-3-decyl diimidazolium (DVImBr) a été réalisée dans l'eau, à 30 °C, pour former des nanogels poly(VEtImBr-co-DVImBr) hydrophiles. Les propriétés antibactériennes de ces nanogels ont été étudiées.

Les pendants hydrophobes de ces nanogels à base de PILs ont été synthétisés *via* la CMRCcP directe, dans l'acétate d'éthyle, de co-monomères contenant des contre-anions bis(trifluoromethanesulfonyl)imide (NTf₂⁻). La capacité à former des surfaces poreuses ordonnées de ces nanogels hydrophobes poly(VEtImNTf₂-co-DVImNTf₂) a été examinée, ainsi que leur conductivité ioniques en films minces.

Des copolymérisations 'mixtes' ont également été étudiées, dans l'optique de former différentes architectures nanogels en utilisant des co-monomères ayant des réactivités très différentes.

Mots clés : Nanogels ; Polymères liquides ioniques ; CMRP

Title : Synthesis of Poly(ionic liquid)-type Nanogels by Cobalt-Mediated Radical Cross-linking Copolymerization, for Coating Applications

Abstract : The syntheses of globular nanogels were first investigated under mild conditions, using a mono- and a divinyl co-monomer with similar reactivities. CMRCcP was implemented on either neutral (vinyl acetate (VAc) and divinyl adipate (DVA)) co-monomers, or ionic liquid co-monomers. Control over each polymerization was ascertained, and dormant cobalt-carbon chain-ends could be re-activated to form "second-generation" nanogels. CMRCcP of *N*-vinyl-3-ethyl imidazolium bromide (VEtImBr) and 1,13-divinyl-3-decyl diimidazolium bromide (DVImBr) was achieved in water at 30 °C, leading to hydrophilic poly(VEtImBr-co-DVImBr) nanogels. The antibacterial activity of these cross-linked structures was investigated. The hydrophobic pendants of these PIL-based nanogels were synthesized *via* direct CMRCcP in ethyl acetate, using bis(trifluoromethanesulfonyl)imide (NTf₂⁻) counter anions. An array of these poly(VEtImNTf₂-co-DVImNTf₂) nanogels was then investigated as possible coatings for porous patterned surfaces, and their ionic conductivity assessed. Different cross-linked architecture were approached, using a mono- and a divinyl co-monomers of completely different reactivities.

Keywords : Nanogels ; Poly(ionic liquid)s ; CMRP

Laboratoire de Chimie des Polymères Organiques (LCPO)

UMR 5629 : 16, avenue Pey Berland _ 33607 PESSAC CEDEX

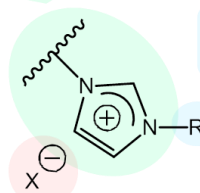
Synthèse de Nanogels à base de Poly(liquides ioniques), par Copolymérisation Radicalaire Réticulante Contrôlée par le Cobalt, pour des Applications de Revêtement

L'acier inoxydable est employé dans de nombreux secteurs, telles que le domaine médical, l'industrie, ou les objets ménagers, pour ne citer qu'eux. Cette abondance d'applications est due à la résistance du matériau à la corrosion et aux produits chimiques ainsi qu'à ses propriétés mécaniques et esthétiques. Cependant, l'acier inoxydable n'est pas antibactérien, et ne peut donc pas se prémunir contre la prolifération de bactéries sur sa surface. Différentes techniques de greffage ont été utilisées pour attacher des biocides sur la surface (l'électrografting par exemple), mais ce sont généralement des procédés en plusieurs étapes, ce qui rend leur utilisation à l'échelle industrielle difficile et/ou coûteuse.

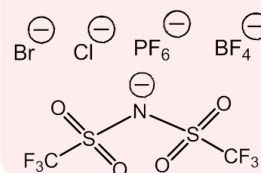
Le but de ce projet est de synthétiser de façon simple, robuste et versatile, de nouveaux polymères cationiques qui pourraient être utilisés comme revêtement antibactériens à long-terme sur l'acier inoxydable. Les copolymères que nous voulons développer sont à base de polymères liquides ioniques (PILs).

Une attention toute particulière a été apportée au PILs dans la littérature de la dernière décennie : en effet, ces polymères combinent les propriétés physico-chimiques des liquides ioniques (Ils) moléculaires – leur stabilité thermique et chimique, leur conductivité ionique élevée, leur solubilité et viscosité modulable – et les propriétés spécifiques des polymères, telles que la capacité de former des films. Les applications des PILs sont nombreuses et variées : ils sont utilisés dans la catalyse, les tensioactifs polymères, les polymères électrolytes, etc. Parmi les PILs, les polymères contenant une fonction imidazolium ont été étudiés plus particulièrement (voir figure ci-contre).

Chaîne polymère avec des fonctions imidazolium



X⁻ = contre-anion



Ici, nous avons fait l'hypothèse que des revêtements à base de PILs de haute masse molaire permettraient de conférer à l'acier inoxydable non seulement des propriétés antibactériennes, mais également d'assurer la durabilité du revêtement. En effet, un polymère de haute masse molaire peut être plus difficile à re-dissoudre après séchage. De ce fait, il était attendu que la déposition et le séchage de PILs antibactériens de haute masse molaire permette d'obtenir des revêtements antibactériens durables. De plus, un moyen simple de jouer sur les propriétés finales du polymère (solubilité, propriétés antibactériennes, durabilité du revêtement) est de substituer le contre-anion ($X^- = Br^-$ ou $N^-(SO_2CF_3)_2$).

Cette thèse de doctorat se situe à la jonction de trois domaines des sciences polymères, c'est-à-dire les polymères liquides ioniques, la polymérisation radicalaire contrôlée et la synthèse d'architectures réticulées. Le but de ce projet est de synthétiser des architectures nanogels par copolymérisation radicalaire réticulante contrôlée par le cobalt (CMRCcP). Il est escompté que ces nanogels permettent d'obtenir des revêtements antibactériens durables, actifs contre les bactéries Gram-positives et Gram-négatives, pour des surfaces d'acier inoxydable.

Cette thèse se divise en six chapitres, tous écrits en anglais, et organisée comme suit.

Le premier chapitre montre un bref état de l'art des polymères biocides (c'est-à-dire les polymères intrinsèquement antibactériens) et de leur utilisation dans les revêtements antibactériens. Les revêtements polymériques antibactériens ont en effet été développés afin d'améliorer les services de santé, et d'empêcher la prolifération des bactéries. Les principaux polymères biocides bio-sourcés (tels que le chitosan et la polylysine) et synthétiques (comme la poly(éthylène imine), la polyguadinine ou les PILs, par exemple) sont d'abord discutés et comparés grâce à leur concentration inhibitrice minimale (MIC). La MIC d'un polymère représente la concentration minimale en polymère pour laquelle la croissance bactérienne est inhibée : plus la MIC d'un polymère est basse, plus ce polymère est un antibactérien efficace.

Les différents types de revêtements polymériques antibactériens sont brièvement discutés. Une attention particulière a été portée aux revêtements polymériques antibactériens utilisés sur des surfaces d'acier inoxydables.

Le second chapitre de cette thèse propose une vue d'ensemble des derniers développements concernant la copolymérisation radicalaire réticulante contrôlée, ou CRCcP

(utilisant les méthodologies ATRP, NMP et RAFT) d'un monomère monovinyle et d'un réticulant divinyle. Ces stratégies permettent la formation de réseaux polymériques réticulés chimiquement, possédant des longueurs de chaîne cinétique contrôlées. La modélisation de ces copolymérisations ainsi que les publications expérimentales ont été discutées dans cet état de l'art. Les trois principaux mécanismes de copolymérisation radicalaire réticulante contrôlée considérés sont la « nitroxide-mediated polymerization » (NMP), l'« atom-transfer radical polymerization » (ATRP), et la « reversible addition-fragmentation chain transfer polymerization » (RAFT).

Plusieurs propriétés propres aux gels issus de la CRCcP sont exposées, comme la possibilité de retarder la gélification ou de fonctionnaliser le gel après polymérisation. La question de l'homogénéité du réseau réticulé (vis-à-vis de l'hétérogénéité des gels issus de la copolymérisation radicalaire réticulée classique) est abordée. Dans des conditions particulières, la CRCcP permet d'obtenir des (nano)gels polymériques, c'est-à-dire des matériaux polymères réticulés solubles de taille inférieure au micron.

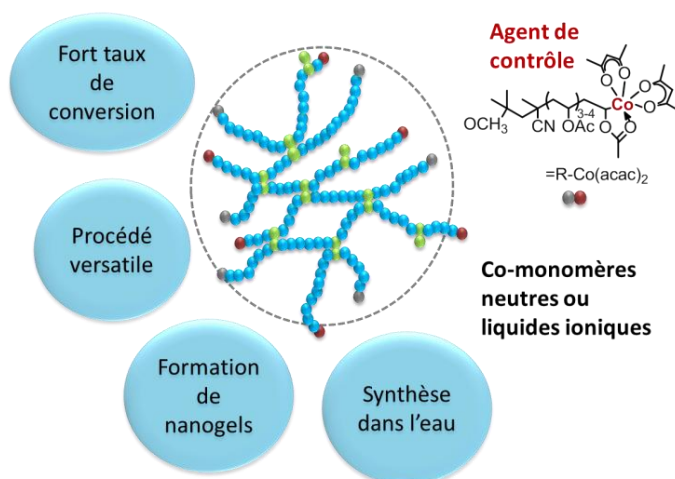
La modélisation de la CRCcP (*via* des modèles statistiques, déterministes et les simulations informatiques) est également traitée. Les principales modélisations et simulations sont comparées entre elles.

Le chapitre bibliographique II a démontré l'intérêt d'utiliser une voie radicalaire réticulante contrôlée pour former des nanogels. Les mécanismes de polymérisation principalement utilisés sont dérivés de la NMP, de l'ATRP et de la polymérisation RAFT. Le chapitre III propose une méthodologie nouvelle pour synthétiser des nanogels aux longueurs de chaînes cinétiques contrôlées, par copolymérisation radicalaire réticulante contrôlée par le cobalt (CMRCcP) d'un monomère monovinyle et d'un réticulant divinyle. Le réticulant est choisi pour sa structure similaire à celle du monomère, et nous faisons l'hypothèse que sa réactivité est semblable à celle du monomère également.

La preuve de concept de cette stratégie a été apportée par la formation de nanogels neutres, issus de la CMRCcP de l'acétate de vinyle (VAc) avec l'adipate de divinyle (DVA) à 40 °C dans l'acétate d'éthyle, en présence d'un amorceur-agent de contrôle alkyl-cobalt(III) préformé. L'une des particularités de ces nanogels est la possibilité de cliver les nœuds de réticulation, par méthanolyse en milieu basique : on obtient alors les chaînes primaires de nanogels. Le contrôle de la polymérisation est alors vérifié par analyse CES. La CMRCcP du VAc et du DVA peut également être réactivée, par un simple ajout de monomère dans le milieu réactionnel.

Des nanogels à base de polymères liquides ioniques ont été obtenus directement par la CMRCcP d'un couple de co-monomères liquides ioniques, le bromure de N-vinyl-3-ethyl imidazolium (VETImBr) et le bromure de 1,13-divinyl-3-decyl imidazolium (DVIImBr). DVIImBr est utilisé comme réticulant ici. Les polymérisations peuvent avoir lieu à 30 °C soit en

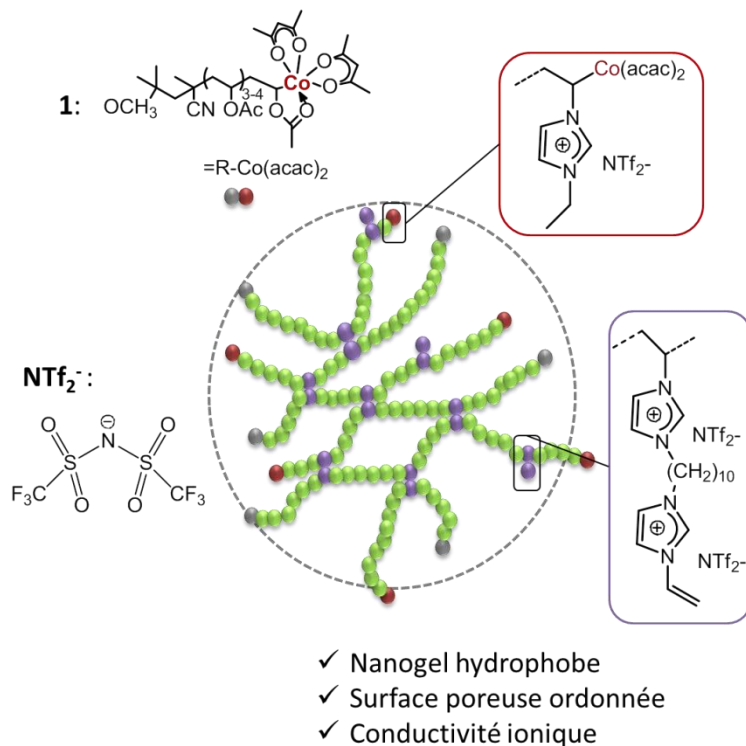
milieu organique, soit dans l'eau, ce qui démontre la robustesse et la versatilité de ce procédé CMRCcP en une étape. Des réactions d'extensions de chaîne des nanogels de PILs ont été réalisées dans l'eau, formant des nanogels « de seconde-génération ». Ces architectures particulières, dites « cœur-écorce », ouvrent de nouvelles voies d'accès à des nanogels chargés fonctionnalisés.



Dans le chapitre IV, la CMRCcP est utilisée sur des couples de co-monomères aux réactivités supposées très différentes. L'objectif est de pouvoir former différentes architectures de nanogels « arms-first » ou « core-first ». Les copolymérisations sont réalisées en présence d'un agent de contrôle alkyl-cobalt(III). Les deux couples de co-monomères utilisés sont (VAc/DVIImBr) et (VETImBr/DVA). Nos tentatives de déterminer exactement les réactivités relatives du VAc et du VETImBr se sont soldées par un échec, leurs réactivités étant trop différentes.

Si la copolymérisation du VETImBr avec le DVA peut éventuellement mener à la formation de nanogels si la concentration en réticulant DVA est suffisamment élevé (un minimum de 8.1 mol% est requis), la synthèse d'un nanogel « core-first » de VAc et de DVIImBr n'est pas possible. Une voie de synthèse alternative en deux étapes est donc employée, formant un nanogel cœur-écorce avec une écorce de chaînes de PVAc, et un cœur de polymères liquides ioniques hydrophobes réticulé. Dans ces conditions, les co-monomères liquides ioniques employés sont hydrophobes afin que les deux étapes de polymérisation puissent avoir lieu dans le même milieu réactionnel, sans avoir besoin de changer le solvant.

Le chapitre V expose la CMRCcP de co-monomères liquides ioniques hydrophobes, contenant un contre-anion bis(trifluoromethanesulfonyl)imide (NTf₂⁻). La copolymérisation



du monomère VEtImNTf₂ et du réticulant DVImNTf₂ en solution dans l'acétate d'éthyle forme des nanogels de polymères liquides ioniques hydrophobes en une étape. Différents paramètres de polymérisation sont étudiés, tels que la température de polymérisation et les concentrations du réticulant et du monomère. La réactivation des liaisons carbone-cobalt en bout de chaînes permet la formation de nanogels « de seconde-génération ».

Les nanogels de poly(VEtImNTf₂-co- DVImNTf₂) ont ensuite été utilisés pour réaliser des revêtements sur des surfaces de mica. Une analyse par microscope de force atomique (AFM) de ces surfaces a révélé la présence de « figures de souffle », mais aussi des pores interconnectés ou d'agrégats : la forme et l'ordre de la surface dépend de la densité de réticulation des nanogels, de leur concentration, et du solvant utilisé (THF/H₂O 98/2 ou THF seul).

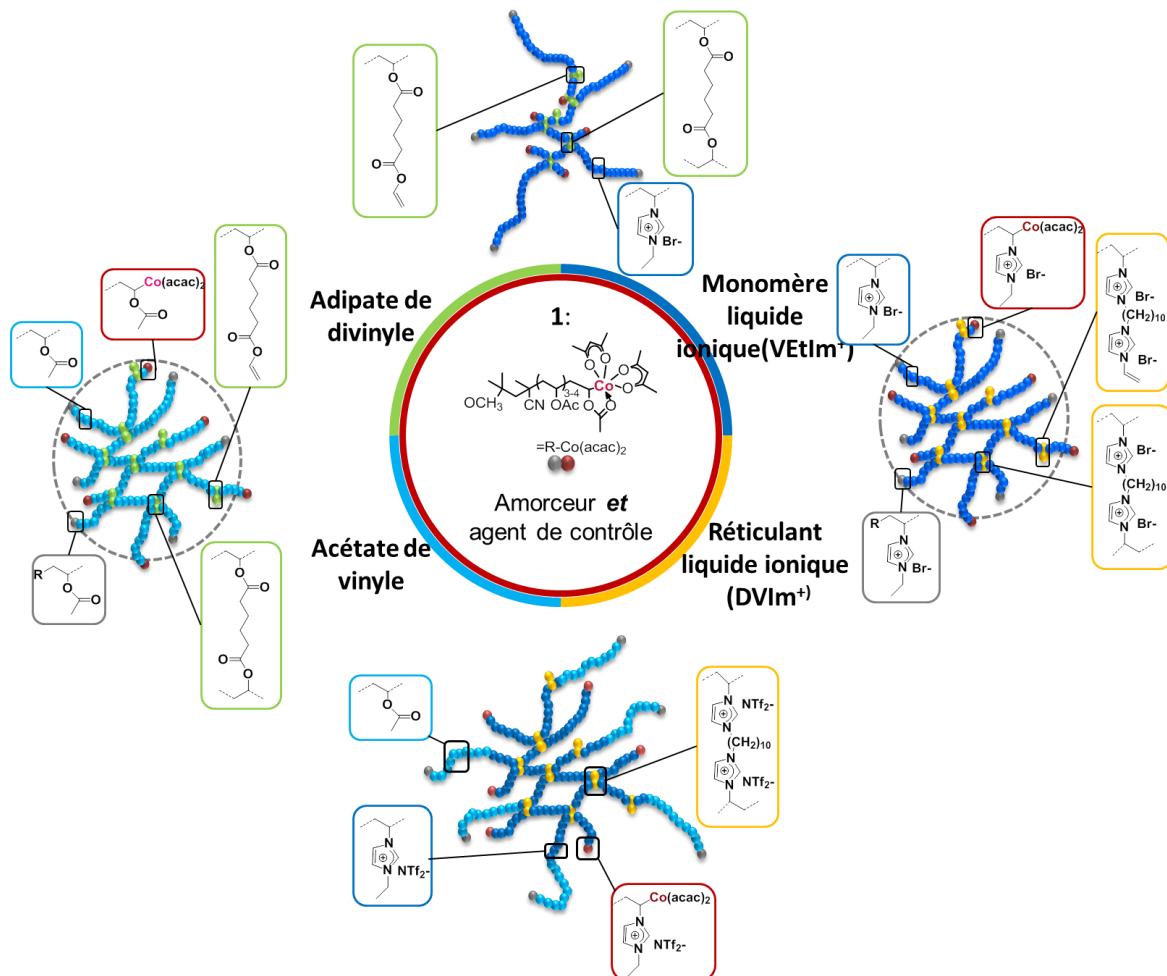
Enfin, la conductivité ionique en couche mince d'un panel de nanogels liquides ioniques hydrophobes de première- et seconde-génération a été étudiée : pour cela, il faut que le nanogel utilisé en couche mince (épaisseur inférieur à 100 nm) soit stable en température jusqu'à 130 °C. Il est intéressant de constater que certains nanogels de seconde-génération peuvent être utilisés, même si le nanogel de première-génération dont ils sont issus n'est pas stable aux températures voulues ; la conductivité ionique la plus élevée ici correspond à un nanogel de seconde-génération (1.9 10⁻⁵ S/cm vs. 5.7 10⁻⁶ S/cm).

Le chapitre VI est une étude préliminaire des propriétés antibactériennes et des propriétés de revêtements des différents copolymères de polymères liquides ioniques hydrophiles réalisés dans les chapitres III et IV. Les copolymères sont différenciés par leur architecture : homopolymères linéaires ou nanogels réticulés. Les nanogels testés sont des copolymères de VEtImBr utilisant un réticulant DVA ou DVImBr.

L'adhérence des revêtements polymères à une surface d'acier inoxydable est évaluée par QCM-D et par mesure de l'angle de contact. La durabilité d'un tel revêtement est déterminée par un test d'immersion dans l'eau.

L'activité antibactérienne des copolymères hydrophiles est d'abord testé en solution contre des bactéries Gram-positives (*S. Epidermis*) et Gram-négatives (*E. Coli*), par la méthode dite « shake-flask », dans lequel les polymères sont au contact des bactéries pendant 18h d'incubation. De ce premier test, il en est ressorti que les nanogels synthétisés dans l'eau semblaient être plus antibactérien que les nanogels synthétisés en milieu organique. Les MIC des copolymères les plus prometteurs ont été évaluées. Un effet d'architecture est confirmé, puisque les nanogels de polymères liquides ioniques ont une MIC plus basse que les homopolymères correspondants (c'est-à-dire les homopolymères de PILs ayant un degré de polymérisation similaire à celui des chaînes primaires des nanogels).

Pour conclure, cette thèse de doctorat a permis de développer une méthodologie nouvelle pour former des nanogels neutres ou liquides ioniques, par voie radicalaire réticulante contrôlée par le cobalt, en une étape (figure ci-dessous).



Les couples de co-monomères utilisés peuvent être neutres, liquides ioniques ou mixtes, donnant lieu à différentes architectures réticulées. Dans chaque cas, il est possible d'obtenir des taux de conversion élevés à partir de conditions de polymérisation relativement douces (30 et 40 °C, en solution). La versatilité et la robustesse du procédé est démontrée par la polymérisation de co-monomères liquides ioniques à 30 °C dans l'eau. La combinaison des structures réticulées et des propriétés propres aux polymères liquides ioniques montre le potentiel de ces nanogels pour la formation de revêtement dans diverses applications. Les applications potentielles sont nombreuses : ici, les nanogels liquides ioniques hydrophiles ont fait l'objet d'une étude préliminaire de leurs propriétés antibactériennes, et les nanogels liquides ioniques hydrophobes ont été utilisés pour former des surfaces poreuses ordonnées (figure de souffle) et pour leur conductivité ionique.

La réactivation des liaisons carbone-cobalt en bout de chaîne permet la synthèse de nanogels « cœur-écorce ».

Les travaux de thèse décrits dans ce manuscrit ont été réalisés en co-tutelle entre le centre d'éducation et de recherche sur les macromolécules (CERM) de l'Université de Liège, et le Laboratoire de Chimie des Polymères Organiques (LCPO) de l'université de Bordeaux, sous l'égide du Dr. Christophe Detrembleur et du Prof. Daniel Taton. Cette thèse a été effectuée dans le cadre du programme IDS-FunMat (International Doctoral School for Functional Materials), et a été financée par l'Université de Liège.

Je tiens à remercier tout d'abord les Prof. Henri Cramail et Prof. Christine Jérôme, qui ont chacun su faire de la place dans leurs laboratoires respectifs pour m'accueillir.

Je voudrais ensuite remercier très chaleureusement mes directeurs de thèse, Prof. Daniel Taton et Dr. Christophe Detrembleur, de m'avoir donné l'opportunité de réaliser cette thèse. J'ai énormément appris à votre contact, tant bien sûr en chimie, que sur le management d'un projet. Ainsi, un grand merci à Dr. Christophe Detrembleur de m'avoir ouvert les portes de la polymérisation radicalaire contrôlée en même temps que celles du CERM. Merci de ton intérêt pour mes architectures de nanogels, et de ton enthousiasme face à quelques moments de doute. Merci également à Prof. Daniel Taton pour votre implication dans mon projet de thèse, votre soutien à toute épreuve, et oui, même votre rigueur quant à ma rédaction : j'ai tenté de limiter au maximum les « mathilderies » dans ces lignes. Merci, enfin, de m'avoir donné un certain degré de liberté dans mes recherches tout en restant présent au moment opportun.

Je remercie Prof. Laurent Billon et Prof. Thomas Junkers d'avoir accepté de porter un regard extérieur sur mes travaux de thèse. Je remercie également Catherine Archambeau et le groupe CRM, qui sont à l'origine du sujet de cette thèse.

J'adresse également mes remerciements aux deux équipes qui m'ont accueillie, à Liège et à Bordeaux, avec enthousiasme et prévenance. Merci à Dr. Anthony Kermagoret, pour nos discussions captivantes sur la CMRP, et sur la recherche en générale. Merci également à Dr. Antoine Debuigne, pour son aide précieuse lors de mes synthèses de nanogels « mixtes ». Merci à Dr. Ian German, pour nos conversations franco-anglaises truffées de nombreux 'tips', pour rédiger un article ou pour choisir un restaurant londonien ! Merci à Grégory Cartigny, qui m'a initiée aux joies de la synthèse de l'alkyl-Cobalt, à Martine Dejeneffe, pour son aide précieuse tout au long de mes deux années passées à Liège, et en particulier de m'avoir appris à me servir du TEM. Merci à Charlotte Dannemark et Laetitia de Fayes, pour leur soutien constant lors des analyses parfois ardues de mes nanogels. Merci à Valérie Collard, pour nos tests antibactériens toujours effectués dans la joie et la bonne humeur ! L'équipe de Bordeaux n'est pas en reste : j'adresse mes sincères remerciements à Amélie Vax pour son aide concernant la SEC, à Anne-Laure Wirotius pour la RMN, Cédric Le Coz pour son aide et sa patience quant au TGA et DSC des mêmes nanogels. Merci à Dr. Karim Aïssou pour son aide très appréciée quant à la conductivité ionique de nos nanogels de PILs, à Emmanuel Ibarboure qui a fait un travail génial pour imager par AFM nos surfaces poreuses nanostructurées, à Prof. Christophe Schatz pour son aide quant à la caractérisation SEC. Merci à Dr. Joan Vignolle pour son accueil dans l'équipe, et l'intérêt qu'il a porté à mes travaux.

Je souhaite également remercier de tout cœur Sophie Boulanger, Enza Esposito, Corine Gonçalves de Carvahlo, Dominique Richard et Catherine Roulinat pour leur présence constante et leur aide continue quant à l'aspect administratif de ma thèse, à Liège comme à Bordeaux. J'apprécie énormément tout ce que vous avez fait pour nous faciliter la vie !

Merci aux doctorants du CERM et du LCPO pour tout ce que nous avons vécu ensemble, pour la bonne ambiance dans les bureaux et les labos, pour les discussions à n'en plus finir et les débats que personne n'a gagné. Merci en particulier à Mathilde, Mathilde, Daniela, Margaux, Zeynep et Rahmet pour tous nos moments (et nos cafés) partagés, pour nos week-end à Paris et nos soirées entre amis. Merci à Winnie et Paul, qui ont facilité mes premiers mois à Bordeaux. Merci à Romain pour nos conversations (que dis-je, nos débats) toujours très intéressantes, à Ana pour tous nos moments de fous-rires, à Camille, Jana, Beste et Sofiem pour leur bonne humeur.

My PhD work would never have been the same had I not been part of IDS, thus, I profusely thank all the PhD students from IDS-FunMat, with whom I spent three unforgettable weeks of lectures and fun (and werewolves) during the training schools! Coming from all over the world, from different cultures and different languages, we all learnt a lot, from our projects of course, but also from each other: I know we will keep in touch. IDS-FunMat is far more than just another program, and I am more thankful for that than I can express! Merci à tous les organisateurs d'IDS qui se démènent pour nous rendre les démarches administratives plus simples : les difficultés ont peut-être été importantes, mais nous avons tous appris beaucoup. Vous nous avez donné non seulement l'opportunité de créer un réseau fort, mais surtout la possibilité de nouer des liens très forts les uns avec les autres. Merci pour tout ce que vous avez fait pour nous ces dernières années, et j'espère de tout cœur que cette initiative va continuer à exister, fusse sous un autre nom.

Merci enfin, à ma famille, qui m'a aidée, épaulée et encouragée sans relâche ces dernières années. Merci à mes parents, à Marie, Aline et Augustin, qui ont toujours su trouver

les mots justes pour m'apporter leur soutien et me pousser à aller de l'avant. Merci de vous être toujours intéressés à ce que je faisais, même si les détails étaient parfois difficiles à saisir. Merci à Léon, mon grand-père, dont la confiance absolue m'a aidée à surmonter les macrogélations de certaines copolymérisations, et le manque de conversion d'autres.

Table of contents

Aim of the thesis	1
<hr/>	
Chapter I	9
<i>From Biocidal Polymers to Antibacterial Coatings</i>	
<hr/>	
Chapter II	51
<i>Recent Advances in Controlled Radical Cross-linking Copolymerization (CRCcP): Experimental and Theoretical Investigations</i>	
<hr/>	
Chapter III	129
<i>Direct One-Pot Synthesis of Poly(vinyl acetate) and Poly(ionic liquid) Nanogels by Cobalt-Mediated Radical Cross-linking Copolymerization</i>	
<hr/>	
Chapter IV	169
<i>Copolymerization of Vinyl/Divinyl Systems with Different Reactivities by Cobalt-Mediated Radical Cross-linking Copolymerization</i>	
<hr/>	
Chapter V	191
<i>Synthesis of Hydrophobic Nanogels of Poly(ionic liquids) by Cobalt-Mediated Radical Cross-linking Copolymerization, and their Use for Patterning Surfaces</i>	
<hr/>	
Chapter VI	243
<i>Coating and Antibacterial Properties of the Poly(ionic liquids) Structures</i>	
<hr/>	
General conclusion and perspectives	271
<hr/>	

Abbreviations

1	cobalt(III)-adduct acting as initiator and control agent in CMRP
AB	Antibacterial
AFM	Atomic force microscopy
ATRP	Atom-transfer radical polymerization
Br ⁻	Bromide anion
CRCcP	Controlled radical cross-linking copolymerization
CMRP	Cobalt-mediated radical polymerization
CMRCcP	Cobalt-mediated radical cross-linking copolymerization
DLS	Dynamic light scattering
DMF	Dimethylformamide
DSC	Differential scanning calorimetry
DVA	Divinyl adipate
DVI	1,13-divinyl-3-decyl diimidazolium
FRCcP	Free radical cross-linking copolymerization
IL	Ionic liquid
ILM	Ionic Liquid Monomer
MeOH	Methanol
MIC	Minimum inhibitory concentration
NMP	Nitroxide-mediated polymerization
NMR	Nuclear magnetic resonance
NTf ₂ ⁻	bis(trifluoromethanesulfonyl)imide anion
PIL	Poly (ionic liquid)
PVAc	Poly(vinyl acetate)
PVOH	poly(vinyl alcohol)
QCM-D	Quartz crystal microbalance coupled with dissipation technique
RAFT	Reversible addition-fragmentation chain transfer
SEC	Size exclusion chromatography
TEM	Transmission electronic microscopy
THF	Tetrahydrofuran
TGA	Thermo-gravimetric analysis
VAc	Vinyl acetate
VEtIm ⁺	<i>N</i> -Vinyl-3-ethyl imidazolium cation

Aim of the thesis

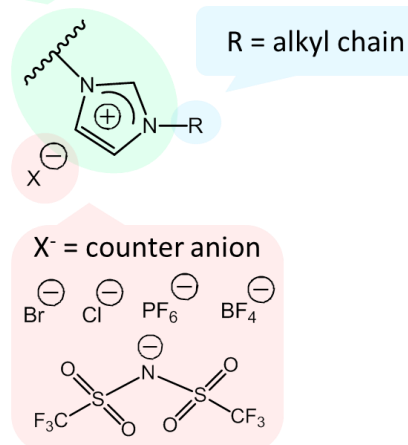
Stainless steel is employed in many areas such as medicine, household appliances, building and food industries, owing to its resistance to corrosion and chemicals, and to its mechanical and aesthetic properties as well. Without particular precautions, however, stainless steel is unable to prevent bacteria from proliferating when ageing. In order to impart antibacterial (AB) properties to stainless steel, surface modification techniques have been developed, for instance, using silver-based inorganic agents¹, or organic biocides such as antibiotics or antimicrobial host-defense peptides^{2, 3}. Diffusion of the AB species out of the coating limits, however, the AB activity over time. Although multiple techniques exist for strongly anchoring the biocides onto the surface (*e.g.* electrografting⁴, cold plasma treatment followed by post-functionalization⁵ or by silane coupling agents^{6, 7}), their implementation at the industrial scale is difficult. Indeed, they are generally based on multi-step synthesis, and/or employ hazardous chemicals and/or toxic molecules, or have high manufacturing costs.

In this project, we propose a simple, robust, precise and environmentally friendly synthetic strategy to new positively charged copolymers that are potentially suitable to achieve stainless steel with long-lasting AB properties. The copolymers that we wish to develop are made of a cationic polymeric ionic liquid -also called poly(ionic liquid) (PIL)- possessing the AB activity.

PILs have emerged in the past 10 years as a new class of polyelectrolytes combining the physicochemical qualities of molecular ionic liquids (ILs), such as chemical and thermal stability, high ionic conductivity, and adjustable solubility and viscosity, with the specific properties of polymers, such as film formation and processability⁸⁻¹⁰. PILs are finding various potential applications as polymer-supported catalysts¹¹, polymeric surfactants¹², polymer electrolytes in electrochemical devices^{13, 14}, etc. Among PILs, those based on imidazolium (cationic) moieties have been the most investigated (see figure below). To the best of our

Aim of the thesis

Polymeric backbone with pendant imidazolium moieties



knowledge, there was only one paper that reported on the AB activity of PILs bearing imidazolium groups when started this PhD thesis¹⁵, though imidazolium-containing organic compounds had also been studied¹⁶. The strong AB activity of these PILs was investigated in aqueous solution but not when they were immobilized on surfaces. The AB activity is

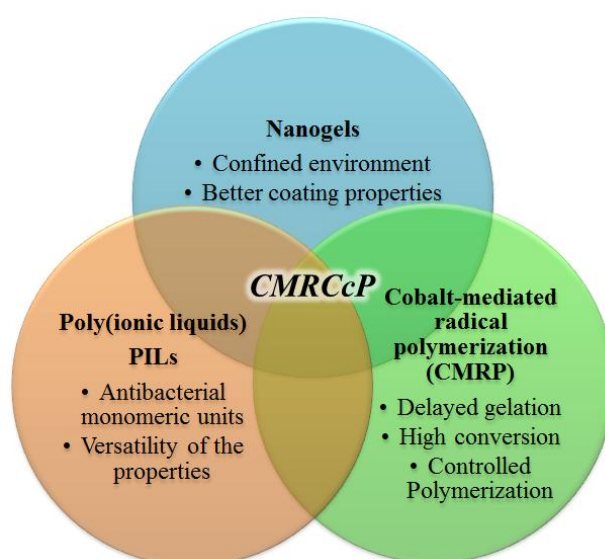
expected to be different because it depends on the organization of the AB groups onto the surface and on their interaction with bacteria. Moreover, due to the lack of anchoring groups, these PILs are not permanently anchored to the surface, so that they will be released in the environment.

We hypothesized that PILs of high molar mass might be useful to impart long-term AB activity to stainless steel. Indeed, high molar mass polymers can be difficult to re-dissolve once they are dried. Therefore, the deposition of AB PILs of high molar mass on the substrate, following by their drying, was expected to lead to AB stainless steel with long activity. Moreover, the variation of both the counter-anion (*e.g.* with X⁻ = Br⁻ or N⁻(SO₂CF₃)₂) and the substituents on the nitrogen atoms of the imidazole backbone are also simple ways to affect both the AB activity and coating durability.

This PhD thesis is at the interface of three fields of polymer science, including polymeric ionic liquids or PILs, controlled radical polymerization and precision synthesis of branched architecture. In this work, we present a simple, versatile, environment-friendly synthesis to novel positively charged PILs of high molar mass, on the form of nanogels, featuring different types of counter-anions. Such PILs have been assessed as antibacterial polymers for stainless steel coatings. The main objective of this PhD thesis was to design

Aim of the thesis

nanogel architectures by the so-called cobalt-mediated radical cross-linking copolymerization (CMRCcP). These coatings were expected to provide long-lasting antibacterial properties when deposited onto stainless steel surfaces, against both Gram-positive and Gram-negative bacteria. Thanks to the controlled character of the CMRCcP methodology, the compositions and the overall structure of all copolymers can be fine-tuned which will help to determine the optimal structure for potent activity, and to better understand the mechanism of antibacterial actions of these AB copolymer materials.



This manuscript is composed of six distinct chapters written in English, and is organized as follow.

The first chapter reports a short state-of-the-art in antibacterial polymers and antibacterial coatings. It focuses on biocidal polymers, meaning polymer which are antibacterial by themselves (contrary to polymers which obtains antibacterial activity *via* stocking and releasing biocides).

Aim of the thesis

Chapter VI is dedicated to the AB activity assessment of the previously synthesized nanogels, compared with their homopolymer counterpart against Gram-positive and Gram-negative bacteria in solution (for hydrophilic nanogels). Preliminary investigations of the formation of antibacterial nanogel coatings on stainless steel are also reported.

This PhD work was carried out in the framework of a collaboration between two universities: the University of Liège in the Center for Education and Research on Macromolecules (CERM, Belgium) and the University of Bordeaux in the Laboratoire de Chimie des Polymères Organiques (LCPO, France), under the joint supervision of Dr. Christophe Detrembleur and Prof. Daniel Taton. It was part of the International Doctorate School in Functional Materials (IDS FunMat), with a scholarship from the Doctorate School of the University of Liège.

References

1. C. Falentin-Daudré, E. Faure, T. Svaldo-Lanero, F. Farina, C. Jérôme, C. Van De Weerd, J. Martial, A. S. Duwez and C. Detrembleur, *Langmuir*, 2012, **28**, 7233-7241.
2. A. Héquet, V. Humblot, J. M. Berjeaud and C. M. Pradier, *Colloids and Surfaces B: Biointerfaces*, 2011, **84**, 301-309.
3. C. Vreuls, G. Zocchi, H. Vandegaart, E. Faure, C. Detrembleur, A. S. Duwez, J. Martial and C. Van De Weerd, *Biofouling*, 2012, **28**, 395-404.
4. M. Ignatova, S. Voccia, S. Gabriel, B. Gilbert, D. Cossement, R. Jérôme and C. Jérôme, *Langmuir*, 2009, **25**, 891-902.
5. E. Stoleru, R. P. Dumitriu, B. S. Munteanu, T. Zaharescu, E. E. Tănase, A. Mitelut, G. L. Ailiesei and C. Vasile, *Appl Surf Sci*, 2016, **367**, 407-417.
6. H. Li, H. Bao, K. X. Bok, C. Y. Lee, B. Li, M. T. Zin and L. Kang, *Biomaterials Science*, 2016, **4**, 299-309.
7. S. J. Yuan, F. J. Xu, S. O. Pehkonen, Y. P. Ting, K. G. Neoh and E. T. Kang, *Biotechnology and Bioengineering*, 2009, **103**, 268-281.

Aim of the thesis

8. J. Yuan, D. Mecerreyes and M. Antonietti, *Progress in Polymer Science*, 2013, **38**, 1009-1036.
9. D. Mecerreyes, *Progress in Polymer Science*, 2011, **36**, 1629-1648.
10. P. Coupillaud and D. Taton, in *Applications of Ionic Liquids in Polymer Science and Technology*, Springer Berlin Heidelberg, 2015, pp. 69-102.
11. P. Coupillaud, J. Vignolle, D. Mecerreyes and D. Taton, *Polymer*, 2014, **55**, 3404-3414.
12. R. Gracia, K. Vijayakrishna and D. Mecerreyes, *Reactive and Functional Polymers*, 2014, **79**, 54-58.
13. C. Pozo-Gonzalo, R. Marcilla, M. Salsamendi, D. Mecerreyes, J. A. Pomposo, J. Rodríguez and H. J. Bolink, *Journal of Polymer Science, Part A: Polymer Chemistry*, 2008, **46**, 3150-3154.
14. M. G. Cowan, M. Masuda, W. M. McDanel, Y. Kohno, D. L. Gin and R. D. Noble, *Journal of Membrane Science*, 2016, **498**, 408-413.
15. G. Garg, G. S. Chauhan, R. Gupta and J. H. Ahn, *Journal of Colloid and Interface Science*, 2010, **344**, 90-96.
16. J. Łuczak, C. Jungnickel, I. Łcka, S. Stolte and J. Hupka, *Green Chemistry*, 2010, **12**, 593-601.

Aim of the thesis

Chapter I

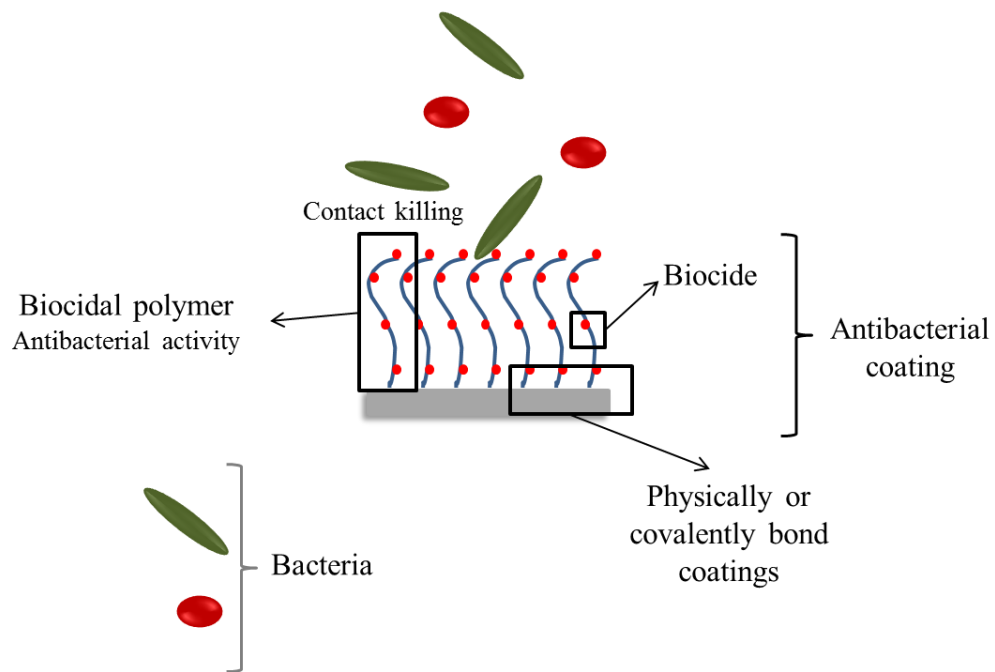
From Biocidal Polymers to Antibacterial Coatings

Abstract

An introduction to the use of biocidal polymers forming efficient long-lasting antibacterial coatings is presented. Antibacterial polymeric coatings have been developed as a mean to improve human healthcare and prevent the proliferation of bacteria.

A presentation of the main biosourced and synthetic biocidal polymers is first given. Their antibacterial activities are compared *via* their minimum inhibitory concentration (MIC). Finally, the different types of antibacterial polymeric coatings are briefly discussed. A special focus is made to antibacterial polymeric coatings applied to stainless steel surfaces.

Graphical abstract



From Biocidal Polymers to Antibacterial Coatings

I. Introduction

- 1.1 Introduction
- 1.2 Scope of the review

II. Biocidal polymers

- II.1 Biosourced biocidal polymers
- II.2 Synthetic biocidal polymers
- II.3 Mode of action

III. Comparison of the polymers: MIC assessment

IV. Antibacterial polymeric coatings

- IV.1 Chemically anchored polymers
- IV.2 Physically anchored polymers
- IV.3 Coatings comparison: antibacterial assessments on surfaces
- IV.4 Antibacterial coatings on stainless steel

V. Outlook

Abbreviations

AB: antibacterial; BC: barnacle cement; DD: degree of deacetylation; LbL: layer-by-layer; MIC: minimum inhibitory concentration; P(4VP): poly(4-vinyl pyridine); PDMAMEA: poly((*N,N*,dimethylamino) ethyl methacrylate); PDOPA: polydopamine; PEG: poly(ethylene glycol); PEI: poly(ethylene imine); PHEAA: poly(*N*-hydroxyethyl acrylamide); PMA: poly(methacrylamide); PMETA: poly(2-(methacryloyloxy)ethyl trimethylammonium chloride); PIL: poly(ionic liquid); PMPC: poly(2-methacryloyloxyethyl phosphorylcholine); QAC: quaternary ammonium compounds; SI-ATRP: surface initiated atom transfer radical polymerization.

I. Introduction

I.1 Introduction

In 2014, the global report on surveillance of World Health Organization highlighted the issue of antimicrobial resistance of Gram-positive and Gram-negative bacteria: amongst the seven most common bacteria were *S. Aureus* (Gram-positive) and *E. Coli* (Gram-negative). Bacterial proliferation and colonization on a surface causes the formation of a biofilm, detrimental in daily life, and more particularly for human healthcare. To solve this issue, considerable efforts have been carried out to find a durable antibacterial coating capable of acting against both Gram-positive and Gram-negative bacteria.

The ability to form durable antibacterial coatings, effective against Gram-positive and Gram-negative bacteria, has been discussed more and more during the past decade. Several strategies have been reported (see Figure I-1), leading to the formation of antibacterial polymeric coatings.

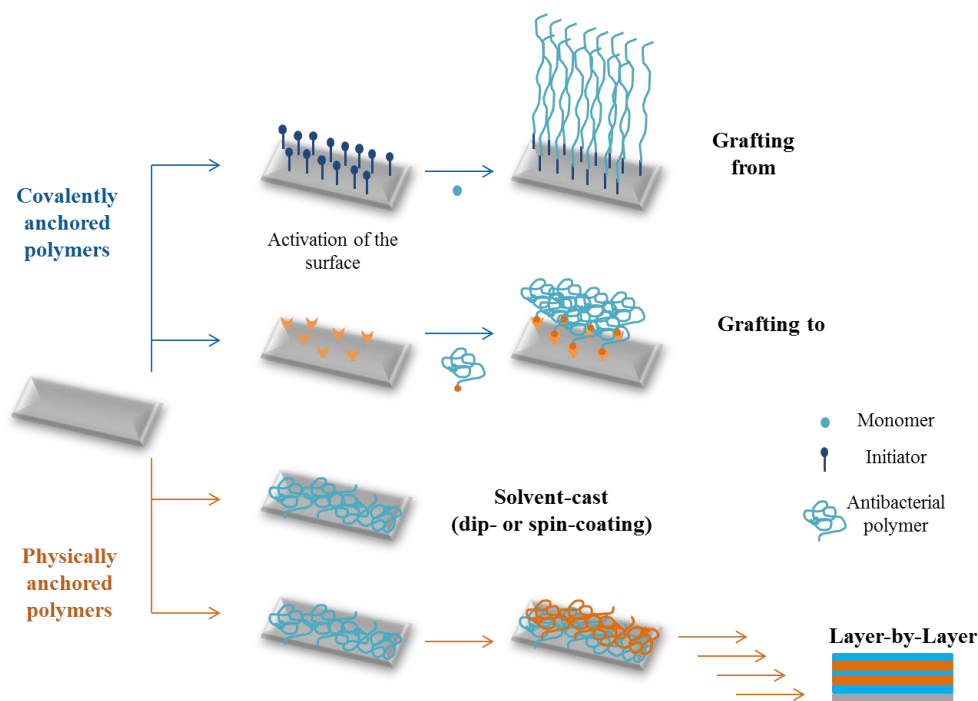


Figure I-1. Coating methods to produce covalently and physically anchored polymer on a surface.

Chapter I: From Biocidal Polymers to Antibacterial Coatings

Antibacterial polymer coatings can be classified, depending on their action mode against bacteria (Figure I-2). On one hand, passive coatings aim to prevent the adhesion of bacteria, usually through steric or electrostatic repulsion. On the other hand, active coatings aim to kill bacteria. In the latter case, active coatings can release biocides in the environment, or kill by contact with the bacteria.

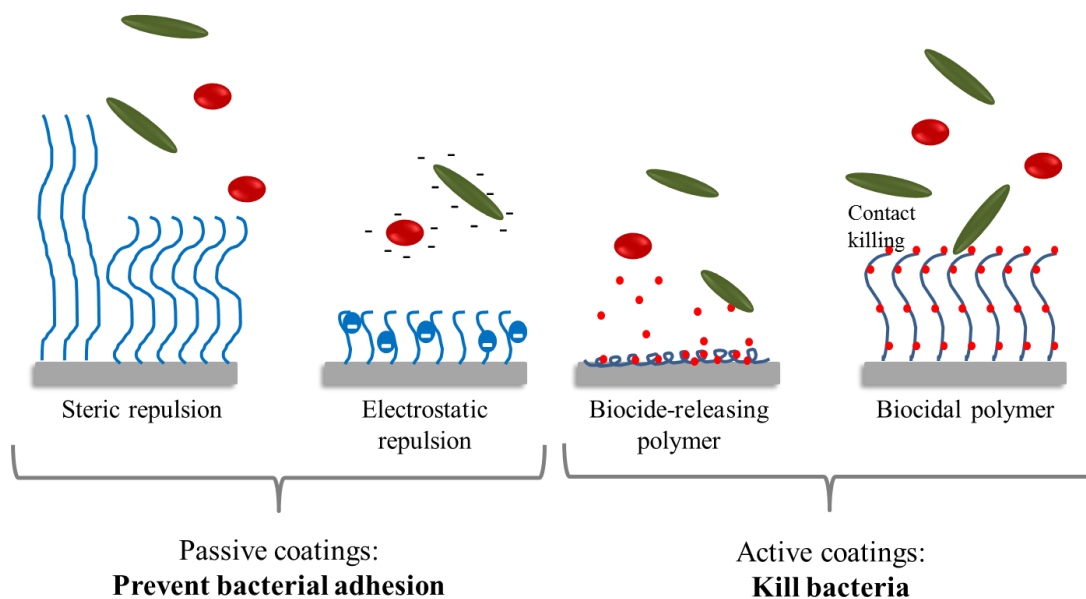


Figure I-2. Representations of the main types of polymeric coatings.

Biocide-releasing coatings have been extensively studied, both inorganic and organic biocides being used (*e.g.* silver nanoparticles, antibacterial peptides). Silver nanoparticles serve as reservoirs of silver ion, which disrupts the bacteria membranes, leading to the death of the cell. However, the permanency of the silver-releasing polymeric coating is relative: once the biocide has been released, the surface is no longer antibacterial. Yin *et al.* have prolonged the antibacterial activity of silver-releasing layer-by-layer (LbL) coating by introducing a nano-structured superhydrophobic surface on top of the polymer coating¹. Silver nanoparticles possess very good antibacterial properties². However, some reports have questioned their effect for human health and its impact on the environment^{3,4}.

Chapter I: *From Biocidal Polymers to Antibacterial Coatings*

I.2 Scope of the chapter

Here, we focus on bio-based and synthetic biocidal polymers, *i.e.* polymers displaying antibacterial activity by themselves, and their use in forming antibacterial long-lasting coatings.

In a coating, polymers are anchored on the surface, either physically by dip- or spin-coating a polymer solution, or covalently by chemical grafting (see Figure I-1). Other non-polymeric coatings, such as essential oil-based coatings⁵, enzymatic coatings⁵, or superhydrophobic surfaces^{6, 7} have been reported in the literature, but will not be further discussed here.

II. Biocidal polymers

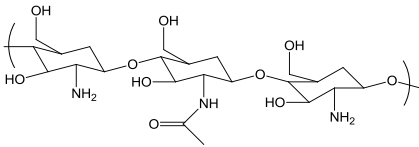
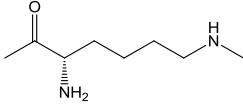
An antibacterial polymer has to address several criteria for implementation as a useful AB coating: i) be easily synthesized; ii) be stable in long-term usage; iii) be insoluble in water once deposited on the surface; iv) must not emit toxic compounds once deposited; v) is active against a broad range of bacteria strains (Gram-positive and Gram-negative bacteria). The main parameters affecting the antibacterial properties of polymers include⁸ the molar mass of the polymer, its charge density, the effect of the counter-ion and the effect of the alkyl chain. The architecture of antibacterial (co)polymers (*e.g.* graft, block copolymers, hyperbranched, nanogels) has also been extensively explored to enhance the antibacterial activity and improve the durability of the coating⁹.

II.1 Biosourced biocidal polymers

In Table I-1 are summarized the main types of biosourced biocidal polymers, which include chitosan and derivatives, and antibacterial polypeptides such as polylysine.

Chapter I: From Biocidal Polymers to Antibacterial Coatings

Table I-1. Structures and principal advantages or drawbacks of the main biosourced antibacterial (co)polymers⁹.

	Advantages	Limitations
<p>Chitosan⁹⁻¹¹</p> 	<p>Natural polymer, with a diversity of molecular weight M_w and degree of deacetylation (DD), as well as chemical modifications.</p> <p>AB to a wide array of bacteria and fungi.</p>	<p>Solubility issues: only soluble in acidic media (water, pH < 6.5)</p>
<p>Polylysine^{12, 13, 14}</p>  <p>ε-PL</p>	<p>Natural polymer, thermo-stable, biodegradable, water-soluble, non-toxic.</p>	

Chitosan is a biosourced, biocompatible polysaccharide, which has been studied for its very wide antibacterial properties against Gram-positive and Gram-negative bacteria, fungi and algae^{10,15}. Numerous studies have been reported, trying to establish links between the antibacterial activity of the chitosan and its molar mass (Figure I-3), and its degree of deacetylation¹⁰. For instance, Takahashi *et al.* have investigated the importance of the latter parameter: a change from 86 to 92% causes a decrease of MIC, from 100 mg/mL to 40 mg/mL¹⁶. While the influence of the molar mass of chitosan over its antibacterial activity has been proven (molar mass of the studied chitosan: 42 to 135 kg/mol.), the trend is not so clear^{10, 17, 18}, but generally, increasing the molar mass of chitosan decreases its MIC. The main drawback remains its poor solubility at pH above 6.5 (Table I-1)^{10, 19}. To circumvent this issue, several studies have investigated the quaternization of chitosan to improve both its solubility and its antibacterial activity^{20,21}, *e.g.* using *N*-(3-chloro-2-

Chapter I: From Biocidal Polymers to Antibacterial Coatings

hydroxypropyl)ethylammonium chloride. The MIC of such chitosan derivatives has been assessed against *S. Aureus* (8-64 $\mu\text{g/mL}$) and *E. Coli* (16-64 $\mu\text{g/mL}$)²²: when the functionalization increases beyond 20%, the MIC increases too.

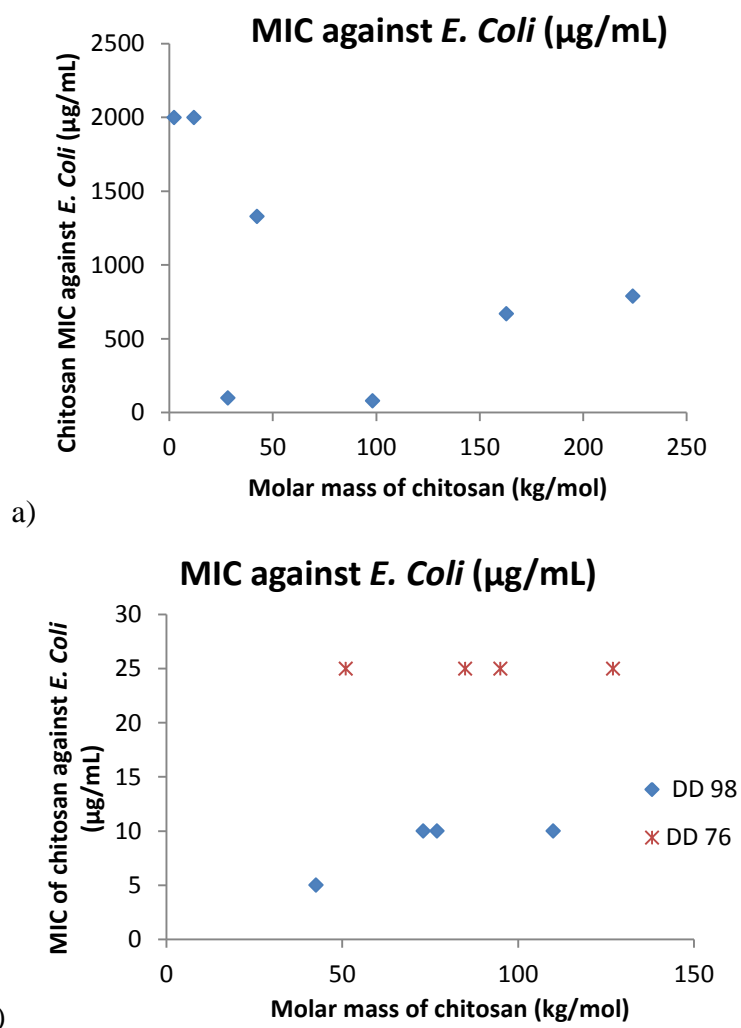


Figure I-3. Variations of MIC of: a) quaternized chitosan, depending on its molar mass¹⁸; b) chitosan, depending on its molar mass and deacetylation degree (MIC determination occurs in acidic solution)¹⁷.

Polypeptides have also been studied for their AB activity^{12, 23}. For instance, the ϵ -polylysine has a MIC of 1 to 8 $\mu\text{g/mL}$ against Gram-positive and Gram-negative bacteria²⁴. A

Chapter I: From Biocidal Polymers to Antibacterial Coatings

large spectrum of applications characterizes ϵ -polylysine, from detergency to drug delivery and use as a dietary agent¹⁴. However, its synthesis remains expensive.

II.2 Synthetic biocidal polymers

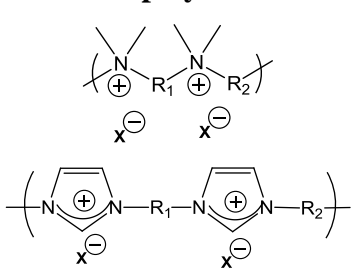
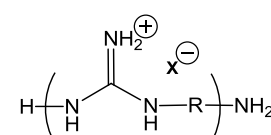
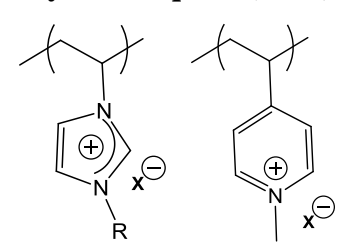
In Table I-2 are summarized the main types of synthetic biocidal polymers: poly(ethylene imine) (PEI), quaternary ammonium compounds (QACs), ionene polymers, poly(guanidines) and poly(ionic liquids) (PILs).

Table I-2. Structures and principal advantages or drawbacks of the main synthetic antibacterial (co)polymers⁹.

	Advantages	Limitations
<p>PEI²⁵</p>	<p>Synthetic, non-biodegradable, cationic.</p> <p>Nontoxic coatings.</p> <p>Main mode of action: rupture of the bacteria membrane walls.</p>	<p>MIC values of PEI quite high, compared to functionalized/modified PEI.</p> <p>AB activity depends on the M_w of the polymer (no activity at low M_w).</p>
<p>Quaternary ammonium compounds (QACs)^a</p> <p>R: spacer group R = alkyl chain benzyl</p>	<p>AB activity depending on the length of the alkyl chain (hydrophobicity).</p> <p>From one biocidal unit per chain to one biocide per monomer unit.</p>	<p>Toxicity on eukaryote cells not studied in-depth.</p>

Table I-2 continued page 18

Chapter I: From Biocidal Polymers to Antibacterial Coatings

<p>Ionene polymers^{26 a}</p> 	<p>Biocidal polymers containing cationic moieties in their backbone, with R₁ and R₂ spacer group which may contain heteroatoms.</p>
<p>Poly(guanidines)^{27, 28 a}</p> 	<p>Wide antibacterial spectrum, non-toxic, water-soluble polymers.</p>
<p>Poly ionic liquids (PILs)^a</p> 	<p>Antibacterial properties reported for imidazolium (structure on the left) and pyridinium (structure on the right) -based PILs. AB activity depends on the molar mass, the counter anion (X⁻)²⁹ and the length of the alkyl chain R. Toxicity on eukaryote cells not studied in depth.</p>

^a Most usual counter anions (X⁻) are : Br⁻, Cl⁻, BF₄⁻, PF₆⁻, N(SO₂CF₃)₂⁻

Cationic (co)polymers have been intensely studied as polymeric antibacterial materials^{30, 31}, as evidenced in Table I-1 and I-2. The influence of the macromolecular characteristics of the polymers on their AB properties has been investigated.

PEI is a synthetic, branched and non-biodegradable polymer that can contain primary, secondary and tertiary amino functions. While unmodified PEI possesses some antibacterial properties, the presence of numerous of amino functions allows for further modification of this polymer with the introduction of AB groups such as quaternary ammonium salts (see Figure I-4)³².

Chapter I: From Biocidal Polymers to Antibacterial Coatings

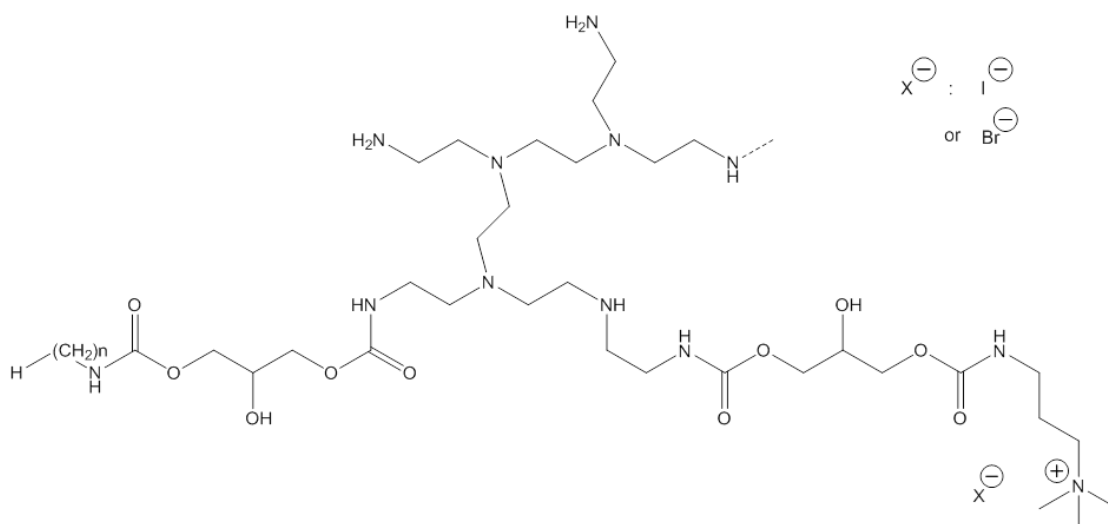


Figure I-4. Schematic representation of modified PEI³²

In 2008, have been studied the antibacterial properties of PEI-based nanoparticles³³ (PEI primary chains cross-linked with dibromopentane³⁴): PEI was alkylated with octyl halides prior to *N*-methylation using CH₃I. The resulting particles size distribution is bimodal (around 7.5 and 140 nm of diameters). These PEI nanoparticles –bimodal in size- are then incorporated in a resin composite for dental implants: 1 wt.% of particle has been enough to stop *S. Aureus* growth for 4 weeks, and to reduce *E. Coli* growth rate of more than 80% during the same period³³. The same group has lately reported the synthesis of ‘PEI-QACs’ particle in the range of 160-190 nm: cross-linked PEI is alkylated with octyl iodide, and further methylated with methyl iodide. Such particles have proven thermally stable up to 161 °C, depending on their cross-linking density. *N*-alkyl-PEI has also been assessed once deposited on a surface; interestingly, these surfaces show no toxicity towards mammalian cells³⁵.

Several other cationic polymers have been studied for antibacterial applications. Cationic polymeric chains containing ammonium or phosphonium as pendent groups, or ammonium groups on their backbone (ionene polymers); typical examples are discussed below.

Chapter I: From Biocidal Polymers to Antibacterial Coatings

While poly(DMAEMA) (Figure I-5) exhibit antibacterial polymer for coatings³⁶ and membrane³⁷ applications, research about quaternized poly(DMAEMA) (co)polymers also abound^{36, 38-42}. For instance, once grafted on a surface³⁸ – here, polyethylene/polypropylene fabric- the killing rate of *E. Coli* bacteria of poly(DMAEMA) was 21%, vs. 100% for quaternized poly(DMAEMA). However, quaternized poly(DMAEMA) is known for its high hemolytic activity⁴³.

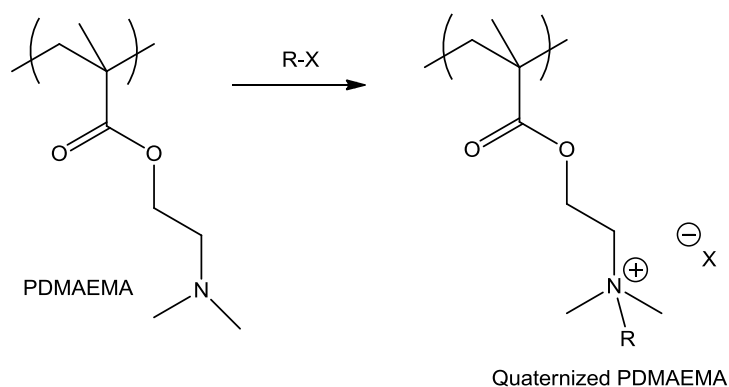


Figure I-5. Quaternization of poly((N,N,dimethylamino ethyl methacrylate).

Cationically charged poly(ionic liquid)s (PILs) have also shown excellent antibacterial properties against Gram-positive and Gram-negative bacteria⁴⁴⁻⁴⁷. Most of AB PILs are based on pyridinium, imidazolium, or phosphonium groups.

Pyridinium-based polymers have been synthesized to mimic biosourced counterparts, *i.e.* polymeric alkylpyridinium salts originated from a marine sponge. In particular, this biosourced polymer is also able to inhibit marine biofilm formation (barnacle settlement) through a reversible non-toxic process⁴⁸, by inhibiting acetylcholinesterase. The process is said reversible as the marine organisms (barnacle) can recover from the antifouling treatment, in filtered natural seawater, after 72 hours of antifouling treatment (*i.e.* 72 hours in a solution of up to 1.6 mg/mL of alkylpyridinium-containing polymers). Sharma *et al.* have demonstrated the influence of the counter anion over the antibacterial activity of PILs⁴⁹:

Chapter I: From Biocidal Polymers to Antibacterial Coatings

depending on the counter anion, the MIC of quaternized poly(4-vinyl-2-hydroxyethyl-pyridinium) against *Bacillus coagulans* range from 65 $\mu\text{g/mL}$ to 4000 $\mu\text{g/mL}$ (Figure I-6).

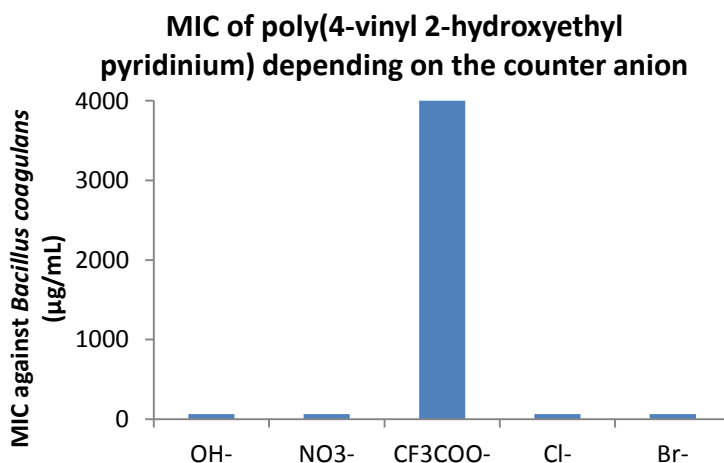


Figure I-6. MIC of poly(4-vinyl 2-hydroxyethyl pyridinium) against *Bacillus Coagulans*, depending on its counter anion⁴⁹.

Gao *et al.* have investigated the influence of both the degree of quaternization and the molar mass of a poly(acrylamide-*co*-4-vinylpyridine) on its antibacterial properties⁵⁰: unexpectedly, the higher the quaternization degree, the higher the antibacterial activity. On the other hand, an increase of molar mass of the quaternized poly(4-vinyl pyridine) block provides a higher antibacterial effect. While pyridinium-based PILs exhibit good antibacterial activity, such copolymers are not biocompatible. They require further chemical modification, or copolymerization with a hydrophilic biocompatible co-monomer, to be used in biomedical applications⁵¹.

Polyanions with a phosphonium counter-cation have been described by Tsuboka *et al.*⁵². The polymers have been grafted from silica nanoparticles, and then tested against *S. Aureus* and *E. Coli*. Only 1 wt.% of such grafted nanoparticles is necessary to completely inhibit the growth of *S. Aureus* in solution, while 5 wt.% are necessary against *E. Coli*.

Chapter I: From Biocidal Polymers to Antibacterial Coatings

In 2010, Jungnickel *et al.*⁴⁷ have reported that imidazolium-type ionic liquids could be antibacterial against both Gram-positive and Gram-negative bacteria: they have focused on 1-alkyl-3-methyl imidazolium derivatives, with an array of possible counter anions (Figure S I-2). Interestingly, they show that the longer the alkyl chain, the lower the MIC of the ionic liquid.

Chauhan *et al.* have investigated the influence of the counter anion on the antibacterial activity of poly(*N*-vinyl-3-(2-sulfoethyl imidazolium betaine))⁵³ of different viscosity and surface morphology. The MIC of the resulting polysulfobetaines vary slightly depending on the counter anion between 2 mg/mL for the chloride counter anion and 16 mg/mL for the acetate counter anion. That has been ascribed to the change of counter anion causing a change in the alignment of the polymer chains; thus, changing the anion influences to a degree the amount of contact between the polymer and the bacteria⁵³.

Other studied polyelectrolytes include ionene polymers, in particular those containing quaternary ammonium on their backbone. Ionene polymers exhibit biocidal properties, which is known since 1973⁵⁴. In particular, Agarwar *et al.* have synthesized a series of alkyloxyethyl ammonium ionenes⁵⁵ displaying not only excellent antibacterial properties (MICs below 10 $\mu\text{g/mL}$ against *E. Coli*), but also a very quick response time. At high concentrations (5000 $\mu\text{g/mL}$), all *E. Coli* bacteria are dead within 10 minutes. At lower concentration (100 $\mu\text{g/mL}$), 90% of bacteria are killed within 2 minutes of contact⁵⁵. When approaching the MIC, the time necessary to achieve such results is longer. The influence of the alkyl chain length and the spacer has also been studied: MIC varied from 10 to 1000 $\mu\text{g/mL}$. The best MIC were obtained either with $R = \text{CH}_3$ and $R' = \text{C}_{12}\text{H}_{24}$, or with $R = \text{C}_8\text{H}_{17}$ and $R' = \text{C}_4\text{H}_8$, C_5H_{10} and C_6H_{12} (see Figure I-7).

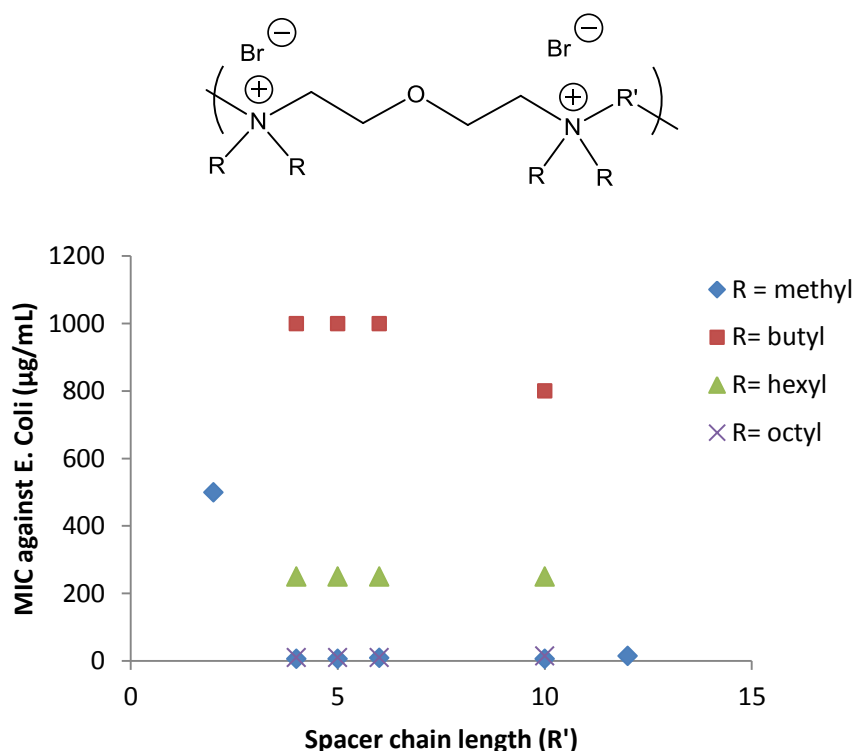


Figure I-7. MIC against *E. Coli* of alkyloxy ethyl ammonium ionene polymers, depending on the chain lengths of the alkyl chain R and the spacer R' .⁵⁵

Poly(guanidines) have also been investigated, due to their high water solubility and biocidal efficiency. Interestingly, an average molar mass of 800 g/mol is sufficient for the polymer to exhibit antibacterial activity⁵⁶. Massimba Dibama *et al.* have investigated the possibility of using guanidine-containing compounds, by attaching guanidine-arms to a benzene core⁵⁷ (see Figure S I-1). Complexes of chitosan with guanidine-based oligomers have been investigated⁵⁸. Agarwal *et al.* have reported the use of poly(guanidines) as macroinitiators for the ring-opening polymerization of caprolactone. The resulting block copolymers have shown good antibacterial activity, with MIC in the range of 37.5-87.5 $\mu\text{g/mL}$ against *E. Coli*, depending on the ratio of each block⁵⁹. Poly(methyl methacrylate-*b*-hexamethylene guanidine hydrochloride) block copolymers have been assessed as

Chapter I: *From Biocidal Polymers to Antibacterial Coatings*

antibacterial films on glass slides⁶⁰. These surfaces have been proven to be active against *E. Coli* bacteria for up to 3 months⁶⁰.

Poly(2-alkyl-2-oxazoline)s (POx) have been compared to passive PEG-based coating⁶¹. POx are water-soluble and biocompatible synthetic polymers, also exhibiting a 'stealth' behavior like PEG⁶¹. Though POx as such, *i.e.* without modification, do not exhibit antibacterial properties, a suitable chemical modification of their chain-ends enhances their antibacterial activity, as proven by Tiller *et al.*⁶². Telechelic POx with quaternary ammonium at chain-ends possess MIC between 200 and 1000 $\mu\text{g/mL}$ against *S. Aureus*, depending on the DP⁶² (respectively for DP = 20 and DP = 96, on a poly(2-ethyl 2-oxazoline) chain). For a similar DP, a change from methyl to ethyl on the oxazoline monomeric unit decreases the MIC from 2000 to 1000 $\mu\text{g/mL}$ ⁶². The authors have also demonstrated that antibacterial activity, *i.e.* MIC value, can be tuned depending on the nature of the chain-ends.

Synthetic biocidal polymers are usually positively charged, the cations being either on pendant chains, or on the backbone. Several parameters influence the antibacterial activity, such as the nature of the counter anion, the molar mass of the polymers, the pendant alkyl chain length.

II.3 Mode of action

Bacteria cells are negatively charged, due to the presence of phosphatidylethanolamine. As such, use of positively charged polymers results in electrostatic interactions between the bacterium cell and the polymer, which then adsorb on the bacterium surface⁹. The polymer adsorption then leads to the disruption of their membrane, and ultimately, to the death of the bacteria³⁵ (Figure I-8).

Chapter I: From Biocidal Polymers to Antibacterial Coatings

The exact mode of action of each type of antibacterial polymer is still not completely known. However, it has been surmised that, in the case of cationically-charged polymers containing pendant alkyl chains, the cations cause electrostatic interaction (thus disrupting the Ca^{2+} ions covering the cell walls), while the hydrophobic pendant alkyl chain are able to infiltrate and disrupt the outer wall of the membrane⁹.

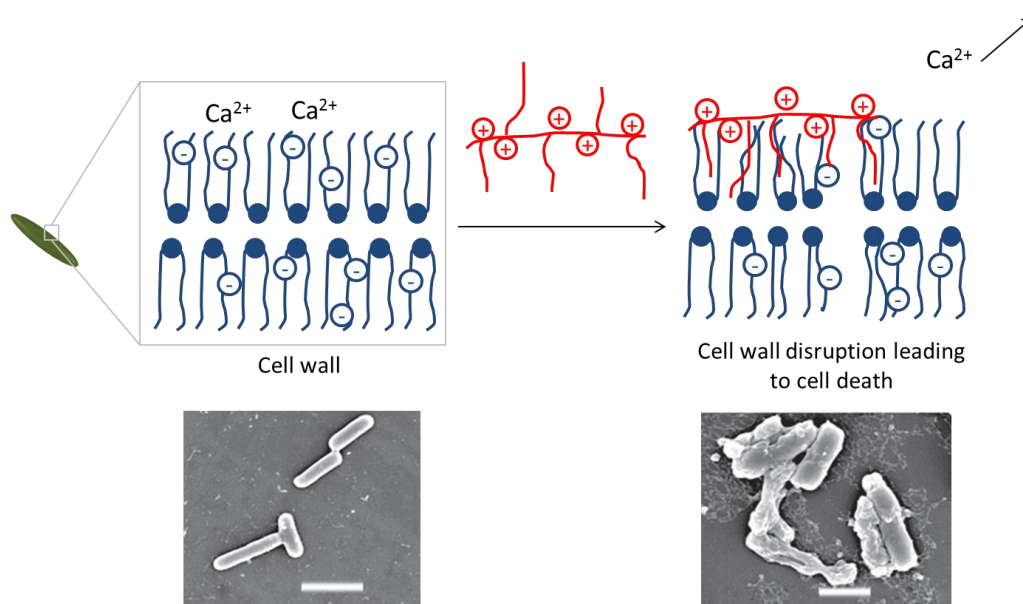


Figure I-8. Accepted antibacterial mechanism of polycationic polymers on bacteria. SEM images are borrowed from Zhou *et al.*⁶³

Several mechanisms of action have been proposed for chitosan⁶⁴, mainly by electrostatic interaction or chelation¹⁰, depending on the pH of the solution. In acidic environment, chitosan can be cationically charged, thus subject to electrostatic interaction with anionically-charged bacterial cell walls. In basic environment, chitosan is not protonated: dispersed in aqueous solution, its antimicrobial activity can be explained by hydrophobic interactions, and chelation of Ca^{2+} and Mg^{2+} cations located on the outer wall of the bacteria cells.

III. Polymer comparison: MIC assessment

Antibacterial polymers can easily be compared *via* the value of their MIC (minimum inhibitory concentration), which represent the minimum necessary concentration of polymer (usually in $\mu\text{g/mL}$) to inhibit bacterial growth in solution. MIC allows comparing the antibacterial activity of polymers in solution, it has to be understood that their antibacterial properties once deposited on a surface may vary.

In Table I-3, we compare the MIC of the polymers reported in literature against Gram-negative *E. Coli* and Gram-positive *S. Aureus* bacteria, both of which have been classified by World Health Organization as two of the seven bacteria of ‘international concern’ (Antimicrobial resistance: global report on surveillance 2014).

Table I-3. Antibacterial activity: MIC against Gram-negative (*E. Coli*) and Gram-positive (*S. Aureus*) bacteria.

Polymer	MIC (<i>E. Coli</i>) $\mu\text{g/mL}$	MIC (<i>S. Aureus</i>) $\mu\text{g/mL}$	Ref.
<i>Chitosan-based polymers</i>			
Chitosan nanoparticles ^b	8	8	65
Chitosan quaternized with <i>N</i> -(3-chloro-2-hydroxypropyl) trimethyl ammonium chloride (up to 44% of quaternization)	16-64	8-64	22
Unmodified Chitosan (DD: 85%)	20	20	15, 66
<i>ϵ-polylysine</i>			
Unmodified ϵ -polylysine	1-8	4-16	24
<i>Guanidine-based polymers</i>			
poly(guanidine-co-caprolactone)	37.5-87.5	- ^a	

Table I-3 continued p.27

Chapter I: *From Biocidal Polymers to Antibacterial Coatings*

poly(<i>N</i>-vinyl guanidine)	34	68	67
<i>PEI –based polymers</i>			
Modified PEI, physically cross-linked nanogels, (Figure S I-3a)	20	7	68
Modified PEI (Figure I-3)	100	^a	32
Unmodified PEI	400	^a	68
<i>PDAMEA-based polymers</i>			
Unmodified PDAMEA	100	100	69
Methylated PDAMEA	16	^a	43
Quaternary ammonium silane copolymers (QACs) (Figure S I-3b)	62.5-125	62.5	70
PEG-polycarbonate functionalized with ammonium	250,000	125,000-250,000	71
<i>PIL-based polymers</i>			
Pyridinium-quaternized poly(norbornenes) (Figure S I-3c)	200	^a	72
Poly(alkyl pyridinium)	300-500	30-100	73
Cellulose-g-PIL₁₀₀ (Figure S I-3d) (PIL unit: imidazolium bromide)	10	39	74
<i>Ionene-based polymers</i>			
Alkyloxy ethylammonium ionene polymers (with different spacer chain length)	^a	10-1000 depending on the alkyl chains	55
<i>Antibiotics</i>			
Ampicillin (antibiotics)	39	39	74

^a MIC of the polymer not assessed for this bacteria. ^b Chitosan nanoparticles are formed spontaneously by adding tripolyphosphate anions to chitosan solution.

As expected, ‘MIC’ of PEG-derivatives is the highest, since PEG in itself is not biocidal. However, it is interesting to note that some of the polymers analyzed here have

Chapter I: *From Biocidal Polymers to Antibacterial Coatings*

similar MIC to ampicillin (an antibiotic known to react to a large array of Gram-positive and Gram-negative bacteria). Studies on the length of the alkyl chains of poly(pyridinium) compounds have shown that the higher the length, the better the antibacterial and antifungal activity⁷³. On the other hand, Agarwal *et al.* have investigated the influence of the alkyl chains on the antibacterial activity of ionene polymers⁵⁵: they show that antibacterial effect is best for either very short alkyl chains (ethyl) or relatively long (octyl).

MIC of a polymer is generally lower once positive charges have been introduced in the structure. It is very interesting to note that several types of polymers possess antibacterial activity similar to antibiotics (ampicillin), or even lower ones. Amongst them are the quaternized chitosans, ϵ -polylysine, and several QACs and PILs.

The effect of the architecture can be observed on the chitosan-based and PEI-based nanostructures: both show better antibacterial effect than their unmodified counterpart. While the modifications of chitosan occur in one-step process, the formation of PEI-based nanostructures requires a cross-linking step prior to its quaternization, which makes it harder to use in industrial settings.

However, though MIC allows comparing polymers against a wide range of bacteria (Gram-positive and Gram-negative), the testing occurs in aqueous solution. As such, hydrophobic copolymers cannot be assessed. Furthermore, the method of deposition may reduce the antibacterial properties of the final coating.

IV. Antibacterial coatings

Polymeric antibacterial coatings are mainly divided into two categories (Figure I-2), depending on their actions to prevent biofouling^{75, 76}: passive coatings, which prevent the bacteria from anchoring themselves onto the surface (*e.g.* PEG brushes^{77, 78}), and active

Chapter I: *From Biocidal Polymers to Antibacterial Coatings*

coatings, which actually kill the bacteria and prevent the formation of a biofilm. Passive coatings generally prevent the adhesion of the bacteria *via* steric or electrostatic repulsion (see Figure I-2) and are mainly composed of PEG-based polymers. Active coatings represent either biocide-releasing polymer (*e.g.* silver nanoparticle-releasing coating⁷⁹⁻⁸¹) or biocidal polymer (*i.e.* the polymer itself is biocidal⁸²).

LbL coating^{1, 79, 83, 84}, the use of catechols⁸⁵⁻⁸⁷, and other grafting to⁸² and grafting from⁸⁸ methods⁸⁹ are particularly efficient to impart long-lasting properties. Grafting the AB polymer to the surface requires a multi-step process that uses organic solvents, making the process more difficult to use in industrial settings.

Some articles have reported the spin-coating of antibacterial polymer to form unwoven fibers on the substrate⁹⁰.

IV.1 Chemically anchored coatings

Chemically-anchored coatings are mainly divided in grafting-from and grafting-to processes (see Figure I-1).

Grafting-from methods require the activation of the substrate surface⁴², prior to the addition of monomer, while grafting-to processes attach a preformed polymer on a surface. While these two methods have been used to access long-lasting antibacterial coatings, the chemical modifications of the substrate surface usually requires a multi-step pathways, along with high temperature and/or the use of several organic solvents.

To enhance the antibacterial activity of the surface, enzymes or peptides have been grafted on the polymer-coated surface⁹¹⁻⁹³.

Recently, a new process to enhance antibacterial activity on poly(lactic acid) (PLA) surface has been engineered, by the grafting of chitosan onto the surface using

Chapter I: From Biocidal Polymers to Antibacterial Coatings

carbodiimides⁹⁴: untreated PLA surface exhibit 52% of antibacterial activity against *E. Coli*, vs. 100% for chitosan-grafted PLA.

Klibanov *et al.* have studied the antibacterial activity of covalently-anchored PEI on glass slides⁹⁵, using acylated NH₂-functionalized glass. Interestingly, first results show that covalently-bound PEI did not form an antibacterial coating. However, once the PEI was alkylated, the biocidal activity increased as well. The antibacterial activity of the coating is also influenced by the length of the alkyl chain: for a methylation, bactericidal efficiency increased up to 18 ± 20 %, while it raised to 90 ± 5 % for a hexyl chain⁹⁵.

Tiller *et al.* have described a grafting process leading to a PEI-QAC hyperbranched coating⁹⁶, using glass slides rendered hydrophilic by immersion in hot piranha solution (H₂SO₄/H₂O₂ = 7/3), and subsequent use of a siloxane coupling agent. Polyureas have been grafted from the siloxane agent, and PEI has been subsequently grafted onto the surface, alkylated with hexyl chains and quaternized with CH₃I. The coating has been proven antibacterial against *S. Epidermidis* (Gram-positive bacteria). The absence of growth inhibition zone around the coated surface further indicates that the coating does not release any biocide.

Antibacterial coatings based on poly(*N*-vinyl-4-hexyl pyridinium bromide) brushes grafted on NH₂-containing glass surface have been reported by Tiller *et al.*⁴⁶: such coated surfaces have been found antibacterial against *S. Aureus* and *E. Coli*. On the other hand, brushes of poly(*N*-vinyl-4-decylpyridinium bromide), under the same protocol, did not exhibit any antibacterial activity⁴⁶.

High density PILs brushes based on imidazolium-type polymer have been grafted on TiO₂⁸² via surface-initiated atom transfer radical polymerization, giving a brush thickness of 80 nm, with antibacterial properties against Gram-negative (*E. Coli*) and Gram-positive (*S. Aureus*) bacteria. Interestingly, the highest biocidal efficiency can be found for PIL brushes

Chapter I: *From Biocidal Polymers to Antibacterial Coatings*

containing either BF_4^- or PF_6^- as counter anions: it is suggested that these counter anions can undergo hydrolysis in water at room temperature, thus releasing fluoride in the environment.

Chen *et al.* have recently reported the synthesis of cross-linked polyurethanes films⁹⁷, containing copolymers of PEG and *N*-(4-hydroxy-3-methoxybenzyl)acrylamide. Such coatings have been tested on glass slides against *E. Coli* with an efficiency of 93% (compared to the blank glass surface). The PEG blocks would act as antifouling agent, while *N*-(4-hydroxy-3-methoxybenzyl)acrylamide block would kill bacteria. Films with increased *N*-(4-hydroxy-3-methoxybenzyl)acrylamide content (from 24 to 45 mol.%) have led to higher antibacterial activity (from 81 to 93 % antibacterial efficiency).

IV.2 Physically anchored coatings

While chemically anchored polymer coatings exhibit good antibacterial activity, the formation of the coating requires a multistep process, generally using several organic solvents. To avoid a costly and time-consuming process which can be difficult to implement in industrial settings, several groups have reported the use of physically anchored polymer coatings (usually *via* dip-coating, spin-coating or more rarely by electrospinning).

Chitosan in particular has been used for antibacterial coatings on textile fibers: Hassan has recently reported the antibacterial coating *via* ionic bonding of a modified poly(styrene sulfonate)-grafted wool fabric with chitosan containing poly[2-(acryloyloxy)ethyl]trimethylammonium chloride⁹⁸; Cheng *et al.* have observed the antibacterial coating of chitosan grafted with 1-Hydroxymethyl-5,5-dimethylhydantoin on cotton fabric⁹⁹ by a dip-coating process.

Layer-by-Layer assembly of chitosan and its derivatives with an anionic polymer has been widely reported¹⁰⁰. Hernandez-Montelongo *et al.* have very recently reported of the LbL assembly of chitosan with hyaluronan^{101, 102}.

Chapter I: *From Biocidal Polymers to Antibacterial Coatings*

Klibanov *et al.* have synthesized an alkylated PEI and have subsequently used it for physically-anchored coating of a glass slide¹⁰³ by a one-step dip-coating process of the substrate in the solution of PEI for one minute. However, the synthesis of the alkylated methylated PEI has necessitated a multi-step process at high temperature (95 °C). Furthermore, the authors have found that the bactericidal efficiency of the surface depends on the molar mass of the polymer: the higher the molar mass, the more efficient the coating. Additionally, the bactericidal efficiency of the ‘painted’ PEI decreases with each spraying of bacteria on the surface¹⁰⁴. However, this effect is reversible: washing the surface allows the bactericidal efficiency to come back to its initial level.

IV.3 Coatings comparison: antibacterial tests on a surface

Comparing the antibacterial activity of surfaces is more difficult than simply comparing the activity of the AB polymer in solution. Contrary to MIC assessment, there is a variety of qualitative and quantitative AB protocol method for the assessment of antibacterial surfaces, and not a single universal protocol method followed by all authors: several tests can be carried out, either qualitative or quantitative. In Table I-4 are inventoried the most usual antibacterial tests on a polymeric surface.

An easy way of comparing covalent and non-covalent coatings is to use the same polymers for both methods of deposition. For instance, Klibanov *et al.* have reported the covalent grafting and non-covalent deposition of an *N*-hexyl, *N*-methyl-PEI on glass slides^{45, 95, 105}. When the polymer is covalently bound to the surface, its bactericidal efficiency is $90 \pm 5\%$ against *S. Aureus*, and $96 \pm 2\%$ against *E. Coli*⁹⁵. On the other hand, when the polymer is only physically anchored to the surface, its bactericidal efficiency is of 100% against both bacteria¹⁰³.

Chapter I: *From Biocidal Polymers to Antibacterial Coatings*

Table I-4. Most usual antibacterial tests on a polymer coating.

Tests	Aim	Notes
Inhibition zone	Is any biocide released?	No use in the case of non-leaching coatings Hard to compare studies
In vitro adhesion test	Viable adherent fraction What is the efficiency of the antibacterial coating (compared to the pristine surface)?	Compares the number of living bacteria cells on the pristine surface and on the coated-one
Live/dead two colors fluorescence	Viability of the bacteria	
Shaking incubator	Is the coating preventing biofouling?	In aqueous conditions
Immersion test	Is the coating stable during immersion in water?	

In Table I-5 are summarized the main differences of the different types of antibacterial polymer coatings: passive/active coatings, physically/covalently anchored coatings.

On the one hand, while passive coatings may prevent biofouling on the surface, they do not inhibit the proliferation of bacteria in the immediate environment. On the other hand, while biocide-releasing coatings have been proven highly efficient antibacterial materials, they only work as long as the biocide is being released.

Unlike passive coatings, biocidal polymeric coatings kill the bacteria by contact, without releasing organic or inorganic biocides. Several coatings methods have been investigated, mainly chemically anchored coatings (*via* grafting from and grafting to methods), and physically anchored coatings (*via* spin- or dip-coating). Physically-anchored coatings do not usually require an activated substrate, unlike most chemically-anchored polymers. Thus, multi-steps processes necessitating high temperatures and/or organic solvents can be avoided.

Chapter I: *From Biocidal Polymers to Antibacterial Coatings*

Table I-5. Comparison of the different types of antibacterial polymeric coatings.

Passive coatings	Prevent the adhesion of the bacteria on the surface	Do not prevent the proliferation of bacteria in the environment
Biocide releasing coatings	Kill the bacteria in the environment	Problem of durability
Biocidal coatings	Kill the bacteria on contact only	Can be long-lasting, provided that biofilm formation is avoided
Physically anchored polymer	Dip-coating, spin-coating Layer-by-Layer	Polymer can be removed more easily Durability of the coating under usage?
Covalently anchored polymer	Grafting from, grafting to	Need multi-step process to activate the surface and polymerize the monomer or graft the polymer Generally use organic solvent(s)

Lately, dual-functional polymeric coatings have been reported^{31, 106, 107}. These coatings can thus present characteristics of more than one of the coatings represented in Figure I-1 and in Table I-5. It enables the surfaces to prevent bacterial adhesion and kill bacteria for instance, or to possess both leaching and non-leaching biocides³⁶.

IV.4 Antibacterial coatings on stainless steel surfaces

Recent studies pertaining to the antibacterial coating of stainless steel surfaces based on biocidal polymers are summarized hereafter (Table I-6). Biocide-releasing coatings for stainless steel will not be discussed here and are reported elsewhere^{31, 79, 108}.

While stainless steel has been widely used, its surface does not exhibit any antibacterial or antifouling activity. Thus, chemical modifications are needed to prevent the proliferation of bacteria on stainless steel surfaces. Interestingly, to insure long-lasting

Chapter I: From Biocidal Polymers to Antibacterial Coatings

property to the coating, most polymers used for this application are either grafted from or to the surface.

Table I-6. Biocidal polymers grafted or casted on stainless steel surfaces

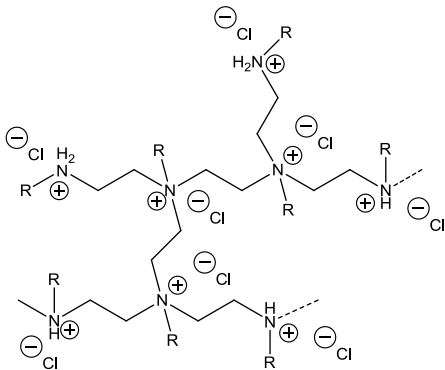
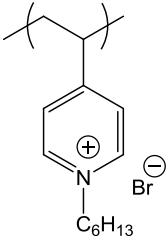
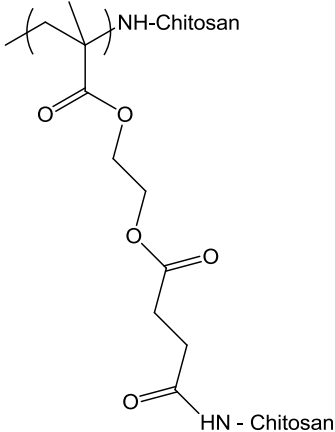
Polymer	Notes	Ref
<p>Hyperbranched PEI quaternized with 1-chlorooctane</p>  <p>with R = CH₃-(CH₂)₇</p>	<p>Grafted from (electrografting) or solvent casted</p> <p>Comparison of the two methods</p>	109
<p>Quaternized P(4VP)</p> 	<p>Grafting from (SI-ATRP)</p> <p>Coupled with TiO₂ (hybrid coating)</p>	110
<p>Chitosan grafted on modified PHEMA brushes</p> 	<p>Polymer brushes modified by the addition of succinid acid to allow the grafting</p> <p>Grafting with barnacle cement and dopamine</p>	111

Table I-6 continued p.36

Chapter I: From Biocidal Polymers to Antibacterial Coatings

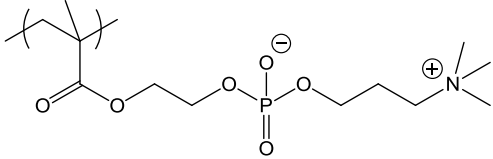
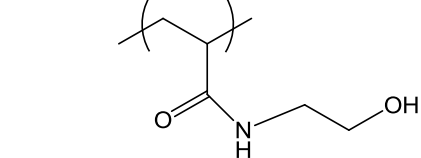
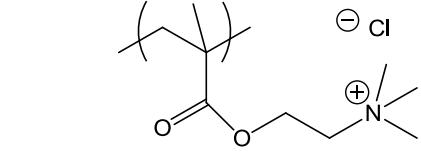
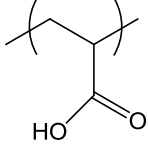
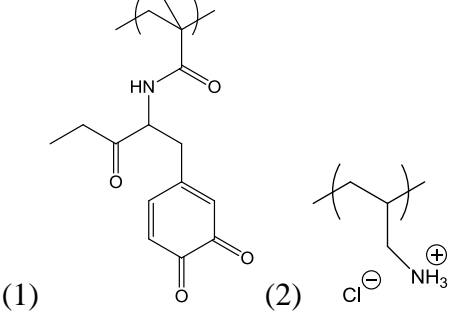
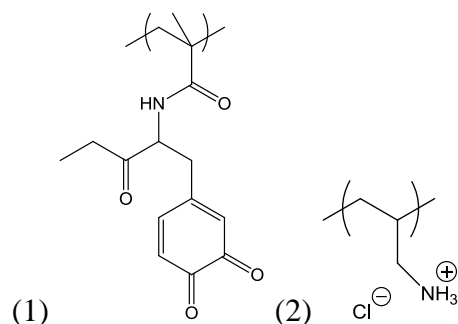
Zwitterionic PMPC	Grafted from (thiol-ene ¹¹² photopolymerization)
	
PHEAA	Grafted to (coupling of azide- ¹¹² functionalized PHEAA)
	
PMETA	Grafted to (coupling of alkyne- ¹¹² functionalized PMETA)
	
Poly(acrylic acid)/Nisin LbL coating	deposited via LbL dip-coating process. ¹¹³ Catechols ensure the adhesion of the coating to the stainless steel surface.
	
PMAox(1) / poly(allylamine) (2) / Nisin LbL coating	15 bilayers of (1)/(2), followed by 5 bilayers of (1)/(3). ¹¹⁴ PMAox stands for poly(methacrylamide), bearing oxidized 3,4-dihydroxyphenylalanine moieties. Shows good antibacterial activity after deposition of nisin. Antibacterial activity against <i>Bacillus Subtilis</i> is lost after immersion in water
	

Table I-6 continued p.37

PMAox (1) / poly(allylamine) (2) / Aqueous based process.

115

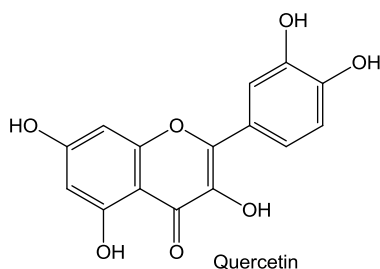
Trypsin LbL coating

Trypsin is a commercially available broad spectrum serine protease. Trypsin is either grafted on the LbL coating using the quinone functions contained in (1), or deposited on the LbL coating.

Quercetin-derivatives

Deposited on the surface

116



Versace *et al.* have described a green chemistry synthesis leading to quercetin-derivatives coatings on stainless steel. These dye-based coatings exhibit good antibacterial activity against *S. Aureus*¹¹⁶.

Ignatova *et al.* have demonstrated that solvent cast hyperbranched PEI could be peeled from stainless steel surface more easily than grafted-from and grafted-onto polymers¹⁰⁹. Stainless steel surfaces have first been electrografted with polyacrylates, the latter being used to covalently bond hyperbranched polymers containing either amines or halide groups. After the second layer has been quaternized, the antibacterial properties of the newly-coated stainless steel have been studied against *S. Aureus*.

Caro *et al.* have studied the grafting of PEG brushes and biocidal enzymes on preformed PEI-coated stainless steel surfaces, in order to enhance their antiadhesion activity⁹¹. PEI has been deposited on the surface, and PEG and enzymes have then been covalently bond to the PEI. PEG brushes have reduced protein adsorption by 97% and bacterial adhesion by 96% (tests effected against *L. ivanovii*), compared to the bare stainless

Chapter I: *From Biocidal Polymers to Antibacterial Coatings*

steel surface. Samples coated with biocidal enzymes have been proven to be highly antibacterial against Gram-positive bacteria (100% of biocidal efficiency)⁹¹. However, this remarkable activity requires a multi steps process to prepare the bare stainless steel, by using several organic solvents and toxic reagents such as sulfochromic acid.

Interestingly, Yuan *et al.* have demonstrated the antibacterial activity of a hybrid coating. Stainless steel surface has been first coated with multilayers nanostructured titanium oxide¹¹⁰. The TiO₂ surface has then been activated, and 4-vinylpyridine has been polymerized by surface initiated atom transfer radical polymerization (SI-ATRP). The subsequent poly(4-vinylpyridine) has been then quaternized with hexyl bromide forming a TiO₂-QPVP-coated surface. The TiO₂-coated and hybrid-coated surfaces have been further tested against Gram-negative *D. Desulfuricans* bacterium. Such multi-steps process is time-consuming, and, again, requires the use of organic solvents. The TiO₂-QPVP-coated surface inhibited almost completely any bacterial activity during 3 days of exposure. After 21 days of exposure, viable adherent fraction is 0.1% of the initial viable adherent fraction on pristine surface. Comparatively, Yuan *et al.* have also investigated the SI-ATRP of 2-dimethylamino-ethyl methacrylate (DMAEMA) on stainless steel¹¹⁷, and its antibacterial activity against *D. Desulfuricans*. SEM images have shown that such coating can prevent biocorrosion of stainless steel. The antibacterial properties have been enhanced further by coupling viologen on the PDMAEMA brushes.

Several processes involving both LbL deposition and grafting methods *via* catechols^{79, 114, 115, 118} have been reported. PDOPA bears 3,4-dihydroxyphenylalanine functions, which are a component of natural adhesives, found for example in mussels. These processes have been researched in order to prevent the use of toxic initiators and the massive use of organic solvents, towards a more sustainable method. For instance, Faure *et al.*⁷⁹ have investigated the use of catechols in LbL processes. Antibacterial peptides^{113, 114} silver nanoparticles⁷⁹, and

Chapter I: From Biocidal Polymers to Antibacterial Coatings

antibiofilm enzymes¹¹⁵ have been grafted on LbL coating. These antibacterial coatings have been synthesized in mild conditions (aqueous solutions, mild temperature). In particular, the authors have compared the antibacterial efficiency of enzyme-grafted and enzyme-deposited LbL coating¹¹⁵: while an enzyme-grafted LbL coating displays a reproducible antibacterial efficiency of $92\% \pm 4\%$, an enzyme-deposited LbL exhibit lower, not reproducible antibacterial efficiency ($58\% \pm 39\%$).

While Faure *et al.* have used preformed dopamine-functionalized polymers to anchor the antibacterial coating⁷⁹, Rittschof *et al.* have suggested another way to use these natural adhesives, to anchor an ATRP initiator to the stainless steel surface¹¹².

Rittschof *et al.* have used a grafting-from method to form zwitterionic polymer-brushes (poly(2-methacryloyloxyethyl phosphorylcholine), (PMPC)) on stainless steel *via* click chemistry reactions on ‘barnacle cement’¹¹². The same cement has been used on different surfaces, to graft preformed brushes of poly(*N*-hydroxyethyl acrylamide) (PHEAA) and poly(2-(methacryloyloxy)ethyltrimethyl ammonium chloride) (PMETA) by click-chemistry coupling. The three surfaces (zwitterionic, PHEAA, PMETA) have been then tested against *E. Coli* and *S. Epidermidis*. Surfaces have been observed *via* SEM, and viable adherent fractions have been calculated (Table I-7). Further investigations have also indicated that the grafted surfaces are stable and durable under various environments. The authors have also investigated the grafted-to of chitosan, using either barnacle cement or polydopamine¹¹¹.

Table I-7. Comparison of the viable adherent fractions on brushes-grafted stainless steel^{111, 112}

Bacteria	PMPC-coated	PHEAA-coated	PMETA-coated	Chitosan-coated
	BC ^a	BC ^a	BC ^a	PDOPA ^b
<i>E. Coli</i>	5%	7%	10%	17%
<i>S. Epidermidis</i>	10%	14%	16%	- ^c

^a Barnacle cement; ^b polydopamine ; ^c viable adherent fraction non studied for this coating.

Chapter I: *From Biocidal Polymers to Antibacterial Coatings*

Brushes of zwitterionic poly(sulfobetaine methacrylate) have been grafted from dopamine-anchored stainless steel surface *via* SI-ATRP by Chang *et al.*¹¹⁹. Such coatings have enabled to reduce the adherent population of bacteria (*E. Coli*) by 98% of reduction of bacterial adhesion against, and more than 99% for *S. Epidermidis*.

Antibacterial coatings on stainless steel have been mainly realized *via* grafting methods (grafting-to, grafting-from, or even LbL followed by the use of catechols). While these pathways allow for long-lasting antibacterial properties, the multi-step processes involved render them usually difficult to use in industrial settings. Nanogel syntheses have been hypothesized as a way to allow for long-lasting antibacterial coating while reducing the length of the processes. A first step in that direction has been realized by Faure *et al.*¹¹⁸: the authors have used Schiff base formation to cross-link preformed polymers of poly(allylamine) and poly(methacrylamide) bearing 3,4-dihydroxy-L-phenylalanine moieties, at pH 10. The resulting nanogels possess a diameter in the range of 20 to 30 nm. These nanogels have been deposited on stainless steel by a LbL process. Active molecules bearing thiols (*e.g.* DispersinB and PEG-SH) have then been grafted on top of the coating, to confer antiadhesion activity to the surface.

V. Outlook

Antibacterial polymeric coatings can be achieved by several methods of grafting and deposition. Both types of physically-anchored and covalently-bonded coatings exhibit antibacterial activity against Gram-positive and Gram-negative bacteria, depending on the nature of the polymer. The main biosourced and synthetic polymer-type used in coatings have been discussed, and compared *via* their MIC assessment. The principal advantages and disadvantages of these antibacterial coatings have been discussed in this introduction (in

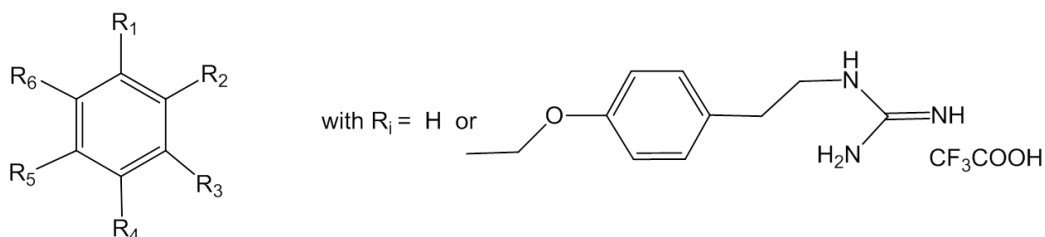
Chapter I: *From Biocidal Polymers to Antibacterial Coatings*

Table I-5). A special focus has been pointed on the different antibacterial coatings applied to stainless steel surfaces.

Interestingly, now that several 'core' families of biocidal polymer have been proven to exhibit good antibacterial activity (as is shown by their MIC in solution), research concerning antibacterial coatings have turned to long-lasting efficiency, and more sustainable methods, to avoid long and costly synthesis and coating processes. Several reports concerning either one aspect or the other have already been reviewed. However, relatively few deal with both longevity and environment-friendly methods.

What remains to be done in that area is a one-step synthesis, one-step coating process of a biocidal polymer, avoiding the use of organic solvents and high temperatures.

Supporting Information



Entry	Position of the arms (i)	MIC against <i>E. Coli</i> ($\mu\text{g/mL}$)	MIC against <i>S. Aureus</i> ($\mu\text{g/mL}$)
1	1	32	16
2	1, 2	8	<1
3	1, 3	16	2
4	1, 4	4	1
5	1, 3, 5	<1	<1
6	1, 3, 4, 6	4	<1
7	1, 2, 3, 4, 5, 6	16	8

Figure S I-1. Evolution of the MIC of a guanidine-containing compound with a benzene core, depending on the number and position of the guanidine ‘arms’.

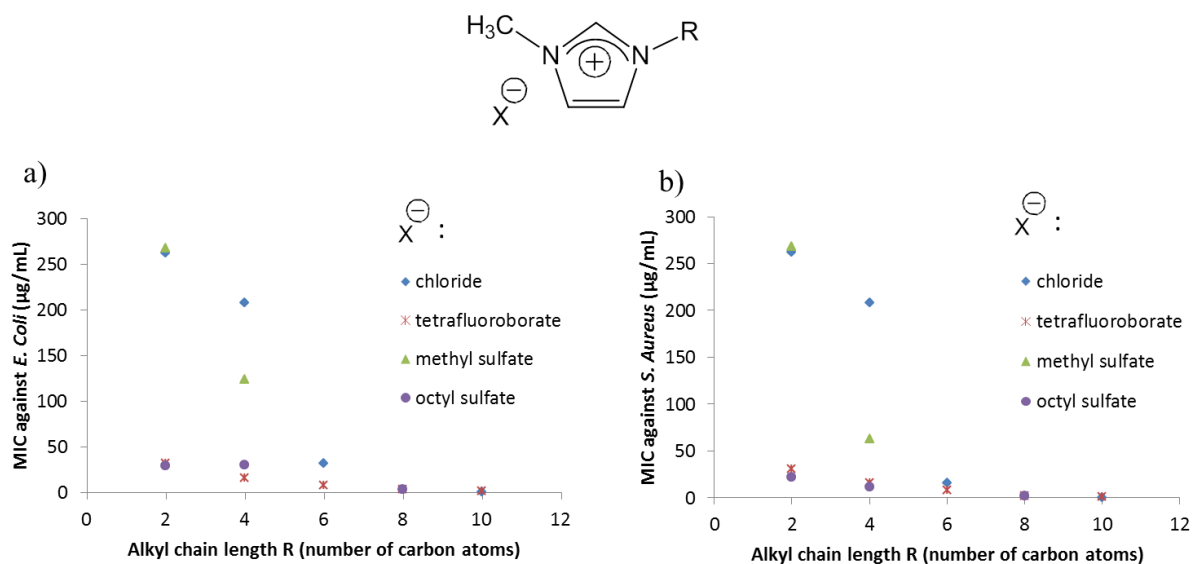


Figure S I-2. Influence of the alkyl chain length and the counter anion over the MIC values of methyl-imidazolium derivatives against: a) *E. Coli*; b) *S. Aureus*.⁴⁷

Chapter I: From Biocidal Polymers to Antibacterial Coatings

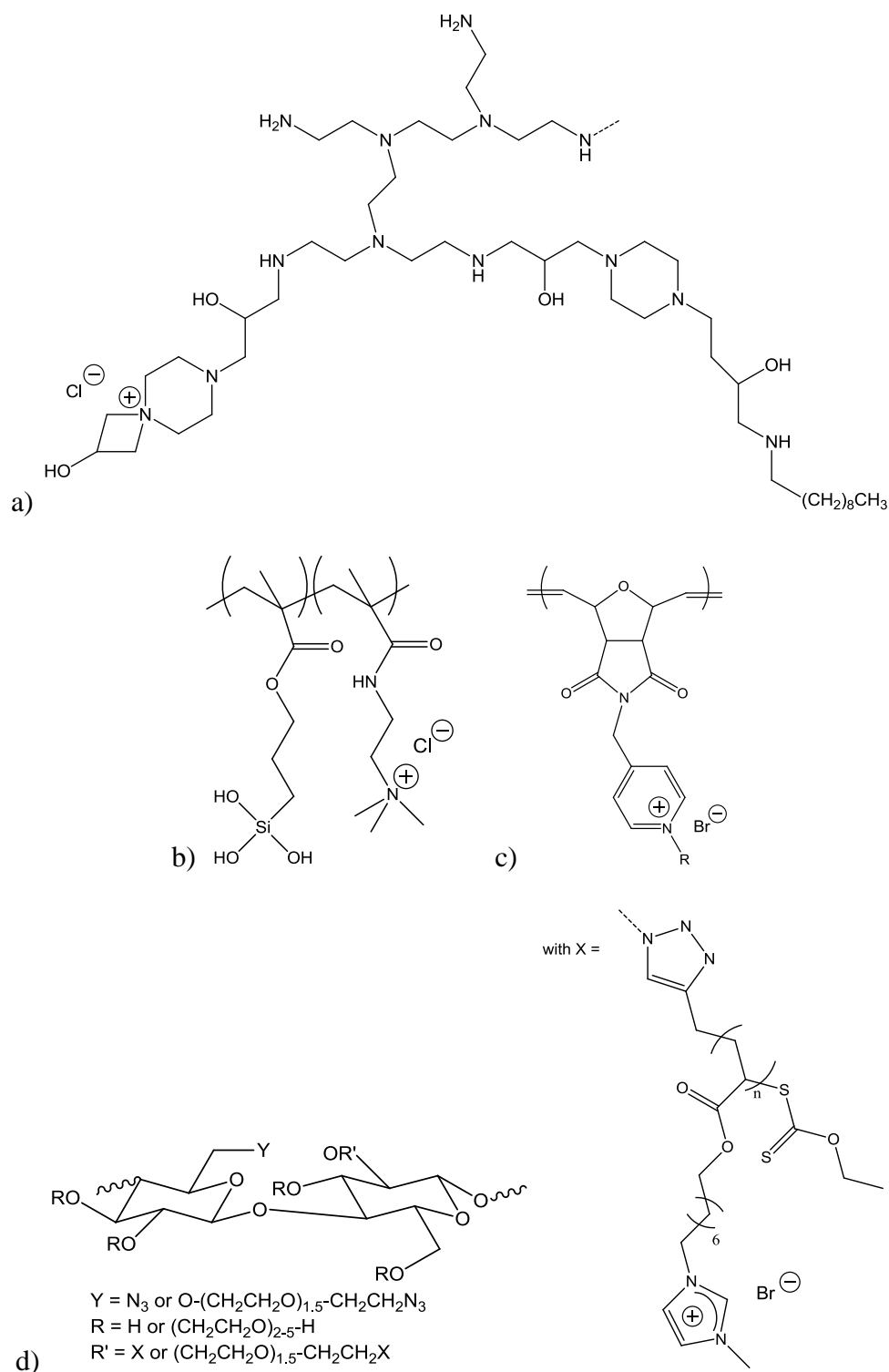


Figure S I-3. Schematic representation of: a) modified PEI after alkylation and cationic modification, to form physically cross-linked waterborne nanogels⁶⁸; b) quaternary ammonium silane copolymer⁷⁰; c) poly(norbornene) quaternized with pyridinium functions⁷² (R= ethyl, butyl, hexyl, octyl or decyl chains); d): graft cellulose-g-methacryloyl imidazolium-based copolymer⁷⁴.

References

1. B. Yin, T. Liu and Y. Yin, *Langmuir*, 2012, **28**, 17019-17025.
2. L. Ge, Q. Li, M. Wang, J. Ouyang, X. Li and M. M. Q. Xing, *International Journal of Nanomedicine*, 2014, **9**, 2399-2407.
3. C. Marambio-Jones and E. M. V. Hoek, *Journal of Nanoparticle Research*, 2010, **12**, 1531-1551.
4. T. Faunce and A. Watal, *Nanomedicine*, 2010, **5**, 617-632.
5. K. Glinel, P. Thebault, V. Humblot, C. M. Pradier and T. Jouenne, *Acta Biomaterialia*, 2012, **8**, 1670-1684.
6. X. Zhang, L. Wang and E. Levänen, *RSC Advances*, 2013, **3**, 12003-12020.
7. M. Spasova, N. Manolova, N. Markova and I. Rashkov, *Appl Surf Sci*, 2016, **363**, 363-371.
8. E.-R. Kenawy, S. D. Worley and R. Broughton, *Biomacromolecules*, 2007, **8**, 1359-1384.
9. A. Jain, L. S. Duvvuri, S. Farah, N. Beyth, A. J. Domb and W. Khan, *Advanced Healthcare Materials*, 2014, **3**, 1969-1985.
10. M. Kong, X. G. Chen, K. Xing and H. J. Park, *International Journal of Food Microbiology*, 2010, **144**, 51-63.
11. D. F. Kendra and L. A. Hadwiger, *Exp. Mycol.*, 1984, **8**, 276-281.
12. S. A. Onaizi and S. S. J. Leong, *Biotechnology Advances*, 2011, **29**, 67-74.
13. N. A. El-Sersy, A. E. Abdelwahab, S. S. Abouelkhiir, D. M. Abou-Zeid and S. A. Sabry, *J. Basic Microbiol.*, 2012, **52**, 513-522.
14. I. L. Shih, M. H. Shen and Y. T. Van, *Bioresour. Technol.*, 2006, **97**, 1148-1159.
15. E. I. Rabea, M. E. T. Badawy, C. V. Stevens, G. Smagghe and W. Steurbaut, *Biomacromolecules*, 2003, **4**, 1457-1465.
16. T. Takahashi, M. Imai, I. Suzuki and J. Sawai, *Biochemical Engineering Journal*, 2008, **40**, 485-491.
17. I. Younes, S. Sellimi, M. Rinaudo, K. Jellouli and M. Nasri, *International Journal of Food Microbiology*, 2014, **185**, 57-63.
18. H. Mellegård, S. P. Strand, B. E. Christensen, P. E. Granum and S. P. Hardy, *International Journal of Food Microbiology*, 2011, **148**, 48-54.

Chapter I: From Biocidal Polymers to Antibacterial Coatings

19. J. Duan, X. Liang, Y. Cao, S. Wang and L. Zhang, *Macromolecules*, 2015, **48**, 2706-2714.
20. W. Sajomsang, S. Tantayanon, V. Tangpasuthadol, M. Thatte and W. H. Daly, *International Journal of Biological Macromolecules*, 2008, **43**, 79-87.
21. W. Sajomsang, S. Tantayanon, V. Tangpasuthadol and W. H. Daly, *Carbohydrate Polymers*, 2008, **72**, 740-750.
22. H. Tan, R. Ma, C. Lin, Z. Liu and T. Tang, *International Journal of Molecular Sciences*, 2013, **14**, 1854-1869.
23. J. S. Rudra, K. Dave and D. T. Haynie, *J. Biomater. Sci. Polym. Ed.*, 2006, **17**, 1301-1315.
24. S. Shima, H. Matsuoka, T. Iwamoto and H. Sakai, *J. ANTIBIOT.*, 1984, **37**, 1449-1455.
25. M. Jäger, S. Schubert, S. Ochrimenko, D. Fischer and U. S. Schubert, *Chemical Society Reviews*, 2012, **41**, 4755-4767.
26. S. R. Williams and T. E. Long, *Progress in Polymer Science (Oxford)*, 2009, **34**, 762-782.
27. P. Feiertag, M. Albert, E. M. Ecker-Eckhofen, G. Hayn, H. Hönig, H. W. Oberwalder, R. Saf, A. Schmidt, O. Schmidt and D. Topchiev, *Macromolecular Rapid Communications*, 2003, **24**, 567-570.
28. P. Vakuliuk, A. Burban, V. Konovalova, M. Bryk, M. Vortman, N. Klymenko and V. Shevchenko, *Desalination*, 2009, **235**, 160-169.
29. J. Guo, Q. Xu, Z. Zheng, S. Zhou, H. Mao, B. Wang and F. Yan, *ACS Macro Letters*, 2015, 1094-1098.
30. A. Carmona-Ribeiro and L. de Melo Carrasco, *International Journal of Molecular Sciences*, 2013, **14**, 9906-9946.
31. A. Charlot, V. Sciannaméa, S. Lenoir, E. Faure, R. Jérôme, C. Jérôme, C. Van De Weerd, J. Martial, C. Archambeau, N. Willet, A. S. Duwez, C. A. Fustin and C. Detrembleur, *Journal of Materials Chemistry*, 2009, **19**, 4117-4125.
32. N. Pasquier, H. Keul, E. Heine, M. Moeller, B. Angelov, S. Linser and R. Willumeit, *Macromolecular Bioscience*, 2008, **8**, 903-915.
33. N. Beyth, Y. Hour-Haddad, L. Baraness-Hadar, I. Yudovin-Farber, A. J. Domb and E. I. Weiss, *Biomaterials*, 2008, **29**, 4157-4163.
34. N. Beyth, I. Yudovin-Farber, R. Bahir, A. J. Domb and E. I. Weiss, *Biomaterials*, 2006, **27**, 3995-4002.

Chapter I: From Biocidal Polymers to Antibacterial Coatings

35. N. M. Milović, J. Wang, K. Lewis and A. M. Klibanov, *Biotechnology and Bioengineering*, 2005, **90**, 715-722.
36. J. W. Xu, Y. Wang, Y. F. Yang, X. Y. Ye, K. Yao, J. Ji and Z. K. Xu, *Colloids and Surfaces B: Biointerfaces*, 2015, **133**, 148-155.
37. T. Cai, W. J. Yang, K. G. Neoh and E. T. Kang, *Industrial and Engineering Chemistry Research*, 2012, **51**, 15962-15973.
38. J. F. Madrid, M. Barsbay, L. Abad and O. Güven, *Radiat. Phys. Chem.*, 2016, **124**, 145-154.
39. B. Wang, T. Jin, Y. Han, C. Shen, Q. Li, J. Tang, H. Chen and Q. Lin, *Int. J. Polym. Mater. Polym. Biomater.*, 2016, **65**, 55-64.
40. H. Yu, Y. Fu, G. Li and Y. Liu, *Holzforschung*, 2013, **67**, 455-461.
41. Z. Dong, H. Wei, J. Mao, D. Wang, M. Yang, S. Bo and X. Ji, *Polymer*, 2012, **53**, 2074-2084.
42. M. Krishnamoorthy, S. Hakobyan, M. Ramstedt and J. E. Gautrot, *Chemical Reviews*, 2014, **114**, 10976-11026.
43. M. Álvarez-Paino, A. Muñoz-Bonilla, F. López-Fabal, J. L. Gómez-Garcés, J. P. A. Heuts and M. Fernández-García, *Biomacromolecules*, 2015, **16**, 295-303.
44. V. Sambhy, B. R. Peterson and A. Sen, *Angewandte Chemie - International Edition*, 2008, **47**, 1250-1254.
45. J. C. Tiller, S. B. Lee, K. Lewis and A. M. Klibanov, *Biotechnology and Bioengineering*, 2002, **79**, 465-471.
46. J. C. Tiller, C. J. Liao, K. Lewis and A. M. Klibanov, *Proceedings of the National Academy of Sciences of the United States of America*, 2001, **98**, 5981-5985.
47. J. Łuczak, C. Jungnickel, I. Łcka, S. Stolte and J. Hupka, *Green Chemistry*, 2010, **12**, 593-601.
48. V. Piazza, I. Dragić, K. Sepečić, M. Faimali, F. Garaventa, T. Turk and S. Berne, *Mar. Drugs*, 2014, **12**, 1959-1976.
49. S. K. Sharma, G. S. Chauhan, R. Gupta and J. H. Ahn, *J. Mater. Sci. Mater. Med.*, 2010, **21**, 717-724.
50. B. Gao, S. He, J. Guo and R. Wang, *Journal of Applied Polymer Science*, 2006, **100**, 1531-1537.
51. P. H. Sellenet, B. Allison, B. M. Applegate and J. P. Youngblood, *Biomacromolecules*, 2007, **8**, 19-23.

Chapter I: *From Biocidal Polymers to Antibacterial Coatings*

52. R. Yamashita, Y. Takeuchi, H. Kikuchi, K. Shirai, T. Yamauchi and N. Tsubokawa, *Polymer Journal*, 2006, **38**, 844-851.
53. G. Garg, G. S. Chauhan, R. Gupta and J. H. Ahn, *Journal of Colloid and Interface Science*, 2010, **344**, 90-96.
54. A. Rembaum, *Appl Polym Symp*, 1973, 299-317.
55. C. Mattheis, M. Zheng and S. Agarwal, *Macromolecular Bioscience*, 2012, **12**, 341-349.
56. M. Albert, P. Feiertag, G. Hayn, R. Saf and H. Hönig, *Biomacromolecules*, 2003, **4**, 1811-1817.
57. H. Massimba Dibama, M. Mourer, R. E. Duval and J. B. Regnouf-De-Vains, *Bioorganic and Medicinal Chemistry Letters*, 2014, **24**, 4791-4793.
58. S. Sun, Q. An, X. Li, L. Qian, B. He and H. Xiao, *Bioresour. Technol.*, 2010, **101**, 5693-5700.
59. H. Wang, C. V. Synatschke, A. Raup, V. Jérôme, R. Freitag and S. Agarwal, *Polymer Chemistry*, 2014, **5**, 2453-2460.
60. O. Aviv, S. Ratner, N. Amir, N. Laout, A. Basu, H. Shadmon, N. Beyth and A. J. Domb, *Polymers for Advanced Technologies*, 2016.
61. R. Konradi, C. Acikgoz and M. Textor, *Macromolecular Rapid Communications*, 2012, **33**, 1663-1676.
62. C. J. Waschinski and J. C. Tiller, *Biomacromolecules*, 2005, **6**, 235-243.
63. Z. X. Zhou, D. F. Wei, Y. Guan, A. N. Zheng and J. J. Zhong, *Journal of Applied Microbiology*, 2010, **108**, 898-907.
64. D. Raafat, K. Von Bargaen, A. Haas and H. G. Sahl, *Applied and Environmental Microbiology*, 2008, **74**, 3764-3773.
65. L. Qi, Z. Xu, X. Jiang, C. Hu and X. Zou, *Carbohydrate Research*, 2004, **339**, 2693-2700.
66. X. F. Liu, Y. L. Guan, D. Z. Yang, Z. Li and K. D. Yao, *Journal of Applied Polymer Science*, 2001, **79**, 1324-1335.
67. L. Bromberg and T. A. Hatton, *Polymer*, 2007, **48**, 7490-7498.
68. S. Chattopadhyay, E. Heine, A. Mourran, W. Richtering, H. Keul and M. Möller, *Polymer Chemistry*, 2016, **7**, 364-369.
69. L. A. B. Rawlinson, S. M. Ryan, G. Mantovani, J. A. Syrett, D. M. Haddleton and D. J. Brayden, *Biomacromolecules*, 2010, **11**, 443-453.

Chapter I: From Biocidal Polymers to Antibacterial Coatings

70. H. Li, H. Bao, K. X. Bok, C. Y. Lee, B. Li, M. T. Zin and L. Kang, *Biomaterials Science*, 2016, **4**, 299-309.
71. Z. X. Voo, M. Khan, Q. Xu, K. Narayanan, B. W. J. Ng, R. Bte Ahmad, J. L. Hedrick and Y. Y. Yang, *Polymer Chemistry*, 2016, **7**, 656-668.
72. T. Eren, A. Som, J. R. Rennie, C. F. Nelson, Y. Urgina, K. Nüsslein, E. B. Coughlin and G. N. Tew, *Macromolecular Chemistry and Physics*, 2008, **209**, 516-524.
73. A. Zovko, M. Vaukner Gabrič, K. Sepčić, F. Pohleven, D. Jaklič, N. Gunde-Cimerman, Z. Lu, R. Edrada-Ebel, W. E. Houssen, I. Mancini, A. Defant, M. Jaspars and T. Turk, *Int. Biodeterior. Biodegrad.*, 2012, **68**, 71-77.
74. F. Joubert, R. P. Yeo, G. J. Sharples, O. M. Musa, D. R. W. Hodgson and N. R. Cameron, *Biomacromolecules*, 2015, **16**, 3970-3979.
75. F. Siedenbiedel and J. C. Tiller, *Polymers*, 2012, **4**, 46-71.
76. A. Muñoz-Bonilla and M. Fernández-García, *Progress in Polymer Science*, 2012, **37**, 281-339.
77. H. Otsuka, Y. Nagasaki and K. Kataoka, *Current Opinion in Colloid and Interface Science*, 2001, **6**, 3-10.
78. I. Banerjee, R. C. Pangule and R. S. Kane, *Advanced Materials*, 2011, **23**, 690-718.
79. C. Falentin-Daudré, E. Faure, T. Svaldo-Lanero, F. Farina, C. Jérôme, C. Van De Weerd, J. Martial, A. S. Duwez and C. Detrembleur, *Langmuir*, 2012, **28**, 7233-7241.
80. J. K. Oh, R. Drumright, D. J. Siegwart and K. Matyjaszewski, *Progress in Polymer Science (Oxford)*, 2008, **33**, 448-477.
81. V. K. Sharma, R. A. Yngard and Y. Lin, *Advances in Colloid and Interface Science*, 2009, **145**, 83-96.
82. Q. Ye, T. Gao, F. Wan, B. Yu, X. Pei, F. Zhou and Q. Xue, *Journal of Materials Chemistry*, 2012, **22**, 13123-13131.
83. S. Pavlukhina and S. Sukhishvili, *Advanced Drug Delivery Reviews*, 2011, **63**, 822-836.
84. W. J. Yang, D. Pranantyo, K. G. Neoh, E. T. Kang, S. L. M. Teo and D. Rittschof, *Biomacromolecules*, 2012, **13**, 2769-2780.
85. D. E. Fullenkamp, J. G. Rivera, Y. K. Gong, K. H. A. Lau, L. He, R. Varshney and P. B. Messersmith, *Biomaterials*, 2012, **33**, 3783-3791.
86. J. Song, H. Kang, C. Lee, S. H. Hwang and J. Jang, *ACS Applied Materials & Interfaces*, 2012, **4**, 460-465.

Chapter I: From Biocidal Polymers to Antibacterial Coatings

87. H. Han, J. Wu, C. W. Avery, M. Mizutani, X. Jiang, M. Kamigaito, Z. Chen, C. Xi and K. Kuroda, *Langmuir*, 2011, **27**, 4010-4019.
88. K. Glinel, A. M. Jonas, T. Jouenne, J. Leprince, L. Galas and W. T. S. Huck, *Bioconjugate Chemistry*, 2009, **20**, 71-77.
89. C. J. Fristrup, K. Jankova and S. Hvilsted, *Soft Matter*, 2009, **5**, 4623-4634.
90. D. G. Yu, J. Zhou, N. P. Chatterton, Y. Li, J. Huang and X. Wang, *International Journal of Nanomedicine*, 2012, **7**, 5725-5732.
91. A. Caro, V. Humblot, C. Méthivier, M. Minier, M. Salmain and C. M. Pradier, *Journal of Physical Chemistry B*, 2009, **113**, 2101-2109.
92. A. Héquet, V. Humblot, J. M. Berjeaud and C. M. Pradier, *Colloids and Surfaces B: Biointerfaces*, 2011, **84**, 301-309.
93. S. Yuan, J. Yin, W. Jiang, B. Liang, S. O. Pehkonen and C. Choong, *Colloids and Surfaces B: Biointerfaces*, 2013, **106**, 11-21.
94. E. Stoleru, R. P. Dumitriu, B. S. Munteanu, T. Zaharescu, E. E. Tănase, A. Mitelut, G. L. Ailiesei and C. Vasile, *Appl Surf Sci*, 2016, **367**, 407-417.
95. J. Lin, S. Qiu, K. Lewis and A. M. Klibanov, *Biotechnology Progress*, 2002, **18**, 1082-1086.
96. L. A. T. W. Asri, M. Crismaru, S. Roest, Y. Chen, O. Ivashenko, P. Rudolf, J. C. Tiller, H. C. van der Mei, T. J. A. Loontjens and H. J. Busscher, *Advanced Functional Materials*, 2014, **24**, 346-355.
97. X. Chen, G. Zhang, Q. Zhang, X. Zhan and F. Chen, *Industrial and Engineering Chemistry Research*, 2015, **54**, 3813-3820.
98. M. M. Hassan, *RSC Advances*, 2015, **5**, 35497-35505.
99. X. Cheng, K. Ma, R. Li, X. Ren and T. S. Huang, *Appl Surf Sci*, 2014, **309**, 138-143.
100. X. Zhu and X. Jun Loh, *Biomaterials Science*, 2015, **3**, 1505-1518.
101. J. Hernandez-Montelongo, E. G. Lucchesi, I. Gonzalez, W. A. A. Macedo, V. F. Nascimento, A. M. Moraes, M. M. Beppu and M. A. Cotta, *Colloids and Surfaces B: Biointerfaces*, 2016, **141**, 499-506.
102. J. Hernández-Montelongo, V. F. Nascimento, D. Murillo, T. B. Taketa, P. Sahoo, A. A. De Souza, M. M. Beppu and M. A. Cotta, *Carbohydrate Polymers*, 2016, **136**, 1-11.
103. D. Park, J. Wang and A. M. Klibanov, *Biotechnology Progress*, 2006, **22**, 584-589.
104. K. Mukherjee, J. J. Rivera and A. M. Klibanov, *Appl. Biochem. Biotechnol.*, 2008, **151**, 61-70.

Chapter I: *From Biocidal Polymers to Antibacterial Coatings*

105. J. Lin, S. Qiu, K. Lewis and A. M. Klibanov, *Biotechnology and Bioengineering*, 2003, **83**, 168-172.
106. L. Moroni, M. Klein Gunnewiek and E. M. Benetti, *Acta Biomaterialia*, 2014, **10**, 2367-2378.
107. Q. Yu, Z. Wu and H. Chen, *Acta Biomaterialia*, 2015, **16**, 1-13.
108. K. Vasilev, J. Cook and H. J. Griesser, *Expert Review of Medical Devices*, 2009, **6**, 553-567.
109. M. Ignatova, S. Voccia, S. Gabriel, B. Gilbert, D. Cossement, R. Jérôme and C. Jérôme, *Langmuir*, 2009, **25**, 891-902.
110. S. J. Yuan, S. O. Pehkonen, Y. P. Ting, K. G. Neoh and E. T. Kang, *ACS Applied Materials and Interfaces*, 2009, **1**, 640-652.
111. W. J. Yang, T. Cai, K. G. Neoh, E. T. Kang, G. H. Dickinson, S. L. M. Teo and D. Rittschof, *Langmuir*, 2011, **27**, 7065-7076.
112. W. J. Yang, T. Cai, K. G. Neoh, E. T. Kang, S. L. M. Teo and D. Rittschof, *Biomacromolecules*, 2013, **14**, 2041-2051.
113. C. Vreuls, G. Zocchi, H. Vandegaart, E. Faure, C. Detrembleur, A. S. Duwez, J. Martial and C. Van De Weerd, *Biofouling*, 2012, **28**, 395-404.
114. E. Faure, P. Lecomte, S. Lenoir, C. Vreuls, C. Van De Weerd, C. Archambeau, J. Martial, C. Jérôme, A. S. Duwez and C. Detrembleur, *Journal of Materials Chemistry*, 2011, **21**, 7901-7904.
115. E. Faure, C. Vreuls, C. Falentin-Daudré, G. Zocchi, C. van de Weerd, J. Martial, C. Jérôme, A. S. Duwez and C. Detrembleur, *Biofouling*, 2012, **28**, 719-728.
116. M. Condat, J. Babinot, S. Tomane, J. P. Malval, I. K. Kang, F. Spillebout, P. E. Mazeran, J. Lalevée, S. A. Andalloussi and D. L. Versace, *RSC Advances*, 2016, **6**, 18235-18245.
117. S. J. Yuan, F. J. Xu, S. O. Pehkonen, Y. P. Ting, K. G. Neoh and E. T. Kang, *Biotechnology and Bioengineering*, 2009, **103**, 268-281.
118. E. Faure, C. Falentin-Daudré, T. S. Lanero, C. Vreuls, G. Zocchi, C. Van De Weerd, J. Martial, C. Jérôme, A. S. Duwez and C. Detrembleur, *Advanced Functional Materials*, 2012, **22**, 5271-5282.
119. J. M. Thomassin, C. Jérôme, T. Pardoën, C. Bailly, I. Huynen and C. Detrembleur, *Materials Science and Engineering R: Reports*, 2013, **74**, 211-232.

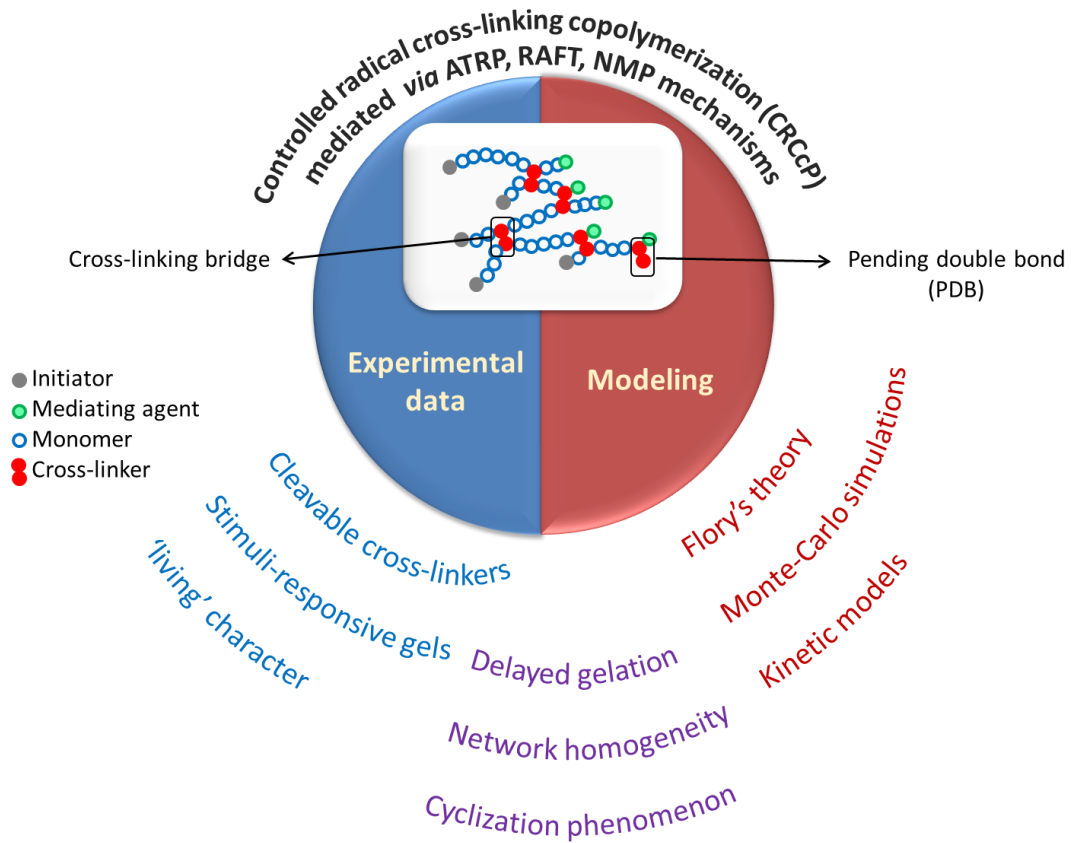
Chapter II

Recent Advances in Controlled Radical Cross-linking Copolymerization (CRCcP): Experimental and Theoretical Investigations

Abstract

This bibliographic chapter inventories recent developments in the field of controlled radical cross-linking copolymerization (CRCcP) involving a monovinyl monomer and a divinyl co-monomer serving as a cross-linker, forming chemically cross-linked networks of controlled kinetic chain length. Both developments in modeling CRCcPs and recent experimental data are presented. The three main mechanisms of controlled radical cross-linking copolymerization include nitroxide-mediated polymerization (NMP), atom-transfer radical polymerization (ATRP) and reversible addition-fragmentation chain transfer (RAFT) polymerization methods. In certain conditions, CRCcP can lead to so-called polymeric (nano)gels that are soluble materials of submicron size range with an internally cross-linked structure. Modeling approaches, such as stochastic, deterministic and computational simulations, allowing for a thorough description of both the CRCcP process and the as-formed nano-, micro- or macrogels are also compared.

Graphical abstract



**Recent Advances in Controlled Radical Cross-linking Copolymerization (CRCcP):
Experimental and Theoretical Investigations**

I. Introduction and scope of the review

I.1 Introduction

I.2 Scope of the review

I.3 Definitions and vocabulary

II. Recent advances in the synthesis of (nano)gels via CRCcP

II.1 CRCcP leading to the formation of nano-, micro- or macroscopic polymeric networks

II.2 From cleavable cross-linkers to labile arms

II.3 How to further delay gelation?

II.4 Homogeneity of the network: swelling ratio and moduli

II.5 Monitoring the cyclization phenomenon *via* NMR spectroscopy

II.6 Stimuli-responsive (nano)gels

II.7 Functionalizing, extending and coupling: taking advantage of the ‘living’ character of CRCcP

II.7.1 Chain extensions

II.7.2 Coupling and functionalization

III. Modeling of controlled radical cross-linking copolymerization

III.1 The model of Flory and Stockmayer (FS), and their derivatives

III.2 Kinetic models

III.2.1 Mono- or multi-radical assumptions

III.2.2 Cyclization

III.2.3 Modeling CRCcP of vinyl/divinyl systems

III.3 Computational simulations in space

III.3.1 Monte-Carlo simulations

III.3.2 Dynamic Lattice Liquid: cooperative motion concept

III.3.3 Comparison of the stochastic models

III.3.4 Comparison with the FS model

III.4 Case study of CRCcP modeling: styrene/divinylbenzene.

IV. Conclusions

I. Introduction and scope of the review

I.1 Introduction

This chapter focuses on the use of controlled radical polymerization in the context of cross-linking copolymerization, involving a monovinyl monomer and a divinyl co-monomer as a cross-linker. This synthetic access to soluble or insoluble polymers exhibiting a three-dimensional internal structure is referred to as the controlled radical cross-linking copolymerization and will be abbreviated as CRCcP. The main factors influencing the structural features of as-formed polymers include the type of polymerization mechanism, *i.e.* the nature of the mediating/controlling agent employed, and obviously the initial experimental conditions selected (mostly, temperature, concentration in co-monomers, and reaction time). Differences in the overall structure of the network grown by CRCcP will be discussed in comparison to networks prepared by the more conventional free-radical cross-linking copolymerization, abbreviated as FRCcP.

Polymerizing multifunctional (co)monomers is of great importance in polymer chemistry, for it opens an easy way to branched (co)polymers. Copolymerization of a monomer and a cross-linker most often occurs either by FRCcP. In the past decade, however, CRCcP has been reported as a versatile method to achieve gel-like structures (nano-, micro and macrogels) with an expectedly different internal structure to materials obtained by FRCcP. In the latter case, initiation stage is generally slow, in contrast to both propagation and termination reactions. The different synthetic methods to nano-, micro- or macrogels by FRCcP is out of the scope of this thesis chapter; interested readers are referred to general reviews or book chapters on that topic¹⁻³.

In a CRCcP process, all polymer chains are supposedly initiated at the same time, an equilibrium being reached between growing polymer chains and dormant ones (*i.e.* polymer chains capped by the controlling agent), with the occurrence of termination reactions being significantly minimized. Key differences between FRCcP and CRCcP mechanisms were first discussed by Ide and Fukuda (Figure II-1), and used liberally afterwards.

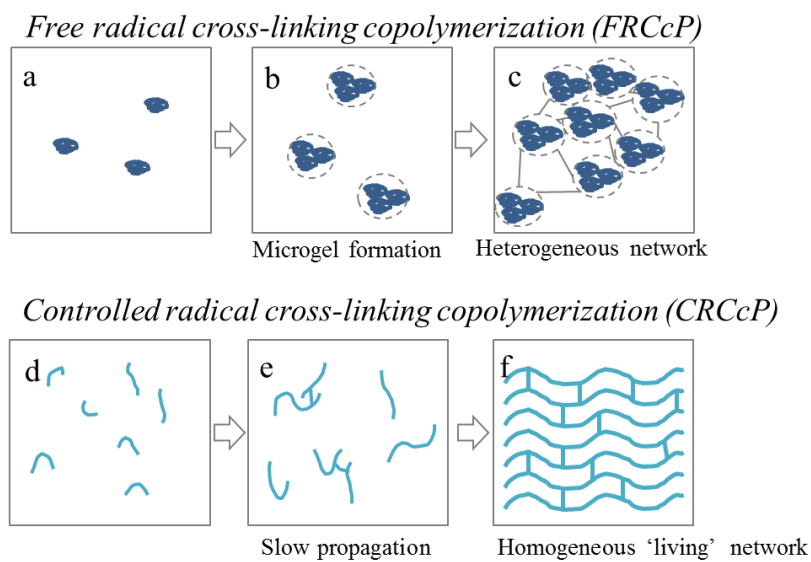
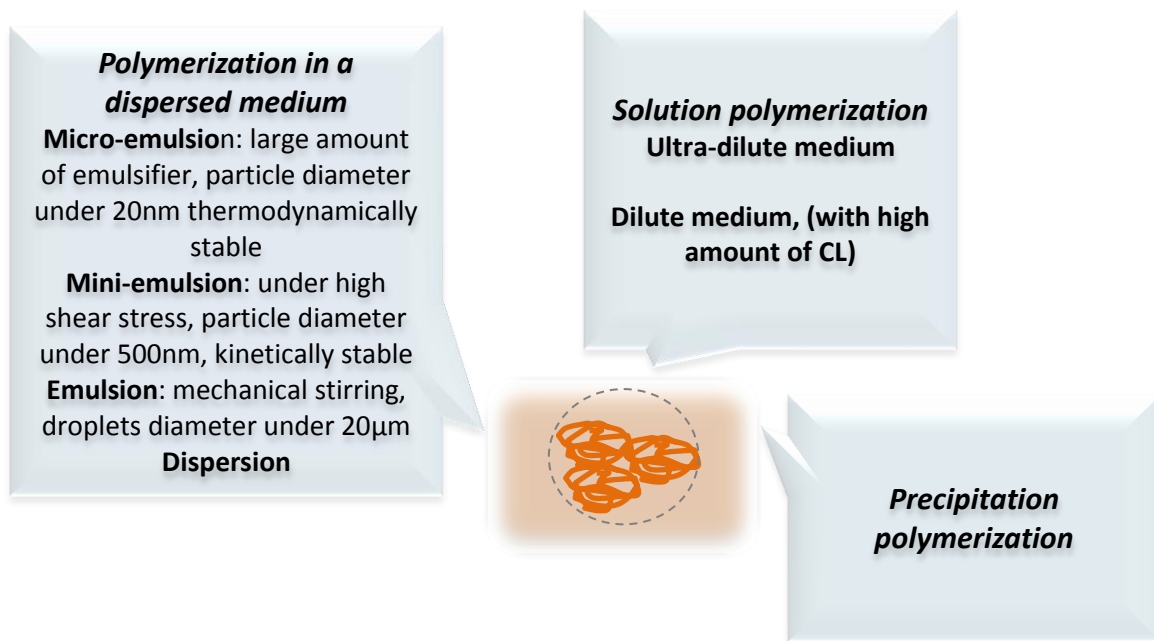


Figure II-1. Schematic representation of the cross-linking copolymerization of a vinyl monomer and a divinyl cross-linker by FRCcP (a, b and c), and by CRCcP (d, e and f), inspired by Ide and Fukuda⁴.

Depending on the initial polymerization conditions, (*i.e.* the presence of a controlling agent, the amount of cross-linker), either an insoluble macrogel or a soluble nanogel or microgel is obtained. IUPAC defines a (polymeric) nanogel as a soluble cross-linked polymer network with a dimension under 100 nm (respectively a microgel for dimensions under 1 μm) or a macrogel, a 3D-network with macroscopic dimensions⁵. Common synthetic methods to obtain nanogels include: i) the post-cross-linking of pre-formed linear polymers, *e.g.* by chemical post-modification of polymer precursors possessing pendant reactive groups, or by

radiation with a high energy source^{6, 7}, and ii) the FRCcP in dispersed media or in highly dilute solution^{3, 8, 9} (see Scheme II-1).

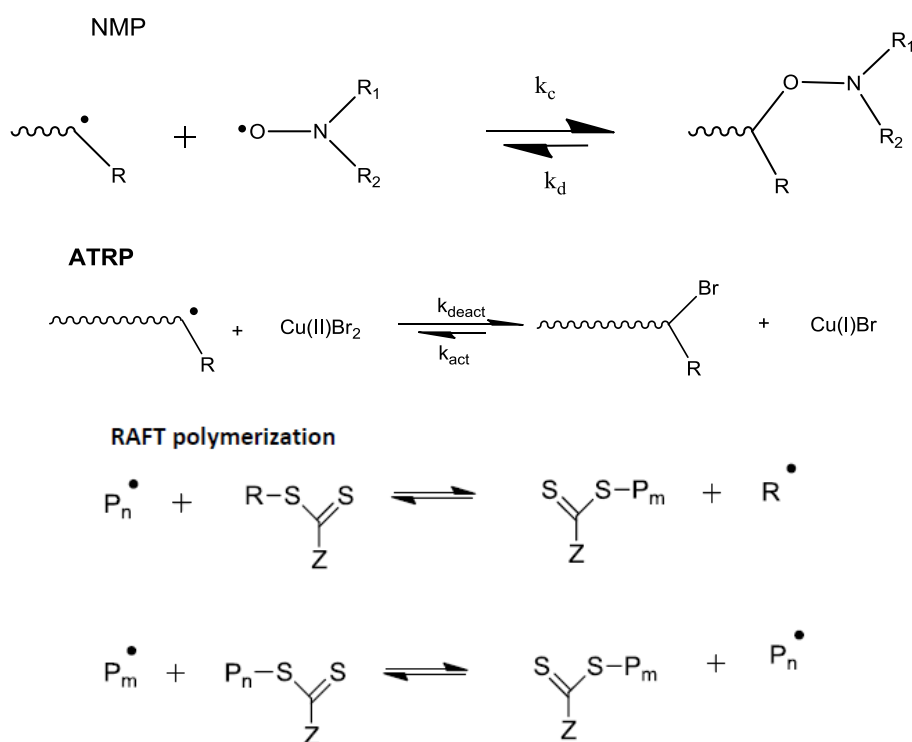


Scheme II-1. Strategies to synthesize nano/microgels *via* free radical cross-linking copolymerization (FRCcP), either in dilute to highly dilute media¹⁰, or in confined media^{11, 12}.

Polymer nanogels made by FRCcP have garnered a significant amount of publications in the past decade, mainly for a potential use in drug delivery¹³⁻¹⁶ and coating^{7, 17, 18} applications. Various properties are targeted for these engineered nanosized compounds, including biodegradability and stealth effect *in vivo* for drug carriers, non-toxicity to eukaryote cells of both the parent nanogel and its biodegraded fractions, stimuli-responsiveness leading to the loading and release of the drugs, and antibacterial or anti-fungi activity for coatings^{7, 19-21}. More specific uses have been also described, for instance, as shuttles between two immiscible phases²² (an aqueous phase and a hydrophobic ionic liquid), or as stabilizers of Pickering emulsions, or as structuring components of porous patterned

coatings¹⁸. This large area of utilizations has led to the synthetic developments of a wide range of nanogels, in particular, hydrophilic compounds.

CRCcP processes have also been developed as a possible means to achieve nano-, micro or macrogels with a more homogeneous internal structure, permitting not only to delay the macrogelation, but also to achieve control over the constitutive chain lengths within the gels. Last but not least, polymer chain-ends can be reactivated in CRCcP-derived gels, chain extension allowing for the synthesis of core-shell architectures. Reported examples of CRCcP will be summarized in this section, and include nitroxide-mediated polymerization (NMP)^{23, 24}, atom-transfer radical polymerization (ATRP)^{25, 26}, and reversible addition-fragmentation chain transfer polymerization (RAFT)²⁷. Each of these methods is schematically summarized below.



Scheme II-2. Mechanisms of NMP, ATRP and RAFT polymerizations^{8, 28-30}.

I.2 Scope of the review

Recent developments in the field CRcCP involving one monovalent monomer with one divalent cross-linker, both from the experimental and modeling viewpoints, will be presented in this chapter. Other synthetic strategies to form polymeric networks or branched architectures, such as dendrimers^{31, 32}, star copolymers^{33, 34}, cross-linked micelles³⁵⁻³⁸ or post-polymerization cross-linking^{27, 39}, will not be covered here. However, a few examples of nano- or microgels obtained *via* the copolymerization of a monovinyl monomer with a divinyl cross-linker using macro-initiator (or macro-CTA in the case of RAFT-mediated polymerizations) will be discussed, as the synthetic process is at the edge of the scope. Recent advances in the “controlled” synthesis of nanogels will be discussed first, though related structures such as micro- and macroscopic networks synthesized *via* CRcCP will be also considered, because the latter structures share some common features, *e.g.* a similar internal structure and, expectedly, a controlled kinetic chain length. Computational investigations aimed, in particular, at differentiating FRCcP and CRcCP processes and at describing the overall structures of CRcCP-derived gels, will be the topic of the second part of this chapter.

I.3 Definitions and vocabulary.

A *monomer* refers to a monovinyl molecule, while a *cross-linker* is a divinyl molecule. The most commonly cross-linkers used are listed in Figure II-4. A *pending double bond (PDB)* is formed when the first double bond of a cross-linker is incorporated in a growing polymer chain, while the second double bond of the molecule remains unreacted (see Scheme II-2). This PDB can be further incorporated to another growing polymer chain, or react with the radical center of its own polymer chain. In the former case, it results in a so-called *intermolecular branching*, or inter-molecular cross-linking. This is the main cause of the molecular weight increase. In the latter case, it forms a ‘loop’ in the network’, and is

referred to as a *cyclization*, or *intramolecular cross-linking* (Figure II-2). Note that cyclizations do not increase the molecular weight, but contributes to the increase in compacity of the final network *via* the formation of loops. A cross-linker thus incorporated generates a *cross-linking bridge* (or *cross-linkage*), between two *primary chains*.

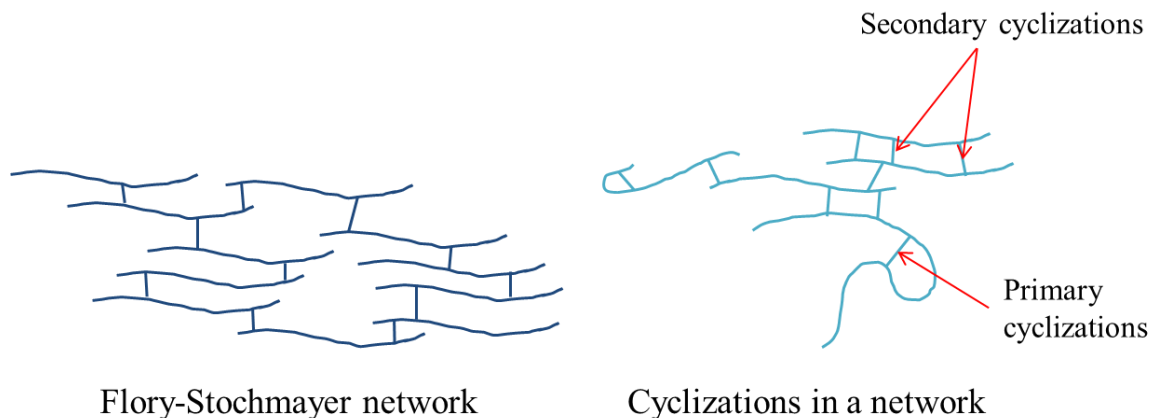
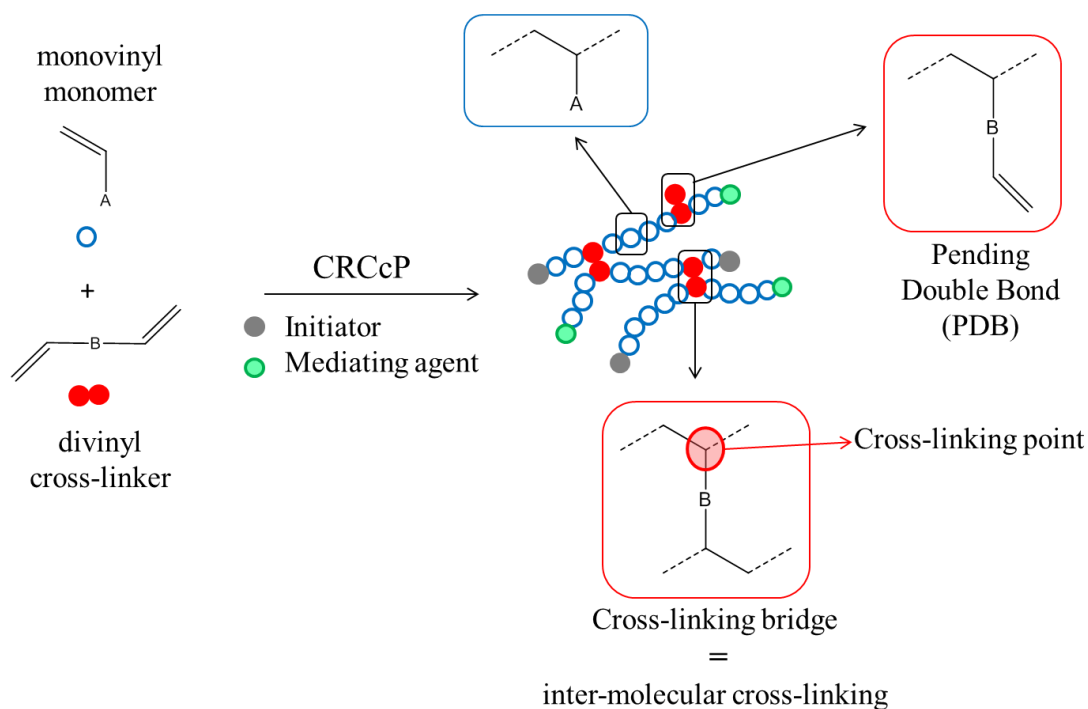


Figure II-2. Network representations: “classical” (on the left, no cyclization), and including cyclization (on the right)⁴⁰.

IUPAC defines gelation as the ‘*process of passing through gel point to form a gel, or network*’⁴¹. As for the gel point, it is defined as the ‘*point of incipient network formation in a process of forming a chemical or physical network*’⁴².

Gelation usually occurs when all values of the molar masses of the growing polymer chains (except the highest one) face a maximum (peak value). Prior to the gelation point, the branched chains are separated, and after the gel point, the polymeric material contains a single macromolecule forming the gelled network, and a decreasing population of smaller molar masses. The gelation phenomenon has been extensively studied, both from modeling and experimental viewpoints. Its occurrence in a given experiment can be predicted theoretically based on computations studies.

Finally, a *nanogel*, according to IUPAC, is a soluble polymeric network with a dimension lower than 100 nm⁵.



Scheme II-3. Schematic representation of the mechanism in a controlled radical cross-linking copolymerization (CRCcP) of a vinyl monomer with a divinyl cross-linker, resulting in the formation of a polymeric network.

The figure II-3 below shows the domain of nanogel formation (as opposed to either linear polymer or macrogel), as well as the influence of the initial monomer concentration. It highlights the fact that nanogels can be obtained by CRccP in homogeneous medium, under a very narrow window of experimental conditions only. For a concentration in cross-linker too low, the resulting copolymer exhibits a poor cross-linking density with lots of PDB's. For higher concentrations in cross-linker, the resulting polymeric network is no longer of nanometric dimensions if it is not a macrogel. In this regard, modeling allows for a better understanding of the nanogel structure and can also help to define the 'border conditions' of synthesis⁴³.

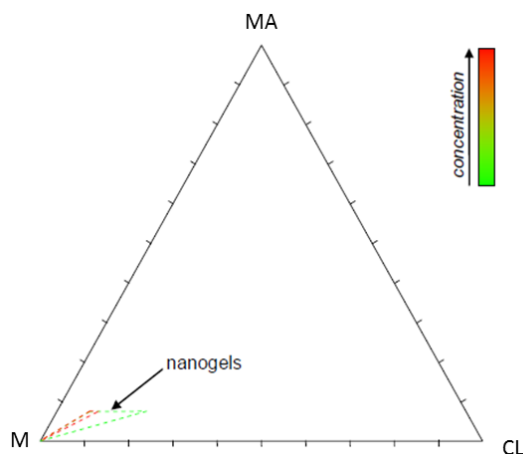


Figure II-3. Ternary diagram monomer (M)/ Cross-linker (CL)/ Mediating agent (MA): domain of nanogel formation and influence of concentration. The concentration in the polymerization medium also influences the domain of nanogel formation.

II. Recent advances in the synthesis of (nano)gels via CRCcP

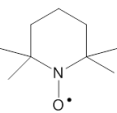
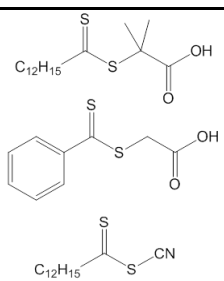
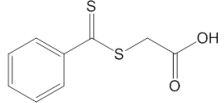
As mentioned above, ATRP^{34, 44, 45}, NMP^{4, 46-48} and RAFT⁴⁹⁻⁵¹ methods have been applied in the context of CRCcP. In most cases, CRCcP has been developed to achieve (nano)gels with a more homogeneous structure, though this has been questioned later on⁵². This section discusses representative examples of synthetic efforts of the past 5-6 years, regarding the synthesis of (nano)gels by CRCcP. Key features of the CRCcP process, including the occurrence of cyclization, the delayed gelation, whether chain extensions or functionalization of the parent nanogels have been performed, as well as the homogeneity of related networks have been considered.

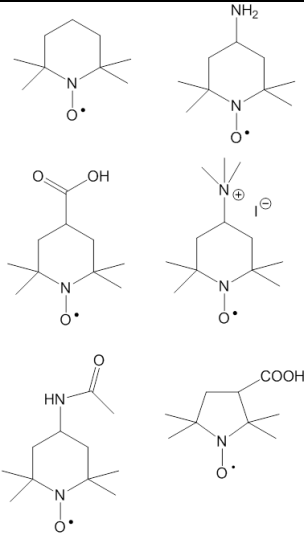
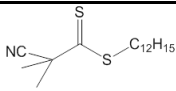
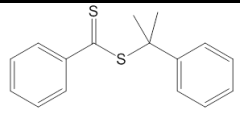
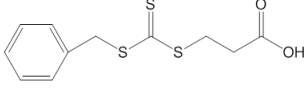
I-1. CRCcP forming nano-, micro or macroscopic polymeric networks.

Tables II-1 through II-3 summarize CRCcP experiments published over the past decade, using NMP, ATRP and RAFT methods. Data are classified according to the type of

monomer used (styrenic monomers in Table II-1; (meth)acrylates and acetate-type monomers in Table II-2; acrylamide monomers in Table II-3). Each table describes the monomer, cross-linker and controlling agent used, as well as the polymerization mechanism (ATRP, RAFT and NMP), and any peculiar properties analyzed in the article (such as its cleaving or stimuli-responsive properties). Chemical structures of the cross-linkers can be found in Figure II-4.

Table II-1. Controlled radical cross-linking copolymerization of styrenic-type monomers.

Entry	M	CL	Control agent	Mechanism	Comments	Ref
1	St	<u>J</u>	TEMPO 	NMP	1 st report	47
2	St	<u>A</u>	PS-TEMPO	NMP		4, 46
3	St	<u>A</u>	TEMPO	NMP	Comparison FRP/NMP, gelation	53
4	St	<u>A</u>		RAFT	Polymer beads synthesized <i>via</i> aqueous suspension	12
	St	<u>A</u>		RAFT		54
Table II-1 continued p.63						

5	St	<u>A</u>		NMP	PS monoliths; study of the link between the nitroxide used and the size of the resulting pores.	55
6	St	<u>A</u>		RAFT	PS monoliths, comparison FRP/RAFT	43
7	St	<u>A</u>	PS-TEMPO or TEMPO or P(S-r-MA)-TEMPO	NMP	Aqueous miniemulsion	48, 56- 58
8	St	<u>A</u>	CuBr / 2,2'-bipyridine	ATRP	Soluble branched copolymers	59
9		<u>A</u>	CuBr / PMDETA	ATRP	Coupling of nanogels	60
10	St	<u>A</u>		RAFT		61
11	St	<u>I</u>		RAFT	Miniemulsion semibatch	62

Cross-linkers are shown in Figure II-4. Articles reporting the modeling of CRCcP of styrene with divinylbenzene are listed further in Table II-10.

Table I-2. Controlled radical cross-linking copolymerization of (meth)acrylate and acetate-type monomers (cross-linkers are shown in Figure II-4).

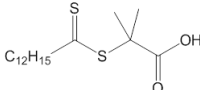
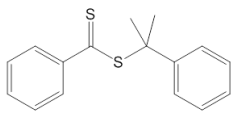
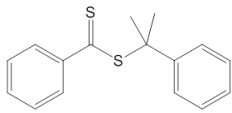
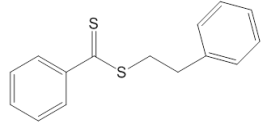
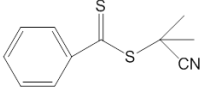
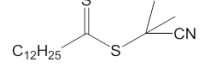
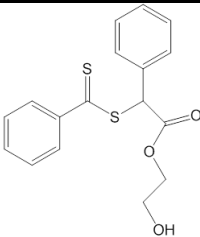
Entry	M	CL	Control agent	CRccP	Properties	Ref
1	HPMA	<u>E, F</u> or <u>H</u>	CuBr / 2,2'-bipyridine	ATRP	Synthesis following Flory and Stockmayer theory	44, 63
2	HPA	<u>E, F</u> or <u>H</u>		RAFT	More than one CL by primary chain without gelation: evidence of cyclization	49
3	MMA	<u>F</u>	or 	ATRP or RAFT	Comparison of the mechanisms	64
4	MMA	<u>F</u>		RAFT	Cyclization study <i>via</i> NMR. Resulting copolymer cleavable into primary chains.	65, 66
5	-	<u>D</u>	CuBr / N,N,N',N'-tetraethyldiethylenetriamine	ATRP	Homopolymerization of dimethacrylates with different PEG lengths. Dynamic experiments, comparison FRP	67
6	-	<u>D</u>		RAFT		68
7	-	<u>C</u>	 		Cyclized single-chain particles	69, 70
8	methacrylates	<u>A</u>		RAFT	Macro-CTA as PNIPAm, thus thermoresponsive	71

Table II-2 continued p.65

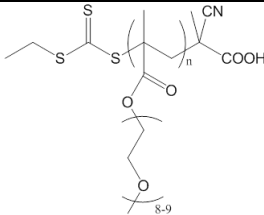
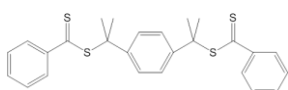
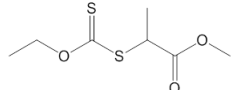
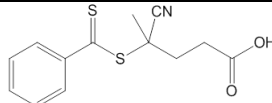
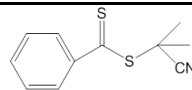
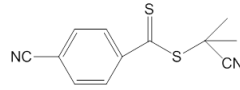
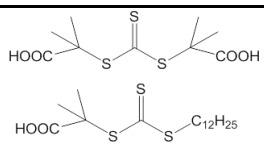
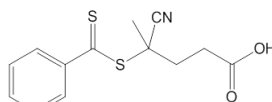
9	methacrylates	<u>D</u>		RAFT	Thermo-responsive material	72
10	methacrylates	<u>D</u>	CuBr / tris (2-pyridylmethyl) amine	ATRP	pH-responsive properties	45
11	BuMA, DMAE MA,	<u>A</u> , <u>C</u> or <u>H</u>		RAFT	Swelling behavior	73, 74
12	MMA, BuMA, St,	<u>A</u> , <u>C</u> or <u>H</u>		RAFT		75
13	VAc	<u>B</u>		RAFT	Resulting copolymer cleavable into primary chains	76
14	PEG diacrylates		see Figure I-4	RAFT	Resulting copolymer cleavable from cross-links and from in-chains	77
15	methacrylates	<u>L</u>		RAFT	Galactose nanogels thermoresponsive polymer	78
16	MMA	<u>C</u>		RAFT		79
17	MMA	<u>C</u>		RAFT	Homogeneity topic	52
18	MMA	<u>P</u> or <u>Q</u>		RAFT	Highly monodisperse	80
19	methacrylate	<u>P</u>		RAFT	Thermo-responsive pH-responsive for CL, x=48	81
20	MA	<u>H</u>	EBrP, CuBr, CuBr ₂ , PMDETA	ATRP		82, 83

Table II-2 continued p.66

21	MA	<u>G</u>	CuBr ₂ / Tris-(2-(dimethylamino) ethyl)amine	ATRP	Highly dilute conditions	10
22	OEOMA	<u>P</u>	CuBr ₂ / tris(2-pyridylmethyl)amine (TPMA)	ATRP	For the CL, x=10	84

Table II-3. Controlled radical cross-linking copolymerization of acrylamide-type monomers (cross-linkers are shown in Figure II-4).

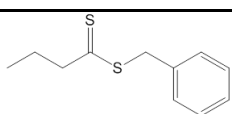
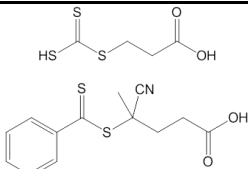
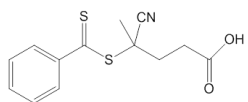
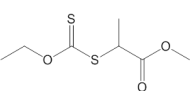
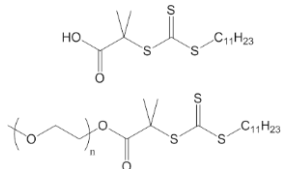
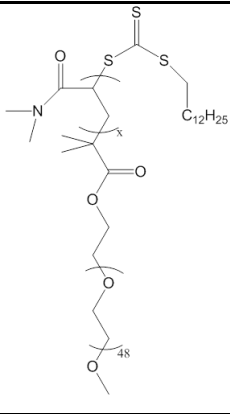
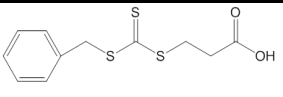
Entry	M	CL	Control agent	Mechanism	Properties	Ref
1	NIPAm	<u>L</u>		RAFT	Thermo-responsive polymer	85
2	NIPAm	<u>L</u>		RAFT	Study of the homogeneity of the network	86
3	N-(2-hydroxypropyl) methacrylamide	<u>M</u>		RAFT	Reduction sensitive polymer	87
4	acrylic acid or acrylamide	<u>L</u>		RAFT		88
5	N,N-diethylacrylamide	<u>L</u>		RAFT		89

Table II-3 continued p.67

<p>6</p>	<p>N,N-diethylacrylamide</p> <p>L</p>		<p>Amphiphilic RAFT agent, aqueous dispersion polymerization</p> <p>RAFT</p> <p>90</p>
<p>7</p>	<p>acrylamide</p> <p>L</p>		<p>Semibatch process</p> <p>RAFT</p> <p>91</p>

In Figure II-4 below, are reported the most usual cross-linkers used in CRCcP mediated by NMP, RAFT or ATRP.

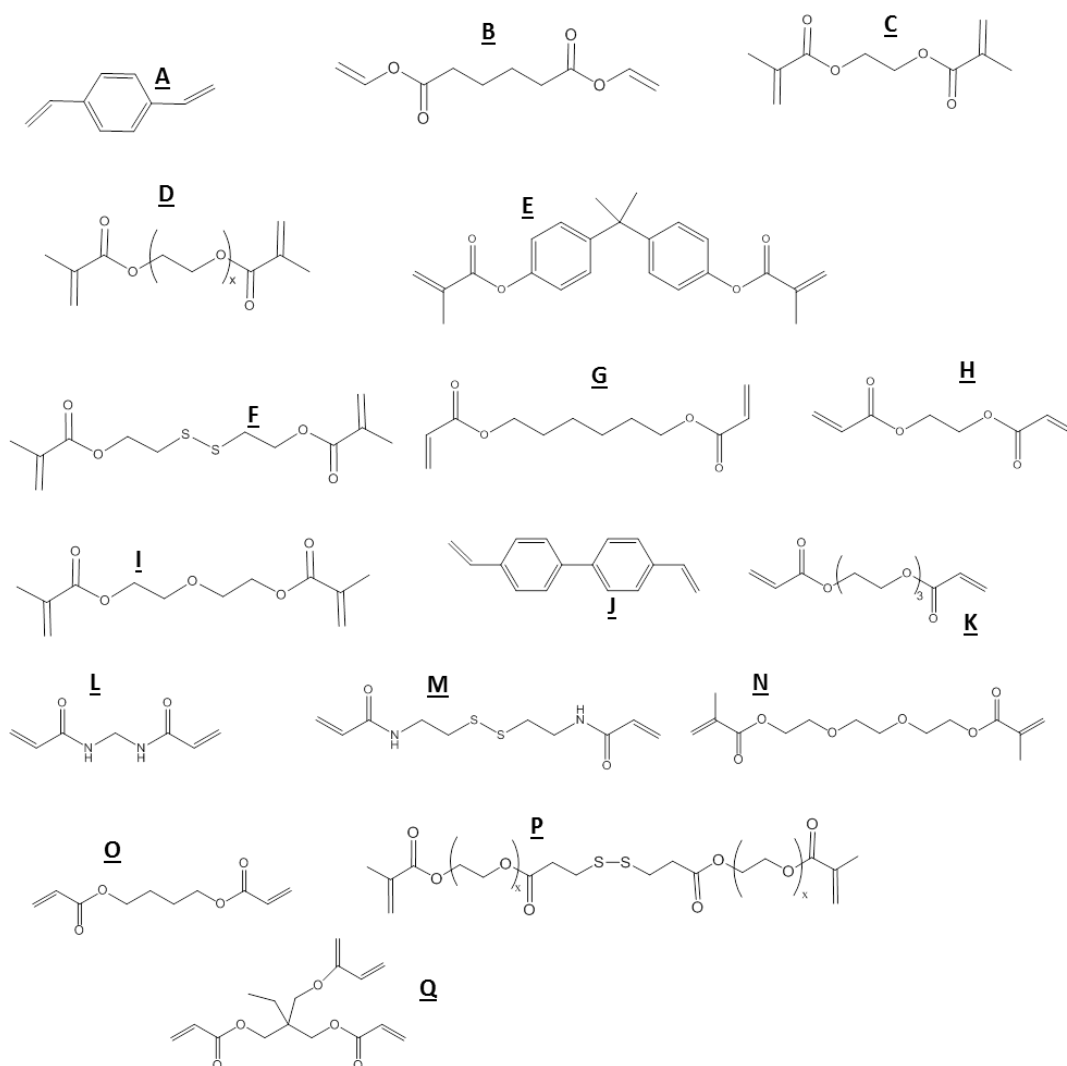


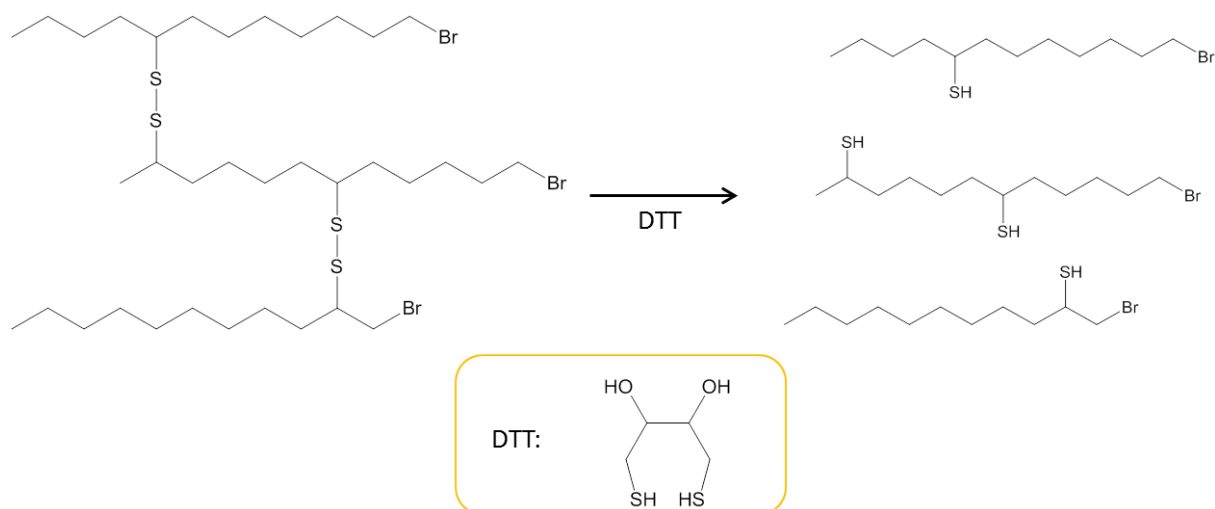
Figure II-4. Most common cross-linkers employed in a context of CRCcP.

II-2. From cleavable cross-linkers to labile arms

Interestingly, investigations that have attempted to gain an insight into the internal structure of CRCcP-derived gels have evidenced narrow distributions of primary chains, through the cleavage of the cross-links. Various divinyl cross-linkers have been used indeed in CRCcP (see Figure II-4), and some of them can be cleaved off. For instance, those featuring a disulfide bond (**F** and **M**) or containing vinyl ester moieties (**B**) can be cleaved off by reduction^{59, 61, 62, 88-90} (Scheme II-4) and by methanolysis⁷⁶ (Scheme II-5), respectively, making the as-obtained gels degradable, and allowing for further characterization of the primary (constitutive) chains.

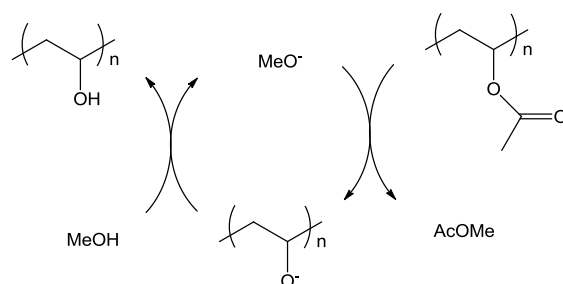
Use of disulfide dimethacrylate cleavable cross-linker (**F**, Figure II-4) has also proven useful to study intracyclization reactions specifically, as reported by Li and Armes⁶³. These authors have indeed evaluated the ratio between intra- and intermolecular cross-linking occurring in ATRP-mediated CRCcP by selecting a cross-linker which, once cleaved, gives very distinct NMR signals from those of the monomer units.

Also in the context of ATRP, Matyjaszewski *et al.* have resorted to the same disulfide-containing cross-linker, but in a different way⁹²: after the synthesis of a core-first poly(n-butyl acrylate)-based nanogel by CRCcP using ethylene glycol diacrylate first (**H**, Figure II-4), the disulfide cross-linker has served to reversibly link together the arms of the star copolymers.



Scheme II-4. Cleaving process of gels containing disulfide bonds in the cross-linking bridges.⁶³

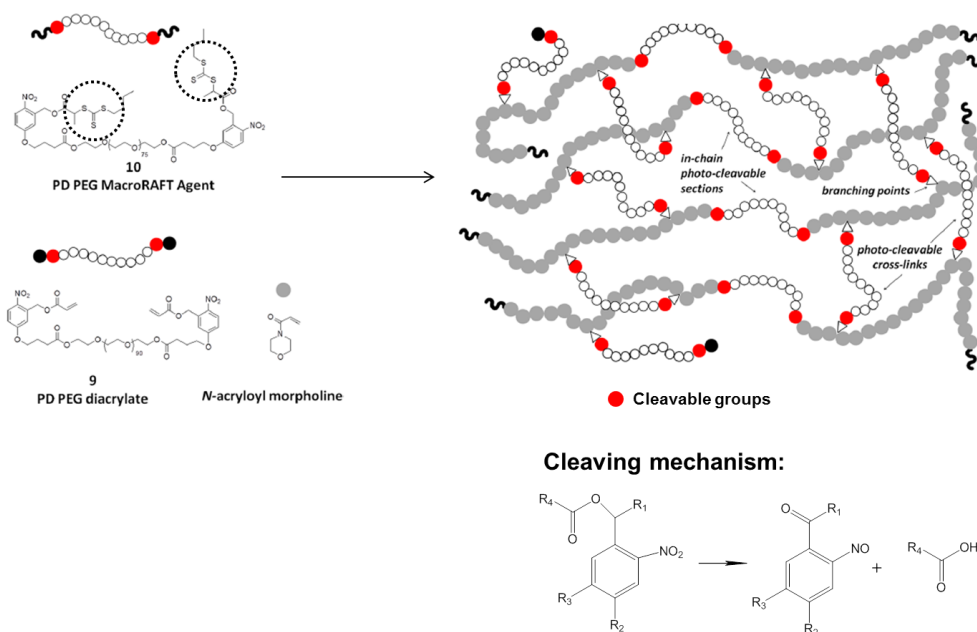
Primary chains formed after chemical cleavage can be analyzed by SEC. This has been exemplified by different groups who have confirmed that constitutive chains are homogeneous in size^{70, 76, 93}. It has been established that, as expected, primary chain length is influenced by the initial monomer to initiator ratio^{76, 82, 86, 94}.



Scheme II-5. Methanolysis of a poly(VAc-DVA) nanogel into constitutive linear chains in the form of poly(vinyl alcohol) after modification.⁷⁶

Evans, Forsythe *et al.* have reported the synthesis of photodegradable hydrogels by RAFT-mediated CRCcP⁷⁷, using a macro-RAFT agent, and a polymeric cross-linker (see Scheme II-6), which put this synthesis at the limit of the scope of this chapter. Once the

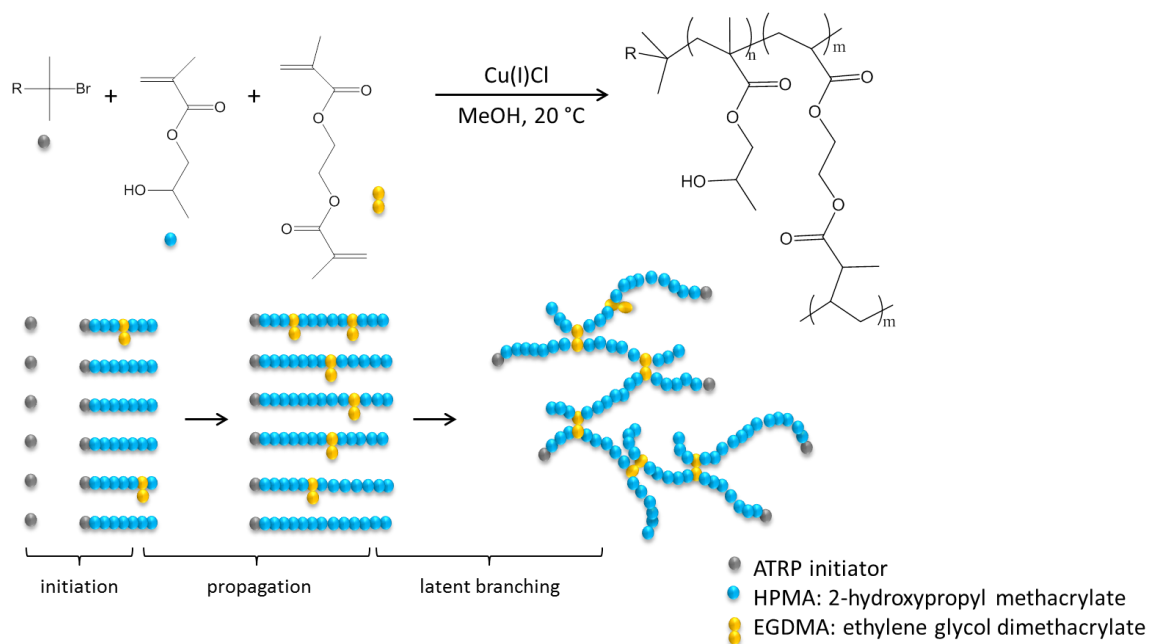
polymeric network has been synthesized *via* RAFT-mediated CRCcP, the photodegradability abilities of both the cross-linker and the RAFT agent allows for subsequent cleavage, either of the ‘primary’ chains (cleaving the cross-linker) or of intra-chain (cleaving the RAFT agents incorporated in the network).



Scheme II-6. Photodegradable RAFT hydrogels: the cleaving mechanism takes place either at the location of the cross-linker, or at the RAFT end groups⁷⁷.

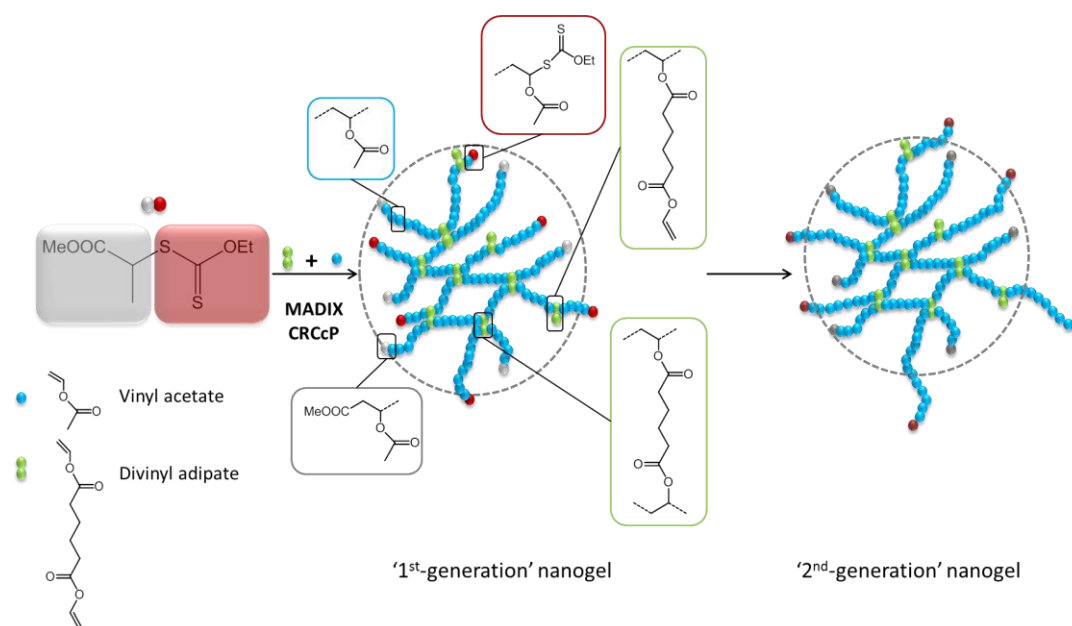
In 2014, Sawamoto *et al.* have described the synthesis of different star-like architectures, either by homopolymerization of a divinyl cross-linker (**C** or **D** with $x=9$), or by CRCcP with a vinyl monomer, namely poly(ethylene glycol) methacrylate, using a pre-synthesized PEGylated macroinitiator⁹⁵. This macroinitiator contains an acid-cleavable acetal function between the PEG chain and the chloride. Thus, after the ATRP-initiated CRCcP, the PEG chains form a shell around the cross-linked copolymer, and can be cleaved under acidic conditions.

Below are two representative schemes of the synthesis of polymeric cross-linked networks mediated either by ATRP (Scheme II-7), or by xanthates in the context of a RAFT-mediated CRCcP (Scheme II-8). Scheme II-7 illustrates the kinetic aspect of CRCcP, particularly concerning the incorporation of the cross-linker and its further branching.



Scheme II-7. Formation of branched copolymers by ATRP-induced CRCcP, using **C** (see Figure I-3) as a cross-linker⁴⁴.

Scheme I-8 below illustrates the ‘living’ character of a CRCcP process, by the possible reactivation of the chain ends to form ‘2nd-generation’ gels.



Scheme II-8. Formation of nanogels of PVAc *via* xanthate-mediated RAFT CRCcP; the xanthate end-chain can be reactivated to obtain ‘2nd-generation nanogels’; the cross-linker used (divinyl adipate) can be further cleaved by methanolysis, resulting in linear chains of poly(vinyl alcohol) corresponding to the primary chains of the nanogels⁷⁶ (see Scheme II-5 above).

II-3. How to further delay gelation?

Flory and Stockmayer theory claims that, as long as cyclization is not taken into account and that all double bonds have the same reactivity, macrogelation occurs when the ratio between the cross-linker and the primary chain is equal or superior to 1.

In the context of FRCcP, Sherrington *et al.* have developed “the Strathclyde route” by resorting to an irreversible chain transfer agent (typically a thiol), as a means to minimize the extent of cross-linking during the synthesis⁹⁶⁻⁹⁸.

In CRCcP, gelation phenomenon is delayed as opposed to FRCcP⁹⁹. This has been reported both experimentally⁹⁹ and computationally¹⁰⁰, which is ascribed to the predominant

dormant state of growing polymer chains, leaving more time for the monomer to diffuse and for the chains to relax.

The most common way to delay gelation is to perform a CRCcP process in solution conditions¹⁰. Zhu *et al.* have studied the relationship between feeding processes and the structure of the final polymeric network¹⁰¹: using *N,N'*-methylene bisacrylamide (**L**, Figure II-4) as a cross-linker (monomer at 7 wt.%), cross-linked networks of different internal structure have been prepared whether a continuous or a semi-batch process has been implemented in RAFT-mediated CRCcP, using different CL/CTA ratios.

Zhu *et al.* have reported that only 6 to 22 % of the cross-linker used in these conditions leads to inter-molecular cross-linking instead of cyclization. They have also found that, for the same ratio of cross-linker, a continuous process leads to a macrogel, while in a semi-batch process in which the cross-linker is added during the polymerization, the final polymers are soluble and highly branched. On the other hand, a batch process gives a more cross-linked copolymer than under a semi-batch process (204 kg/mol *vs.* 100 kg/mol).

Several groups have developed synthetic approaches to delay gelation in ATRP-mediated CRCcP. Zhu *et al.* have polymerized a same divinyl monomer (poly(ethylene glycol) dimethacrylate, **D** with $x=6$ in Figure II-4) in bulk at 70 °C, mediated *via* ATRP-induced CRCcP (for comparison, in FRCcP, gelation occurs at low conversions, *i.e.* less than 10%)¹⁰². No auto-acceleration of the propagation has been noted, in contrast to FRCcP. At high conversion however, the polymerization resembles more a FRCcP process due to the lack of mobility of the chains, which induces an increase in the concentration of radicals.

Zhao, Poly *et al.*¹⁰³ have developed another approach that consists in dramatically enhancing - or even suppressing- cyclization at the early stages of ATRP-mediated CRCcP. In this scenario, *i.e.* at high chain concentration, both intermolecular cross-linking and linear chain growth are as likely to occur, and cyclization is less probable. On the other side of the

spectrum, Wang *et al.* have developed the so-called *in situ* deactivation enhanced ATRP (DE-ATRP) to access ‘single cyclized polymers’ or ‘single knot nanoparticles’, as depicted in Figure II-5⁶⁹. Use of a small amount of a reducing agent (10% of Cu^{II}) allows shifting the equilibrium towards the formation of dormant species. Intramolecular reactions are thus more likely to occur, as opposed to intermolecular cross-linking (see Figure II-8). The growth boundary of the polymer chains is much more restrictive in a DE-ATRP mechanism than described in Flory and Stockmayer’s model. Polymer chains are submitted to a growth boundary. Each growing chain thus forms a 3D-network, and the polymer chains are maintained *via* intramolecular cross-linking containing only one active center (see Figure II-6).

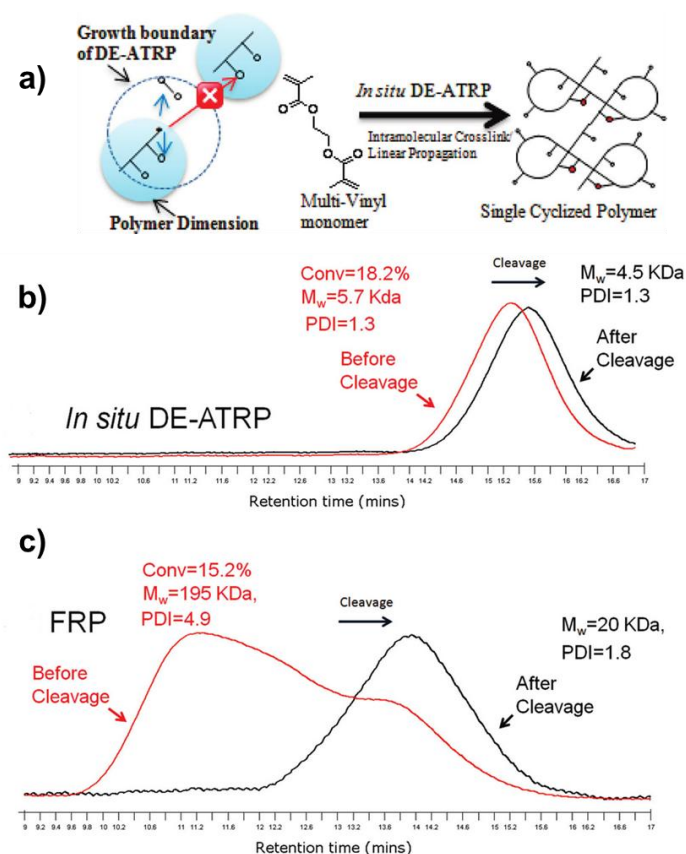


Figure II-5. a) In-situ deactivation-enhance atom transfer radical polymerization (DE-ATRP) mechanism and formation of single chain cyclized polymer; SEC traces of the branched architectures before and after cleavage, synthesized b) by DE-ATRP; c) by FRCcP.⁶⁹

Gelation does not occur until relatively high conversion is reached, since it is only during the last stages that intermolecular branching takes place, forming chemically cross-linked networks. Note that these results relate to the *homopolymerization* of a multi-vinyl monomer (C, Figure II-4), and not to CRCcP, strictly speaking. Here, the authors have reached 55% conversion before the formation of a macrogel, owing to the fact that each growing chain contains a PDB. Such a high conversion is only possible due to the high proportion of dormant species in the medium: under similar conditions, FRCcP leads to macrogelation at 7% of monomer conversion only. Furthermore, the *in situ* DE-ATRP and vinyl oligomer combination enable syntheses in relatively concentrated medium (monomer ratio of 28 w/v%).

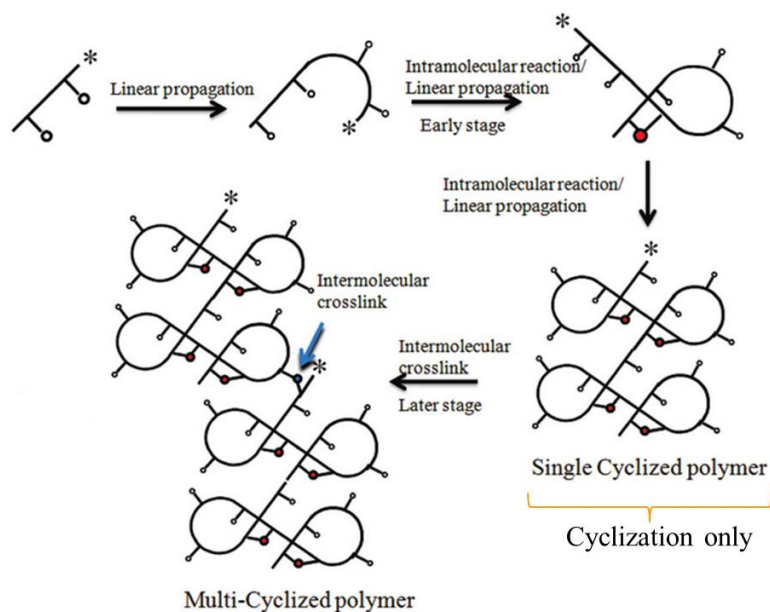


Figure II-6. Propagation mechanism of *in situ* deactivation enhanced ATRP (DE-ATRP); the low monomer concentration and the addition of Cu(II) leads to extensive cyclization; once single-chain cyclized polymers form, inter-molecular cross-linking occurs at a later stage of the process.

Lately, the homopolymerization of divinyl monomers *via* DE-ATRP has been applied in other conditions aimed at increasing both the concentration in monomer, and the monomer/initiator ratio, as a means to suppress primary cyclization (the length of the primary chains being so small that cyclization is indeed less likely to occur).

Wang *et al.* have then explored a similar process, *i.e.* the 3D network formation from parent polymer chains, *via* the RAFT-induced CRCcP of ethylene glycol dimethacrylate (C, in Figure II-4, and Figure II-7)⁹³. The RAFT polymerization occurs under concentrated solutions, [C] = 36.6 wt.%, with a significant delay of gelation. These data have been confirmed by subsequent cleavage of an acid-cleavable divinyl monomer⁹³.

At low conversion (7%), cleaving the FRCcP-synthesized polymer has resulted in a steep decrease of the molar mass (from 74 to 14 kg/mol), while cleaving the RAFT-mediated polymer shows only a very slight change (from 7 to 5 kg/mol): cyclization would thus be predominant during RAFT polymerization of C, especially in the first stages, while intermolecular cross-linking would occur later.

On the other hand, the gel synthesized *via* FRCcP is formed of several smaller primary chains, which shows that both inter-molecular cross-linking and cyclization take place during the copolymerization. Interestingly, the authors have taken advantage of the remaining PDBs to post-functionalize the cyclized single-chain polymers.

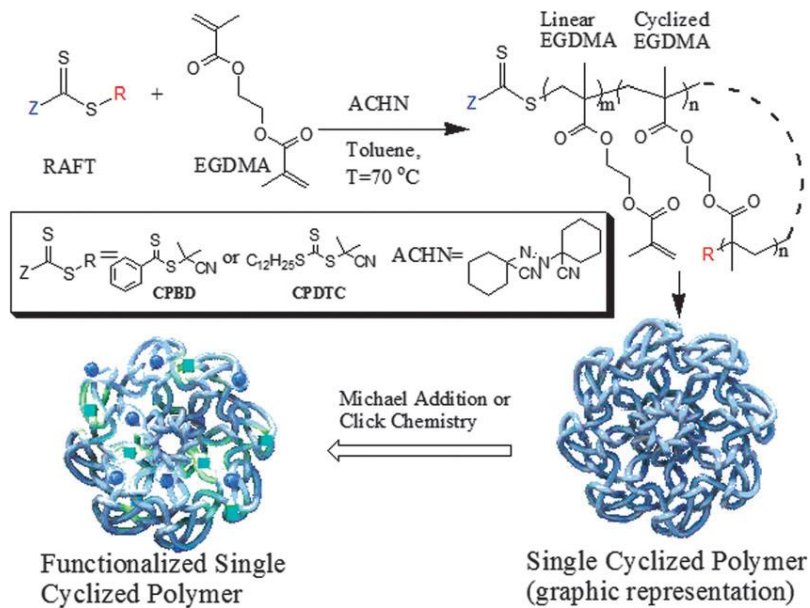


Figure II-7. Homopolymerization of ethylene-glycol dimethacrylate *via* RAFT polymerization, and subsequent formation of a 3D single cyclized chain⁹³, (ACHN was used as initiator).

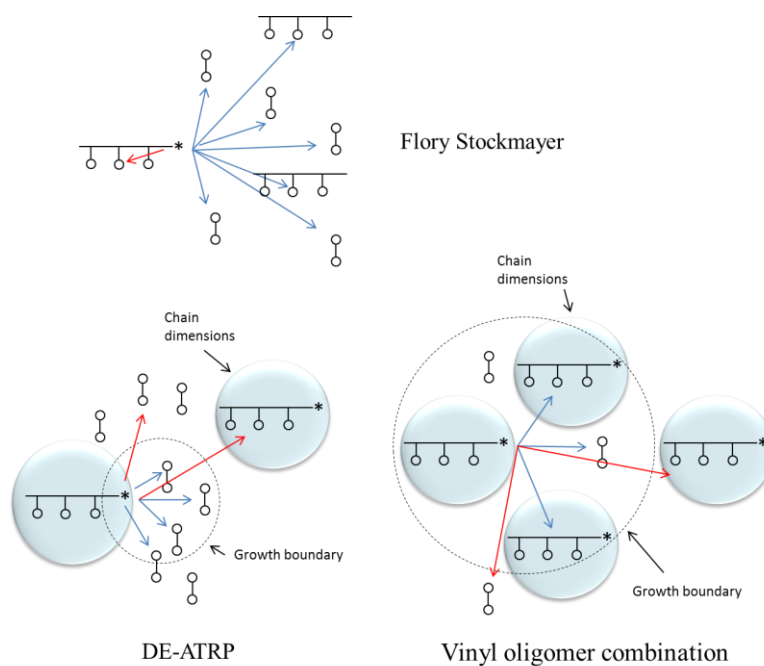


Figure II-8. Schematic representation of: a) FRCcP according to Flory's theory; b) DE-ATRP⁶⁹; c) vinyl oligomer combination¹⁰³.

II-4. Homogeneity of the network: swelling ratio and moduli.

As mentioned above, CRCcP methods have been anticipated to access to nanogels with a better network homogeneity^{68, 104}, compared to FRCcP, with the assumption that cross-linking points can be regularly distributed within the structure. This can be highly beneficial in specific applications, such as in drug delivery systems, which can require controlled structure so as to tune the kinetics of drug release and the possible degradation of the cross-linked polymer⁸. In Figure II-2 are compared an ‘ideal’ network (based on Flory and Stockmayer theory), and networks presenting first and second cyclizations.

However, the possibility to really achieve more homogeneous (nano)gels by CRCcP, as opposed to FRCcP,¹⁰⁵ has been recently questioned⁵². It is worth reminding that heterogeneity characterizing FRCcP-derived gels is due, in particular, to very fast chain growth, depleting the immediate environment of the radicals from monomer species, which is followed by rapid termination limiting the monomer diffusion and/or chain relaxation, thereby favoring extensive intramolecular cross-linkings (cyclizations)⁴. In contrast, much more primary chains start growing simultaneously in a CRCcP process from the early stage of the process. Their growth is also much slower, leaving enough time for the growing chains to relax and for the monomer to diffuse. Hence, intermolecular cross-linking reactions are more likely to occur in CRCcP, compared to FRCcP. Differences between FRCcP and CRCcP methods have been supported by experimental findings, both at the macroscopic level (*e.g. via* elastic or swelling analyses)^{94, 106} and microscopically, for instance through light scattering measurements. Thus, CRCcP-made networks exhibit higher swelling ratios and seem to be softer than those obtained by FRCcP.

While modeling the NMP-mediated CRCcP of styrene and divinylbenzene, Penlidis *et al.* have concluded that NMP gels are more homogeneous than those made by FRCcP.

Modeling thus agrees with experimental data, and shows a lesser extent of cyclization in the controlled process¹⁰⁷ (see discussion further).

Experimentally, homogeneity of the network is usually determined by swelling/deswelling experiments^{4, 86}, morphological behavior studies, or by light scattering analyses^{61, 108}. The swelling/deswelling method has allowed comparing the density of the cross-linking points. The more cross-linked a network is, the slower the swelling ratio is.

The first study of homogeneity of a cross-linked PS-based network synthesized *via* CRCcP has been reported by Ide and Fukuda who have resorted to NMP of styrene and divinylbenzene (**A**, Figure II-4)^{4, 46}. The as-obtained polymeric networks have been qualified as ‘more homogeneous’ than their FRCcP-synthesized counterparts, based both on swelling ratios and on concentration in PDBs before gelation.

Kowalewski, Matyjaszewski *et al.*¹⁰⁶ have compared both the swelling ratio and the water retention (the deswelling kinetic, as well as the final percentage of water remaining in the gel) of an ATRP-derived copolymer based on of 2-(2-methoxyethoxy)ethyl methacrylate and ethylene glycol dimethacrylate (**C**, Figure II-4), using either ‘high’ cross-linkage (M/CL=100/1) or ‘low’ cross-linkage (M/CL=400/1) ratios. In the ‘high’ cross-linkage case, ATRP-gels have shown a greater water uptake than FRCcP-gels, though both have released similar amounts of water during deswelling measurements. Thus, ATRP-derived gels would retain more water than FRP-derived ones, for ‘high’ cross-linkage. For gels of ‘low’ cross-linkage, the swelling analysis gives similar results, both gels retaining a high fraction of water during deswelling analysis; this has been described as a ‘skin effect’.

Yu, Zang *et al.*¹⁰⁹ have come to similar conclusions *via* another analysis method. These authors have indeed compared the glass transition temperature (T_g) of various gels synthesized by FRCcP, and ATRP- or RAFT-induced CRCcP of oligo(ethylene glycol) methyl ether methacrylate with oligo(ethylene glycol) dimethacrylates (**D**; Figure II-4). A

broader distribution of T_g values has been correlated to a lesser homogeneity of the network, more cross-linked areas having a different T_g than looser ones¹⁰⁹.

Gels synthesized *via* CRCcP also show a narrower $\tan \delta$ value than FRCcP-derived gels. However, it has been also found that the longer the size of the cross-linker (*e.g.* **D** in Figure II-4) is, the more homogeneous the network is (*i.e.* a lower cross-linking density).⁶⁸

Table II-4. Relevant literature on network homogeneity, especially in comparison between CRCcP mechanisms and conventional radical cross-linking copolymerization (RCC).

Groups	CRCcP: more homogeneous?	Remarks	Ref.
Ide and Fukuda	Yes	<i>Method:</i> comparison of the cross-linking density at gel point in networks synthesized <i>via</i> NMP or FRP. <i>Results:</i> NMP networks closer to Flory's theory than FRP, they conclude that NMP networks were more homogeneous.	4
Lu et al.	No Yes (deswelling experiments)	<i>Method:</i> swelling and visual aspects (de-visu observations), <i>Results:</i> contradictory. After swelling in water, gels formed <i>via</i> CRCcP seem less homogeneous than <i>via</i> FRCcP (RAFT gels turn turbid, while FRP gels stayed transparent). However, de-swelling ratios indicate that RAFT gels are more homogeneous than FRCcP ones.	86
Matyjaszewski, Kowalewski et al.	Yes	<i>Method:</i> swelling/deswelling experiments. <i>Results:</i> skin effect (keeping the water in the gels, especially at high temperature)	106

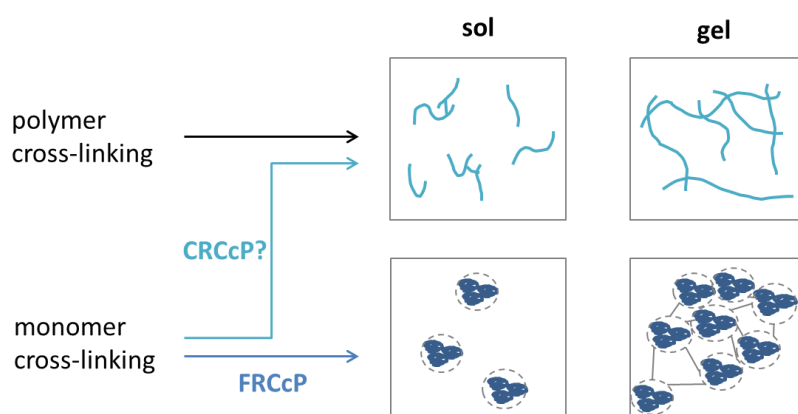
Table II-4 continued p. 81

Zhu et al.	Yes	<p><i>Method:</i> follow up via DSC, DMA and swelling ratio.</p> <p><i>Results:</i> $\tan \delta$ narrower for CRCcP than FRCcP, cross-linking density and heterogeneity increases with conversion. The longer the cross-linker, the more homogeneous the network (lower cross-linking density).</p> <p>Noteworthy, conversion in FRCcP experiments are 10% higher than for CRCcP networks. Mild autoacceleration of the propagation is observed for CRCcP reactions.</p>	67, 68
Zhu et al.	Yes	<p><i>Method:</i> dynamic experiment (T_g)</p> <p><i>Results:</i> networks from FRP have broader distribution of glass transition than networks from CRCcP. The broader the distribution of glass transition temperature, the less homogeneous the network (highly reticulated area have different T_g than very loose ones). Hence, networks from CRCcP (either RAFT or ATRP) are more homogeneous than networks from FRCcP.</p>	109
Norisuye, Fukuda et al.	Yes	<p><i>Method:</i> Light scattering experiment during the copolymerizations (FRCcP and RAFT)</p> <p><i>Results:</i> The cooperative diffusion in semi-dilute conditions increases more gradually for RAFT than for FRP; the translational diffusion of large aggregates is much lower in RAFT than in FRCcP, and only appears towards the end of the polymerization. Cross-linking in RAFT-mediated CRCcP occurs more randomly than in FRCcP, resulting in a more homogeneous final network. Updating the ‘model’ first published by Ide and Fukuda</p>	61

(Figure I-1) by the cross-linked polymers in Scheme I-9.

Oppermann <i>et al.</i>	No	<p><i>Method:</i> shear modulus and swelling ratio</p> <p><i>Results:</i> Comparison between FRCcP and RAFT-derived gels based on similar moduli values. RAFT gels are not more homogeneous than FRCcP gels, they only appear more homogeneous because their cross-linking density is significantly lower than FRCcP-derived gels.</p>	52
--------------------------------	----	--	----

As mentioned above, by comparing the internal structure of gels prepared both by free-radical and controlled routes, Oppermann *et al.*⁵² have stated that gels obtained by CRCcP appear to be more homogeneous only because they are much less densely cross-linked (reduced cross-linking efficiency) as compared to FRCcP⁵². Eventually, a “controlled” gel would not be more homogeneous than a “non controlled” gel, only if both related gels exhibit the same effective network density. In other words, CRCcP-derived gels do not necessarily show a more even distribution of cross-link points.



Scheme II-9. Schematic representation of the RCC of a vinyl monomer and a divinyl cross-linker in FRCcP *vs.* CRCcP, as reported by Fukuda and Norisuye⁶¹: before gelation, a) CRCcP-derived gels are loosely cross-linked, which leads to b) loosely cross-linked network

after gelation. On the other hand, c) FRCcP-derived gels before gelation show evidence of microgel formation; d) after gelation, these microgels are integrated in the macroscopic polymer network.

What authors generally agree on is that: i) differences in macroscopic properties between CRCcP and FRCcP networks are due to a distinct cross-linking ‘environment’, be it cross-linking density or proportion of cyclized structures; ii) the concentration in co-monomers dramatically influences the inter- vs. intra-molecular reactions, affecting the cross-linking density; iii) CRCcP network formation does not pass by a ‘microgel stage’, as is usual in FRCcP.

II-5. Monitoring the cyclization phenomenon *via* NMR spectroscopy.

Investigations into CRCcP have employed various analytical tools in order to monitor the microstructure of the obtained gels, and in particular, to account for the extent of intermolecular vs. intramolecular cross-linking. In this regard, NMR spectroscopy has proven a relevant method. Cyclization/intra-molecular cross-linking causes the polymeric network to stray from ideality in Flory’s theory^{103, 111, 112}. These events eventually lower the cross-linking density (intramolecular cross-linkings do not contribute per se for the branching of growing chains; see Figure II-2).

Armes *et al.* have determined the extent of cyclization (intramolecular branching) *via* a thorough characterization by NMR spectroscopy of nanogels made by RAFT-mediated CRCcP of MMA and DSDMA (**E**, Figure II-4)^{65, 66}. Their working hypothesis relies on Flory and Stockmayer theory, *i.e.* all double bonds exhibit the same reactivity, making the consumption of monomer and cross-linker fully statistical. Unlike Flory’s proposition, however, PDBs can be subjected to cyclizations.

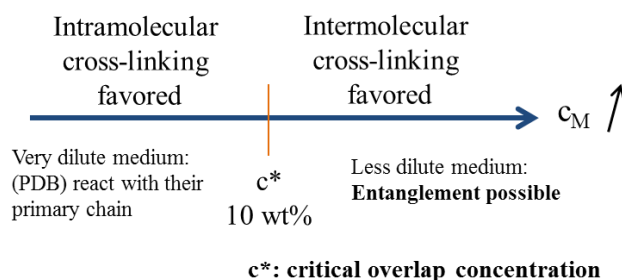
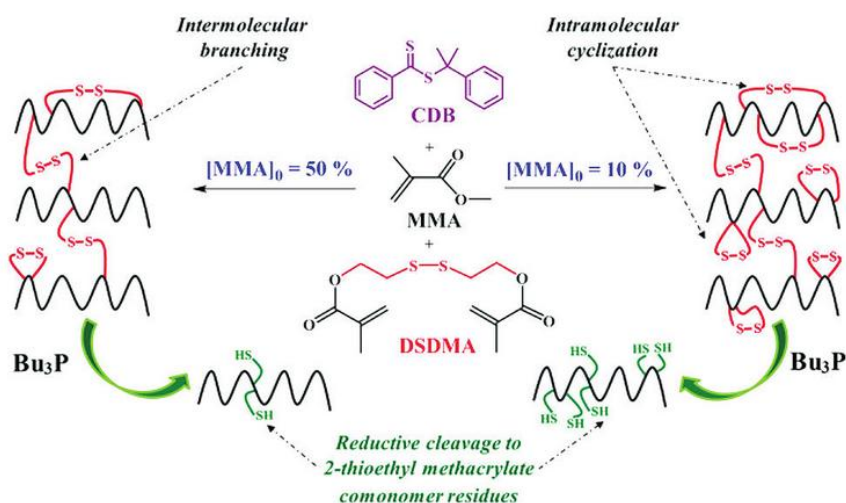


Figure II-9. Expected evolution of the intra- vs. inter-molecular cross-linking as a function of the concentration of monomer; when the concentration of double bonds (from monomer and cross-linker) increases, less cross-linker is needed to attain gelation⁶⁴.

A first indication of the competition between inter-molecular cross-linking and cyclization can be seen by comparing the SEC traces of the copolymers and primary chains with that of the homopolymer, in a qualitative manner only, as demonstrated by Wang *et al.* (in Figure 5b and c) [69]. The disulfide bond in DSDMA allows for subsequent cleavage of the gel formed by RCC. If the elution time of the primary chains is the same as that of the PMMA homopolymer, it is assumed that mostly cyclization takes place. In contrast, if primary chains are shorter (elution time smaller) than the homopolymer, intermolecular cross-linking are predominant.

Armes *et al.* have also established that NMR studies enable a more quantitative evaluation of these two events. Their hypothesis is that intramolecular cross-linking causes a broadening of the NMR peaks. This is due to the fact that the disulfide bond of the cross-linker is characterized by its dihedral angle (almost 90°), which renders the adjacent protons more sensitive to their immediate environment. Interestingly, the cross-linker used, once cleaved, shows different proton signals than those of the monomer: this allows for the differentiation *via* ¹H NMR of the monomer unit with the ‘cross-linker’ units.



Scheme II-10. CRCcP of MMA and DSDMA (**F** in Figure I-3) via RAFT, and subsequent cleavage of disulfide bonds contained in the cross-linking points⁶⁵.

By deconvolution of the parent peak into Gaussian curves, intermolecular cross-linking has been assigned to the Gaussian curve at the exact chemical shift predicted by modeling (red curve in Figure II-10), while other peaks have been ascribed to intramolecular cross-linking (blue curves in Figure II-10).

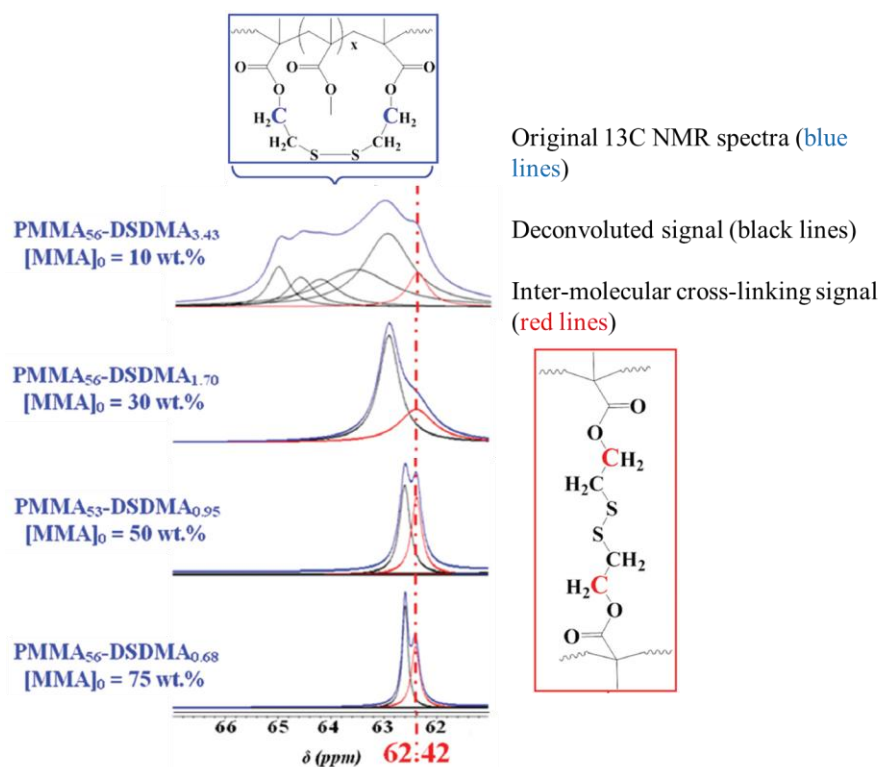


Figure II-10. Deconvolution of the ^{13}C NMR spectra resulting from the RAFT-mediated CRCcP of MMA with DSDMA. The deconvoluted signal in red matches the expected chemical shift of the carbon atom of the cross-linker, and is attributed to inter-molecular cross-linking. All the other deconvoluted signals are ascribed to intra-molecular cross-linking (= cyclization).

Strengths and weaknesses to the use of either ^1H and ^{13}C NMR for monitoring the cyclization phenomenon are listed below in Table II-5. Investigations by ^1H and ^{13}C NMR spectroscopy^{65, 66} have led to a similar ratio between inter- and intramolecular cross-linking (see Table II-5), with the notable exception of CRCcP occurring in highly concentrated medium (50 wt.% of monomer), which has not been explained. In addition, the assignment of the integrals of the deconvolution to either inter or intramolecular branching has not been justified.

Table II-5. Comparison of the studies of cyclization in a gel *via* ^1H and ^{13}C NMR spectroscopy monitoring.

	^1H NMR	^{13}C NMR
Calculated inter-molecular ratio	0.61	0.59
+	Faster spectroscopy (abundance of ^1H proton compared to ^{13}C).	Better separation of the peaks. Should be better for copolymerizations not using disulfide cross-linkers.
-	Less accurate study (overlapping of several peaks).	Poor signal-to-noise ratio. Shifting of the peaks when the cyclization increases.

II-6. Stimuli responsive (nano)gels.

Thermo-responsive nanogels are quite sought after⁹⁰ mostly in the biomedical field. A well-known thermo-responsive polymer is poly(*N*-isopropylacrylamide) (= PNIPAm) possessing a lower critical solution temperature (LCST) around 37 °C. Licea-Claverie *et al.* have reported the synthesis of thermo-responsive core-shell structures, by copolymerizing divinylbenzene with (meth)acrylates *via* RAFT, using PNIPAm this time as a macro-chain transfer agent (macro-CTA)⁷¹. On the other hand, nanogels of PNIPAm have also been synthesized using NIPAm as the monomer¹¹³ (Figure II-11) and either *N,N'*-methylenebis(acrylamide) (**L**, Figure II-4)⁸⁶ or 1,6-hexanediol diacrylate (**G**, Figure II-4) as a cross-linker.

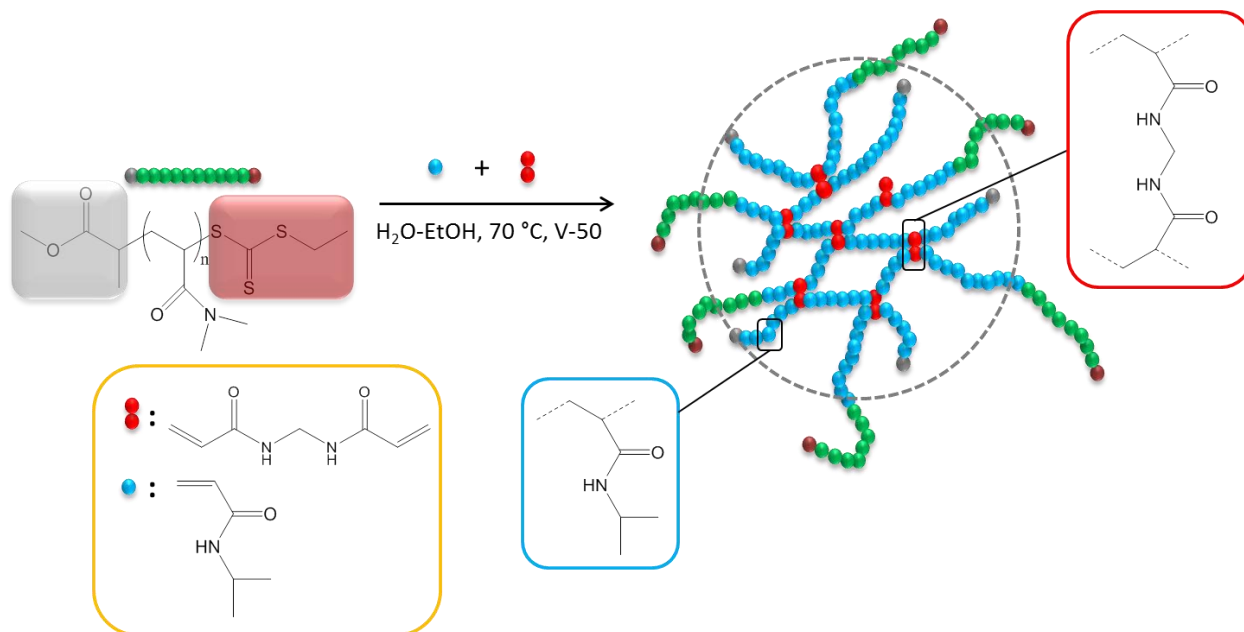


Figure II-11. RAFT-mediated CRCcP forming thermo-responsive nanogels based on PNIPAm¹¹³.

An *et al.* have also described the RAFT-induced CRCcP of di(ethylene glycol) methyl ether methacrylate and poly(ethylene glycol) methyl ether methacrylate with poly(ethylene glycol) dimethacrylate (**D**, Figure II-4 with $x=14-15$) as a cross-linker, using a PEG macroinitiator. Related nanogels prove thermo-responsive, and the PEG corona endows the copolymers with biocompatibility⁷². The nanogels obtained have shown enhanced stability compared to linear polymers, either in saline medium or bovine serum albumine, which bodes well for further bio-related applications.

Thermo-responsive nanogels based on galactose shell with a cross-linked core of di(ethylene glycol)methylethyl methacrylate, 2-lactobionamidoethyl methacrylamide and *N,N'*-methylene bisacrylamide (**L** in Figure II-4) for a use in drug delivery applications have been synthesized *via* RAFT by Narain *et al*⁷⁸. At low temperature (4 °C), the cross-linked core can swell in aqueous medium, allowing the encapsulation of iodoazomycin arabinofuranoside, a drug that has been proven effective for imaging, during treatment against

carcinoma. At high temperature (37 °C), the cross-linked core would collapse, trapping the drug inside. The nanogels have been further proven non-toxic and biodegradable.

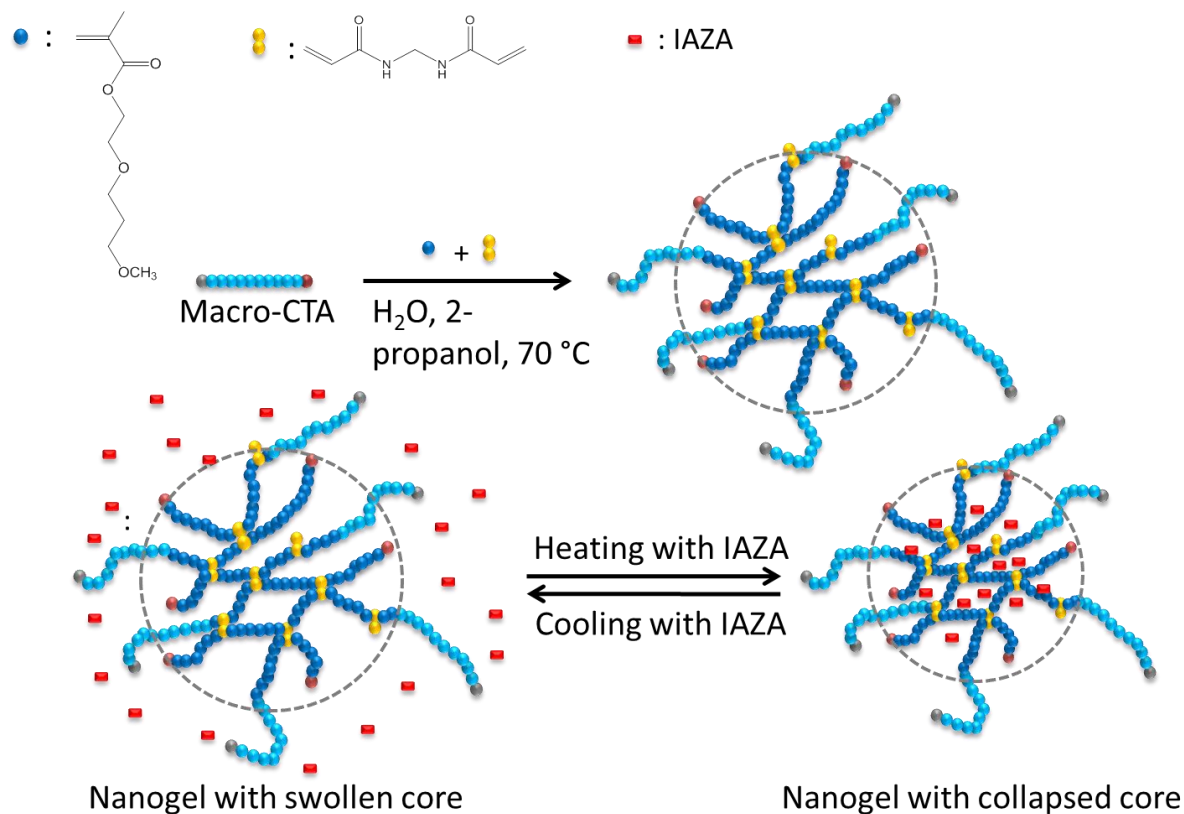


Figure II-12. RAFT-mediated CRCcP of di(ethylene glycol) methylethyl methacrylate with different methacrylate-type cross-linkers with galactose macro-CTA⁷⁸.

Forbes and Peppas have compared the properties of nanogels synthesized *via* ARGET-ATRP (reverse ATRP technique using Cu(II) catalyst instead of Cu(I) as controlling agent) and by UV-initiated CRCcP. They have copolymerized poly(ethylene glycol) methyl ether methacrylate, 2-(diethylamino) ethyl methacrylate, *ter*-butyl methacrylate with tetra ethylene glycol dimethacrylate (**D** in Figure II-4 with $x=4$) as cross-linker¹¹⁴. ATRP-induced nanogels have shown narrower molar mass distributions and glass transition temperatures than UV-initiated copolymers. The pH-responsive behavior of these nanogels could be tuned, from a continuous response (with UV-initiation) to a discontinuous one (with ATRP). The authors

have suggested that this pH-responsive behavior is likely the result of a more homogeneous structure for ATRP-initiated nanogels.

Nanogels of *N*-(2-hydroxypropyl)methacrylamide and *N,N'*-bis(acryloyl)cystamine (**M**, Figure II-4) synthesized by RAFT-mediated CRCcP in inverse emulsion can behave as reduction-sensitive compounds⁸⁷ that are able to release an encapsulated drug (*e.g* a protein) under reductive conditions, as reported by Klok *et al.* The diameter of these nanogels varies from 100 to 200 nm, which eventually characterizes them as microgels more than nanogels.

II-7. Functionalizing, extending and coupling: taking advantage of the ‘living’ character of CRCcP

As already emphasized, chains of CRCcP-derived nanogels can be re-activated, and various derivatized structures of controlled chain length can be achieved: from hairy nanogels, to core-shell structures to macroscopic networks (see Figure II-13). These compounds show great potential in different fields, such as drug delivery,⁸ antibacterial polymers, mono- or multilayer coatings, or adhesives⁹. As such, the nanogels have to be well-defined (hence the control over the polymerization), and functionalized, to answer specific needs, or deliver a drug to a specific part of the body for instance.

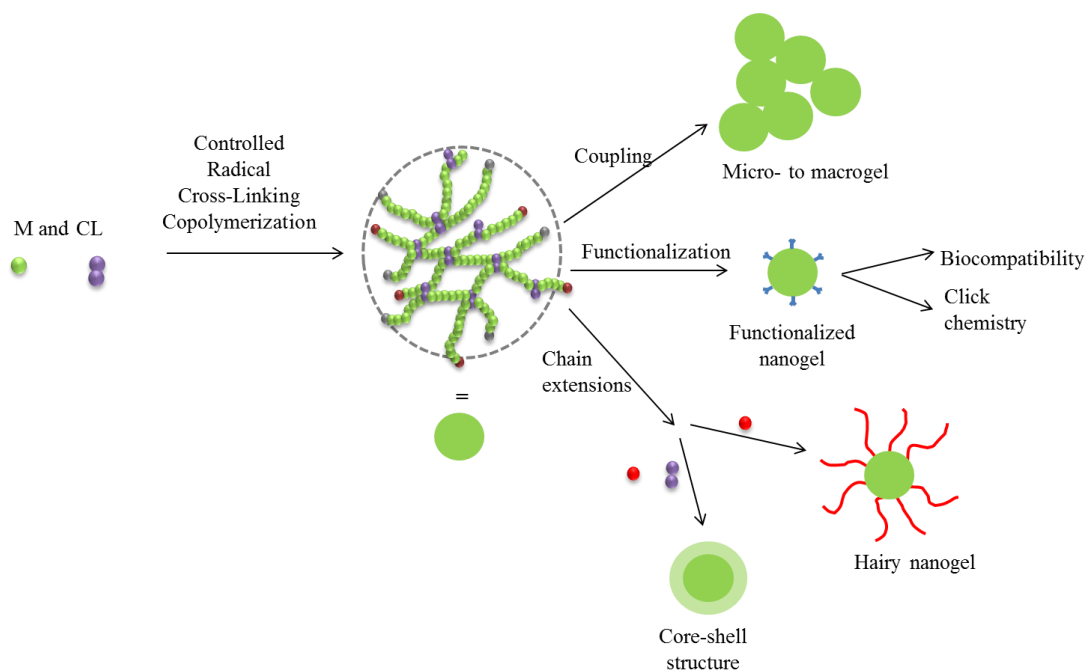


Figure II-13. The controlled character of CRCcP offers possibilities to derivative various architectures *e.g.* core-shell, hairy nanogel, functionalized or coupled nanogels. No new feed of mediating agent is added during the second-generation reaction.

II.7.1 Chain extensions

Adding a new monomer feed to the reaction medium allows the polymerization to resume, resulting in the formation of a core-shell structure. For instance, Zhang *et al.* have reported the one-pot synthesis of microgels of surprisingly narrow dispersity (in the range of 1.01), using ethylene glycol dimethacrylate (**C**, Figure II-4) *via* so-called atom transfer radical precipitation polymerization (ATRPP)¹¹⁵. In comparison, FRCcP leads either to polydisperse particles for a low amount of cross-linker, or to coagulation for a high concentration of cross-linker. Using ATRP-mediated CRCcP - instead of FRCcP - further allows the functionalization of the particles, either adding a co-monomer in the polymerization, or grafting polymer brushes (here, poly(2-hydroxyethyl methacrylate)) onto the surface.

Core-shell structures have been obtained by Perrier *et al.*⁷⁹, by chain extension with styrene, of a parent poly(MMA-*r*-EGDMA) nanogel generated by RAFT-mediated CRCcP,

forming star-like cross-linked copolymers. Near total conversion (>97%) is obtained without gelation and without losing the control over the polymerization. Thermal analyses performed by DSC have shown two glass transition temperatures: one corresponding to the PS arms, while the other being attributed to the parent nanogel.

II.7.2 Coupling and functionalization

Large surface area is one of the main characteristics of nanogel, which allows the branched copolymers to be tailored *via* functionalization, and thus better suit the final application. Functionalization of nanogels has been reported *via* different means, depending on the targeted applications. Two types of functionalization are predominant. This can be achieved i) before or during the copolymerization¹¹⁶ through the use of the parent nanogel as a macro-initiator or as a macromolecular chain transfer agent (macro-CTA), or ii) at the completion of the copolymerization, involving a reaction between functions already present on the nanogel –including the remaining PDBs.

The former method has been reported by An *et al.*¹¹³, following RAFT-derived dispersion polymerization of NIPAm, using *N,N'*-methylene bisacrylamide (**L** in Figure II-4) as cross-linker, and poly(*N,N*-dimethylamino acrylamide) as macro-CTA. This strategy has effectively yielded a core-shell structure with a thermoresponsive core. The diameter of the final nanogel has been found to increase with the ratio of cross-linker, and increasing the ratio of monomer over macro-CTA results in the formation of microgels.

Tai *et al.* have described thermoresponsive gels¹¹⁶ made from PEG-based monoacrylates and up to 30% of ethylene glycol dimethacrylate (**C** in Figure II-4). Lately, Xiong *et al.* reported the synthesis of ionic liquids nanogels *via* RAFT, and have then functionalized them with poly(*N*-isopropylamide) *via* surface grafting polymerization¹¹⁷. Highly monodispersed PMMA microgels, synthesized *via* RAFT with either dipropylene glycol

diacrylate or trimethylolpropane triacrylate as cross-linker, have been further functionalized by Zeng *et al.*, with poly(2-hydroxyethyl methacrylate) brushes grafting onto, *via* surface-initiated RAFT¹¹⁸.

Matyjaszewski *et al.* and Saunders *et al.* have independently reported the combination of controlled radical polymerization and click chemistry (CuAAC)^{60, 119} to achieve coupling cross-linked polymeric networks. Saunders *et al.* have shown that colloidal stability has not been impaired by the coupling of the polymeric particles, while functionalization remains possible, due to the remaining PDB (see Figure II-14). Wang *et al.* have taken advantage of the remaining PDBs on their 3D single chain cyclized nanogel synthesized *via* RAFT homopolymerization of ethylene glycol dimethacrylate (C, Figure II-4) to functionalize the vinyl double bonds with 2-mercaptoethanol *via* Michael addition⁹³.

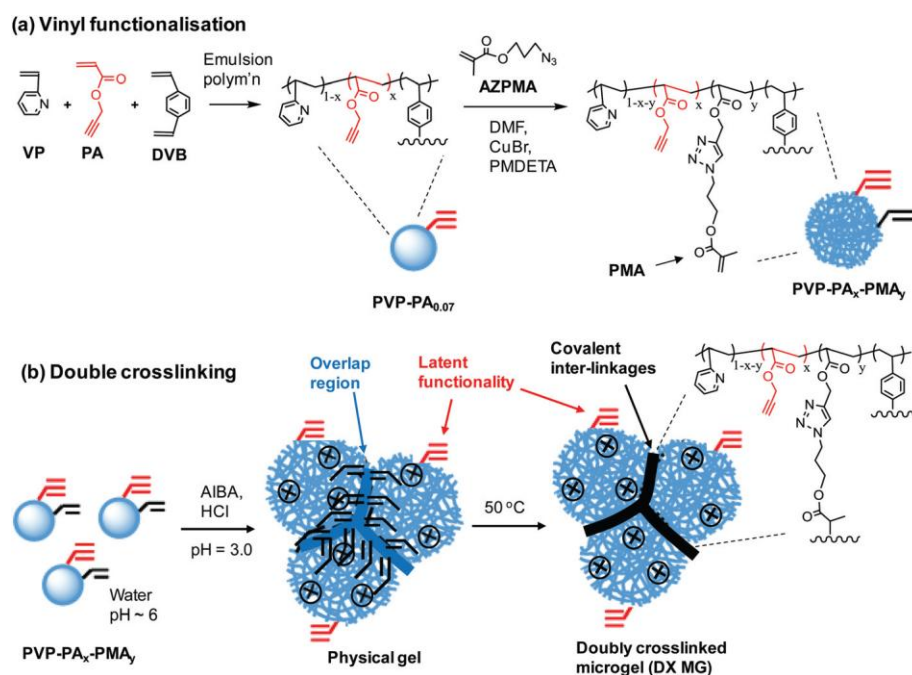


Figure II-14. Synthesis of doubly cross-linked microgels as depicted by Saunders *et al.*⁶⁰

Copyright RSC.

Zhuang, Zhang *et al.* have reported the RAFT-induced CRCcP of vinylbenzyl chloride with divinylbenzene (**A**, Figure II-4). After depositing the gel on graphene sheets, they have used the chloride function in Friedel-Craft reactions, to ensure the stability of the structure¹²⁰. In this case, the RAFT-derived gels have been used as precursors to 3D-network of graphene nanosheets, and contributes to the porosity of the final material.

Thus, CRCcP mediated by NMP, ATRP and RAFT mechanisms has been proven a very efficient method for forming polymeric networks of nano-, micro- or macroscopic dimensions. The equilibrium between propagating and dormant species allows for: i) a delayed gelation, but even more interestingly, ii) the relaxation of the chains and diffusion of the monomer during the copolymerization, leading to very different polymer networks than those obtained by FRCcP.

While CRCcP-derived networks have been thought to be more homogeneous than FRCcP-derived gels, this assumption has recently been questioned by Oppermann *et al.* These authors have indeed reported that CRCcP-derived gels are viewed as more homogeneous than FRCcP ones, because their cross-linking density is lower. Another important aspect of the architecture is the ratio of cyclization reactions during the copolymerization: all PDBs engaged in cyclization are PDBs that will not contribute to the increase of the network size. Last but not least, the 'living' character of CRCcP allows for further functionalization and/or coupling of the gels, and for chain extension reactions.

III. Modeling of controlled radical cross-linking copolymerization

As discussed in the previous section, various characterization methods have been employed to probe the internal structure of nanogels, including NMR spectroscopy, SEC,

DLS, TEM or AFM imaging, rheology, conductimetry¹. In recent years, several research groups have also developed computational modeling of CRCcP processes. The main results of these modeling are assessed in this section and will be compared between them, while pointing out some limitations. Main hypotheses of each type of model are first presented.

There are three distinct possibilities for modeling a polymerization reaction in general (Fig. II-15), including: i) the deterministic models –based on differential equations, ii) the statistical (or stochastic) models – based on statistics with one master equation, as first developed by Flory and Stockmayer, and finally iii) the computational simulations¹²¹.

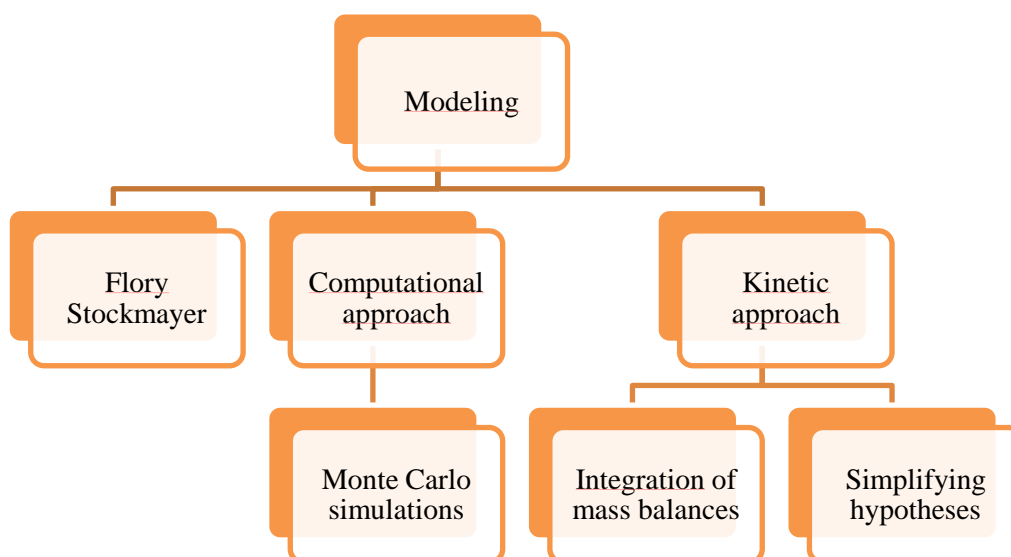


Figure II-15. Approaches used to model CRCcP, and main related models reported.

Several decades ago, Gillespie had already stated the main differences between stochastic approach vs. deterministic models¹²². The two following formalisms have been proposed for mathematically describing the time behavior of a spatially homogeneous chemical system:

i) the *kinetic approach* regards the time evolution as a continuous, wholly predictable process which is governed by a set of coupled, ordinary differential equations, referred to as the “reaction-rate equations”;

ii) the *statistical approach* relates to the time evolution as a “random-walk” process governed by a single differential-difference equation called the “master equation”.

The former approach is derived from differential equations, while the most common stochastic approach corresponds to the Flory and Stockmayer model, or variations of this model, in particular to take cyclization reactions into account.

A more recent approach is referred to as the *computational simulation in space*; a prime example of it is the Monte Carlo simulation (MC).¹²³ This simulation is run using model hypotheses (see paragraphs III.1.2 and III.1.3). The MC simulation is not to be confused with the Kinetic Monte Carlo (KMC) model, which will not be discussed here, since to the best of our knowledge, no KMC model has been applied to CRCcP.

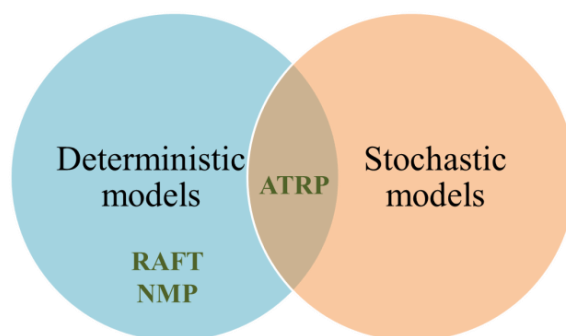


Figure II-16. Repartition of models most often used in the description of CRCcP processes.

To the best of our knowledge, the modelling CRCcP *via* the stochastic method has only been reported in the context of ATRP, independently by Matyjaszewski *et al.* and Armes *et al.*^{44, 123, 124}.

III.1 The Flory and Stockmayer model, and their derivatives.

Statistical or stochastic models give estimations of the kinetics. One limitation of this approach, however, is that only average properties of the copolymers can be calculated, since the “history” of the polymerization is ‘re-calculated’ by the models. Time is not seen as a continuum, but as a succession of time intervals during which elementary reactions can occur. Furthermore, the 3 main statistical models, namely, the Flory Stockmayer (FS), the “off lattice” (OL), and the so-called dynamic lattice liquid (DLL) models ignore the detailed chemical structure of the final compounds (monomer, cross-linker, initiator, solvent, etc). Since these models are statistical, they are based on the repetition of a large number of modeling experiments, in order to access the mean values of the properties. A comparison of these three models is proposed in paragraph III.1.4.

Polanowski, Matyjaszewski *et al.* have modelled ATRP-mediated CRCcP *via* FS, OF or DLL methods. Main differences between these three models in this context include the occurrence of cyclization, differences in the reactivity of the different double bonds, and the “cooperative movement concept” of DLL (see Figure II-17).

The first model of a FRCcP is the one developed by Flory (1941)^{111, 125} and Stockmayer (1943)^{112, 126, 127}. The model of Stockmayer describes a radical cross-linking copolymerization. It is adapted from the model published by Flory several years before, on gelation behavior during polycondensation. Flory introduced a parameter α , defined as the probability that two polymer chains be part of the same cross-linked macromolecule. As such, gelation occurs when α reaches the value of 1: the model considers that gelation occurs as long as there is at least one cross-linking unit per polymer chain.

Stockmayer's model is based on several hypotheses: i) the chemical nature of the monomer and cross-linker does not matter; ii) all double bonds exhibit the same reactivity during the whole polymerization; iii) solvent dilution is not taken into account; iv) cyclization does not occur, v) cross-linking reactions are irreversible.

On the basis of these hypotheses, Stockmayer's model allows determining the monomer conversion at which gelation occurs. However, because the model only gives average values, the dispersity of molar mass distribution cannot be determined in this way.

Experimentally, the position of the double bond, *i.e.* in the monomer, in the cross-linker, or PDB's of a growing polymer chain, can have a dramatic influence on its reactivity, which is not considered by the model. Several experimental studies have demonstrated that medium dilution influences the occurrence of cyclization^{65, 66}.

On this basis, the FS model often predicts the occurrence of the gelation point before that observed experimentally. This is because FS model considers that gelation takes place as long as there is at least one cross-linking unit per polymer chain. In reality, all PDB's consumed *via* intramolecular cross-linking are *de facto* not available for intermolecular cross-linking. Thus, the amount of cross-linker that can be incorporated in the polymeric network per primary chain can be higher than 1.

Two important parameters of the FS model include the branching density (ρ), and the weight-average degree of polymerization of the primary chains (denoted as P). Stockmayer has stated that gelation occurs if $\alpha_c \rho (P - 1) = 1$, *i.e.* one cross-linking point per primary chain. This is true as long as cyclization is absent¹²⁷.

Armes and Billingham have used this product, ρP , to compare two cross-linkers (C and E in Figure II-4), on the grounds that their reactivity should be similar. However, E is characterized by a higher steric hindrance compared to C. In the latter case, the product ρP is

equal to 0.99, meaning that while the copolymer is still soluble, the system is very close to the gel point. In the case of **E**, the ratio of cross-linker has to be increased by 10% before the product ρP reaches the value of 1. The authors thus hypothesized that this difference was due to the occurrence of cyclization with **E**, while the system was deemed ‘ideal’ with **C** (only intermolecular cross-linking in this case).⁴⁴

While Stockmayer’s theory is very useful to model gelation, and obtain average values of molar mass, it has been established that its simplifying hypotheses generally underestimate the conversion at gel point. In order to obtain a more complete set of data, kinetics models have been developed.

III.2 Kinetic models

A kinetic model considers the polymerization as a set of interdependent differential equations. Once the interdependent equations are solved, it allows accessing both average data and the accurate distribution of molar mass¹²⁸. While FS models a “reconstructed history of the polymerization” based on statistics, *i.e.* data extracted from the model represent a statistical probability of what the experimental data is, kinetic approaches preserve the “history of the polymerization” *via* the solution of differential equations¹²⁹.

Copolymerizations are modeled as systems of differential equations describing the concentration evolution of both reagents and products. It is a popular modeling method as it is based on mathematical calculations, viewing time as a continuous parameter.

In particular, full chain length dispersity of nanogels can be obtained *via* these methods, by merely counting each of the resulting possible copolymers and their probabilities. However, because it is based on interdependent differential equations, several assumptions have to simplify the problem set, to reduce the computing time (see Figure II-18 below).

For instance, the method of the moments is one of the most used tools to solve differential equations of a deterministic model. Zhu *et al.* have recently published a review on this method¹²⁹.

It has first been used in modeling by Bamford and Tampa in the 1950s¹³⁰. Since then, it has proven its versatility in modeling of conventional and controlled radical polymerization, in solution, in continuous or batch processes¹²⁹.

In simplifying the mass balance equations, the method of the moments allows determining average properties of final polymers but not, for example, their full molar masses distribution or the distribution of the branching density. It also eliminates the dependence of the polymerization rate constant on the kinetic chain length, but this limitation has been overcome by using other models^{131, 132}. While these simplifications may be used in simple examples, their execution in a concept of CRCcP may be confusing.

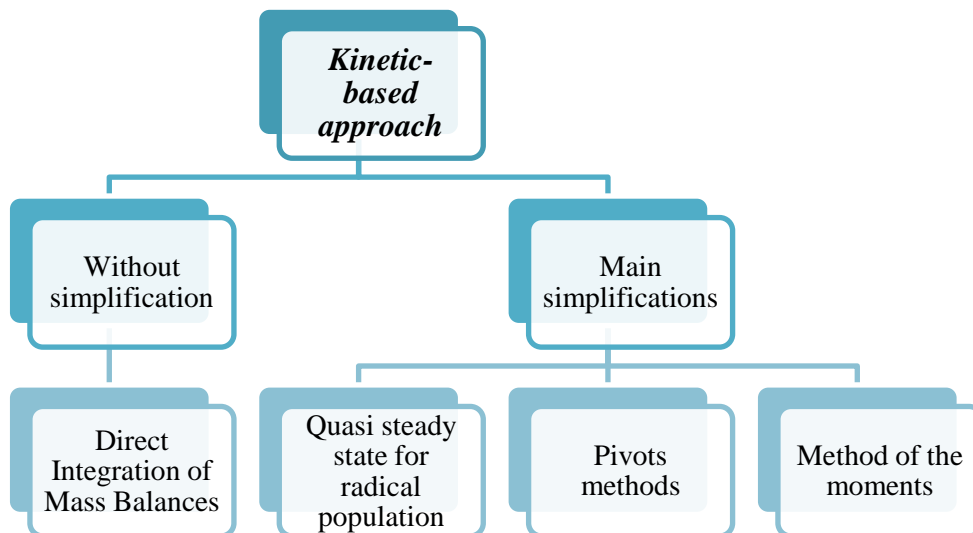


Figure II-18. Kinetic-based approaches of modeling CRCcP, and the most common simplifications used.

The most usual simplifications include the quasi stationary state approximation (QSSA) of radical species, the ‘mono-radical assumption’, *i.e.* considering only one radical

per macromolecule, or the ‘mono-capping assumption’, *i.e.* only one capping/dormant end per macromolecule, and the assumption of equal reactivity for all double bonds. Hereafter are compared the main hypotheses made in modeling CRCcP *via* deterministic tools.

While the direct integration of mass balances allows accounting, not only for the average properties, but also for the molar mass distribution, it is yet time-consuming, especially considering that the differential equations are interdependent.

Zhu *et al.* have published several articles pertaining to the kinetic modeling of controlled radical polymerizations^{121, 133}. They have also reported the modeling of RAFT-induced CRCcP in semi-batch conditions, in the specific case where triethylene glycol dimethacrylate (**N**, Figure II-4)⁶² or *N,N'*-methylene bis(acrylamide) (**L**, Figure II-4)⁹¹ has been employed as a cross-linker. They have used the pseudo-kinetic rate constant and the method of the moments to simplify differential equations. Noteworthy, they have differentiated *primary cyclization* (the formation of ‘loops’ on a primary chain) and *secondary cyclization* (the formation on a cross-linking bridge between two primary chains already connected). Second cyclization is included in the branching density with inter-molecular cross-linking. They have found that gelation can be delayed - or even suppressed - by adjusting the feeding ratio of cross-linker. For their system, gelation occurs at 70% of conversion in batch, and over 90% in semibatch process. On the other hand, the higher the instantaneous concentration in cross-linker is, the higher the cross-linking density is.

Poly, Taton *et al.* have also developed a very simple kinetic model describing a CRCcP process¹³⁴. They have hypothesized that: i) all radical centers are initiated at the same time; ii) the characteristic propagation time is longer than the species diffusion; iii) no termination or other side reaction occurs; iv) the reactivity of the radicals does not depend on the length of the growing polymer chains. They have restricted the cross-linkers used to those of divinyl symmetrical structure, and have considered that the formation of a cross-linking

bridge is not reversible. This model has led to two parameters: α_{inter} , which corresponds to the degree of cyclization in the polymer, and the β parameter, defined as the proportionality ratio between the volume of a macromolecule, and the sum of volumes of its monomeric units. As such, the latter parameter can be viewed as an indicator of the swelling ratio. However, these simplifications also prevent the model from accessing the real “history of the polymerization”.

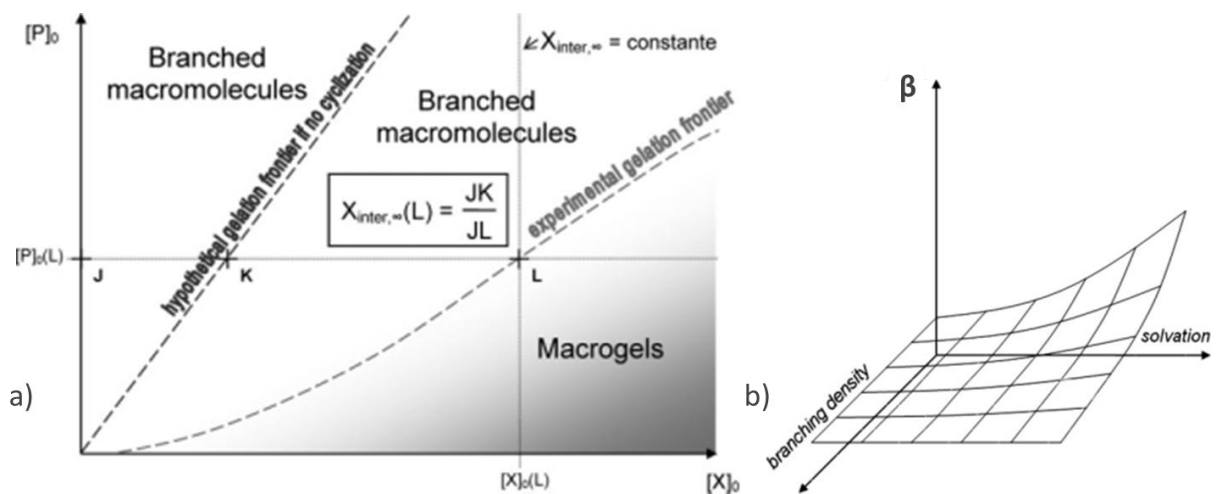


Figure II-19. Results of the deterministic model of Taton, Poly *et al.*¹³⁴: a) determination of the proportion of inter-molecular cross-linking from gelation frontiers, for complete conversion of double bonds and a fixed value of concentration; b) qualitative dependence of β on solvation and branching density.

III.3.1 Mono-or multi-radical assumptions

The assumption of “multi-radical macromolecules” is a controversial subject¹³⁵. While this possibility does not exist for linear polymers (there is only one active or dormant radical per macromolecule), the case of cross-linked polymer is more complex. As long as only cyclization (intramolecular cross-linking) occurs, there is still only one active or capped chain end. However, as soon as intermolecular cross-linking takes place, more than one active or dormant radical may exist on the same polymer chain.

Lazzari and Storti¹³⁶ have explained that only a handful of radicals are in fact active at any given time, and that the equilibrium between active and dormant chains always favors the dormant ones. Hence, there is usually only one active radical per macromolecule, but intermolecular cross-linking events allow several dormant centers to coexist in a same chain¹⁰⁰. The presence of dormant chain ends actually seems to favor intermolecular cross-linking (as opposed to intra-molecular, which would occur in the case of multi-radical macromolecules).

III.3.2 Cyclization

A few groups have attempted to either minimize the occurrence of cyclization⁹⁴ or, in contrast, to made it predominant^{69, 70, 137} (see for instance the *in situ* DE-ATRP, described in section II-3 of this chapter). It is worth reminding that the deviation of the experimental gel point, from that calculated by the FS theory is explained by the occurrence of intramolecular cross-linking (=cyclization). It is thus crucial to quantify the extent of cyclizations in CRCcP, since these events lower the number of PDBs available for intermolecular branching⁴⁰. Most of the deterministic approaches modeling a CRCcP accounts for intramolecular cross-linking, as reported by the groups of Fukuda⁶¹, Zhu⁹⁴, Penlidis¹³⁸ or Giudici^{53, 139}.

For instance, Penlidis *et al.* have established that in NMP-derived CRCcP, the dilution, the concentrations in cross-linker and the ratio monomer/initiator play a predominant role on the occurrence of cyclization¹⁰⁷: for instance, the presence of the nitroxide mediating agent in the copolymerization medium decreases the occurrence of cyclization. They have verified their findings by studying NMP-mediated CRCcP of styrene with divinylbenzene. The effect of dilution on increased cyclization has also been demonstrated by Giudici *et al.*⁵³, which has been further established *via* SEC/RI/MALLS measurements. Zhu *et al.*⁹⁴ have reported that i)

Flory's criterion (ρP) is a good approximation of the gel point, as long as cyclization is absent from the process, and ii) cyclization significantly delays the gelation.

III.3.3 Modeling CRCcP of vinyl/divinyl systems

The groups of Penlidis and Vivaldo-Lima^{100, 138, 140}, and of Zhu⁹⁴ have modeled CRCcP processes induced by ATRP, NMP and/or RAFT of a vinyl/divinyl system. For this purpose, the authors have not taken into account specifications regarding the chemical structure of the monomer or the cross-linker⁹⁴. In Table II-6 are compared the methods reported by Penlidis and Vivaldo-Lima, and Zhu regarding the RAFT-mediated CRCcP of a vinyl/divinyl systems.

This method has been employed with the view at simplifying calculations. The model developed by Penlidis *et al.* has assessed the delayed gelation observed experimentally¹⁴⁰.

The so-called pseudo-kinetic rate constant method may be used for long polymer chains, or if the co-monomer ratio in the polymer is far from 0.5. The latter assumption is generally valid in CRCcP, the amount in cross-linker being most often low compared to the amount in vinyl monomer. While Zhu *et al.* count the active and dormant chain-ends in a macromolecule, Vivaldo-Lima, Penlidis *et al.* differentiate the active radical centers, the RAFT agent capping moieties, the RAFT agent located between two polymeric segments, and the RAFT agents placed at the end of a polymer chain (Figure II-19).

Table II-6. Comparison of the models of RAFT-mediated CRCcP developed by Penlidis, Vivaldo-Lima *et al.*¹⁴⁰; and Zhu *et al.*⁹⁴

	Penlidis and Vivaldo-Lima ¹⁴⁰	Zhu ⁹⁴
Method	Method of the moments ¹²⁹	Method of the moments ¹²⁹
Hypotheses	i) Multifunctional macromolecules; ii) Pseudo-kinetic rate constant; iii) 3 different types of dormant radical centers (vinyl monomer, divinyl cross-linker, PDB); iv) all primary chains have the same kinetic length post-gelation	i) Neglect of intermediate radicals; ii) Pseudo-kinetic rate constant ¹⁴¹
Polymer denomination	Using the number of monomer units, the number of active centers, the total number of RAFT capping agents, the number of RAFT agents attached to 2 segments of the polymer, the number of RAFT agents attached to the polymer during the reversible chain transfer.	Using the number of monomer units, the number of radical centers, and the number of RAFT capping agents.
Results	Delayed gelation as [RAFT] increases; Studies of homopolymerization of styrene, and copolymerization of styrene with divinylbenzene; Hypothesis (iv) leads to a dispersity of 1 post-gelation, which is recognized as unrealistic	Delayed gelation as [RAFT] increases; Cyclization significantly delays the gelation; Highly cross-linked copolymers can only be observed near the gelation, or in the final stage of cross-linking (in the absence of gelation)

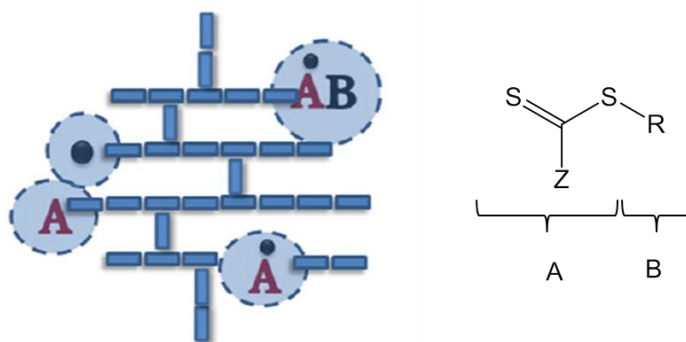


Figure II-19. Representation of the growing macromolecule with active radical centers, dormant chain ends, and RAFT agent placed either at the end of a chain, or between two polymeric segments, described by Vivaldo-Lima, Penlidis *et al*¹⁴⁰

Since both ATRP and NMP are based on the persistent radical effect^{23, 25}, while RAFT polymerization is based on a degenerative transfer¹⁴², modeling these CRP methods leads to different sets of propagation equations.

The deterministic models do not account for the detailed structure of the chemical compounds, so the fact that the controlling agent is a nitroxide- or a copper-based species should not influence the model that much. NMP needs higher temperature than ATRP, but in a model, temperature can be translated as a parameter with a ‘low’ and ‘high’ level. Ideally, the copolymerization of indefinite vinyl and divinyl co-monomers should be compared for the three types of mechanisms. This has been realized by the groups of Vivaldo-Lima and Penlidis who have reported models of NMP, ATRP and RAFT-mediated CRCcP of vinyl and divinyl co-monomers (not taking into account their structures)^{100, 138, 140}. The method of the moments has been applied for the three processes, in order to simplify the differential equations. Changes between the models from the three types of CRCcP (NMP, RAFT or ATRP) are not due to a change in the conditions or the chemical structures of the reagents used, but rather to differences in the polymerizations’ mechanisms.

III.3 Computational simulations in space*III.3.1 Monte-Carlo simulations*

While kinetic approaches are accurate, they need extensive calculations. To circumvent this inconvenient, computational simulations in space have been studied.

Computational simulations in space are based on the percolation theory and imply a finite number of molecules in the simulated ‘space’, *i.e.* border conditions are of utmost importance. Since the simulation only takes into account a limited number of molecules, the border conditions must reflect the outer copolymerization medium without changing the growth of the polymer chains inside the borders^{123, 143}. The most usual computational simulation is called Monte Carlo simulation (MC, see Scheme II-11). This MC simulation allows to skip the resolution of a set of differential equations (see table II-7). However, MC simulations need the support of a model (usually a derivative from FS). Furthermore, the expected results of such simulations are usually: i) the monomer conversion at which gelation occurs; ii) the average molar mass of the polymer.

Table II-7. Advantages and limitations of Monte-Carlo simulations.

Advantages	Limitations
Statistical simulation algorithm exact	Multiple runs to ensure the statistical probability are respected
No approximation of dt by Δt	Restricted to a finite number of molecules
Easy to code	Computational time-consuming
No need of large memory space	Need a ‘reliable’ and uniform random number generator
No set of differential equations	

Armes *et al.* have resorted to a MC simulation to study the consumption of the cross-linker during ATRP-mediated CRCcP of 2-hydroxypropyl methacrylate and ethylene glycol dimethacrylate (**C**; Figure II-4)⁴⁴. Interestingly, the authors have proven that their ATRP-

derived CRCcP has a behavior close to ideal according to the FS model, meaning that all double bonds have similar reactivity, and almost no cyclization has been observed.

Matyjaszewski *et al.* have also employed this simulation to model the CRCcP of methyl acrylate and ethylene glycol dimethylacrylate *via* ATRP¹⁴⁴. The authors have compared two MC simulations, based either on an OL model or on a DLL one. They have observed that a simulation based on OL model essentially gives the same results as a simulation based on the FS theory. However, the MC simulation based on the DLL model (cooperative motion concept) predicts much more accurately the gel point of the CRCcP. It also shows that decreasing the expected DP of the primary chains allows delaying the gelation.

The MC simulation can also predict the microstructure of nanogels and does not require so many assumptions or hypotheses as in deterministic models. Advantages and limitations of the MC simulations are presented in Table II-7. Until now, MC has mostly been used to model ATRP systems^{144, 145}. Below are described two models used in MC simulations, the off lattice (OL) model and the dynamic lattice liquid (DLL) model. OL and DLL models are then compared to FS.

III.3.2 Off lattice: an update of Flory and Stockmayer theory.

The off lattice (OL) model is a derivatives on the FS theory, to allow cyclization phenomena to be taken into account, albeit with a low probability. However, in contrast to the dynamic lattice liquid (DLL) model, the OL model does not take into account the spatial distribution of PDBs. Gao, Polanewski and Matyjaszewski¹⁴⁴ have used the OL model in the context of ATRP-initiated CRCcP assuming that: i) termination and chain transfer reactions are negligible, and ii) the reactivity of the vinyl groups is constant and independent of the kinetic chain length. A comparison of this model with FS can be found on paragraph *III.3.4*.

III.3.3 Dynamic Lattice Liquid: cooperative motion concept.

The DLL model is based on cooperative motions^{146, 147}, explicated below in Figure II-17. In this model, all lattice sites are occupied by one molecule (density factor $F=1$), be it a molecule of solvent, initiator, monomer, cross-linker, or monomer unit. Each lattice particle is assigned a vector, the direction of which is random. It is also assumed that related systems have some excess volume, so that molecules have enough space to vibrate around their position defined by lattice sites. The principle of the DLL model is that for a single diffusion step, *i.e.* a molecule (= lattice particle) moving to a neighboring lattice site, a cooperative movement of its neighbors must take place, resulting in the occupation of the newly vacant lattice site. A molecule can move only if its movement is compensated by the cooperative rearrangement of the molecules around it. After this movement, all lattice sites must still be occupied by one molecule (no lattice site may contain 2 molecules, or be empty). It is important to note that the algorithm takes into account a 2-D polymeric system.

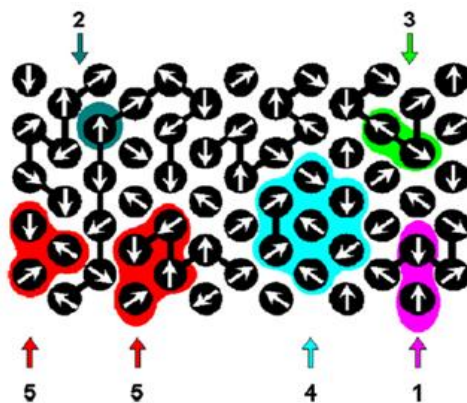


Figure II-17. Illustration of the vector field representing attempts of molecular displacements toward neighbouring lattices sites in the dynamic lattice liquid model. Local situations 1 to 4 are unsuccessful, while the two situations labelled ‘5’ will evolve, no polymer chain would be broken, no lattice sites would be left empty or two crowded. Copyright AIP Publishing¹⁴⁶

III.1.4 Comparison of the FS model with the computer simulations

The FS, OL and DLL models are all statistical: they reconstruct the “polymerization history”, based on the probability of collisions between molecules. As such, only average properties of the polymers can be obtained. In Table II-8 are compared the principles and hypotheses of the three stochastic models

Table II-8. Comparison of the principles and hypotheses of FS model with off lattice (OL) and dynamic lattice liquid (DLL) models.

<i>Flory Stockmayer (FS)</i>	<i>Off Lattice (OL)</i>	<i>Dynamic Lattice Liquid (DLL)</i>
Monomers placed in a virtual reaction space	Monomers placed in a virtual reaction space	Cooperative motion concept, based on rearrangements of beads within closed dynamic loops.
No size and dimension	No size and dimension	
No coordinate or specific position in space	No coordinate or specific position in space	Enables efficient treatment of the diffusion problems in mixtures.
No cyclization.	Limited cyclization.	Accounts for cyclization, and for the spatial distribution of pendent vinyl groups.
All the double bonds have the same reactivity.	Does not take into account the position of pendent vinyl groups (simulated gelation occurs before experimental one).	
Does not account for dilution	Does not account for dilution	Accounts for dilution
Expected results: gel point	Expected results: gel point	Expected results: gel point
	Often used for proteins folding/ interaction.	Valid even at high conversion.

Several groups have applied FS-based approaches in the context of a CRCcP. For instance, Polanowski and Matyjaszewski^{123, 124} have compared the three models (FS, OL,

DLL) that have been further challenged with a same set of CRCcP experimental data. Common hypotheses in the three models are as follows: i) the chemical structures of the components of the medium do not influence the copolymerization; ii) each elementary step of the process is irreversible; iii) all vinyl double bonds possess the same reactivity, and iv) no termination reaction takes place. . Simulated gel points have been estimated *via* the FS, OL and DLL models, and compared to the experimental value. Table II-9 compares the gel points simulated to the experimental one.

Table II-9. Comparison of the experimental gel point with simulated ones, using : i) FS model ; ii) MC simulation with an OL model ; iii) MC simulation with a DLL model.

	<i>Experimental gel point</i>	FS simulated	OL simulated	DLL simulated
Monomer conversion (%)	78	58	61	83

Note also that FS and OL models do not account for solvent dilution^{124, 144}. On the other hand, the DLL model predicts the gelation much more accurately, with an error of 6% of monomer conversion, though usually slightly over-estimating the experimental value. DLL also accounts for the dilution effect, since the ‘lattice sites’ match either the monomer, cross-linker, monomer unit or solvent. Thus, DLL seems to be a more accurate way to model CRCcP¹⁴⁴. Further modeling *via* DLL has shown that gelation occurs *via* the cross-linking of already cross-linked polymers; the cross-linked copolymers involved in the gelation process already containing more than 50 primary chains¹²³.

Table II-10 below summarizes and compares hypotheses and limitations possible for i) statistical models, ii) Monte-Carlo simulations and iii) deterministic models.

Table II-10. Comparison of the stochastic, Monte-Carlo and deterministic models, and their outcomes.

	FS model	Monte-Carlo simulations	Kinetics models
Time-consuming	✓	✓	✓
Complex equations	X	X	✓
Several runs	✓	✓	X
Possibility of multi-radicals	X	✓	✓
Different reactivities	X	✓	✓
Accounts for cyclization	X	✓	✓
Average molar mass of the polymers	✓	✓	✓
Molar mass distribution and dispersity	X	X	✓
History of the polymerization	X	X	✓

A colored cell shows that the model is not the best for this hypothesis or result.

X : the hypothesis or result is not possible *via* the modeling process

✓ : the hypothesis or result is possible *via* the modeling process

III.4 Case study of CRCcP modeling: styrene/divinylbenzene

The copolymerization of styrene and divinylbenzene has been widely reported and modeled in the literature, including by FRCcP^{148, 149} and CRCcP, firstly by Penlidis *et al.* in the latter case¹⁰⁷. Copolymerization of styrene and divinylbenzene has also been achieved

under various conditions (see Table II-11), leading to dispersed polymeric networks or monolithic copolymers.

Table II-11. Controlled radical cross-linking copolymerizations of styrene (St) with divinylbenzene (DVB). In the case of modeling data, the hypotheses and main results are listed.

group	CRP method	Notes	ref
Solomon <i>et al.</i>	NMP	Copolymerization of styrene with DVB in solution, to form statistical microgels (<i>via</i> one step vinyl/divinyl copolymerization) or star microgel (<i>via</i> the arm-first approach, not available in FRP). SEC spectra show multimodal peaks. First report of CRccP of styrene and divinylbenzene.	2, 47, 150
Penlidis, Vivaldo-Lima <i>et al.</i>	NMP	Modeling Hypotheses: i) mono-radical assumption, ii) mono-function assumption, iii) gelation point for $M_n > 10^7$ g/mol., iv) diffusion controlled equations, v) accounts for termination Use of the method of the moments to simplify equations Results: Model fit exp. data up to 80% of conversion, more homogeneous network, control agent delays the gelation, do not influence the composition (no change of reactivity).	107
	NMP	Modeling Bayesian approach (detailed in Scheme II-13): Bayesian design determines the optimal experimental conditions (given previous reports) for an aimed outcome. The selected factors are the	151

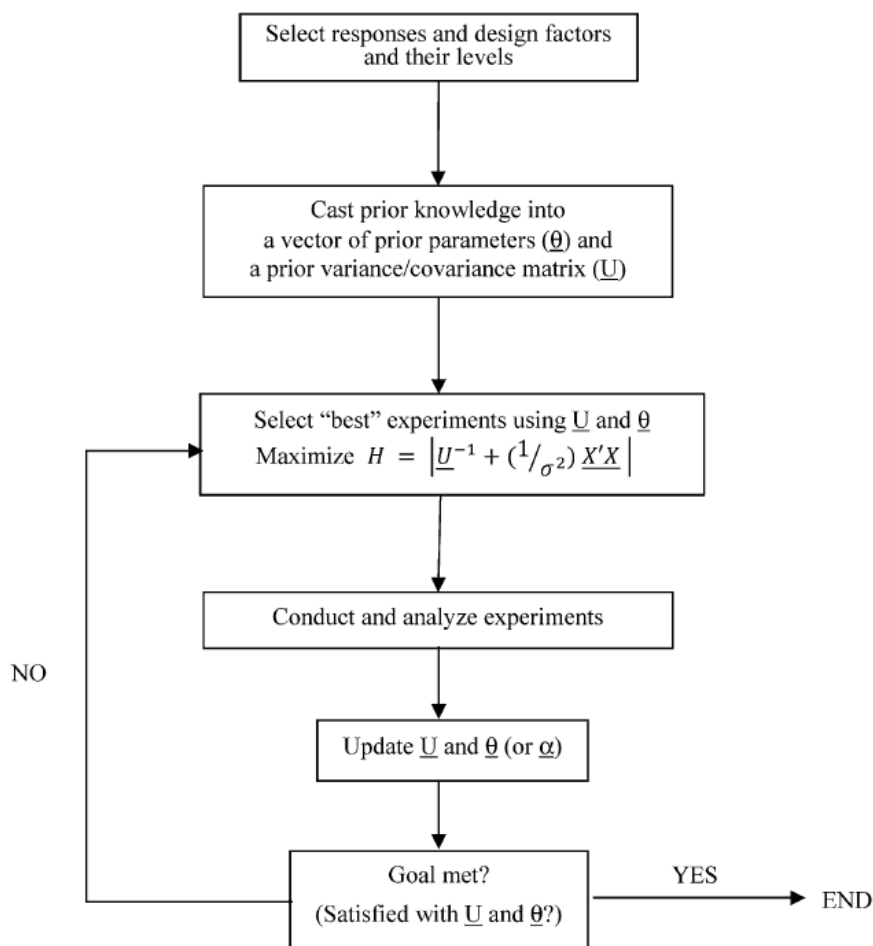
	main conditions susceptible of influencing the outcome (here, temperature, [St] and [DVB]) Results: conversion at gel point decrease when [N] increases; conversion at gel point decreases when [DVB] increases, minimal number of lab experiments in order to understand the relative influence of each factor.	
	Modeling Hypotheses: follow the Bayesian approach, multifunctional assumption, Results: conversion at gel point higher for NMP (60% vs 7% for FRCcP), higher swelling ratio (54% vs 35% for FRCcP), but levels down at high conversion, loss of control for [DVB]/[N] increasing (gelation as earlier as 56% of conversion). Evolution of molar masses and gel point were modeled with accuracy, loss of 'livingness' after gel point (too viscous).	54
	Experimental data. Synthesis of copolymer in aqueous suspension via NMP.	
	NMP Influence of the temperature and experimental conditions of the reactions. Comparison FRCcP vs NMP-mediated CRCcP of the system and influence on gelation.	53
Dias, Costa et al.	Modeling of cyclization in the St/DVB system. Hypotheses: Kinetic mechanism Results: Cyclization occurs when there are at least 3 monomer units between the radical and the pending double bond. The effect of cyclization is less visible on systems with a lower amount of DVB (5% compared to 50%).	139
	RAFT Synthesis of PS/DVB beads <i>via</i> aqueous suspension	12

		Three different RAFT agents used, change of the experimental conditions.	
Fréchet et al.	NMP	PS macroporous monolith (for chromatographic applications) via solution copolymerization. Results: control over the pores size by varying the reaction temperature, and the cross-linking density.	55, 152
Moad, Lima et al.	RAFT	Aim: PS monolith with added functionalities comparison of modeling of FRCcP /RAFT Hypotheses: diffusion-controlled copolymerization (high CL content modeled as well) Results: effect of [RAFT] on the synthesis (conversion and molar masses) <i>To fit the exp. data, some parameters had to take unrealistic values;</i> <i>Calculations time-consuming (for computer)</i>	43
	NMP	CRCcP in aqueous miniemulsion at 125°C, with 1%mol of DVB. Pending double bond conversion was determined by NMR and GC. Comparison of the particles size with different homogenizations methods. The polymerization rate and cross-linking density are lower in miniemulsion than in bulk.	48
Zetterlund, Okubo et al.	NMP	CRCcP in aqueous miniemulsion at 125°C, with 8.2%mol of DVB. Comparison of the gel point with Flory and Stockmayer theory (occurrence of cyclization, heterogeneity). Influence of the primary chain length on gelation: the higher the primary chain length, the lower the conversion at gel point (since they are more pending double bond on the chain).	57
	NMP	Comparison FRCcP and NMP-mediated CRCcP, in	153

		<p>micro-suspension, with 1%mol DVB.</p> <p>Mechanical properties remain constant for the particles synthesized via FRCcP whatever the monomer conversion. However, these properties increase nearly linearly with the conversion in nitroxide-mediated CRCcP. This is explained by the differences in network formation between FRP and NMP (even at low conversion, microgels are formed in FRCcP, but absent in NMP).</p>	
	NMP	<p>Copolymerization in aqueous miniemulsion and toluene solution at 125°C, with 3%mol of DVB.</p> <p>Deviation from FS theory influenced by the presence of hydrophobic tetradecane in large amount: experimental gelation occurs before the theoretical one. That is explained as an effect of the oil-water interface ([PDB] higher near the interface than in the droplets).</p> <p>This interface effect is further explored by using hydrophilic macroinitiator, to increase the concentration of styrene and PDB near the interface.</p>	58, 154, 155
Bibiao <i>et al.</i>	ATRP	<p>CRCcP of St with DVB (amount ranging from 3.3 to 20%mol) to form soluble branched copolymers.</p> <p>Conversions were determined by GC, and molecular weight confirmed by GPC.</p> <p>DVB is then used as cross-linker (around 3%mol) in the copolymerization of styrene and acrylonitrile.</p>	156

Penlidis *et al.* have made use of experimental data from previous literature for the so-called Bayesian model (see Scheme II-13 below), which allows determining the optimal experimental conditions for a targeted outcome. Selected factors include the temperature and concentrations of the monomer and cross-linker. These factors can be given different values

(or levels), to study their influence over the final copolymer architecture. The prior knowledge about the copolymerization is then used to design three ‘optimal’ experiments that can be used to compare the relative influence of each factor on the final copolymer. Since the model can incorporate data from other reports, it is a better fit for the experimental data.



Scheme II-13. Bayesian process used by Nabifar, Hernandez-Ortiz, Vivaldo-Lima and Penlidis¹⁵¹ for modeling the nitroxide-mediated CRCcP of styrene and divinylbenzene, using experimental data already reported.

Costa *et al.* have modeled the St/DVB CRCcP *via* NMP, and also investigated the same synthesis *via* RAFT copolymerization in aqueous suspension¹². On the experimental data front, the group of Zetterlund and Okubo has studied the nitroxide-mediated CRCcP of styrene and divinylbenzene in dispersed media^{48, 57, 58, 154}. Comparing experimental data with

the FS model, they have found that gelation occurs sooner in the process when the nitroxide-mediated CRCcP occurs in dispersed media, instead of in solution⁵⁷.

IV. Conclusions

Controlled radical cross-linking copolymerization (CRCcP) is an ever-increasing field of research. The control exercised over the copolymerization, the delayed gelation due to the equilibrium between active and dormant species, the possibility for functionalizing, extending primary chains or coupling copolymers, to cite just a few, make CRCcP a very versatile methodology to directly access highly branched copolymers. While (nano)gels synthesis *via* CRCcP has been extensively applied to numerous comonomers, the characterization of the resulting copolymers is often more difficult than for linear counterpart.

Modeling of CRCcP has been developed, *via* three main approaches, including the stochastic, the computational and the deterministic ones. Each of these methods possesses its own advantages and weaknesses. A common drawback drawback is the need to make hypotheses in order to actually solve the different equations, be it the master equation of a statistical model, or the differential equations of a deterministic approach. However, models have shown a good fit to CRCcP experimental data, which opens up opportunities to anticipate the effect of the internal structure of related networks on their overall properties.

The comparison of homogeneity of the CRCcP-derived and FRCcP-based networks has not yet been answered. FRCcP and CRCcP have been compared *via* several methods, such as light scattering, dynamic experiments or swelling ratio of macrogels. While CRCcP delays gelation through its dormant/active chains mechanism, gel point can be pushed further in the polymerization kinetics *via* several processes, none the least in situ deactivation-enhanced atom transfer radical polymerization.

CRCcP offers undeniable advantages to polymer synthesis: apart from the proven control over the length of the primary chains, the ‘livingness’ of the polymerization enables the syntheses of various complex macromolecular or supra-macromolecular designs. Indeed, while the control achieved is not yet total, the enthusiasm for CRCcP is ever-increasing. Several processes of post-polymerization coupling of the nanogels have been evoked, as well as combining two types of mechanisms during the same synthesis.

The following chapters of this thesis report the synthesis of nanogels *via* a cobalt-mediated radical cross-linking copolymerization, abbreviated as CMRCcP. Such nanogels have been first designed using vinyl acetate and divinyl adipate as cross-linker. Then, synthesis of nanogels made of ionic liquid monomeric units has been achieved *via* the same CMRCcP method, leading to either hydrophilic or hydrophobic compounds depending on the counter anion. The resulting ionic liquid-based materials have been studied for coating applications on different substrates.

References

1. D. Taton, in *Macromolecular Engineering: Precise Synthesis, Materials Properties, Applications*, 2011, vol. 2, pp. 1007-1056.
2. S. Abrol, M. J. Caulfield, G. G. Qiao and D. H. Solomon, *Polymer*, 2001, **42**, 5987-5991.
3. H. Gao and K. Matyjaszewski, *Progress in Polymer Science*, 2009, **34**, 317-350.
4. N. Ide and T. Fukuda, *Macromolecules*, 1998, **32**, 95-99.
5. IUPAC, *Pure Appl. Chem.*, 2007, **79**, 1801-1829.
6. A. Concheiro and C. Alvarez-Lorenzo, *Advanced Drug Delivery Reviews*, 2013, **65**, 1188-1203.
7. D. J. Siegwart, J. K. Oh and K. Matyjaszewski, *Progress in Polymer Science*, 2012, **37**, 18-37.
8. J. K. Oh, R. Drumright, D. J. Siegwart and K. Matyjaszewski, *Progress in Polymer Science*, 2008, **33**, 448-477.

9. N. Sanson and J. Rieger, *Polymer Chemistry*, 2010, **1**, 965-977.
10. W. Li, J. A. Yoon, M. Zhong and K. Matyjaszewski, *Macromolecules*, 2011, **44**, 3270-3275.
11. K. Min and K. Matyjaszewski, *Central European Journal of Chemistry*, 2009, **7**, 657-674.
12. M. A. D. Gonçalves, V. D. Pinto, R. C. S. Dias, J. C. Hernández-Ortiz and M. R. P. F. N. Costa, *Macromolecular Symposia*, 2013, **333**, 273-285.
13. A. J. Sivaram, P. Rajitha, S. Maya, R. Jayakumar and M. Sabitha, *Wiley Interdisciplinary Reviews: Nanomedicine and Nanobiotechnology*, 2015, **7**, 509-533.
14. D. M. Eckmann, R. J. Composto, A. Tsourkas and V. R. Muzykantov, *Journal of Materials Chemistry B*, 2014, **2**, 8085-8097.
15. R. T. Chacko, J. Ventura, J. Zhuang and S. Thayumanavan, *Advanced Drug Delivery Reviews*, 2012, **64**, 836-851.
16. J. K. Oh, S. A. Bencherif and K. Matyjaszewski, *Polymer*, 2009, **50**, 4407-4423.
17. E. Faure, C. Falentin-Daudré, T. S. Lanero, C. Vreuls, G. Zocchi, C. Van De Weerd, J. Martial, C. Jérôme, A. S. Duwez and C. Detrembleur, *Advanced Functional Materials*, 2012, **22**, 5271-5282.
18. J. Poly, E. Ibarboure, J. F. Le Meins, J. Rodriguez-Hernandez, D. Taton and E. Papon, *Langmuir*, 2011, **27**, 4290-4295.
19. G. Liu and Z. An, *Polymer Chemistry*, 2014, **5**, 1559-1565.
20. H. Kawaguchi, *Polymer International*, 2014, **63**, 925-932.
21. X. Zhang, S. Malhotra, M. Molina and R. Haag, *Chemical Society Reviews*, 2015, **44**, 1948-1973.
22. T. Ueki, S. Sawamura, Y. Nakamura, Y. Kitazawa, H. Kokubo and M. Watanabe, *Langmuir*, 2013, **29**, 13661-13665.
23. J. Nicolas, Y. Guillaneuf, C. Lefay, D. Bertin, D. Gimes and B. Charleux, *Progress in Polymer Science*, 2013, **38**, 63-235.
24. R. B. Grubbs, *Polymer Reviews*, 2011, **51**, 104-137.
25. K. Matyjaszewski, *Macromolecules*, 2012, **45**, 4015-4039.
26. K. Matyjaszewski and J. Xia, *Chemical Reviews*, 2001, **101**, 2921-2990.
27. A. E. Smith, X. Xu and C. L. McCormick, *Progress in Polymer Science*, 2010, **35**, 45-93.
28. T. Fukuda and A. Goto, in *Polymer Science: A Comprehensive Reference, 10 Volume Set*, 2012, vol. 3, pp. 119-157.

29. M. U. Kahveci, Y. Yagci, A. Avgeropoulos and C. Tsitsilianis, in *Polymer Science: A Comprehensive Reference, 10 Volume Set*, 2012, vol. 6, pp. 455-509.
30. P. J. Lutz and F. Peruch, in *Polymer Science: A Comprehensive Reference, 10 Volume Set*, 2012, vol. 6, pp. 511-542.
31. D. Konkolewicz, S. Perrier, D. Stapleton and A. Gray-Weale, *Journal of Polymer Science, Part B: Polymer Physics*, 2011, **49**, 1525-1538.
32. A. M. Caminade, D. Yan and D. K. Smith, *Chemical Society Reviews*, 2015, **44**, 3870-3873.
33. L. Espinosa-Pérez, J. C. Hernández-Ortiz, P. López-Domínguez, G. Jaramillo-Soto, E. Vivaldo-Lima, P. Pérez-Salinas, A. Rosas-Aburto, A. Licea-Claverie, H. Vázquez-Torres and M. J. Bernad-Bernad, *Macromolecular Reaction Engineering*, 2014, **8**, 564-579.
34. K. Matyjaszewski and N. V. Tsarevsky, *Journal of the American Chemical Society*, 2014, **136**, 6513-6533.
35. V. Schmidt, R. Borsali and C. Giacomelli, *Langmuir*, 2009, **25**, 13361-13367.
36. C. F. Van Nostrum, *Soft Matter*, 2011, **7**, 3246-3259.
37. E. S. Read and S. P. Armes, *Chemical Communications*, 2007, 3021-3035.
38. R. K. O'Reilly, C. J. Hawker and K. L. Wooley, *Chemical Society Reviews*, 2006, **35**, 1068-1083.
39. C. Legros, M. C. De Pauw-Gillet, K. C. Tam, S. Lecommandoux and D. Taton, *Polymer Chemistry*, 2013, **4**, 4801-4808.
40. J. E. Elliott and C. N. Bowman, *Macromolecules*, 1999, **32**, 8621-8628.
41. IUPAC, *Pure Appl. Chem.*, 2007, **79**, 1801.
42. IUPAC, *Pure Appl. Chem.*, 2007, **79**, 1801.
43. P. López-Domínguez, J. C. Hernández-Ortiz, K. J. Barlow, E. Vivaldo-Lima and G. Moad, *Macromolecular Reaction Engineering*, 2014, **8**, 706-722.
44. I. Bannister, N. C. Billingham, S. P. Armes, S. P. Rannard and P. Findlay, *Macromolecules*, 2006, **39**, 7483-7492.
45. D. C. Forbes and N. A. Peppas, *Polymer*, 2013, **54**, 4486-4492.
46. N. Ide and T. Fukuda, *Macromolecules*, 1997, **30**, 4268-4271.
47. S. Abrol, P. A. Kambouris, M. G. Looney and D. H. Solomon, *Macromolecular Rapid Communications*, 1997, **18**, 755-760.
48. P. B. Zetterlund, M. N. Alam, H. Minami and M. Okubo, *Macromolecular Rapid Communications*, 2005, **26**, 955-960.

49. C.-D. Vo, J. Rosselgong, S. P. Armes and N. C. Billingham, *Macromolecules*, 2007, **40**, 7119-7125.
50. D. Konkolewicz, A. Gray-Weale and S. Perrier, *Polymer Chemistry*, 2010, **1**, 1067-1077.
51. J. Poly, D. James Wilson, M. Destarac and D. Taton, *Macromolecular Rapid Communications*, 2008, **29**, 1965-1972.
52. R. Scherf, L. S. Müller, D. Grosch, E. G. Hübner and W. Oppermann, *Polymer*, 2015, **58**, 36-42.
53. M. A. D. Gonçalves, V. D. Pinto, R. C. S. Dias, M. R. P. F. N. Costa, L. G. Aguiar and R. Giudici, *Macromolecular Reaction Engineering*, 2013, **7**, 155-175.
54. A. J. Scott, A. Nabifar, J. C. Hernández-Ortiz, N. T. McManus, E. Vivaldo-Lima and A. Penlidis, *European Polymer Journal*, 2014, **51**, 87-111.
55. C. Viklund, A. Nordström, K. Irgum, F. Svec and J. M. J. Fréchet, *Macromolecules*, 2001, **34**, 4361-4369.
56. M. N. Alam, P. B. Zetterlund and M. Okubo, *Macromolecular Chemistry and Physics*, 2006, **207**, 1732-1741.
57. Y. Saka, P. B. Zetterlund and M. Okubo, *Polymer*, 2007, **48**, 1229-1236.
58. P. B. Zetterlund, N. Alam and M. Okubo, *Polymer*, 2009, **50**, 5661-5667.
59. Q. Ren, F. Gong, C. Liu, G. Zhai, B. Jiang, C. Liu and Y. Chen, *European Polymer Journal*, 2006, **42**, 2573-2580.
60. R. Farley, S. Halacheva, J. Bramhill and B. R. Saunders, *Polymer Chemistry*, 2015, **6**, 2512-2522.
61. T. Norisuye, T. Morinaga, Q. Tran-Cong-Miyata, A. Goto, T. Fukuda and M. Shibayama, *Polymer*, 2005, **46**, 1982-1994.
62. X. Li, W.-J. Wang, B.-G. Li and S. Zhu, *Macromolecular Reaction Engineering*, 2015, **9**, 90-99.
63. Y. Li and S. P. Armes, *Macromolecules*, 2005, **38**, 8155-8162.
64. J. Rosselgong, S. P. Armes, W. R. S. Barton and D. Price, *Macromolecules*, 2010, **43**, 2145-2156.
65. J. Rosselgong and S. P. Armes, *Macromolecules*, 2012, **45**, 2731-2737.
66. J. Rosselgong and S. P. Armes, *Polymer Chemistry*, 2015, **6**, 1143-1149.
67. Q. Yu, M. Zhou, Y. Ding, B. Jiang and S. Zhu, *Polymer*, 2007, **48**, 7058-7064.
68. Q. Yu, Y. Zhu, Y. Ding and S. Zhu, *Macromolecular Chemistry and Physics*, 2008, **209**, 551-556.

69. Y. Zheng, H. Cao, B. Newland, Y. Dong, A. Pandit and W. Wang, *Journal of the American Chemical Society*, 2011, **133**, 13130-13137.
70. B. Newland, Y. Zheng, Y. Jin, M. Abu-Rub, H. Cao, W. Wang and A. Pandit, *Journal of the American Chemical Society*, 2012, **134**, 4782-4789.
71. L. A. Picos-Corrales, A. Licea-Claverie and K. F. Arndt, *Journal of Polymer Science, Part A: Polymer Chemistry*, 2012, **50**, 4277-4287.
72. W. Shen, Y. Chang, G. Liu, H. Wang, A. Cao and Z. An, *Macromolecules*, 2011, **44**, 2524-2530.
73. T. C. Krasia and C. S. Patrickios, *Macromolecules*, 2006, **39**, 2467-2473.
74. M. Achilleos, T. Krasia-Christoforou and C. S. Patrickios, *Macromolecules*, 2007, **40**, 5575-5581.
75. M. Achilleos, T. M. Legge, S. Perrier and C. S. Patrickios, *Journal of Polymer Science, Part A: Polymer Chemistry*, 2008, **46**, 7556-7565.
76. J. Poly, D. J. Wilson, M. Destarac and D. Taton, *Macromolecular Rapid Communications*, 2008, **29**, 1965-1972.
77. F. Ercole, H. Thissen, K. Tsang, R. A. Evans and J. S. Forsythe, *Macromolecules*, 2012, **45**, 8387-8400.
78. S. Quan, Y. Wang, A. Zhou, P. Kumar and R. Narain, *Biomacromolecules*, 2015, **16**, 1978-1986.
79. B. Liu, A. Kazlauciusas, J. T. Guthrie and S. Perrier, *Macromolecules*, 2005, **38**, 2131-2136.
80. J. Tan, X. Rao, J. Yang and Z. Zeng, *RSC Advances*, 2015, **5**, 18922-18931.
81. M. A. M. Oliveira, C. Boyer, M. Nele, J. C. Pinto, P. B. Zetterlund and T. P. Davis, *Macromolecules*, 2011, **44**, 7167-7175.
82. H. Gao, K. Min and K. Matyjaszewski, *Macromolecules*, 2007, **40**, 7763-7770.
83. H. Gao, K. Min and K. Matyjaszewski, *Macromolecules*, 2009, **42**, 8039-8043.
84. K. O. Jung, D. J. Siegwart, H. I. Lee, G. Sherwood, L. Peteanu, J. O. Hollinger, K. Kataoka and K. Matyjaszewski, *Journal of the American Chemical Society*, 2007, **129**, 5939-5945.
85. Q. Chen, Y. Xu, X. Cao, L. Qin and Z. An, *Polymer Chemistry*, 2014, **5**, 175-185.
86. Q. Liu, P. Zhang, A. Qing, Y. Lan and M. Lu, *Polymer*, 2006, **47**, 2330-2336.
87. H. Wutzel, F. H. Richter, Y. Li, S. S. Sheiko and H. A. Klok, *Polymer Chemistry*, 2014, **5**, 1711-1719.

88. D. Taton, J. F. Baussard, L. Dupayage, J. Poly, Y. Gnanou, V. Ponsinet, M. Destarac, C. Mignaud and C. Pitois, *Chemical Communications*, 2006, **18**, 1953-1955.
89. J. Rieger, C. Grazon, B. Charleux, D. Alaimo and C. Jérôme, *Journal of Polymer Science, Part A: Polymer Chemistry*, 2009, **47**, 2373-2390.
90. C. Grazon, J. Rieger, N. Sanson and B. Charleux, *Soft Matter*, 2011, **7**, 3482-3490.
91. D. Wang, X. Li, W. J. Wang, X. Gong, B. G. Li and S. Zhu, *Macromolecules*, 2012, **45**, 28-38.
92. J. Kamada, K. Koynov, C. Corten, A. Juhari, J. A. Yoon, M. W. Urban, A. C. Balazs and K. Matyjaszewski, *Macromolecules*, 2010, **43**, 4133-4139.
93. Y. Zheng, B. Newland, H. Tai, A. Pandit and W. Wang, *Chemical Communications*, 2012, **48**, 3085-3087.
94. R. Wang, Y. Luo, B.-G. Li and S. Zhu, *Macromolecules*, 2008, **42**, 85-94.
95. T. Terashima, S. Nishioka, Y. Koda, M. Takenaka and M. Sawamoto, *Journal of the American Chemical Society*, 2014, **136**, 10254-10257.
96. R. Baudry and D. C. Sherrington, *Macromolecules*, 2006, **39**, 1455-1460.
97. P. Besenius, S. Slavin, F. Vilela and D. C. Sherrington, *Reactive and Functional Polymers*, 2008, **68**, 1524-1533.
98. M. Chisholm, N. Hudson, N. Kirtley, F. Vilela and D. C. Sherrington, *Macromolecules*, 2009, **42**, 7745-7752.
99. Q. Yu, Z. Qin, J. Li and S. Zhu, *Polymer Engineering & Science*, 2008, **48**, 1254-1260.
100. J. C. Hernández-Ortiz, E. Vivaldo-Lima, M. A. Dubé and A. Penlidis, *Macromolecular Theory and Simulations*, 2014, **23**, 429-441.
101. D. Wang, W. J. Wang, B. G. Li and S. Zhu, *AIChE Journal*, 2013, **59**, 1322-1333.
102. Q. Yu, F. Zeng and S. Zhu, *Macromolecules*, 2001, **34**, 1612-1618.
103. T. Zhao, Y. Zheng, J. Poly and W. Wang, *Nat Commun*, 2013, **4**, 1873-1881.
104. K. Matyjaszewski and N. V. Tsarevsky, *Nature Chemistry*, 2009, **1**, 276-288.
105. J. Bastide and L. Leibler, *Macromolecules*, 1988, **21**, 2647-2649.
106. J. A. Yoon, C. Gayathri, R. R. Gil, T. Kowalewski and K. Matyjaszewski, *Macromolecules*, 2010, **43**, 4791-4797.
107. J. C. Hernández-Ortiz, E. Vivaldo-Lima, L. M. F. Lona, N. T. McManus and A. Penlidis, *Macromolecular Reaction Engineering*, 2009, **3**, 288-311.
108. J. Bastide, L. Leibler and J. Prost, *Macromolecules*, 1990, **23**, 1821-1825.
109. Q. Yu, S. Xu, H. Zhang, Y. Ding and S. Zhu, *Polymer*, 2009, **50**, 3488-3494.

110. M. Roa-Luna, G. Jaramillo-Soto, P. V. Castañeda-Flores and E. Vivaldo-Lima, *Chemical Engineering and Technology*, 2010, **33**, 1893-1899.
111. P. J. Flory, *Journal of the American Chemical Society*, 1941, **63**, 3083-3090.
112. W. H. Stockmayer and H. Jacobson, *The Journal of Chemical Physics*, 1943, **11**, 393.
113. Y. Xu, Y. Li, X. Cao, Q. Chen and Z. An, *Polymer Chemistry*, 2014, **5**, 6244-6255.
114. D. C. Forbes and N. A. Peppas, *Polymer*, 2013, **54**, 4486-4492.
115. J. Jiang, Y. Zhang, X. Guo and H. Zhang, *Macromolecules*, 2011, **44**, 5893-5904.
116. H. Tai, A. Tochwin and W. Wang, *Journal of Polymer Science, Part A: Polymer Chemistry*, 2013, **51**, 3751-3761.
117. Y. Zuo, N. Guo, Z. Jiao, P. Song, X. Liu, R. Wang and Y. Xiong, *Journal of Polymer Science, Part A: Polymer Chemistry*, 2015, **54**, 169-178.
118. J. Tan, M. Yu, X. Rao, J. Yang and Z. Zeng, *Polymer Chemistry*, 2015, **6**, 6698-6708.
119. P. L. Golas and K. Matyjaszewski, *Chemical Society Reviews*, 2010, **39**, 1338-1354.
120. W. Zhao, Z. Hou, Z. Yao, X. Zhuang, F. Zhang and X. Feng, *Polymer Chemistry*, 2015, **6**, 7171-7178.
121. E. Mastan, X. Li and S. Zhu, *Progress in Polymer Science*, 2015, **45**, 71-101.
122. D. T. Gillespie, *Journal of Physical Chemistry*, 1977, **81**, 2340-2361.
123. P. Polanowski, J. K. Jeszka and K. Matyjaszewski, *Polymer*, 2010, **51**, 6084-6092.
124. P. Polanowski, J. K. Jeszka, W. Li and K. Matyjaszewski, *Polymer*, 2011, **52**, 5092-5101.
125. P. J. Flory, *Journal of Physical Chemistry*, 1942, **46**, 132-140.
126. W. H. Stockmayer, *The Journal of Chemical Physics*, 1943, **11**, 45-55.
127. W. H. Stockmayer, *The Journal of Chemical Physics*, 1944, **12**, 125-131.
128. E. Mastan, D. Zhou and S. Zhu, *Journal of Polymer Science Part A: Polymer Chemistry*, 2014, **52**, 639-651.
129. E. Mastan and S. Zhu, *European Polymer Journal*, 2015, **68**, 139-160.
130. C. H. Bamford and H. Tompa, *Transactions of the Faraday Society*, 1954, **50**, 1097-1115.
131. S. Zhu and A. E. Hamielec, *Macromolecules*, 1989, **22**, 3093-3098.
132. D. R. D'Hooge, M. F. Reyniers and G. B. Marin, *Macromolecular Reaction Engineering*, 2009, **3**, 185-209.
133. E. Mastan, X. Li and S. Zhu, *Progress in Polymer Science*, 2015.
134. J. Poly, D. J. Wilson, M. Destarac and D. Taton, *Journal of Polymer Science Part A: Polymer Chemistry*, 2009, **47**, 5313-5327.

135. R. C. S. Dias and M. R. P. F. N. Costa, *Macromolecular Theory and Simulations*, 2005, **14**, 243-255.
136. S. Lazzari, S. Hamzehlou, Y. Reyes, J. R. Leiza, M. R. P. F. N. Costa, R. C. S. Dias and G. Storti, *Macromolecular Reaction Engineering*, 2014, **8**, 678-695.
137. A. Aied, Y. Zheng, B. Newland and W. Wang, *Biomacromolecules*, 2014, **15**, 4520-4527.
138. J. C. Hernández-Ortiz, E. Vivaldo-Lima and A. Penlidis, *Macromolecular Theory and Simulations*, 2012, **21**, 302-321.
139. L. G. Aguiar, M. A. D. Gonçalves, V. D. Pinto, R. C. S. Dias, M. R. P. F. N. Costa and R. Giudici, *Macromolecular Reaction Engineering*, 2014, **8**, 282-294.
140. J. C. Hernández-Ortiz, E. Vivaldo-Lima, M. A. Dubé and A. Penlidis, *Macromolecular Theory and Simulations*, 2014, **23**, 147-169.
141. H. Tobita and A. E. Hamielec, *Polymer*, 1991, **32**, 2641-2647.
142. A. Gregory and M. H. Stenzel, *Progress in Polymer Science*, 2012, **37**, 38-105.
143. D. Konkolewicz, S. Sosnowski, D. R. D'Hooge, R. Szymanski, M. F. Reyniers, G. B. Marin and K. Matyjaszewski, *Macromolecules*, 2011, **44**, 8361-8373.
144. H. Gao, P. Polanowski and K. Matyjaszewski, *Macromolecules*, 2009, **42**, 5925-5932.
145. I. Bannister, N. C. Billingham and S. P. Armes, *Soft Matter*, 2009, **5**, 3495-3504.
146. P. Polanowski and T. Pakula, *The Journal of Chemical Physics*, 2002, **117**, 4022-4029.
147. P. Polanowski and T. Pakula, *The Journal of Chemical Physics*, 2003, **118**, 11139-11146.
148. O. Okay, *Progress in Polymer Science*, 2000, **25**, 711-779.
149. K. Dušek and M. Ilavský, *Journal of Polymer Science: Polymer Symposia*, 1975, **53**, 57-73.
150. L. Pille, A. G. Jhingran, E. P. Capareda and D. H. Solomon, *Polymer*, 1996, **37**, 2459-2464.
151. A. Nabifar, J. Hernandez-Ortiz, E. Vivaldo-Lima and A. Penlidis, *Macromolecular Symposia*, 2013, **324**, 19-32.
152. E. C. Peters, F. Svec, J. M. J. Fréchet, C. Viklund and K. Irgum, *Macromolecules*, 1999, **32**, 6377-6379.
153. T. Tanaka, T. Suzuki, Y. Saka, P. B. Zetterlund and M. Okubo, *Polymer*, 2007, **48**, 3836-3843.

154. P. B. Zetterlund, Y. Saka and M. Okubo, *Macromolecular Chemistry and Physics*, 2009, **210**, 140-149.
155. M. N. Alam, P. B. Zetterlund and M. Okubo, *Polymer*, 2009, **50**, 1632-1636.
156. G. Haidan, H. Wenyan, Z. Dongliang, G. Fanghong, L. Chunlin, Y. Yang, C. Jianhai and J. Bibiao, *Polymer*, 2008, **49**, 4101-4108.

Chapter III

Direct One-Pot Synthesis of Poly(vinyl acetate) and Poly(ionic liquid) Nanogels by Cobalt-Mediated Radical Cross-Linking Copolymerization

Abstract.

The bibliographic chapter has demonstrated the interest of using controlled radical cross-linking copolymerization to achieve polymeric nanogels. The reported methods include nitroxide-mediated radical polymerization, atom-transfer radical polymerization and reversible addition-fragmentation chain-transfer polymerization.

Here, nanogels of controlled kinetic chain length were synthesized by cobalt-mediated radical cross-linking copolymerization (CMRCcP) involving a vinyl monomer and a divinyl cross-linker. This strategy was first validated to achieve neutral poly(vinyl acetate) nanogels by CMRCcP of vinyl acetate and divinyl adipate as cross-linker, at 40 °C, in presence of a pre-synthesized alkyl-cobalt(III) precursor serving both as initiator and controlling agent, using ethyl acetate as solvent.

Poly(ionic liquid) nanogels were then directly obtained by CMRCcP of *N*-vinyl-3-ethyl imidazolium bromide, in presence of 1,13-divinyl-3-decyl diimidazolium bromide as cross-linker. Polymerizations could be conducted either in an organic solvent, *e.g.* dimethyl formamide or, more interestingly, in aqueous solution, demonstrating the robustness and the versatility of this one-step CMRCcP process. Chain extensions of PIL nanogels were also carried out in water, with the formation of core-shell structures, opening new avenues in the design of functionalized charged nanogels.

This part of the work has been published in Polymer Chemistry, RSC, DOI: 10.1039/C6PY00112B.

Introduction

IUPAC defines nanogels as soluble polymer networks with a dimension lower than 100 nm¹. Their three-dimensional internal structure results from both intra- and intermolecular cross-linking reactions. Owing to their low viscosity in comparison to linear homologues of same molar mass, nanogels find applications in coatings at high solid content², or as additives for organic binders³. Specifically, hydrophilic nanogels have emerged, mainly as novel carriers for drug delivery applications⁴⁻⁶. Common synthetic methods to obtain nanogels include: i) the post-cross-linking of pre-formed linear polymers, *e.g.* by chemical post-modification of polymer precursors possessing pendant reactive groups, or by radiation with a high energy source^{7, 8}, and ii) the free-radical cross-linking copolymerization (RCC) in dispersed media or in highly dilute solution⁹⁻¹². As predicted by Flory¹³ and Stockmayer^{14, 15}, RCC conducted under rather high concentrated solution, or in presence of high content of cross-linker, rapidly leads to macrogels, which eventually correspond to interconnected nano- and microgel particles. Furthermore, RCC provides little control over the internal network structure: both the kinetic chain length and the distribution of cross-link points within the final network are highly heterogeneous. This is attributed to both a very fast chain growth and extensive intramolecular cross-linking (cyclization) forming nano/microgels.

Controlled radical polymerization (CRP) methods have been anticipated to allow access to nano-, micro- and macrogels with a higher structural homogeneity^{9, 16-19}. In specific applications such as drug delivery for which structural homogeneity is momentous for controlling the kinetic of drug release, resorting to CRP is thought to be beneficial over conventional free-radical polymerization (FRP). In a RCC operating by CRP, indeed, much more primary chains start growing simultaneously from the early stage of the process, and chain growth is much slower favoring chain relaxation and translational diffusion²⁰. Hence intermolecular cross-linking reactions are more likely to occur, compared to a RCC by FRP.

Differences between FRP and CRP methods, in a context of RCC, have been supported by experimental findings both at the macroscopic level (e.g. *via* elastic or swelling analyses)^{18, 21} and microscopically through light scattering measurements. For instance, CRP-made networks exhibit higher swelling ratios and seem to be softer than those obtained by FRP. These differences have been often interpreted as being due to the formation of a more homogeneous network structure by CRP, compared to FRP. This, however, has been recently questioned by Oppermann *et al*²². Indeed, according to these authors, gels obtained by CRP appear to be more homogeneous only because they are much less densely cross-linked (reduced cross-linking efficiency) as compared to FRP²². Eventually, a CRP gel would not be more homogeneous than an FRP gel, if both compared gels had the same effective network density. In other words, CRP-derived gels do not necessarily exhibit a more even distribution of cross-link points.

Yet, the use of a controlling agent in RCC not only provides a better control of the kinetic chain length, but also enables the gel point to be postponed and to introduce larger amounts of cross-linker²³⁻²⁶. Last but not least, dormant chain-ends can be reactivated in gels prepared by CRP, allowing for chain extension and synthesis of core-shell structures^{9, 27}. “Controlled” RCC process can be implemented by nitroxide-mediated polymerization (NMP)^{28, 29}, reversible addition–fragmentation chain transfer (RAFT)³⁰⁻³² and atom transfer radical polymerization (ATRP)^{8, 26, 33, 34}. Here we wish to describe nanogel synthesis induced by a particular CRP method, referred to as the cobalt-mediated radical polymerization (CMRP) using Co(acac)₂ as controlling agent^{35, 36}. This technique is particularly suited to control the polymerization of nonconjugated vinyl monomers -also called less activated monomers (LAM) in the context of the RAFT process³⁵ -such as vinyl esters (vinyl acetate (VAc)³⁷, vinyl levulinate (VLV)³⁸ or vinyl ester 1,2,3 triazolium³⁹), vinyl chloride (VC)⁴⁰, *N*-vinylpyrrolidone (NVP)⁴¹, or *N*-vinyl-3-alkyl-imidazolium bromide (VRImBr)^{42, 43} or

bis(trifluoromethylsulfonyl)imide (VRImTf₂N)⁴⁴ monomers. VAc has been here tested first so as to validate the possibility to achieve nanogels by cobalt-mediated radical cross-linking copolymerization (CMRccP). This method has then been applied to VRImBr.

Polymerization of the latter monomers leads to cationically charged polymers entering in the category of so-called poly(ionic liquid)s (PILs)⁴⁵⁻⁴⁸. PILs are polymeric versions of ILs, representing a new class of polyelectrolytes of tunable solubility, showing an anhydrous ionic conductivity up to 10⁻⁵ S/cm at room temperature⁴⁹, and a broad range of glass transition temperatures. Owing to their combined properties emanating from IL units and their polymeric nature, PILs find potential applications in areas, such as analytical chemistry⁵⁰, biotechnology, gas separation⁵¹, dispersants, solid ionic conductors for energy, catalysis⁵², etc⁵³. Exchange of the counterion (= metathesis reaction) provides an additional method for the variation of PIL properties⁵⁴.

In this contribution, synthesis of both PVAc and PIL nanogels of controlled chain length is described. CMRccP of VAc (or VRImBr) using divinyladipate (or an IL-type) cross-linker is performed in solution, in presence of a pre-synthesized alkyl-cobalt(III) complex (R-Co(acac)₂, **1**) as a single-component initiator/mediating agent. The capacity to further extend these nanogels is also explored. The synthesis of nanogels composed of a neutral poly(vinyl acetate-co-divinyl adipate) central core and a cationic poly(vinyl imidazolium-co-divinyl imidazolium) outer shell is also described.

Experimental part

Materials

Dimethylformamide (DMF, Aldrich, 99.8%) and methanol (MeOH, HPLC grade) were dried over molecular sieves and degassed by bubbling Argon during 15 minutes. Milli-Q

water and acetone were degassed by bubbling Argon during 30 minutes. 2,2,6,6-tetramethylpiperidine 1-oxy (TEMPO) (98%, Aldrich) was used as received. The alkylcobalt(III) ($R\text{-Co}(\text{acac})_2$) was synthesized as already reported⁵⁵. *N*-Vinyl-3-ethyl imidazolium bromide (VETImBr) was synthesized as reported in the literature⁵⁴. 1,13-Divinyl-3-decyl diimidazolium bromide (DVIImBr) was synthesized following the same strategy. Vinyl acetate (VAc) was dried on calcium hydride to eliminate water, and cryo-distilled prior to use. Divinyl adipate (DVA, Aldrich, >99%) was employed as received.

Characterization

Molar masses and dispersities of PVAc-type samples were determined by SEC in THF eluent, Jasco pump equipped with a set of 3 TSK gel HXL (4 000, 3 000, and 2 000) 7.5_300 mmSEC columns, a RI Jasco detector and a UV Jasco detector at 290 nm connected in series (flow rate 1mL.min⁻¹). Molar masses and dispersities of hydrophilic polymers (*i.e.* of poly(*N*-Vinyl-3-ethyl imidazolium bromide) (PVEtImBr) and of poly(vinyl alcohol) (PVA) obtained after methanolysis of poly(vinyl acetate) (PVAc)-based samples) were determined by aqueous size exclusion chromatography (SEC), in an eluent containing NaCl (0.1M) and trifluoroacetic acid (TFA, 0.1% vol), at 30 °C (pressure: 540 PSI; flow rate: 1 mL/min), with a SEC equipped with a pre-column (PSS NOVEMA Max analytical 10 micron, 8.0Í50 mm) and a linear column (PSS NOVEMA Max analytical linear S micron 8.0Í300 mm). Molar masses and dispersities of PVEtImBr were also evaluated, after anion exchange of bromide anions by bis(trifluoromethylsulfonyl)imide anions, by SEC in THF in an eluent containing 10 mM LiTf₂N, according to the procedure reported by Matyjaszewski *et al.*⁵⁰. ¹H NMR spectra of the reaction medium and final product were recorded at 25 °C with a Bruker spectrometer (400 MHz), in DMSO-d₆. Weight loss during SEC experiments, and in particular after filtration step on 0.2 µm filter prior to injection, was evaluated by column-free SEC equipped with an

Optilab rex detector, in THF containing 10 mM LiTf₂N at 25 °C. Nanogel solutions at 1 mg/mL in THF containing 10 mM LiTf₂N were injected with and without filtration step. Peak area of each run corresponds to the concentration of the sample. Comparison of the peak areas with and without filtration determines the possible weight loss of nanogels during filtration (results are summarized in Figure SIII-5).

Transmission electron microscopy (TEM) images were recorded on a Hitachi H7650 microscope working at 80 kV equipped with a GATAN Orius 11 Megapixel camera. Samples were prepared via deposition of a drop of polymeric solution on a TEM grid, and subsequent absorption of solution excess.

Syntheses

Typical copolymerization of vinyl acetate (VAc) with divinyl adipate (DVA) via CMRccP in ethyl acetate.

In a typical experiment, DVA (0.12 g , 6 mol.%, $6 \cdot 10^{-4}$ mol.) was introduced in a Schlenk tube and degassed by at least three successive vacuum-Argon cycles, followed by 20 minutes under vacuum. To this initial mixture, 10 mL of dried degassed ethyl acetate were added under Argon. Vinyl acetate (1mL, 10^{-2} mol.) was then added under Argon. The flask was thermostated at 40 °C and a solution of alkyl-cobalt(III) initiator (1.1 mL, $1.6 \cdot 10^{-4}$ mol., solution at 1.5 M) in CH₂Cl₂ was then added. The reaction medium was stirred. Aliquots were taken out regularly, to monitor the monomer conversion by ¹H NMR. Samples for THF SEC were quenched by adding TEMPO in the vials and ethyl acetate was removed by dialysis against MeOH before SEC analysis. The results of these syntheses are shown in Table III-1 and Figures III-1 and III-3.

Chapter III : *Direct One-Pot Synthesis of Nanogels by CMRCcP*

Synthesis of PVAc nanogel (with 4 mol.% DVA) and resumption by N-vinyl-3-ethyl imidazolium bis(trifluoromethylsulfonyl)imide.

DVA (0.08 g, 4 mol.%, 4.10^{-4} mol.) was introduced in a Schlenk tube and degassed by at least three successive vacuum-Argon cycles, followed by 20 minutes under vacuum. To this initial mixture, 10 mL of dried degassed ethyl acetate were added under Argon. Vinyl acetate (1 mL, 10^{-2} mol.) was then added under Argon. The flask was thermostated at 40° C and a solution of alkyl-cobalt(III) initiator (1.1 mL, $1.6 \cdot 10^{-4}$ mol., solution at 1.5M) in CH_2Cl_2 was then added. The reaction medium was stirred. An aliquot was removed after 120h to check the conversion and molecular parameters. The reaction medium was then rapidly transferred to a flask containing degassed VEtImNTf₂ (2 g, 5.10^{-3} mol.) and the mixture was stirred for 48h at 30°C. Results are summarized in Figure III-5 and SIII-4.

Typical procedure for the methanolysis of PVAc nanogels.

In a typical experiment, a solution of NaOH in MeOH at 10 g.L⁻¹ (volume V) was added under strong stirring into the same volume V of the polymeric solution in MeOH at 100 g.L⁻¹. During hydrolysis, poly(vinyl alcohol) precipitates and, after several hours of reaction, the polymer was recovered by decantation followed by purification by several cycles of decantation/ supernatant removal/ addition of a minimal amount of water to solubilize the polymer. Mechanism is summarized in Figure SIII-2.

Typical copolymerization of N-vinyl-3-ethyl imidazolium bromide (VEtImBr) with 1,13-divinyl-3-decyl diimidazolium bromide (DVIImBr) via CMRccP in organic solvent.

VEtImBr (1 g, $6.2 \cdot 10^{-3}$ mol.), and divinyl imidazolium DVIImBr (0.1 g, 4.8 mol.%) were introduced in a Schlenk tube and degassed by 3 vacuum-argon cycles, and 12 mL of dry, degassed solvent were added. The solvent was either dimethylformamide (DMF) or a mixture

of DMF and methanol (MeOH) (8/4) (v/v). The flask was thermostated at 30 °C and a solution of alkyl-cobalt(III) initiator (0.40 mL, $7.4 \cdot 10^{-5}$ mol., solution at 1.18M) in CH_2Cl_2 was then added. The reaction medium was stirred. Aliquots were regularly removed for determining the conversion by ^1H NMR. Samples for SEC H_2O were quenched by TEMPO and DMF is removed by dialysis before SEC H_2O (results are summarized in Table S4, and in Figure S5). Samples for SEC in THF undergo an anion exchange before SEC THF. The results of these syntheses are shown in Table III-2, entries 1 to 6 and Figure III-6.

Aqueous copolymerization of N-vinyl-3-ethyl imidazolium bromide (VETImBr) and 1,13-divinyl-3-decyl diimidazolium bromide (DVIImBr) via CMRCcP.

A solution of alkyl-cobalt(III) initiator (0.40 mL, $7.4 \cdot 10^{-5}$ mol., solution at 1.18 M) in CH_2Cl_2 was introduced in a Schlenk tube already degassed by 3 vacuum-argon cycles. The CH_2Cl_2 was then evaporated under vacuum. The Schlenk tube was put under argon again, and the alkyl-cobalt(III) adduct was solubilized in 0.5 mL of previously degassed acetone. VETImBr (1g, $6.2 \cdot 10^{-3}$ mol.), and divinylimidazolium DVIImBr (0.1 g, 4.8 mol.%) were introduced in another Schlenk tube and degassed by 3 vacuum-Argon cycles, and 12 mL of milli-Q water were added. The second Schlenk tube was degassed by bubbling Argon during 30 minutes, and the solution of ionic liquid monomer in water was added to the first Schlenk tube, containing the solution of alkyl-cobalt(III) adduct. The reaction medium was stirred at 30 °C. Aliquots were regularly withdrawn for determining the conversion by ^1H NMR. Samples for SECs were quenched by TEMPO, and samples for THF SEC were submitted to an anion exchange before injection. The results of these syntheses are shown in Table III-2, entries 7 to 9 and Figure III-6 (reaction monitoring on Table SIII-3, entries 7-9).

For nanogels of second-generation (chain extensions), the copolymerization was not quenched, but a fresh feed of VETImBr (respectively a mix of VETImBr with 5 mol.% of

DVImBr) was added to the copolymerization medium. No new Cobalt(III)-adduct **1** is added. Results are summarized Figure III-9.

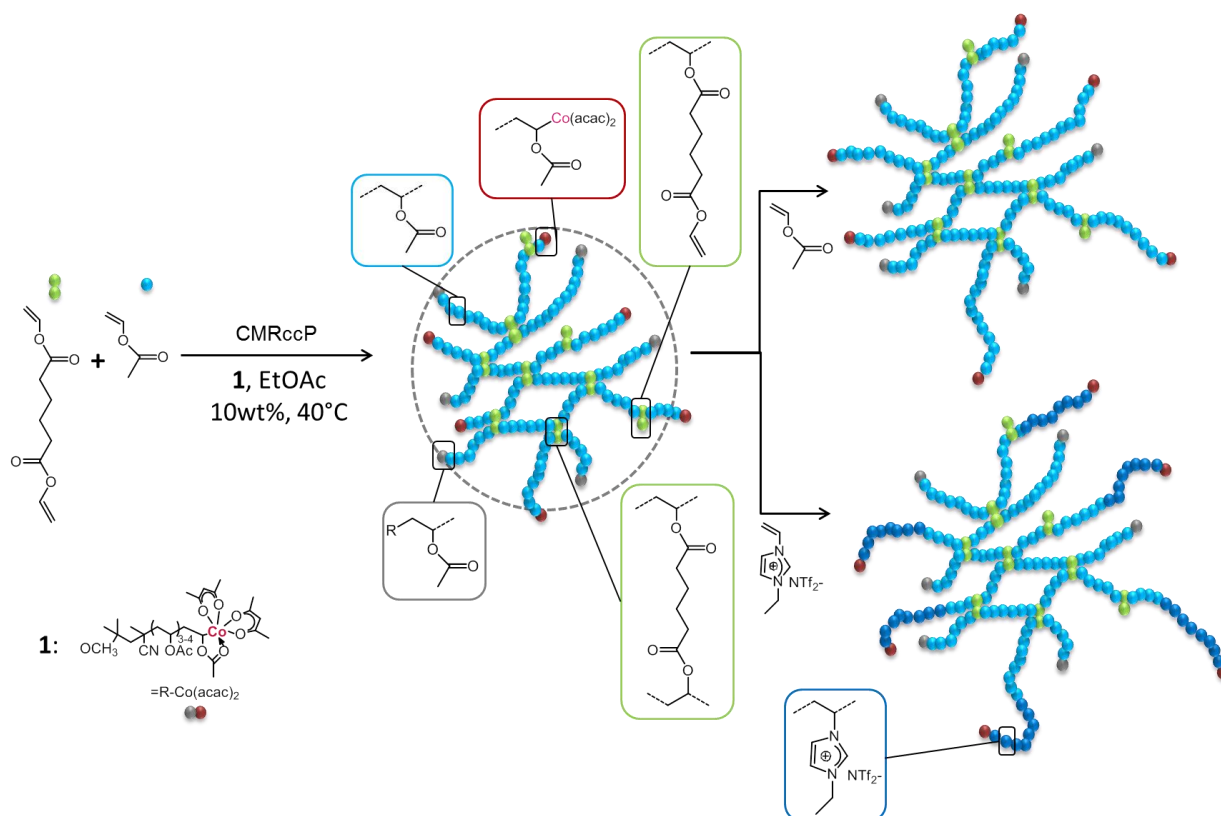
Anion exchange

The aliquot undergoing anion exchange - from bromide to bis(trifluoromethanesulfonyl)imide NTf₂⁻, was first solubilized in deionized water⁵⁶. Then, under stirring, 2 equivalents of LiNTf₂ were added to the aqueous solution. The solutions became turbid almost instantly, since the polymer PVetImNTf₂ precipitates in aqueous medium. However, to complete the anion exchange on branched imidazolium-type nanogels, the medium had to be stirred several days (a complete exchange is observed after 6 days of stirring). Then, the polymers were washed several times with deionized water, to eliminate the LiBr salt formed during the anion exchange.

Results and discussion

Poly(vinyl acetate) nanogels as validation of the concept

PVAc nanogels were first considered in order to validate the principle of CMRccP. VAc, indeed, is the benchmark of the LAM family, the polymerization of which can be controlled by xanthates or dithiocarbamates as RAFT agents^{57, 58}, or by CMRP⁵⁹⁻⁶¹. Here CMRccP of VAc was carried out using divinyl adipate (DVA) as the cross-linker, owing to the structural analogy of DVA with VAc. Synthesis of PVAc nanogels by xanthate-mediated RAFT polymerization was previously reported⁵⁷. CMRccP was carried out in presence of the preformed alkyl-cobalt(III) adduct (R-Co(acac)₂ denoted as **1**) as mediating agent, using various VAc/DVA/**1** ratios (Scheme III-1).



Scheme III-1. Cobalt-mediated radical cross-linking copolymerization of VAc and DVA mediated by **1** in ethyl acetate, and chain extension reactions. The ‘second-generation’ of nanogels was synthesized using either vinyl acetate or *N*-vinyl-3-ethyl imidazolium bis(triflimide) (VETImNTf_2^-).

As mentioned above, CMRP mediated by $\text{Co}(\text{acac})_2$ is a method of choice to achieve linear PVAc samples with a narrow molar mass distribution and controlled molar masses. This was confirmed here as shown in Table III-1, entry 1. On the other hand, it has been established in a previous report that the two double bonds of DVA are of equal reactivity⁵⁷. Initial experiments were performed in bulk at 40 °C. In such conditions, however, soluble PVAc samples were achieved only for low monomer conversions (conversion of 40% of vinyl groups only, after 8 hours of reaction), before macrogelation occurred (Figure SIII-1), whatever the DVA content (see Table SIII-1). In the absence of DVA, the SEC traces were monomodal and narrow ($M_w/M_n \sim 1.1$), while they became rapidly multimodal in the presence

of DVA with an important increase of the dispersity with the monomer conversion or the content of DVA, in line with expectations for nanogels prepared by RCC. The shift of the SEC traces towards the higher molar mass side confirmed the incorporation of DVA units (Table SIII-1).

Table III-1. Cobalt-mediated radical polymerization of vinyl acetate and its copolymerization with divinyl adipate in ethyl acetate at 40 °C.

Entry	DVA (mol.%)	[VAc]/[1]	Conv. ^a (%)	M _n (g/mol) ^b	M _p (g/mol) ^b	M _w / M _n ^b
1	0	60	100	11700	13400	1.4
2	2	60	100	5500	10700	2.4
3	4	60	100	4300	11900	2.6
4	6	60	100	16600	39400	2.8
5	6	120	90	17100	87200	3.4
6	6	180	73	18500	97500	4.4

Conditions: 40 °C, [VAc] = 10 wt% in ethyl acetate. ^a Determined by ¹H NMR in CDCl₃. ^b

Determined by SEC in THF.

Copolymerizations leading to 1st-generation nanogels of PVAc

Better results, *i.e.* higher monomer conversion (up to 90%, as determined by ¹H NMR) with no evidence of macrogel formation, were obtained when carrying out CMRccP in ethyl acetate as solvent (at a VAc concentration of 10 wt%). Increasing the DVA concentration from 2 to 6 mol.% led to higher molar masses and dispersities, for a given concentration of R-Co(acac)₂ **1** (Table III-1, entries 1-4; Fig. III-1a and Table SIII-2). Likewise, lower amounts in **1** gave higher molar masses for a fixed amount of DVA (Table III-1, entries 4-6). Figure III-2 shows the final copolymer, denoted as poly(VAc-co-6 mol.% DVA) (Table III-1, entry 4) after precipitation and subsequent solubilization in THF at 1% w/v, imaged by transmission

electron microscopy (TEM). The formation of spherical nanostructures was clearly evidenced, with a statistical analysis of images giving an average value of 12 ± 2 nm, in agreement with the definition of nanogels¹.

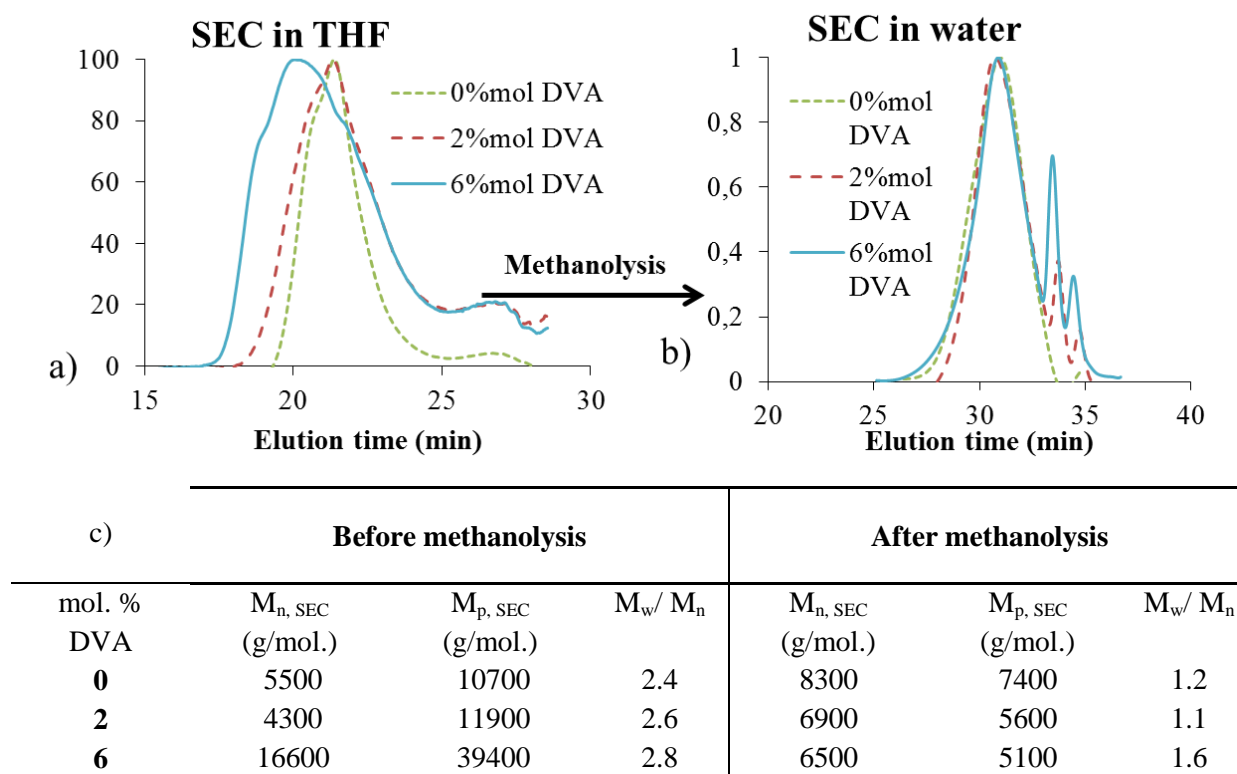


Figure III-1. a) SEC traces (in THF) of PVAc and poly(VAc-co-DVA) nanogels prepared with different contents of DVA before methanolysis (entries 1,2 and 4, Table 1); b) SEC traces (in water) for PVA after methanolysis of the parent PVAc and poly(VAc-co-DVA) nanogels; c) corresponding molecular characteristics of the different copolymer samples.

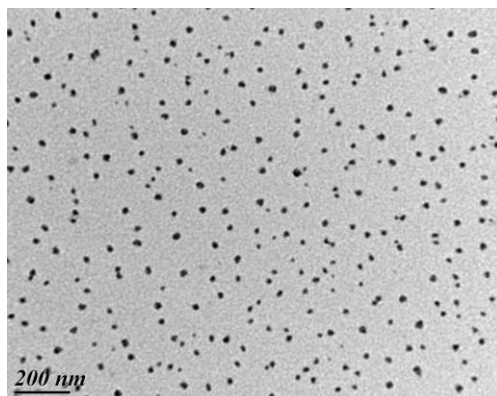


Figure III-2. TEM imaging of the precipitated poly(VAc-co-DVA) nanogel (Table II-1, Entry 4). After purification, the compound is re-dissolved in THF at a concentration of 1% w/v, and a drop is deposited on the TEM grid.

Another interest in using DVA as cross-linker is that the crosslinks can be cleaved by a simple basic treatment in methanol (= methanolysis, see mechanism in Figure SII-2), yielding individual poly(vinyl alcohol) (PVA) chains having the same chain length than that of the constitutive (primary) chains of the parent poly(VAc-co-DVA) nanogels¹⁰. Methanolysis was thus carried out using a catalytic amount of NaOH (see experimental section). Molar masses of resulting linear PVA's, as determined by aqueous SEC (Fig. III-1b), proved nearly the same for a fixed VAc/**1** ratio, and were close to the value of a PVA sample obtained after methanolysis of a linear PVAc sample prepared using the same ratio. On the other hand, lower amounts in **1** increased the length of the primary chains, as illustrated in Figure III-3b. This supported that the constitutive chain length of parent poly(VAc-co-DVA) nanogels directly depended on the initial concentration of the mediating agent (**1**) during CMRCcP, and was independent of the amount of cross-linker for a fixed amount of **1**.

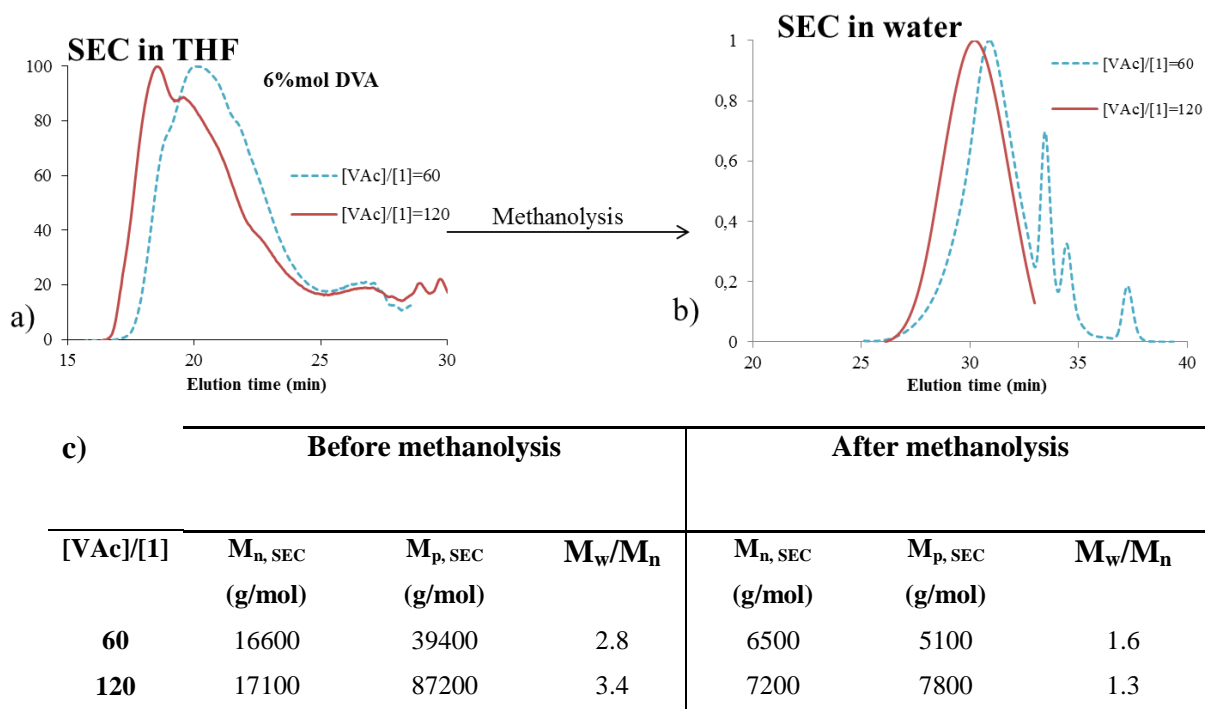


Figure III-3. a) SEC traces in THF of poly(VAc-co-DVA 6 mol.%) nanogels before methanolysis for two different [VAc]/[1] ratios (Table 1, entry 4 for [VAc]/[1] = 60 and entry 5 for [VAc]/[1] = 120); b) SEC traces (in water) of PVA after methanolysis (primary chain length); c) molecular characteristics of the different polymers.

Coating properties of PVAc-based nanogels

While solutions of poly(VAc-co-DVA) nanogels were observed *via* TEM imaging, their surface properties were also investigated by atomic force microscopy (AFM) on a freshly cleaved mica surface. The polymeric solution (0.1 mg/mL in THF) was spin-coated to obtain homogeneous coatings of relatively even depth. We thus noted the formation of a uniform polymeric coating on mica (Figure III-4). The concentration of the polymeric solution is low enough (*i.e.* 0.1 mg/mL) to note the presence of lone nanogels and aggregates on this surface. Contrary to the honeycomb-like structures observed by Poly *et al.*⁶⁹ with their PVAc nanogels made by RAFT at 10 mg/mL, no long-range order was discernable at this concentration (0.1 mg/mL in THF).

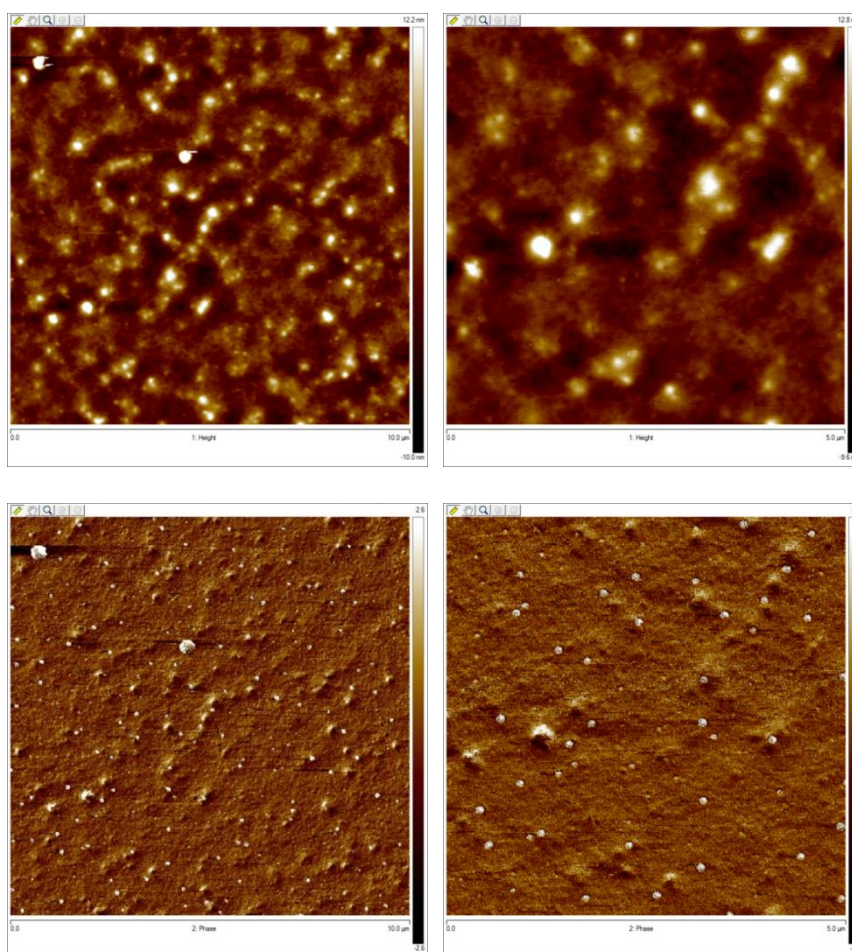


Figure III-4. AFM imaging of the poly(VAc-co-DVA 6 mol.%) nanogel, on 10 and 5 μm , both on height (first row) and phase (second row). Conditions: poly(VAc-co-DVA 6 mol.%) nanogel (0.1 mg/mL in THF) deposited on mica surface *via* spin-coating at 2000 rpm.

Chain extension reactions leading to 2nd-generation nanogels of PVAc

As already emphasized, dormant C-Co(III) chain-ends are expectedly preserved in (nano)gels prepared by CMRCcP, in contrast to ‘conventional’ RCC by FRP, hence further modifications as well as chain extensions can be implemented. Introduction of a fresh feed of degassed VAc containing 5 mol.% DVA to a “first-generation” poly(VAc-co-DVA 4 mol.%) nanogel solution ($[\text{VAc}]/[\mathbf{1}] = 60$) indeed resumed the copolymerization, with no need for adding **1** further. Note here that DVA was added during the chain extension reaction in order to facilitate the observation of the chain extension as noted elsewhere⁵⁷. This 2nd-generation

synthesis resulted in core-shell-type nanogels, following a core-first approach. This is exemplified in Figure SIII-3 showing a chain extension of a parent poly(VAc-co-DVA) nanogel with a new load of VAc/DVA. One can note a clear shift toward higher molar masses after chain extension, witnessing that C-Co(III) chain ends were accessible to grow a “second-generation” nanogel based on PVAc. Comparison of the aqueous SEC trace of the methanolized product highlights the chain-extension of the primary chains.

Even more interestingly, synthesis of nanogels with a PVAc-based inner core and a PIL-based outer shell was attempted (Scheme III-1). For this purpose, PIL chains featuring hydrophobic bis(trifluoromethylsulfonyl)imide (Tf_2N^-) anions were grown from a “first-generation” poly(VAc-co-DVA 4 mol.%) nanogel. This strategy is based on our recent investigations demonstrating that CMRP of ionic liquid monomers (ILMs) with Tf_2N^- counter-anions can be controlled⁴⁴. *N*-Vinyl-3-ethyl imidazolium bis(trifluoromethylsulfonyl)imide, denoted as VEtImNTf₂, was thus added to a solution of a poly(VAc-co-DVA) nanogel precursor formed at complete monomer conversion (copolymerization similar to Scheme III-1, Table 1, entry 3). SEC analysis evidenced the chain extension of the poly(VAc-co-DVA) nanogel with the shift of the elugram towards the higher molar mass side (Figure SIII-4a). Figure III-5 shows the ¹H NMR spectrum of the resulting nanogel with characteristic signals of the two monomer units in the polymer chain. By comparison of the integration of the signal of $-\text{CH}_2-\text{CH}-\text{O}-$ (proton **b**) of VAc at 4.8 ppm and of the signal of aromatic protons **h** of imidazolium ring at 7.8 ppm, the composition of the nanogel can be determined : VAc/VEtImNTf₂ = 19.

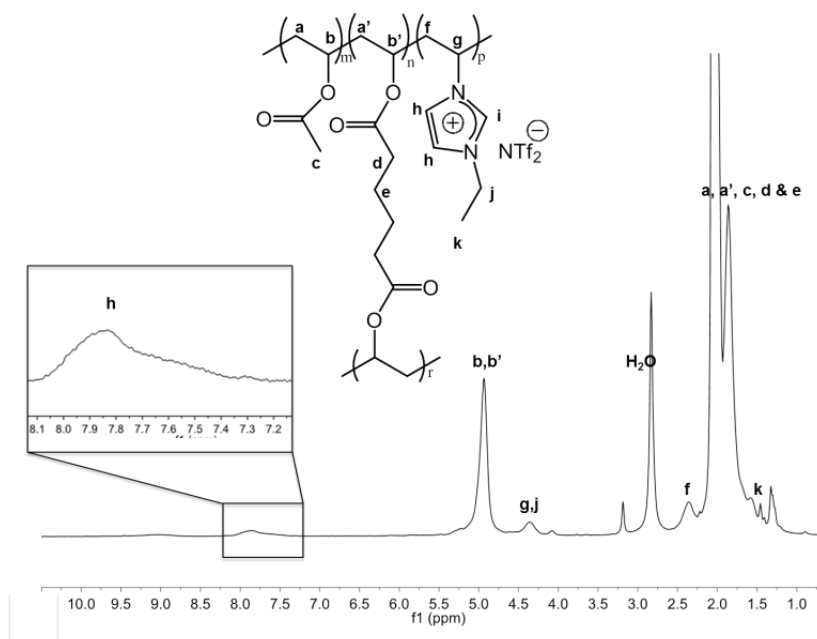
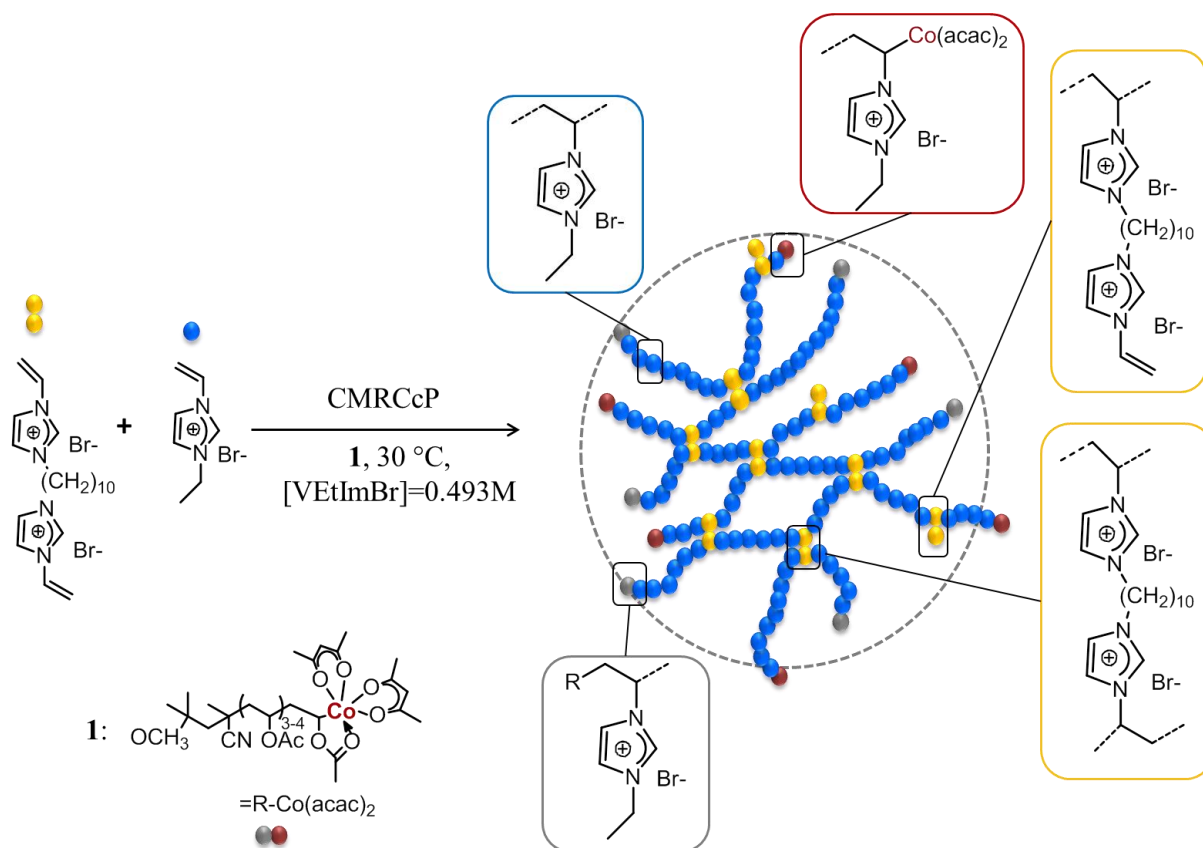


Figure III-5. ^1H NMR spectrum of the poly(VAc-co-DVA 4 mol.%) after chain extension reaction with VEtImNTf₂, in acetone-d₆.

PIL-based nanogels

Of particular interest, ILMs of *N*-vinyl-3-alkylimidazolium-type with bromide (Br⁻) counter-anions can not only be polymerized in organic media *via* CMRP, for instance, in DMF or in DMF/MeOH mixture^{43, 62}, but also directly in water under mild conditions⁵⁶. On this basis, and having established the proof of concept of CMRccP through the synthesis of neutral PVAc nanogels, we examined the possibility to directly achieve hydrophilic PIL nanogels by this method. Previous works have very recently reported on the synthesis of branched PILs by RCC.⁶³⁻⁶⁵ To the best of our knowledge, however, there is only one example that has described the synthesis of PIL nanogels by RCC, using RAFT polymerization in this case⁶⁶. Shape-persistent PIL nanogels could be of practical interest, for instance, as additives in coatings or as membranes for CO₂ capture) or in highly added value applications, *e.g.* in medical diagnostic tests, antibody purifications, or drug delivery systems⁶⁷.



Scheme III-2. Synthesis of nanogels of poly(*N*-vinyl-3-ethyl imidazolium bromide) in organic and aqueous media.

We selected hydrophilic ILMs, namely, *N*-vinyl-3-ethyl imidazolium bromide, denoted as VETImBr, and 1,13-divinyl-3-decyl diimidazolium bromide (DVIImBr) as cross-linker, again due to the structural similarity of DVIImBr with VETImBr. CMRCcP experiments were conducted at $30\text{ }^\circ\text{C}$, in presence of the same $R\text{-Co}(\text{acac})_2$ **1**, either in DMF, or in a mixture of methanol and DMF (1/2 vol.), or directly in aqueous solution. Scheme III-2 illustrates these syntheses. Both the effect of a variation in the concentration of DVIImBr (2.9 mol % and 4.8 mol % relatively to VETImBr) and the solvent nature at a given amount of DVIImBr were examined.

Main results are summarized in Table III-2 and include the homo-CMRP of VETImBr and its copolymerization with DVIImBr. For the sake of clarity, SEC traces of soluble samples synthesized in the three different solvents, and obtained after anion exchange, are compared in

Figure III-6. Control of VEtImBr was first verified, through the increase of molar masses and the production of low dispersities, under the same conditions used for copolymerization experiments (10 wt%, 30 °C, [VEtImBr]/[1] = 60).

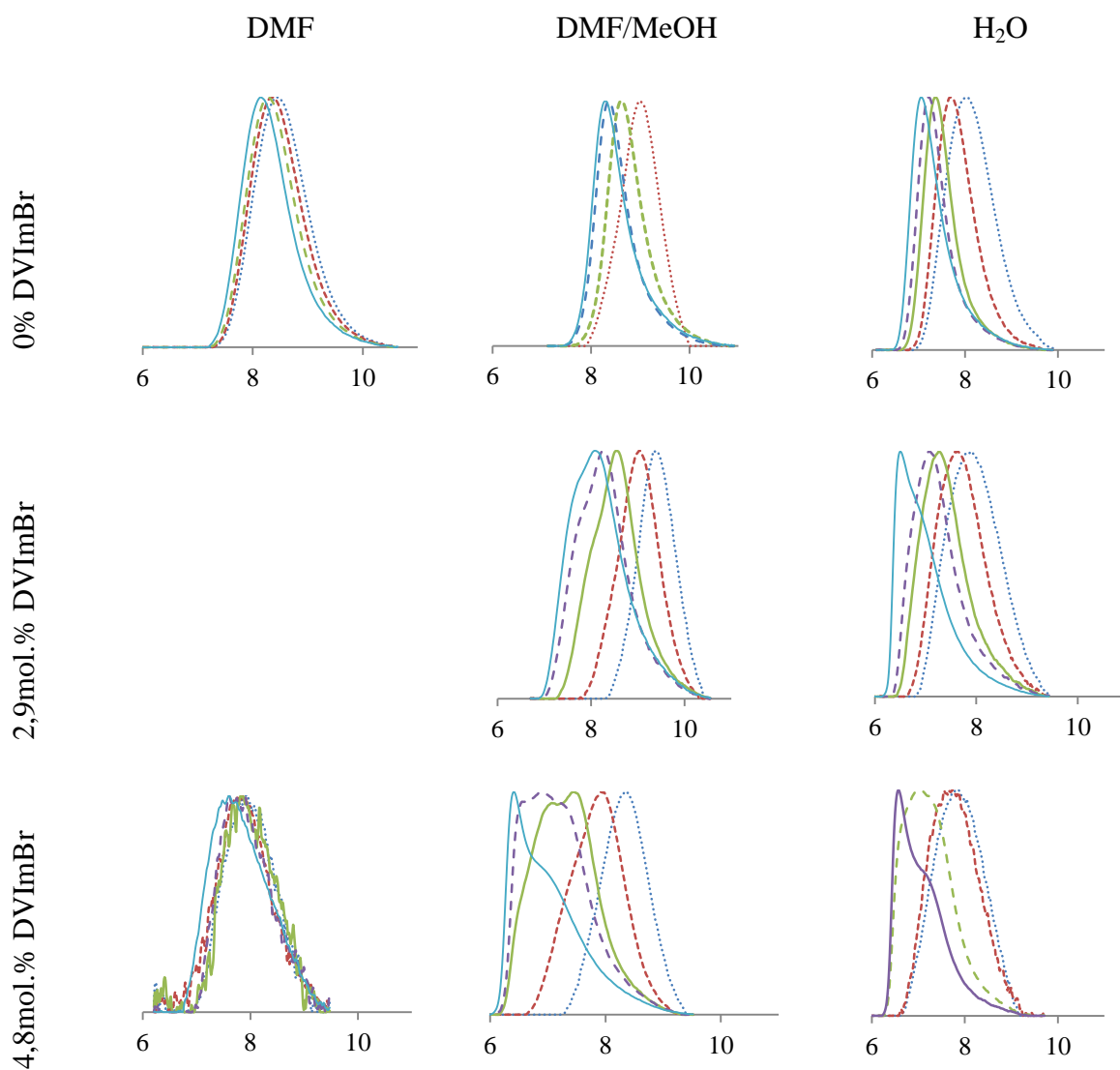


Figure III-6. SEC traces (in THF with 10mM LiTf₂N after anion exchange) for the homopolymerizations of *N*-vinyl-3-ethyl imidazolium bromide (VEtImBr) and its copolymerizations with different amounts of 1,13-divinyl-3-decyl diimidazolium bromide (DVImBr) in various solvents. SEC traces are ordered by solvent nature (per column) and by amount of cross-linker (DVImBr) (per row). Complete data on reaction monitoring are given on SI (Table SIII-3).

Table III-2. Cobalt-mediated polymerization of *N*-vinyl-3-ethyl imidazolium bromide and its copolymerization with different amounts of 1,13-divinyl-3-decyl diimidazolium bromide in various solvents (polymerization monitoring are detailed in Table SIII-3).

Entry	Solvent	DVImBr (%mol)	Conv. ^a (%)	M _n ^b (g.mol ⁻¹)	M _p ^b (g.mol ⁻¹)	M _w /M _n ^b
1	DMF	0	100	14800	20000	1.25
2	DMF	2.9	100	- ^c	- ^c	- ^c
3	DMF	4.8	95	- ^c	- ^c	- ^c
4	DMF/MeOH	0	75	11900	17800	1.27
5	DMF/MeOH	2.9	85	15300	20900	1.38
6	DMF/MeOH	4.8	81	24900	37100	1.63
7	H ₂ O	0	87	21200	35600	1.36
8	H ₂ O	2.9	82	28500	78300	1.59
9	H ₂ O	4.8	gel	-	-	-

Conditions: 30 °C; [VEtImBr]/[**1**] = 60; [VEtImBr]₀ = 0.493M, 30 h of polymerization.^a

Conversion was calculated by ¹H NMR in deuterated DMSO.^b Molar masses were determined by SEC in THF after anion exchange using PS calibration.^c Most of the polymer was removed after filtration of the solution on a 0.2 μm filter, thus preventing the SEC analysis itself.

Copolymerizations leading to the formation of 1st-generation nanogels of PIL in organic media

CMRccP's carried out in solution in DMF gave lower polymerization rates as the amount of DVImBr increased (polymerization monitoring is provided in Table SIII-3, SD):

conversion was almost complete after 4 hours for CMRccP with 2.9 mol.% of DVImBr, while a conversion of 77% was reached after the same period of time using 4.8 mol.% DVImBr (near quantitative conversion was noted for CMRP of VEtImBr, *i.e.* in absence of DVImBr, after 4h). Transmission electron microscopy (TEM) analysis of the purified poly(VEtImBr-*co*-DVImBr 4.8 mol.%) nanogel showed spherical objects with a diameter around $35 \text{ nm} \pm 6 \text{ nm}$ (Figure III-7a). For TEM analysis, residual monomer was removed by precipitation in diethyl ether, followed by redissolution of the nanogel in water (1 wt%) and deposition onto the TEM grid. Importantly, no filtration of the samples was carried out prior to TEM analyses, confirming the absence of aggregates.

As reported elsewhere⁵⁰, SEC analysis of poly(vinyl *N*-alkylimidazolium bromide)s is not straightforward and requires an anion-exchange, from Br^- to Tf_2N^- , prior to injection in THF containing 10 mM LiTf_2N . Nevertheless, when the anion exchange was applied to our Br-containing PIL nanogels, the resulting Tf_2N -containing products proved hardly soluble in this eluent. SEC analyses were therefore not always reliable because part of the polymer was eliminated when filtering the sample on a $0.2 \mu\text{m}$ filter prior to analysis; only a signal of low intensity was observed (Figure III-6). The linear PILs prepared without DVImBr were however totally soluble and SEC analysis could be performed (Figure III-6 first row).

We then turned to the use of a mixture of DMF and MeOH (8/4, v/v) as solvent for CMRccP (entries 4-6, Table III-2). Such a mixture has previously been reported to decrease the CMRP rate of VEtImBr, as compared to DMF⁴³. After 24 h of reaction, conversions were in the range 81-85%, irrespective of the concentration in DVImBr. After 8 hours, conversions for CMRP of VEtImBr and CMRccP using 2.9 mol.% of DVImBr reached 75% in both cases (Table SIII-3). In contrast to nanogels prepared in DMF, those prepared in DMF/methanol were soluble in the SEC eluent after anion exchange. This was evidenced by free-column

refractometric measurements before and after filtration of the nanogel samples. No significant loss of mass occurred during the filtration step prior to injection in SEC (Figure SIII-5a).

For a same conversion, higher molar masses and dispersities were obtained in the presence of DVImBr than for in the case of the homopolymerization of VEtImBr (Table SIII-3), with SEC shapes characteristic of the formation of branched architectures (Figure III-6). The multimodality of SEC traces is characteristic of the formation of nanogels⁶⁸. Both the Br-containing linear and nanogel samples were also analyzed by SEC in aqueous media (using 0.1M NaCl and 0.1 vol% trifluoroacetic acid as eluent, see experimental section). Although some interactions of PILs with the SEC columns could not be totally ruled out in these conditions, Figure SII-6 shows unimodal shapes for PILs prepared in absence of DVImBr with a rather low dispersity, whereas multimodal chromatograms can be observed for PIL nanogels with a high dispersity (Table SIII-4).

Copolymerizations leading to the formation of 1st-generation nanogels of PIL in water

Even more interesting, water could be directly employed as solvent for a new series of CMRccP experiments, both DVImBr and VEtImBr being soluble in aqueous media⁵⁶, as well as the resulting branched PILs. However, R-Co(acac)₂ **1** being insoluble in water, a low amount of acetone was added to ensure homogeneous conditions. In contrast to CMRccP's performed in DMF, rates in water were not significantly affected by the incorporation of DVImBr. At 8 hours of reaction, for instance, conversion was 73% for CMRP of VEtImBr, and 72% and 78%, respectively, for the CMRccP using 2.9 mol.% and 4.8 mol.% of DVImBr (Table SIII-3). However, while in organic solvents, copolymerizations could be run during 30h without macrogelation, the reaction performed in water with 4.8 mol.% of DVImBr (Table III-2, entry 9) formed a macrogel overnight.

The PIL nanogel prepared in water with 4.8 mol.% DVImBr before macrogelation occurs, *i.e.* after 8h of reaction and 78% conversion (Table SII-3, entry 9), was imaged by TEM after purification and subsequent re-dissolution in water (Figure III-7b). Two major populations were observed: a population was likely due to the aggregation of individual nanogels, while the other seemed to correspond to necklaces of nanogels. Individual nanogels were found in the 20-50 nm size range. Formation of necklaces might be explained either by the development of intermolecular cross-linking occurring at the completion of the CMRccP, or simply to a drying artifact. Hydrophilic nanogels were then subjected to the anion exchange reaction, forming hydrophobic PIL derivatives. The latter materials were dissolved in THF and deposited on a carbon TEM grid (Figure III-7c). The above necklaces of nanostructures were not further observed, indicating that these unexpected arrangements were merely due to drying artifacts.

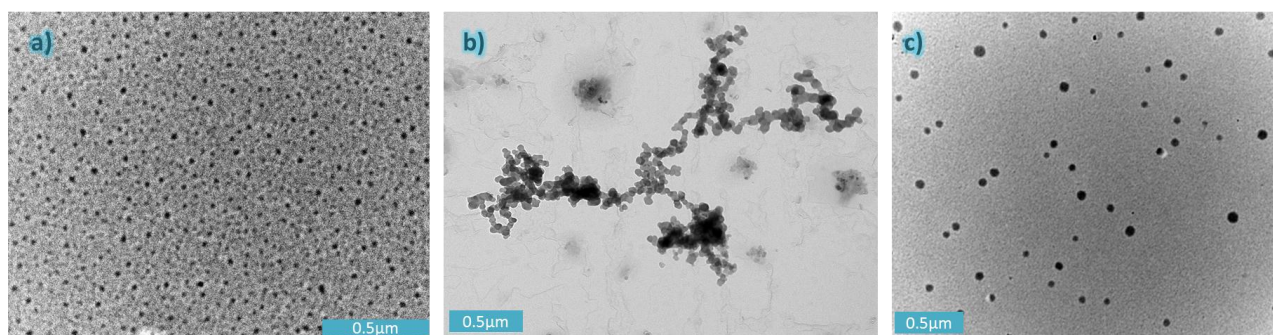


Figure III-7. TEM imaging of: a) poly(VEtImBr-*co*-DVImBr 4.8 mol.%) synthesized in DMF (scale bar: 500 nm); b) poly(VEtImBr-*co*-DVImBr 4.8 mol.%) synthesized in H₂O (scale bar: 500 nm); c) the latter copolymer, after anion exchange and dissolution in THF (scale bar: 500 nm).

Figure III-6 shows the increase of the sample molar mass with the monomer conversion with multimodal SEC traces and an increase in dispersity (Table SIII-3). Further

evidence of intermolecular cross-linking is shown by the kinetics of the CMRccP using 2.9 mol.% of DVImBr where an increase of the conversion of 2% doubled the peak molar mass (M_p) of the copolymer (from 39700 to 78300 $\text{g}\cdot\text{mol}^{-1}$). Refractometric analysis of a typical nanogel sample prepared with 4.8 mol.% DVI (sample Table SIII-3, entry 9) evidences that no significant loss of mass occurred during the filtration (on a 0.2 μm filter) of the samples prior to injection in SEC (Figure SIII-5b). Nanogel samples prepared under these conditions after $\text{Br}^-/\text{Tf}_2\text{N}^-$ exchange are therefore soluble in THF and are not forming aggregates higher than 200 nm.

Nanogel formation in the presence of DVImBr was also evidenced by SEC analysis of Br-containing PILs in aqueous media, *via* the formation of multimodal SEC traces as well and high dispersities (Figure SII-6, Table SIII-4).

The solvent effect could be accounted by examining, for instance, experiments using 4.8 mol.% of DVImBr (entries 3, 6 and 9, Table SII-3; see also CMRP of VEtImBr in Table SII-3 entries 1, 4 and 7 for comparison). DMF gave rapid reaction kinetics with nanogels that were not totally soluble in the SEC eluent, while both the DMF/MeOH mixture and the aqueous solution induced slower reaction rates. Interestingly, for the same conversion of vinyl group, the copolymerization performed in water with 2.9 mol.% of DVImBr (Table III-2, entry 8) achieved higher molar masses than CMRccP carried out in DMF/MeOH with 4.8 mol.% of DVImBr (Table III-2, entry 6). Furthermore, while M_n values remained close (28800 *vs.* 24900 g/mol), the peak molar mass, M_p , more than doubled (78300 *vs.* 37100 g/mol) indicating a difference in the nanogel structure. In the aqueous solvent, intermolecular cross-linking might be more favored than in organic media, leading to higher M_p values. This is supported by the fact that only the CMRccP conducted in water (with 4.8 mol.% of DVImBr) led to macrogelation at high conversion.

Coating properties of PIL-based nanogels

For comparison purposes, nanogels were analyzed by AFM on a freshly cleaved mica surface. A poly(V_{EtIm}Br-*co*-D_{VIm}Br 4.8 mol.%) sample synthesized in H₂O during 8 hours (copolymerization stopped before macrogelation occurs, see entry 9, Table III-2) was thus solubilized in methanol at a concentration of 0.1 mg/mL, which was the same concentration used for the AFM imaging with PVAc nanogels. The surface observed was very different to that observed previously for PVAc nanogels. For a polymer solution at 0.1 mg/mL, the surface showed some cracks (Figure III-8a and b). After a dilution by a factor 10, and subsequent spin-coating, individual nanogels and aggregates could be directly observed on mica.

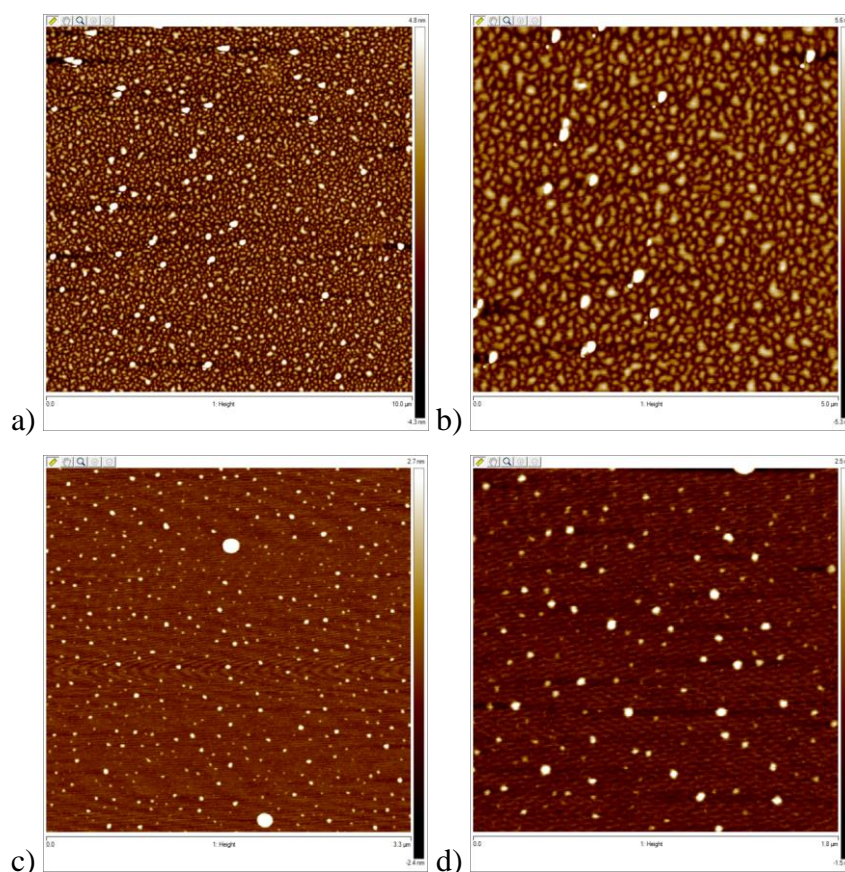
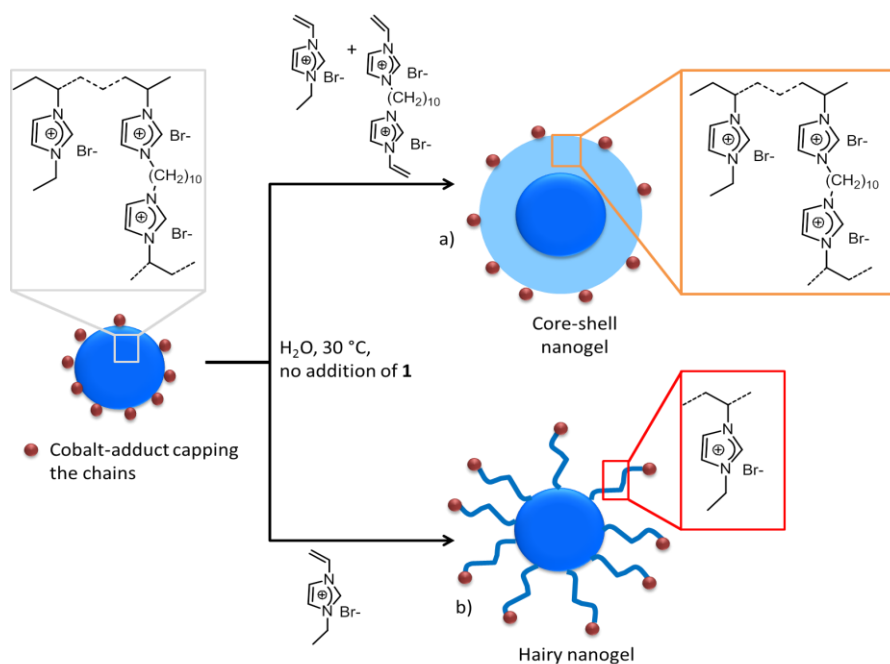


Figure III-8. AFM height imaging of the PIL nanogels poly(V_{EtIm}Br-*co*-D_{VIm}Br 4.8mol.%) synthesized in H₂O during 8 hours (copolymerization stopped before macrogelation occurs) on a freshly cleaved mica surface. The images show the state of the

surface for the spin-coating 2000 rpm at 0.1 mg/mL (first row) and 0.01 mg/mL (second row), at different scale: a) 10 μm , b) 5 μm , c) 3 μm and d) 1 μm .

Chain extension reaction leading to the formation of 2nd-generation nanogels of PIL, in water

To demonstrate that PIL nanogels thus prepared in water could be reactivated, a chain extension experiment was performed. To a solution of the 1st-generation poly(VEtImBr-co-DVImBr 4.8 mol.%) nanogel prepared in water until 88% conversion, an aqueous solution of VEtImBr containing 0, 2.9 or 4.8 mol.% of DVImBr ($[\text{VEtImBr}]/[\mathbf{1}] = 60$) was added. Monomer conversions were above 75% in all cases after 24h of polymerization (Figure III-9a). SEC traces showed a shift to the higher molar masses, attesting that the C-Co bond could be reactivated (Figure III-9a). When DVImBr was present for chain extension, a very high molar mass peak was observed on the SEC traces ($M_p = 329\,500$ g/mol), which was assigned to inter-nanogels cross-linking. TEM imaging showed well-defined spherical nanostructures for the 2nd-generation, in a range of 40-70 nm diameter (Figure III-9b). These experiments thus demonstrated that CMRccP was robust enough to be performed in water with a high chain-end fidelity, enabling the production of second generation PIL nanogels.



Scheme III-3. Chain extension reactions on PIL-based nanogels with: a) a mixture of VEImBr and DVImBr; b) VEImBr only.

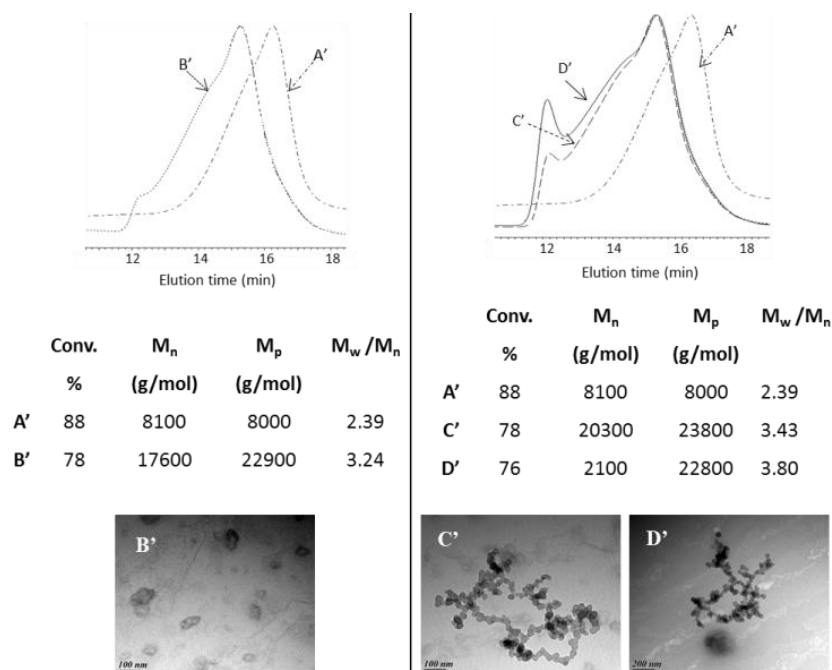


Figure III-9. a) and b) aqueous SEC traces and macromolecular parameters of 1st (A') and 2nd generation of PILs nanogels prepared in the absence (B') and presence of 2.9 mol.% (C') or 4.8 mol.% (D') DVImBr; and b) TEM imaging of the corresponding 2nd generation of

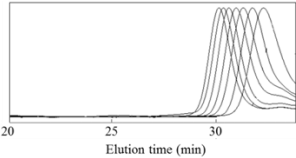
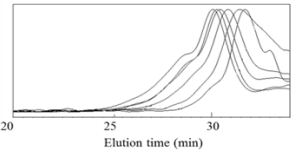
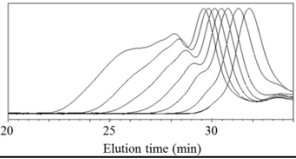
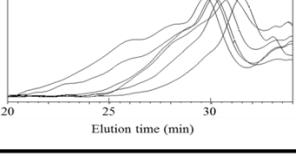
nanogels (B' in the absence of DVImBr; C' in the presence of 2.9 mol.% DVImBr, and D' in the presence of 4.8 mol.% DVImBr).

Conclusions

Neutral and positively charged nanogels based on poly(vinyl acetate) (PVAc) and poly(*N*-vinyl-3-ethyl imidazolium bromide), respectively, were prepared by one-step cobalt-mediated radical crosslinking copolymerization (CMRccP) in solution. The pre-synthesized alkyl-cobalt(III) mediating agent enables to introduce rather larger amounts of cross-linker without the occurrence of macrogelation. Use of divinyl adipate as cross-linker allowed cleaving the cross-linked points of PVAc nanogels and accounting that control over the constitutive chain length could be achieved. The particle size could be fine-tuned by varying the initial monomer/cross-linker/mediating agent ratio. Furthermore, dormant carbon-cobalt(III) chain-ends could be reactivated, enabling the synthesis of core-shell structures, following a divergent approach. Last but not least, robustness and efficacy of this strategy were demonstrated through its direct implementation in aqueous solution for the production of poly(ionic liquid) (PIL) nanogels. Core-shell nanostructures with a PVAc core and a PIL shell were also accessible by chain extension of a PVAc nanogel by a hydrophobic *N*-vinyl imidazolium salt. Exchange of the counter-ion (not exploited here, except for the purpose of characterization) could provide an additional means to vary the PIL nanogels properties. All these attributes make CMRccP-derived nanogels versatile nano-sized polymeric materials for varied applications, from coatings to catalysis or biomaterials. Work is currently in progress in our groups to exemplify this CMRccP method to other types of ionic liquid monomers and to valorize PIL nanogels in specific applications, including catalysis and as antimicrobial coatings.

Supporting Information

Table SIII-1. Kinetics data for the copolymerization of VAc with DVA bulk at 40 °C, with [VAc]/[I] = 60.

Entry	DVA (% mol)	Time (h)	conv (%) ^a	M _n (g/mol) ^b	M _p (g/mol) ^b	M _w /M _n ^c
1	0 	2	12	1300	1600	1.17
		4	27	2500	2700	1.08
		5	29	3100	3300	1.07
		7	34	4100	4500	1.07
2	2 	2	16	1700	2100	1.28
		4	23	2500	3200	1.59
		5	20	4400	4000	1.38
		7	29	5700	4700	1.50
3	4 	2	10	1500	2000	1.31
		4	22	2300	3400	1.66
		5	26	2900	3900	1.88
		7	37	4500	5400	2.94
4	6 	2	6	2000	2400	1.53
		4	19	3200	3900	1.69
		5	22	4500	4600	2.05
		7	26	11100	5800	3.35

^a Determined by ¹H NMR in CDCl₃. ^b Determined by SEC in THF using PS calibration.

Table SIII-2. Kinetics of the polymerization of vinyl acetate and its copolymerizations with divinyl adipate in ethyl acetate at 40 °C.

Entry	DVA (mol.%)	time (h)	conv (%) ^a	M _n ^b (g/mol)	M _p ^b (g/mol)	M _w /M _n ^b
1	2	8	21	- ^c	- ^c	- ^c
		24	40	2200	3400	1.4
		48	60	- ^c	- ^c	- ^c
		120	100	5500	10700	2.4
2	4	8	24	1300	1600	1.17
		24	43	2100	2600	1.4
		48	58	3800	5400	1.9
		120	100	4300	11900	2.6
3	6	8	18	- ^c	- ^c	- ^c
		24	38	2200	2900	1.5
		48	59	4700	6100	2.3
		120	100	16600	39400	2.8

^a Determined by ¹H NMR in CDCl₃. ^b Determined by SEC in THF using PS calibration. ^c Not determined. Conditions: [VAc]/[**1**] = 60, [VAc] = 0.493M, x mol.% DVA, 40 °C, ethyl acetate.

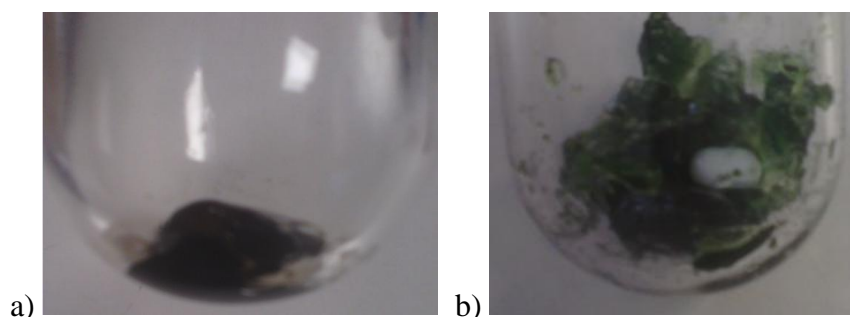


Figure SIII-1. Photograph of: a) a macrogel after 14h of copolymerization (VAc + 4 mol.% DVA, 40 °C, bulk, [VAc]/[**1**] = 60); b) the same compound, after addition of 4 ml of CDCl₃.

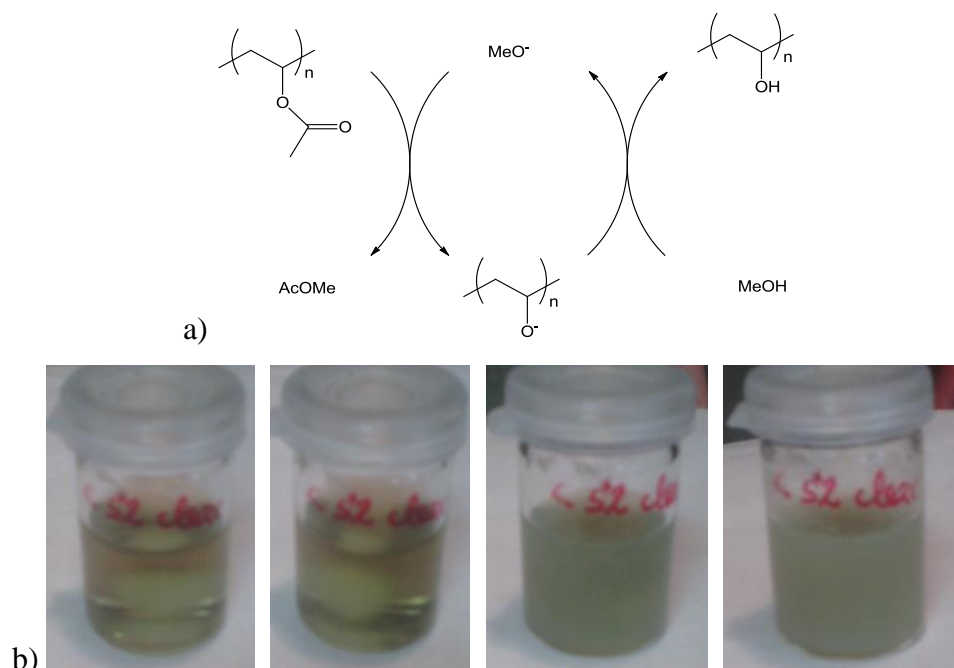
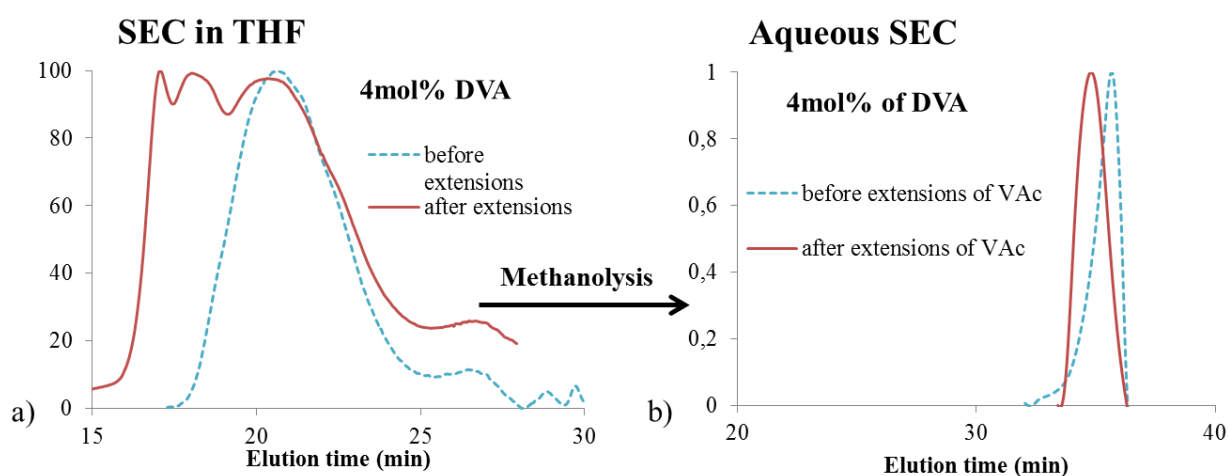


Figure SIII-2. a) Methanolysis process from PVAc to poly(vinyl alcohol); b) macroscopic changes on a poly(VAc-co-DVA) nanogel. While the poly(VAc-co-DVA) nanogels are soluble in methanol, the linear poly(vinyl alcohol) or PVOH, is not.



	Conv. (%)	M_n (g/mol)	M_p (g/mol)	M_w/M_n
1st generation	70	10000	16000	2.1
c) 2nd generation	30	19100	545900	8.6

Figure SIII-3. a) SEC traces (in THF) of a chain extension polymerization on a poly(VAc-co-DVA 4 mol.%) nanogel before methanolysis; b) SEC traces (in water) of primary chains of linear PVA (of the 1st and 2nd generation nanogels) after methanolysis in water; c) molecular

characteristics for the 1st and 2nd generation of nanogels. Conditions: [VAc]/[1] = 60, [VAc] = 0.493M, 40 °C, [VAc]/[DVA] = 4, in ethyl acetate.

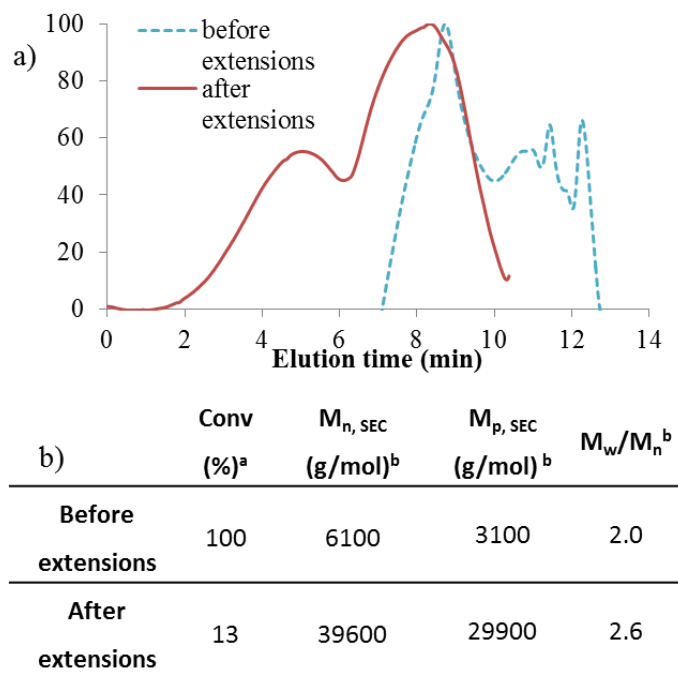


Figure SIII-4. a) SEC traces (in THF containing 10 mM LiTf₂N) of the 1st-generation poly(VAc-DVA) nanogel corresponding to Table 1, entry 3 (blue, dotted line) and the same nanogel after chain extensions with *N*-vinyl-3-ethyl imidazolium NTf₂ (red, plain line); b) macromolecular characteristics of the nanogel before and after chain extension.

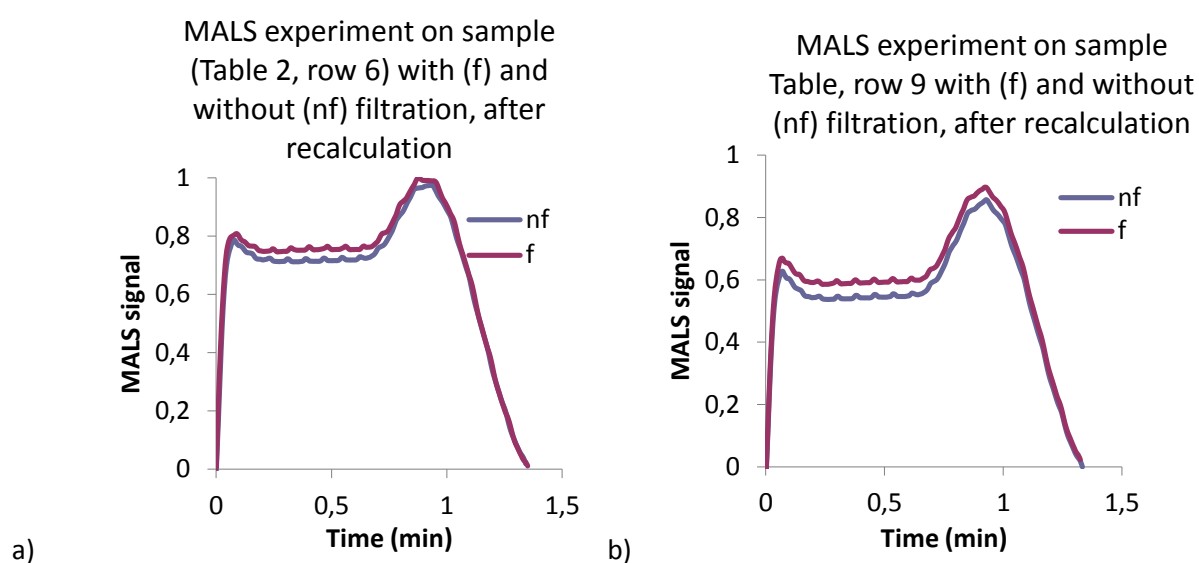


Figure SIII-5. MALS measurement of: a) the nanogel synthesized in DMF/MeOH mixture (Table 2, entry 6); b) the nanogel synthesized in water (Table 2, entry 9), before (nf) and after

(f) filtration of the sample. The very slight difference in peak area can be ascribed to the shearing of the solvent during filtration.

Table SIII-3. Complete follow-up on kinetics data of the poly(VEtImBr-DVImBr) nanogels, via ^1H NMR and SEC in THF.

Entry	Solvent	%mol DVImBr	Time (h)	Global conv (%) ^a	M_n^b (g/mol)	M_p^b (g/mol)	M_w/M_n
1	DMF	0	0.25	70	11800	16000	1.26
			1	85	13600	18100	1.24
			4	98	14800	20000	1.25
2^b	DMF	2.9	0.25	50	- ^c	- ^c	- ^c
			1	83	- ^c	- ^c	- ^c
			4	96	- ^c	- ^c	- ^c
			8	98	- ^c	- ^c	- ^c
3^b	DMF	4.8	0.25	42	11700	14600	1.23
			1	59	13000	14400	1.23
			4	77	12000	15200	1.24
			30	95	13500	19900	1.32
4	DMF/MeOH	0	1	33	8400	9000	1.15
			2	53	9800	13000	1.22
			4	64	12100	16500	1.22
			8	75	11900	17800	1.27
5	DMF/MeOH	2.9	0.25	14	5500	6100	1.15
			1	33	7900	8600	1.21
			4	63	11900	14300	1.29
			8	75	14600	18300	1.33
			24	85	15300	20900	1.38
6	DMF/MeOH	4.8	0.25	17	9000	9600	1.17
			1	37	13700	13800	1.24
			4	56	21400	21800	1.45
			24	81	24900	37100	1.63
7	H ₂ O	0	0.25	25	10100	12600	1.28
			1	40	13600	17300	1.22
			4	68	18700	25000	1.23
			8	73	20400	29700	1.30
			24	87	21300	34800	1.36
			30	87	21200	35600	1.36
8	H ₂ O	2.9	0.25	19	12100	14700	1.27
			1	40	12900	16300	1.26
			4	61	14900	19000	1.29

			8	72	22500	32900	1.41
			24	80	23700	39700	1.48
9	H ₂ O	4.8	0.25	82	28800	78300	1.59
			1	21	12500	15300	1.28
			4	36	14200	15600	1.27
			8	64	22300	28900	1.30
			24	78	26600	70700	1.42
			24	gel			

^a Determined by ¹H NMR in DMSO-d₆. ^b Determined by SEC in THF with LiTf₂N. ^c Not determined. Conditions: [VETImBr]/[**1**] = 60, [VETImBr] = 0.493M, x mol.% DVI, 30 °C.

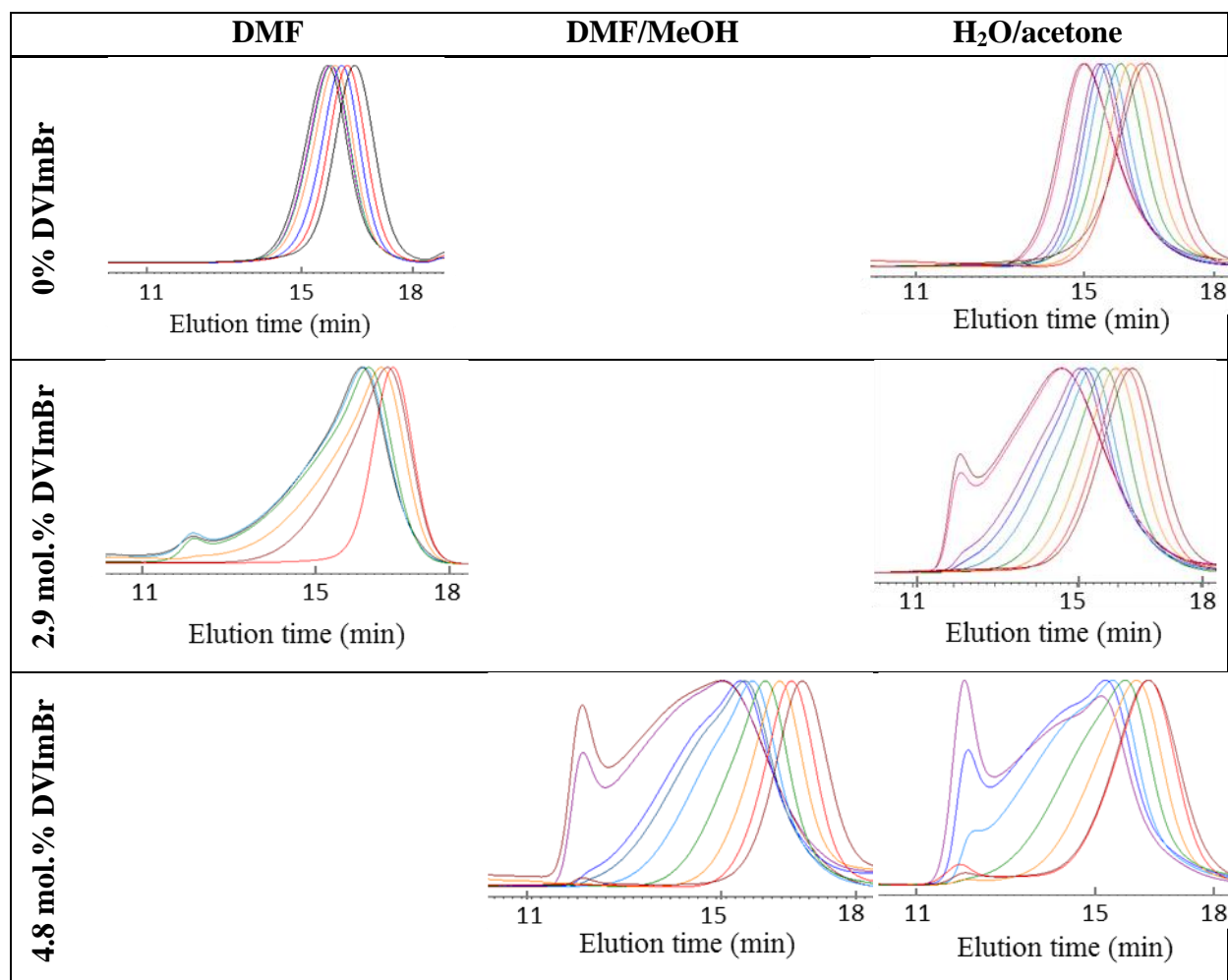


Figure SIII-6. Aqueous SEC chromatograms for the kinetics of copolymerization of VETImBr with DVIImBr.

Table SIII-4. Complete follow-up on kinetics data of the poly(VEtImBr-co-DVImBr) nanogels, via ¹H NMR and aqueous SEC.

Entry	mol.% DVIm Br	Polymerization solvent	Polymerization time (h)	Global conversion(%) ^a	M _n , aq (g/mol) ^b	M _p , aq (g/mol) ^b	M _w / M _n , aq
1	0	DMF	0.25	47	4200	5000	1.28
			1	66	6800	7700	1.37
			4	87	9000	10600	1.43
2	2.9	DMF	0.25	44	5100	4900	2.11
			1	71	6800	5900	2.18
			4	87	9600	9500	2.16
			6	90	9800	10200	2.18
3	4.8	DMF	0.25	42	- ^c	- ^c	- ^c
			1	59	- ^c	- ^c	- ^c
			4	77	- ^c	- ^c	- ^c
			30	95	- ^c	- ^c	- ^c
6	4.8	DMF/MEOH	0.25	17	2800	3700	1.74
			1	37	5800	7000	1.69
			4	56	11200	13700	2.45
			24	81	19200	26900	4.10
7	0	H ₂ O	0.25	25	4300	6100	2.10
			1	40	6800	9600	1.64
			4	68	10700	16500	1.64
			24	87	14800	28600	1.91
8	2.9	H ₂ O	0.25	19	5000	7200	2.08
			1	40	8700	11400	2.00
			4	61	15100	20800	2.42
			24	80	21600	41200	2.7
9	4.8	H ₂ O	0.25	21	5100	7400	2.14
			1	36	8700	10200	2.55
			4	64	17800	18500	3.45
			8	78	- ^c	- ^c	- ^c
			24	gel	- ^c	- ^c	- ^c

^a Determined by ¹H NMR in DMSO-d₆. ^b Determined by SEC in water (containing 0.1M NaCl and 0.1vol% TFA) ^c not determined. Conditions: [VEtImBr]/[**1**] = 60, [VEtImBr] = 0.493M, x mol.% DVI, 30 °C.

References

1. IUPAC, *Pure Appl. Chem.*, 2007, **79**, 1801-1829.
2. N. Sanson and J. Rieger, *Polymer Chemistry*, 2010, **1**, 965-977.
3. R. Pelton, *Advances in Colloid and Interface Science*, 2000, **85**, 1-33.
4. S. Nayak and L. Andrew Lyon, *Angewandte Chemie - International Edition*, 2005, **44**, 7686-7708.
5. R. T. Chacko, J. Ventura, J. Zhuang and S. Thayumanavan, *Advanced Drug Delivery Reviews*, 2012, **64**, 836-851.
6. J. K. Oh, R. Drumright, D. J. Siegwart and K. Matyjaszewski, *Progress in Polymer Science (Oxford)*, 2008, **33**, 448-477.
7. J. Liu, C. Detrembleur, S. Mornet, C. Jerome and E. Duguet, *Journal of Materials Chemistry B*, 2015, **3**, 6117-6147.
8. C. Legros, M. C. De Pauw-Gillet, K. C. Tam, S. Lecommandoux and D. Taton, *European Polymer Journal*, 2014, **62**, 322-330.
9. H. Gao and K. Matyjaszewski, *Progress in Polymer Science (Oxford)*, 2009, **34**, 317-350.
10. J. Poly, D. James Wilson, M. Destarac and D. Taton, *Macromolecular Rapid Communications*, 2008, **29**, 1965-1972.
11. J. Rosselgong, S. P. Armes, W. Barton and D. Price, *Macromolecules*, 2009, **42**, 5919-5924.
12. E. Faure, C. Falentin-Daudré, T. S. Lanero, C. Vreuls, G. Zocchi, C. Van De Weerd, J. Martial, C. Jérôme, A. S. Duwez and C. Detrembleur, *Advanced Functional Materials*, 2012, **22**, 5271-5282.
13. H. Gao, A. Miasnikova and K. Matyjaszewski, *Macromolecules*, 2008, **41**, 7843-7849.
14. P. J. Flory, *Journal of the American Chemical Society*, 1941, **63**, 3083-3090.
15. W. H. Stockmayer and H. Jacobson, *The Journal of Chemical Physics*, 1943, **11**, 393.
16. W. H. Stockmayer, *The Journal of Chemical Physics*, 1943, **11**, 45-55.
17. J. K. Oh, S. A. Bencherif and K. Matyjaszewski, *Polymer*, 2009, **50**, 4407-4423.
18. K. Matyjaszewski and N. V. Tsarevsky, *Nature Chemistry*, 2009, **1**, 276-288.
19. J. A. Yoon, C. Gayathri, R. R. Gil, T. Kowalewski and K. Matyjaszewski, *Macromolecules*, 2010, **43**, 4791-4797.

20. Q. Yu, Y. Zhu, Y. Ding and S. Zhu, *Macromolecular Chemistry and Physics*, 2008, **209**, 551-556.
21. W. A. Braunecker and K. Matyjaszewski, *Progress in Polymer Science (Oxford)*, 2007, **32**, 93-146.
22. R. Wang, Y. Luo, B.-G. Li and S. Zhu, *Macromolecules*, 2008, **42**, 85-94.
23. R. Scherf, L. S. Müller, D. Grosch, E. G. Hübner and W. Oppermann, *Polymer (United Kingdom)*, 2015, **58**, 36-42.
24. H. Gao, P. Polanowski and K. Matyjaszewski, *Macromolecules*, 2009, **42**, 5925-5932.
25. D. Konkolewicz, S. Sosnowski, D. R. D'Hooge, R. Szymanski, M. F. Reyniers, G. B. Marin and K. Matyjaszewski, *Macromolecules*, 2011, **44**, 8361-8373.
26. P. Polanowski, J. K. Jeszka, W. Li and K. Matyjaszewski, *Polymer*, 2011, **52**, 5092-5101.
27. P. Polanowski, J. K. Jeszka and K. Matyjaszewski, *Polymer*, 2010, **51**, 6084-6092.
28. J. Rosselgong and S. P. Armes, *Macromolecules*, 2012, **45**, 2731-2737.
29. H. Kawaguchi, *Polymer International*, 2014, **63**, 925-932.
30. S. Quan, Y. Wang, A. Zhou, P. Kumar and R. Narain, *Biomacromolecules*, 2015, **16**, 1978-1986.
31. N. Ide and T. Fukuda, *Macromolecules*, 1997, **30**, 4268-4271.
32. N. Ide and T. Fukuda, *Macromolecules*, 1998, **32**, 95-99.
33. G. Moad, *Polymer International*, 2015, **64**, 15-24.
34. M. Achilleos, T. Krasia-Christoforou and C. S. Patrickios, *Macromolecules*, 2007, **40**, 5575-5581.
35. A. Gregory and M. H. Stenzel, *Progress in Polymer Science*, 2012, **37**, 38-105.
36. D. J. Siegart, J. K. Oh and K. Matyjaszewski, *Progress in Polymer Science (Oxford)*, 2012, **37**, 18-37.
37. T. Terashima, S. Nishioka, Y. Koda, M. Takenaka and M. Sawamoto, *Journal of the American Chemical Society*, 2014, **136**, 10254-10257.
38. A. Debuigne, R. Poli, C. Jérôme, R. Jérôme and C. Detrembleur, *Progress in Polymer Science (Oxford)*, 2009, **34**, 211-239.
39. M. Hurtgen, C. Detrembleur, C. Jerome and A. Debuigne, *Polymer Reviews*, 2011, **51**, 188-213.
40. Y. Piette, A. Debuigne, V. Bodart, N. Willet, A. S. Duwez, C. Jérôme and C. Detrembleur, *Polymer Chemistry*, 2013, **4**, 1685-1693.

41. A. Debuigne, N. Willet, R. Jérôme and C. Detrembleur, *Macromolecules*, 2007, **40**, 7111-7118.
42. M. M. Obadia, G. Colliat-Dangus, A. Debuigne, A. Serghei, C. Detrembleur and E. Drockenmuller, *Chemical Communications*, 2015, **51**, 3332-3335.
43. C. Detrembleur, A. Debuigne, M. Hurtgen, C. Jérôme, J. Pinaud, M. Fèvre, P. Coupillaud, J. Vignolle and D. Taton, *Macromolecules*, 2011, **44**, 6397-6404.
44. D. Cordella, A. Kermagoret, A. Debuigne, C. Jérôme, D. Mecerreyes, M. Isik, D. Taton and C. Detrembleur, *Macromolecules*, 2015, **48**, 5230-5243.
45. S. Livi, J. Duchet-Rumeau, J. F. Gérard and T. N. Pham, *Macromolecular Chemistry and Physics*, 2015, **216**, 359-368.
46. D. Mecerreyes, *Progress in Polymer Science (Oxford)*, 2011, **36**, 1629-1648.
47. Y. Men, D. Kuzmich and J. Yuan, *Current Opinion in Colloid and Interface Science*, 2014, **19**, 76-83.
48. J. Yuan, D. Mecerreyes and M. Antonietti, *Progress in Polymer Science*, 2013, **38**, 1009-1036.
49. R. Sood, B. Zhang, A. Serghei, J. Bernard and E. Drockenmuller, *Polymer Chemistry*, 2015, **6**, 3521-3528.
50. H. He, M. Zhong, B. Adzima, D. Luebke, H. Nulwala and K. Matyjaszewski, *Journal of the American Chemical Society*, 2013, **135**, 4227-4230.
51. B. J. Adzima, S. R. Venna, S. S. Klara, H. He, M. Zhong, D. R. Luebke, M. S. Mauter, K. Matyjaszewski and H. B. Nulwala, *Journal of Materials Chemistry A*, 2014, **2**, 7967-7972.
52. P. Coupillaud, J. Pinaud, N. Guidolin, J. Vignolle, M. Fèvre, E. Veaudecenne, D. Mecerreyes and D. Taton, *Journal of Polymer Science, Part A: Polymer Chemistry*, 2013, **51**, 4530-4540.
53. J. Lu, F. Yan and J. Texter, *Progress in Polymer Science (Oxford)*, 2009, **34**, 431-448.
54. R. Marcilla, J. A. Blazquez, J. Rodriguez, J. A. Pomposo and D. Mecerreyes, *Journal of Polymer Science, Part A: Polymer Chemistry*, 2004, **42**, 208-212.
55. A. Debuigne, Y. Champouret, R. Jérôme, R. Poli and C. Detrembleur, *Chemistry - A European Journal*, 2008, **14**, 4046-4059.
56. D. Cordella, A. Kermagoret, A. Debuigne, R. Riva, I. German, M. Isik, C. Jérôme, D. Mecerreyes, D. Taton and C. Detrembleur, *ACS Macro Letters*, 2014, **3**, 1276-1280.
57. J. Poly, D. J. Wilson, M. Destarac and D. Taton, *Macromolecular Rapid Communications*, 2008, **29**, 1965-1972.

58. S. Harrisson, X. Liu, J. N. Ollagnier, O. Coutelier, J. D. Marty and M. Destarac, *Polymers*, 2014, **6**, 1437-1488.
59. R. Bryaskova, C. Detrembleur, A. Debuigne and R. Jérôme, *Macromolecules*, 2006, **39**, 8263-8268.
60. A. Debuigne, J. R. Caille, N. Willet and R. Jérôme, *Macromolecules*, 2005, **38**, 9488-9496.
61. M. Hurtgen, A. Debuigne, C. A. Fustin, C. Jérôme and C. Detrembleur, *Macromolecules*, 2011, **44**, 4623-4631.
62. P. Coupillaud, M. Fèvre, A. L. Wirotius, K. Aissou, G. Fleury, A. Debuigne, C. Detrembleur, D. Mecerreyes, J. Vignolle and D. Taton, *Macromolecular Rapid Communications*, 2014, **35**, 422-430.
63. Y. Xiong, J. Liu, Y. Wang, H. Wang and R. Wang, *Angewandte Chemie - International Edition*, 2012, **51**, 9114-9118.
64. R. Marcilla, M. Sanchez-Paniagua, B. Lopez-Ruiz, E. Lopez-Cabarcos, E. Ochoteco, H. Grande and D. Mecerreyes, *Journal of Polymer Science, Part A: Polymer Chemistry*, 2006, **44**, 3958-3965.
65. M. J. Muldoon and C. M. Gordon, *Journal of Polymer Science, Part A: Polymer Chemistry*, 2004, **42**, 3865-3869.
66. Y. Zuo, N. Guo, Z. Jiao, P. Song, X. Liu, R. Wang and Y. Xiong, *Journal of Polymer Science, Part A: Polymer Chemistry*, 2015, **54**, 169-178.
67. J. Ramos, J. Forcada and R. Hidalgo-Alvarez, *Chemical Reviews*, 2013, **114**, 367-428.
68. Y. Li and S. P. Armes, *Macromolecules*, 2005, **38**, 8155-8162.
69. J. Poly, E. Ibarboure, J. F. Le Meins, J. Rodriguez-Hernandez, D. Taton and E. Papon, *Langmuir*, 2011, **27**, 4290-4295.

Chapter IV

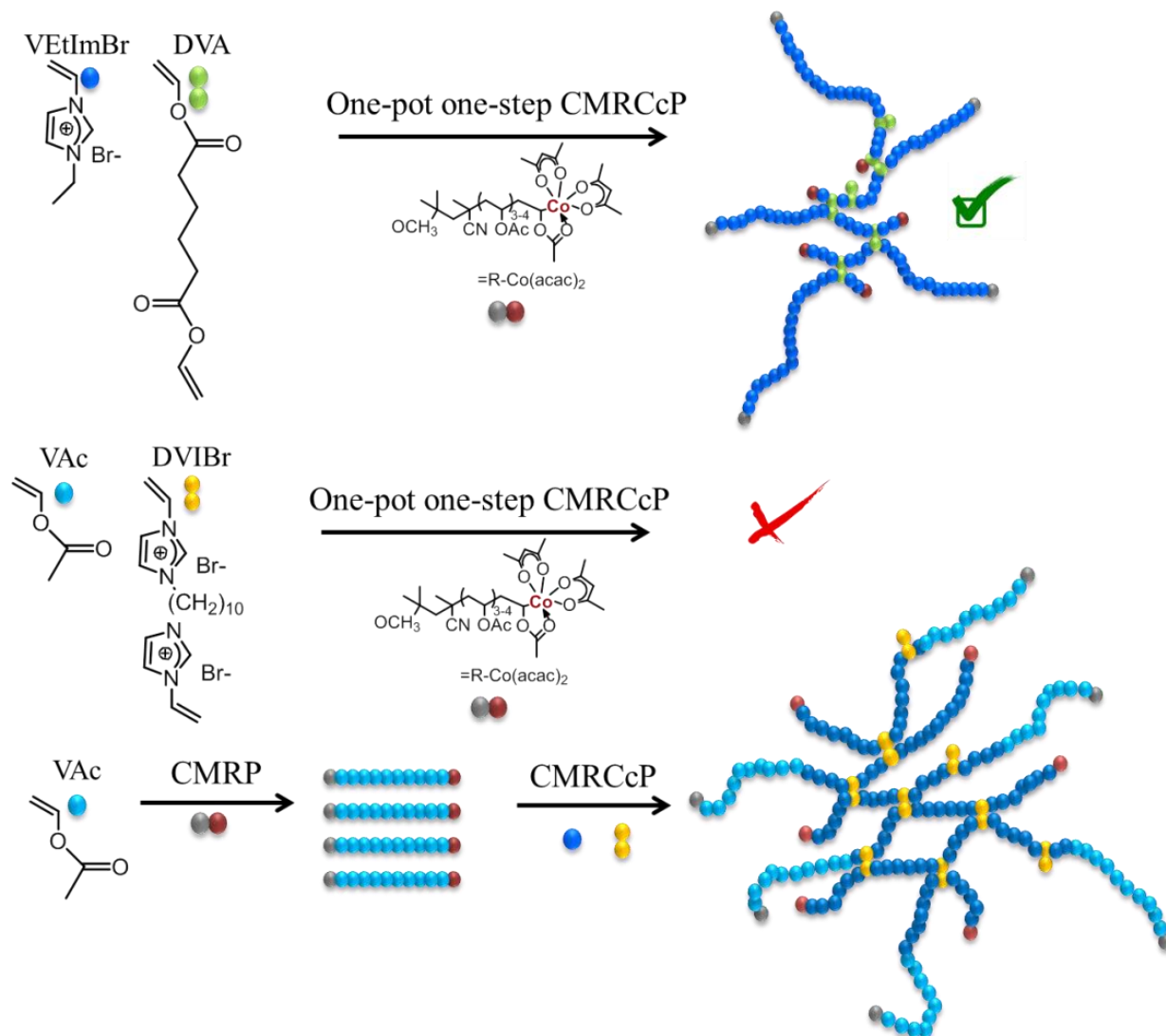
Cobalt-Mediated Radical Copolymerization of Ionic Liquid and Non-ionic Liquid Vinyl and Divinyl Monomers of Different Reactivity by for Nanogels' Synthesis.

Abstract.

We previously reported the use of cobalt-mediated radical cross-linking copolymerization (CMRCcP) as a means to access poly(vinyl acetate)-based and poly(ionic liquid)-based nanogels of controlled kinetic chain length. Cross-linkers were selected for their similarities in structure with the vinylic monomer, their relative reactivities being supposedly similar. We now report the application of CMRCcP to a vinyl and a divinyl co-monomer system of different reactivities. As in our previous works, the CMRCcP method utilizes an alkyl-cobalt (III) adduct acting as both initiator and controlling agent. The vinyl/divinyl systems studied include vinyl acetate and 1,13-divinyl-3-decyl diimidazolium bromide (VAc/DVImBr), on the one hand, and *N*-vinyl-3-ethyl imidazolium bromide and divinyl adipate (VEtImBr/DVA) on the other hand.

While the copolymerizations of VEtImBr with DVA can eventually lead to the formation of nanogels, depending on the concentration of DVA, the synthesis of a 'core-first' nanogel employing VAc/DVImBr could not be achieved, owing to highly unfavorable reactivity ratios between the two co-monomers. An alternative route is thus implemented to achieve a star-like nanogel consisting of a poly(ionic liquid)-based cross-linked core and poly(vinyl acetate) chains forming the corona.

Graphical abstract



Introduction

Major efforts in functional materials science relate to the synthesis of well-defined and shape-persistent polymeric architectures. In this context, the synthesis of star-like (co)polymers has been thoroughly investigated. Originally achieved by anionic polymerization^{1, 2}, star-like polymers can now be designed by controlled radical polymerization^{3, 4}. Star-like polymers that are characterized by a cross-linked core from which emanate polymeric arms, *i.e.* showing a core-shell structure, represent a subclass of star-like polymers. Both properties and applications of star-like polymers are similar to those found with dendrimers, but the synthetic cost is far less important. The main feature of these branched polymers is a lower viscosity in comparison to that of a linear homologue of same molar mass.

As highlighted in the previous chapters, controlled radical cross-linking copolymerization (CRCcP) has been proven effective to directly achieve nanogels and related core-shell star-like structures^{5, 6} (see Chapter II). Several controlled radical polymerization methods, such as atom transfer radical polymerization (ATRP)^{7, 8}, reversible addition fragmentation chain transfer (RAFT) polymerization⁹ or nitroxide-mediated radical polymerization (NMP)^{10, 11}, have been successfully applied to this end. Here we wish to describe cross-linked copolymer synthesis induced by a particular controlled radical polymerization method, referred to as the cobalt-mediated radical polymerization (CMRP) using $\text{Co}(\text{acac})_2$ as controlling agent^{12, 13}. We disclose here a new methodology using vinyl acetate and *N*-vinyl imidazolium-type cross-linker. This copolymerization will be subjected to the marked differences of reactivity of the two co-monomers.

Polymerizing *N*-vinyl-3-alkyl imidazolium bromide (VRImBr) ionic liquid-type monomers has already been proven effective *via* CMRP¹⁴⁻¹⁶. Control over the copolymerization allows a larger array of architectural possibilities, with the formation of block copolymers by sequential copolymerization of different VRImBr monomers¹⁶ or of VRImBr with other neutral vinyl monomers such as vinyl acetate (VAc)¹⁴.

In contrast, little is known about the direct copolymerization of an ionic liquid monomer with a neutral co-monomer and, *a fortiori* with a neutral cross-linker. A few nanogels containing ionic liquid monomer units¹⁷ or cross-linkers¹⁸ have been reported, as well as the synthesis of PIL-based nanogels either *via* conventional radical cross-linking copolymerization^{19, 20} or very recently *via* RAFT-mediated CRCcP²¹.

In Chapter III, we have reported on the direct copolymerization of a vinyl/divinyl system exhibiting a structural similarity and that can be controlled by an adduct of cobalt(III). These copolymerization leads to the formation of globular nanogel-type copolymers. Before we describe the application of CMRCcP to the synthesis of hydrophobic poly(ionic liquid)-based nanogels (Chapter V), we here report the CMRCcP involving both a neutral monomer and a hydrophilic ionic liquid co-monomer with a very different reactivity. The vinyl/divinyl systems have thus been mixed: therefore, vinyl acetate is copolymerized with an ionic liquid-type cross-linker, while an ionic liquid-type monomer is copolymerized with divinyl adipate. Our initial expectation was to achieve star-shaped nanogels in this way, *via* one pot CMRCcP.

Core-first or arms-first methods based on CRCcP⁵ have already been reported as a means to derive star-like compounds consisting of a nanogel part (Figure IV-1). For instance, the monovalent monomer is polymerized first, forming long arms, before a cross-linking agent is added²²⁻²⁵. Alternatively, the cross-linker is polymerized in dilute conditions, which is followed by the addition of the vinyl monomer^{3, 26}. The main difference between these two methods is not only reflected in the cross-linking density of the core -core-first-derived nanogels having a more cross-linked core than nanogels obtained by the arm-first method- but also in the position of the dormant/active chain ends. Active chain ends are indeed located around the core of nanogels obtained following the arm-first method, while they are localized at the periphery of the shell in the case of core-first nanogels. Coupling reactions or chain extensions can also be carried out after a core-first process, while this will be more problematic with arm-first -derived nanogels.

While two-step syntheses of arm-first or core-first nanogel have been described at several occasions these past years^{5, 27, 28}, one-step synthesis of star-like nanogels has been rarely investigated. Östürk *et al.*²⁹ have described the one-step synthesis of star-like polymers by simultaneously polymerizing the arms *via* RAFT polymerization, and the core by ring-opening polymerization in the presence of a trifunctional initiator.

Here, we call ‘one step’ the direct cross-linking copolymerization of a vinyl monomer with a divinyl cross-linker. Thus, the formation of such star-like architecture in one-step was investigated here, by changing the relative reactivities of the monomer/cross-linker system. The vinyl/divinyl systems consisted of either *N*-vinyl-3-ethyl imidazolium bromide in conjunction with divinyl adipate (VETImBr/DVA), or vinyl acetate in presence of 1,13-divinyl-3-decyl diimidazolium bromide (VAc/DVImBr). The VETImBr/DVA couple was expected to form arm-first nanogels, while VAc/DVImBr was thought to lead to core-first nanogels, as illustrated in Figure IV-1.

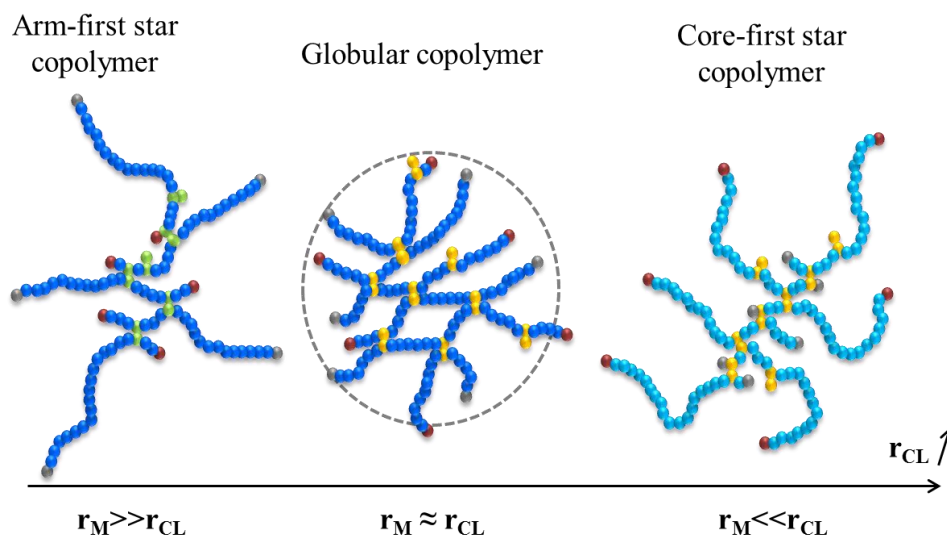


Figure IV-1. Changes in the architecture of the nanogel, depending on the relative reactivities of monomer and cross-linker, during direct CRCcP.^{5, 30}

Experimental section

Materials

Dimethylformamide (DMF) and methanol (MeOH) were dried over molecular sieves and degassed by bubbling argon during 15 minutes. 2,2,6,6-Tetramethylpiperidine 1-oxy (TEMPO) (98%, Aldrich) and divinyl adipate (DVA) were used as received. The alkyl-cobalt(III) was synthesized as already reported³¹. *N*-vinyl-3-ethyl imidazolium bromide (VETImBr) and 1,13-divinyl-3-decyl diimidazolium bromide (DVImBr) were synthesized following a previously reported strategy³². *N*-vinyl-3-ethyl imidazolium bis(trifluoromethanesulfonyl)imide (VETImNTf₂) and 1,13-divinyl-3-decyl diimidazolium bis(trifluoromethanesulfonyl)imide (DVImNTf₂) were obtained after anion exchange from bromide to bis(trifluoromethanesulfonyl)imide.

Syntheses

Copolymerization of N-vinyl-3-ethyl imidazolium bromide (VETImBr) and DVA in solution, in presence of the alkyl-cobalt(III) adduct.

In a typical procedure, VETImBr (1 g, $6.2 \cdot 10^{-3}$ mol.), and divinyl adipate (8.1 mol.%, 0.1g) were introduced in a Schlenk tube and degassed by 3 vacuum-argon cycles, and 12 mL of dry, degassed mixture of DMF and methanol (8/4, v/v) were added. The flask was thermostated at 30 °C and a solution of alkyl-cobalt(III) (0.25 mL, $7.4 \cdot 10^{-5}$ mol., solution at 1.18M) in CH₂Cl₂ was added. The reaction medium was stirred. Aliquots were regularly taken out for the conversion by ¹H NMR. Samples for SEC H₂O were quenched by TEMPO and dialyzed against water to remove DMF before SEC H₂O. Results are summarized in Table IV-1, and in Figures IV-4 and IV-5.

Copolymerization of vinyl acetate (VAc) with 1,13-divinyl-3-decyl diimidazolium bromide (DVImBr), in presence of the alkyl-cobalt(III) adduct.

In a typical experiment, DVImBr (4 mol.%, 0.08 g) was introduced in a Schlenk tube, and degassed by three vacuum-argon cycles. 12 mL of dry, degassed DMF were then added to the medium. The flask was thermostated at 40 °C, and vinyl acetate (0.53 g, $6.2 \cdot 10^{-3}$ mol.) was introduced in the Schlenk tube. A solution of alkyl-cobalt(III) (0.25 mL, $7.4 \cdot 10^{-5}$ mol., solution at 1.18M) in CH₂Cl₂ was added. The reaction medium was stirred. Aliquots were regularly withdrawn for the conversion by ¹H NMR. Samples for SEC H₂O were quenched by TEMPO and precipitated to remove any residual monomer and cross-linker. Results are summarized in Table IV-2.

Two-step polymerization to form core-shell nanogels with a cross-linked ionic liquid core and poly(vinyl acetate) shell.

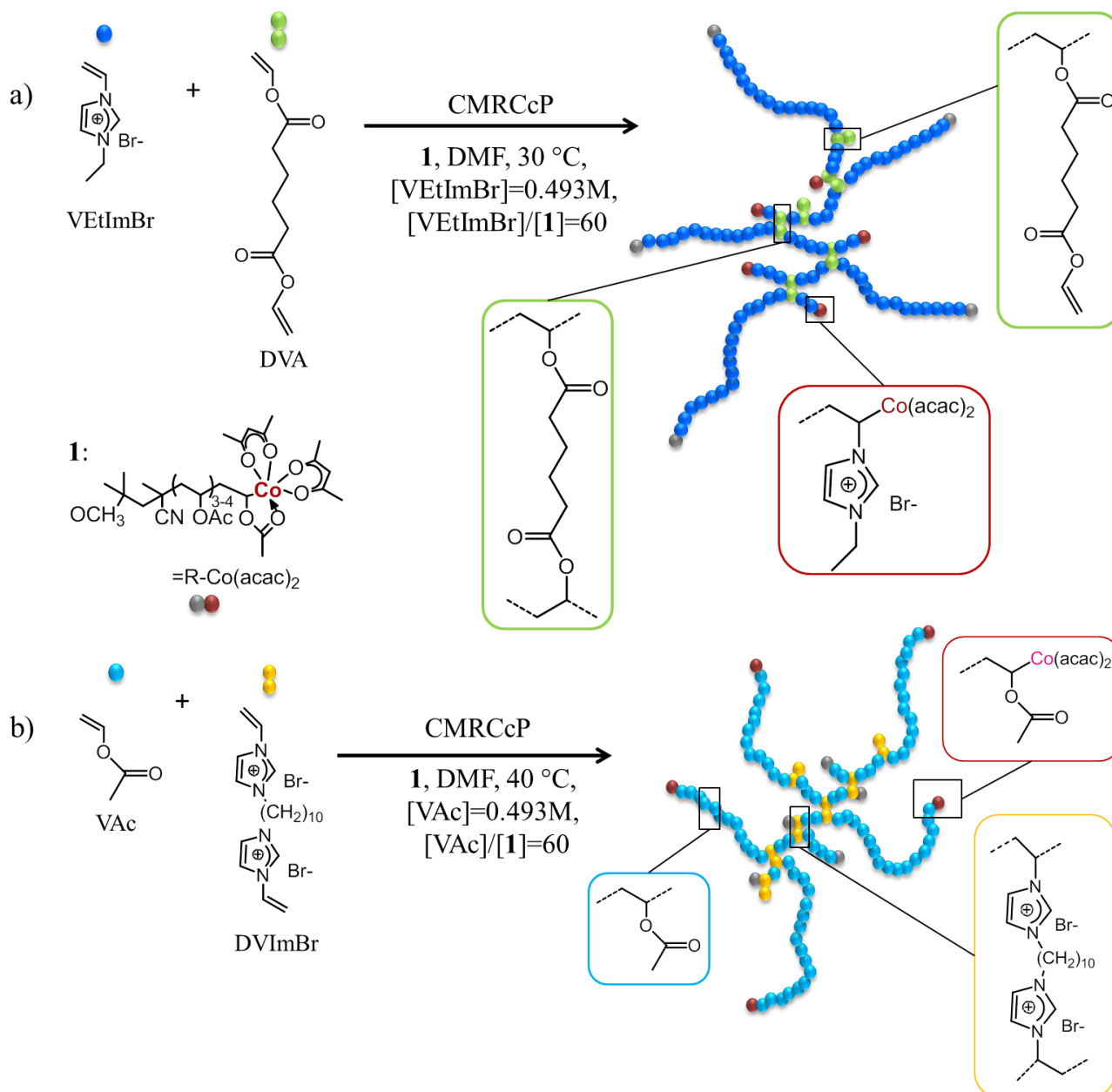
First step: 2 mL of dry, degassed ethyl acetate were added to a Schlenk tube. Vinyl acetate (0.5 mL) was then introduced in the Schlenk tube, and the medium is thermostated at 40 °C. A solution of alkyl-cobalt(III) (0.5 mL, $1.48 \cdot 10^{-4}$ mol., solution at 1.18M) in CH₂Cl₂ was added. The homopolymerization occurred over 48h.

Second step: *N*-vinyl-3-ethyl imidazolium bis(trifluoromethanesulfonyl)imide VEImNTf₂ (2 g, $6.2 \cdot 10^{-3}$ mol.) and 1,13-divinyl-3-decyl diimidazolium bis(trifluoromethanesulfonyl)imide DVImNTf₂ (0.12 g, 5 mol.%) was added along with 10 mL of cryo-distilled ethyl acetate, so that the monomer concentration was [VEImNTf₂] = 0.493M. The polymerization occurred at 30 °C for 24 h. A schematic representation of the process can be seen in Scheme IV-2. Results are summarized in Figures IV-6 and IV-7.

Characterization

Molar masses and dispersities of PVAc-type samples were determined by SEC in THF eluent, Jasco pump equipped with a set of 3 TSK gel HXL (4 000, 3 000, and 2 000) 7.5_300 mm

SEC columns, a RI Jasco detector and a UV Jasco detector at 290 nm connected in series (flow rate $1\text{ mL}\cdot\text{min}^{-1}$). Molar masses and dispersities of hydrophilic polymers (*i.e.* of poly(*N*-vinyl-3-ethyl imidazolium bromide) PILs nanogels were determined using SEC in water containing NaCl (0.1 M) and TFA (0.1%v) at 30°C (flow rate: 1 mL /min) using a Waters SEC equipped with a pre-column (PSS NOVEMA Max analytical 10 micron, 8.050 mm) and a linear column (PSS NOVEMA Max analytical linear S micron 8.0300 mm). Molar masses and dispersities of hydrophobic nanogels containing poly(*N*-vinyl-3-ethyl imidazolium bis(trifluoromethanesulfonyl)imide) were evaluated by SEC in THF containing 10 mM LiTFSI, according to the procedure reported by Matyjaszewski *et al.*³³ ^1H NMR spectra of the reaction medium and final product were recorded at 25°C with a Bruker spectrometer (400 MHz), in DMSO-d_6 .



Scheme IV-1. Cobalt-mediated radical cross-linking copolymerization and expected resulting copolymer of: a) *N*-vinyl-3-ethyl imidazolium bromide (VEtImBr) and divinyl adipate (DVA); b) vinyl acetate (VAc) and 1,13-divinyl-3-decyl diimidazolium bromide (DVIImBr).

Results and discussion

CMRCcP was applied to a vinylic/divinylic, neutral and ionic liquid, mixture of co-monomer. Thus, VAc was copolymerized in presence of 1,13-divinyl-3-decyl diimidazolium bromide

(DVImBr), whereas VEtImBr was copolymerized with divinyl adipate (DVA). As discussed in Chapter II, vinyl acetate-type monomers were expected to polymerize slower than vinyl imidazolium-type co-monomers. We investigated that point further by determining the relative reactivities between vinyl acetate (VAc) and *N*-vinyl-3-ethyl imidazolium bromide (VEtImBr). Related reactivity ratios were determined at 30 °C and 40 °C, *i.e.* at the temperature at which CMRCcP was implemented.

Determination of reactivity ratios

We used the terminal model for copolymerization. This model is based on the assumption that the reactivity of each monomer is independent of the degree of polymerization. We resorted to the method of Fineman and Ross³⁴, based on the protocol by Hurtgen *et al.*¹⁴. These copolymerization experiments were conducted both at 30 °C and 40 °C.

The method of Fineman and Ross is based upon the fact that the ratio of the consumption of each monomer at a defined time *t*, dM_1/dM_2 is equal to the ratio of the incorporation of each monomer unit in the copolymer chains dm_1/dm_2 ; this ratio is given by the instantaneous copolymer composition equation:

$$\frac{d[M_1]}{d[M_2]} = \frac{dm_1}{dm_2} = \frac{[M_1]}{[M_2]} \cdot \frac{r_1 \cdot [M_1] + M_2}{r_2 \cdot [M_2] + M_1}$$

with r_1 and r_2 as the reactivity ratios which show the preference for each monomer to react with itself, or with the other monomer. This equation can be rewritten as follow:

$$y = x \cdot r_1 - r_2$$

with $y = \frac{[M_2]}{[M_1]} \cdot \left(1 - \frac{d([M_1])}{d([M_2])}\right)$ and $x = \frac{d([M_1])}{d([M_2])} \cdot \frac{[M_2]^2}{[M_1]^2}$

Once the y ratio is plotted as a function of the x parameter, r_1 can be deduced as the slope of the linear regression of the graph, r_2 corresponding to the intercept. It was assumed that the reactivity of the vinyl imidazolium monomer was similar to that of the divinyl imidazolium cross-linker, as were the reactivities of vinyl acetate and divinyl acetate. Therefore, reactivity ratios between VEtImBr with divinyl acetate (DVA), and between VAc with divinyl imidazolium (DVImBr) were assumed to be similar than those for the copolymerization of VAc and VEtImBr at 30 °C and at 40 °C. It is worth reminding that the former temperature is the one that allowed for nanogels synthesis based on PILs while nanogels based on poly(vinyl acetate) were synthesized at 40 °C.

The consumption of each monomer was monitored by ^1H NMR spectroscopy. By this method, the relative reactivities were estimated to be $r_{\text{VEtImBr}} = 26$ and $r_{\text{VAc}} = 0.3$ at 30 °C, and $r_{\text{VEtImBr}} = 19$ and $r_{\text{VAc}} = 1$ at 40 °C. The differences between the two pairs of reactivity ratios could be due to the 10 °C difference, knowing that the rate constant of propagation (k_p) is proportional to the exponential of the reaction temperature. However, the correlation factors were not good enough to accurately assess the values of the reactivity ratios calculated.

Another protocol was used, as described by Hurtgen *et al.* in 2011³⁵. Instead of determining the dm_1/dm_2 ratio at very low conversion (less than 15 mol.%), $[M_1]$ and $[M_2]$ were determined by ^1H NMR over time, and $d[M_1]/dt$ and $d[M_2]/dt$ were obtained from the plots of $\ln([M]_0/[M]_t)$ vs. time, for both monomers, in which the experimental points were fitted with a linear regression. The slope of the straight line corresponding to the apparent constant of propagation (k_p), it could be used to calculate the $d[M]/dt$ variation for each monomer at different reaction time. High conversion of each monomer was a prerequisite in this case to calculate the reactivity ratios in this way.

Figure IV-3 below shows that only a fraction of VAc polymerizes (around 2%), even after 30 hours, while the conversion of VEtImBr was already higher (26%).

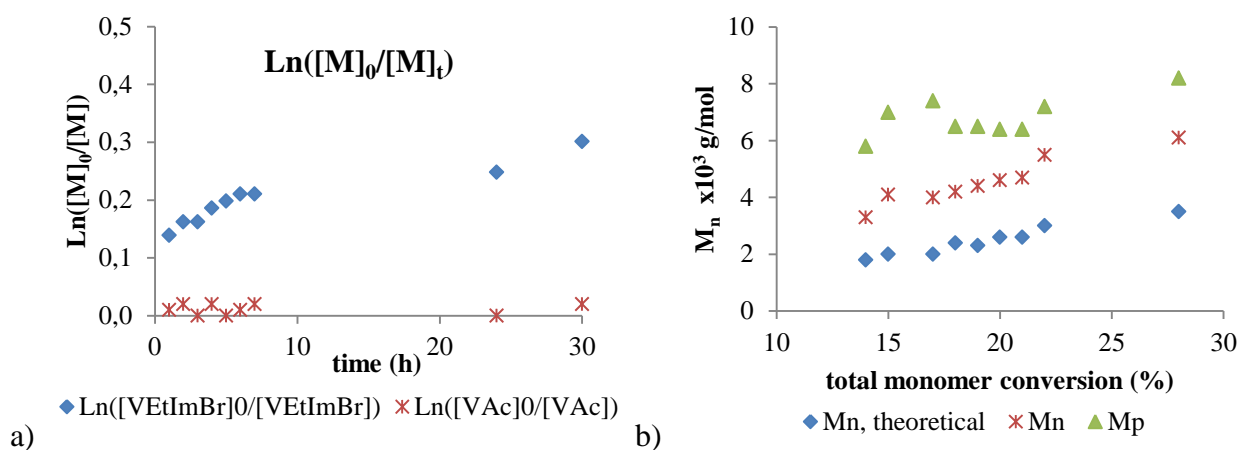


Figure IV-3. Copolymerization in a solution of DMF of VEtImBr and VAc ($[\text{VEtImBr}]/[\text{VAc}] = 1$, $([\text{VEtImBr}] + [\text{VAc}])/[\mathbf{1}] = 60$) at 30 °C initiated by **1**: a) kinetic plot; b) evolution of the molar mass of the polymer vs. total conversion. The theoretical molar mass is calculated by the equation

$$M_{n, \text{theoretical}} = (\text{conv.}_{\text{VEtImBr}} \times M_{n, \text{VEtImBr}}) + (\text{conv.}_{\text{VAc}} \times M_{n, \text{VAc}}).$$

It turned out that the relative reactivities between VEtImBr and VAc were so different that a quantitative approach was not possible. In particular, the reactivity of VEtImBr was much higher than that of VAc.

Relative reactivities and incidence on nanogels' structures

Because of this huge difference in reactivity between the two monomers it was not possible to quantify r_{VAc} and r_{VEtImBr} values. Figure IV-3 shows that VEtImBr was indeed much more rapidly consumed than VAc. Therefore, depending on the nature of the monomer and cross-linker used, and based on their different reactivity ratios, different nanogels structures might be produced during the one pot CMRCcP process. Thus, copolymerization VAc with DVIImBr should lead to a core-first nanogel, while the copolymerization of VEtImBr with DVA should provide an arm-first nanogel.

SEC traces of the CMRCcP of VEtImBr with DVIImBr shows a gradual increase in intensity of a second peak, around 12 minutes of elution, corresponding to the progressive incorporation of DVIImBr on the primary chains based on PVEtImBr (Figure IV-4a). Such a peak was not detected in

SEC traces of copolymers resulting from the copolymerization of VEtImBR with 2.9 and 4.8 mol.% of DVA, and results were similar to those the VEtImBr homopolymerization (Table IV-1). In contrast, SEC traces of the copolymerization monitoring of VEtImBr in presence of 8.1 mol.% of DVA revealed the incorporation of DVA, after a shape very similar to the homopolymerization was first noted (see Table IV-1).

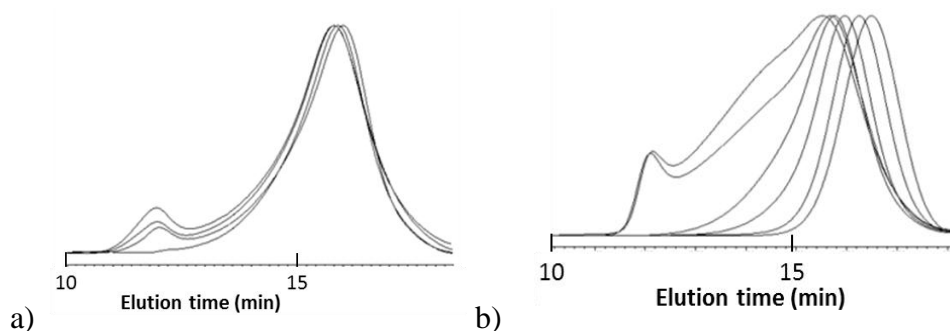


Figure IV-4. Aqueous SEC traces of the copolymerization of VEtImBr a) with 4 mol.% of DVImBr; b) with 8.1 mol.% of DVA (eluent containing NaCl (0.1 M) and TFA (0.1 v%)).

Conversions, as determined by ^1H NMR, show the incorporation of up to 20% of DVA cross-linker for the CMRCcP experiments consisting of 2.9 and 4.8 mol.% of DVA (Table IV-1, entries 1 and 2). However, SEC traces of the same are very similar to those observed for the homopolymerization of VEtImBr, *i.e.* no cross-linking was noted.

All these results (conversion by ^1H NMR and SEC data) thus suggest that homopolymerization of VEtImBr occurred first, which was followed by the cross-linking through the polymerization of DVA forming the core (Table IV-1 and Figure IV-5). As expected, when the concentration in cross-linker increases, the total conversion decreased, and a higher dispersity was noted.

Table IV-1. Copolymerization of VEtImBr and DVA in DMF, at 30 °C, in presence of **1** ([VEtImBr]/[**1**] = 60).

Entry	DVA (mol%)	time (h)	Conv (DVA, %) ^a	Conv (VEtImBr, %) ^a	M _n (g/mol) ^b	M _p (g/mol) ^b	M _w /M _n ^b
1	0	0.25	- ^c	47	4200	5000	1.28
		1	- ^c	66	6800	7700	1.35
		2	- ^c	80	8400	94000	1.30
		4	- ^c	87	9000	10600	1.40
1	2.9	0.5	0	26	2200	2800	1.55
		1	1	61	5300	6550	1.44
		2	4	75	6800	8400	1.41
		6	20	88	8150	10400	1.42
2	4.8	0.5	0	29	2700	3200	1.42
		1	6	54	4700	5700	1.36
		2	10	66	6800	8200	1.37
		6	20	80	7900	10200	1.50
3	8.1	0.5	0	17	3700	4900	1.65
		1	2	33	7400	9500	1.85
		2	10	58	9600	11900	2.14
		6	40	58	14400	13400	4.60

^a determined by ¹H NMR in DMSO; ^b determined *via* aqueous SEC (eluent containing NaCl (0.1 M) and TFA (0.1 v%)); ^c no DVA in this polymerization.

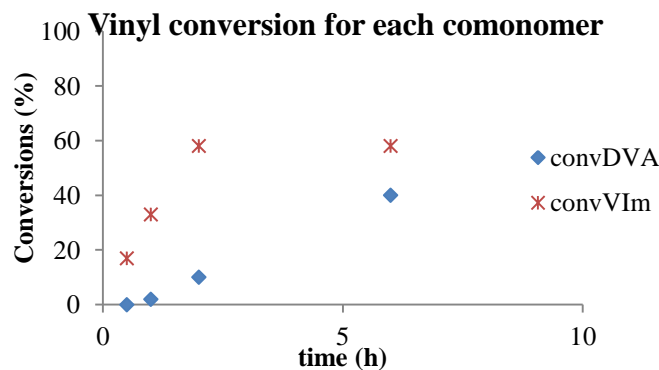
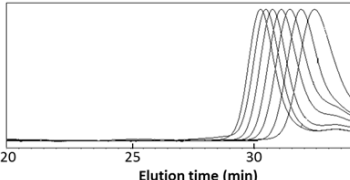
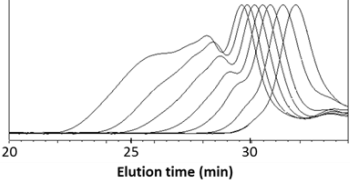
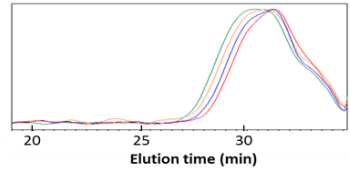
**Figure IV-5.** Conversion of VEtImBr and DVA, as a function of time, during the copolymerization experiments reported in Table IV-1, entry 3.

Table IV-2. Kinetics of the (co)polymerizations of VAc with a cross-linker (CL= DVA or DVImBr) at 40 °C in presence of **1** ([VAc]/[**1**] = 60) in DMF.

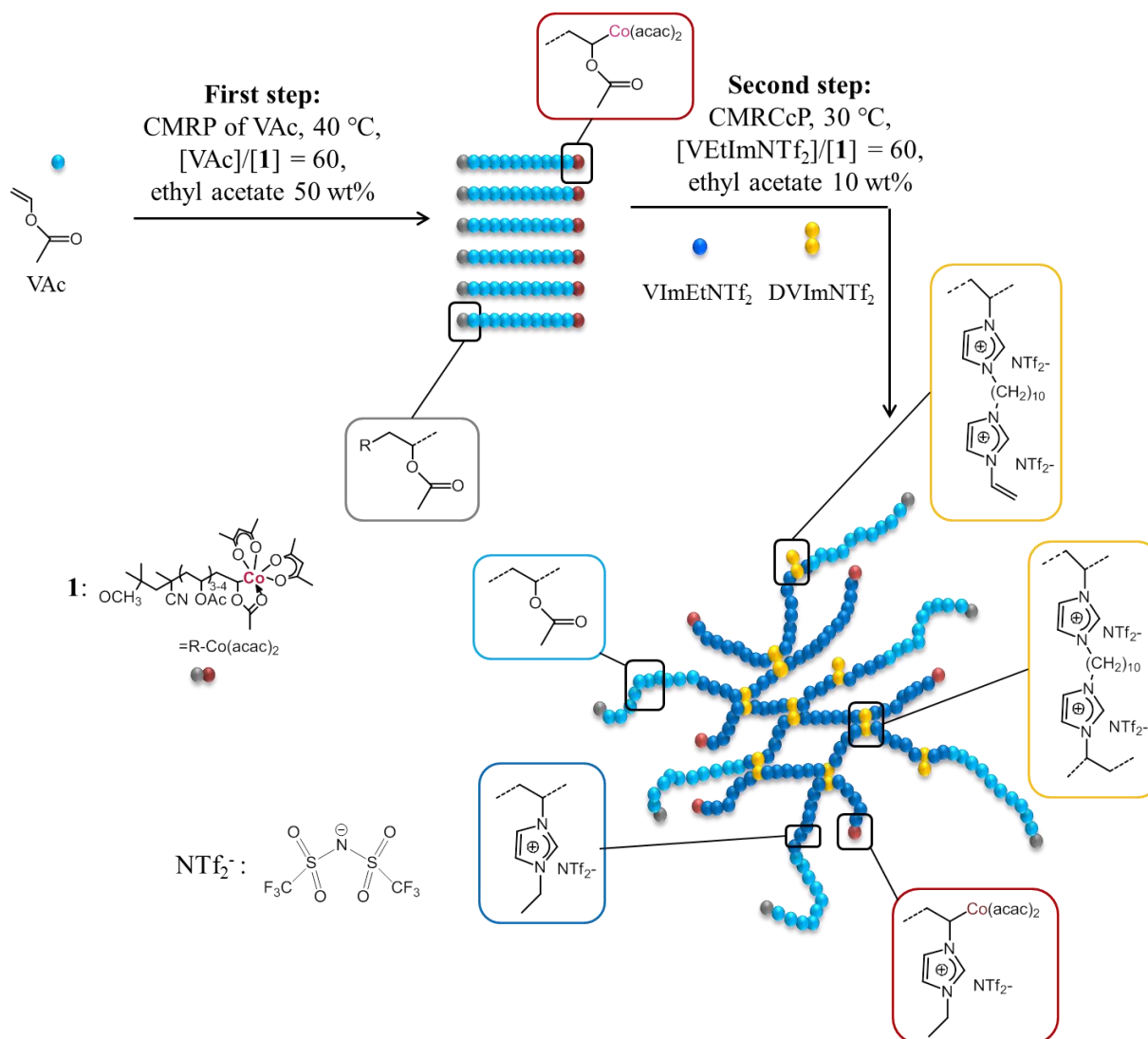
CL	mol% CL	time (h)	Conversion (%) ^a	M _n (g/mol) ^b	M _p (g/mol) ^b	M _w /M _n ^b
-	0	2	12	1300	1600	1.17
		3	21	1800	2200	1.12
		5	29	3100	3300	1.07
		7	34	4100	4500	1.07
						
DVA	4	2	10	1500	2000	1.31
		4	22	2300	3400	1.66
		6	28	4000	4600	2.20
		8	37	5600	6100	4.33
						
DVImBr	4	2	10	3400	4500	1.29
		4	16	3500	4300	1.41
		6	20	2900	4500	1.69
		8	23	3000	4500	1.70
						

^a determined by ¹H NMR in DMSO; ^b determined *via* DMF SEC.

Given the relative reactivities of DVImBr and VAc, it was expected that DVImBr would react first during CMRCcP, so that poly(vinyl acetate) arms could be grown afterwards. However, when monitoring this copolymerization by ¹H NMR and SEC, the formation of a branched structure was noted. The conversion (23 %) was yet too low to ascertain that a core-first nanogel was formed: after the beginning of the polymerization of DVImBr, the conversion did not progress, and vinyl acetate was not polymerized further. This absence of conversion could be ascribed to the marked difference between VAc and DVImBr reactivities.

While an ‘arm-first’ approach can be achieved *via* the one-step CMRCcP of VEtImBr and DVA, the ‘core-first’ one-step synthesis was not feasible to access core-shell star-like structures.

To overcome the lack of reactivity of VAc during its CMRCcP with DVImBr, a two-step pathway was investigated (Scheme IV-2) as a means to achieve the synthesis of a nanogel with a PIL-based core and PVAc corona. To avoid the need for a change of solvents when switching from the homopolymerization of VAc arms to the formation of the PIL-based core by CMRCcP, the IL co-monomers here consisted of a bis(trifluoromethanesulfonyl)imide (NTf₂⁻) counter-anion. More details will be provided in the next chapter, regarding the CMRCcP of NTf₂-containing *N*-vinyl monomers. Thus, a two-step reaction was implemented in degassed ethyl acetate. It was expected that the reactivity of VEtImNTf₂ would be different compared to that of VEtImBr, but the reactivities of VEtImNTf₂ and DVImNTf₂ were supposedly similar.



Scheme IV-2. Two-step synthesis of arm-first poly(VETImNTf₂-co-DVImNTf₂) nanogel with a PVAc shell. Conditions: homopolymerization of VAc occurs at 40 °C *via* CMRP in ethyl acetate (50 wt.%), copolymerization of VETImNTf₂-DVImNTf₂ occurs at 30 °C *via* CMRccP in ethyl acetate (10 wt.%). The ratio [monomer]/[**1**] is always maintained at 60.

First, vinyl acetate was polymerized by CMRP in ethyl acetate in the presence of the same cobalt(III) adduct acting as both initiator and controlling agent (conversion: 75%). This first step occurred over 48h, in concentrated solution of ethyl acetate. Since we previously noted that vinyl acetate did not polymerize anymore once vinyl imidazolium was introduced in the reaction medium, removal of the remaining vinyl acetate was not deemed necessary.

The second feed of co-monomer added thus consisted of VEtImNTf₂ and DVIImNTf₂ in ethyl acetate, *i.e.* with bis(trifluoromethanesulfonyl)imide (NTf₂⁻) as the counter anion. The copolymerization medium was thermostated at 30 °C, and stirred for 4 days under an argon atmosphere.

The carbon-cobalt bond at chains ends of the CMRP-derived precursors were expected to be reactivated in chain extension experiments. The PVAc precursors were thus employed as macroinitiators for the copolymerization of a mixture of VEtImNTf₂ and DVIImNTf₂.

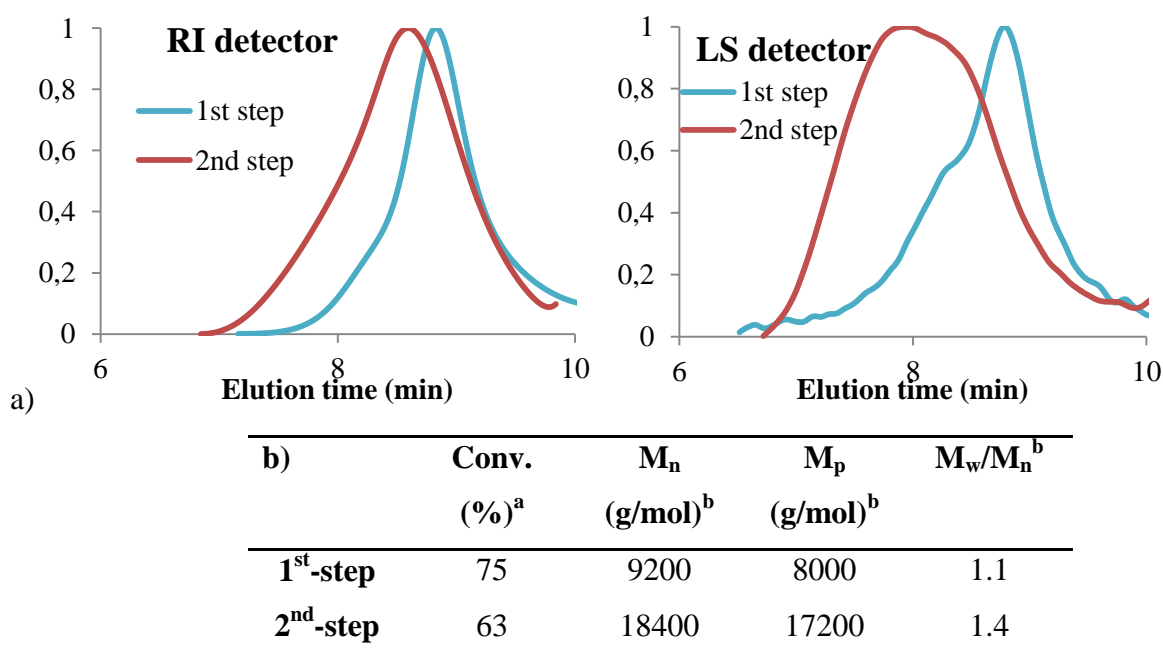


Figure IV-6. a) SEC traces and b) macromolecular characteristics of the polymers resulting from the first step (homopolymerization of VAc, in blue) and second step (after formation of a NTf₂-containing PIL-based cross-linked core, in red). ^a determined by ¹H NMR in acetone-d₆; ^b determined *via* THF SEC (eluent THF with 10 mM LiNTf₂).

A typical NMR spectrum of the resulting copolymer, after chain extension, is shown in Figure IV-7. By comparison of the integration of the signal of -CH₂-CH-O (proton b) with the H₃C-O of **1** (proton l), a DP of 40 was calculated for the VAc-based arms (first step). The

copolymerization was successful, as could be observed by both the conversions of each step and the increase of molar masses and dispersities.

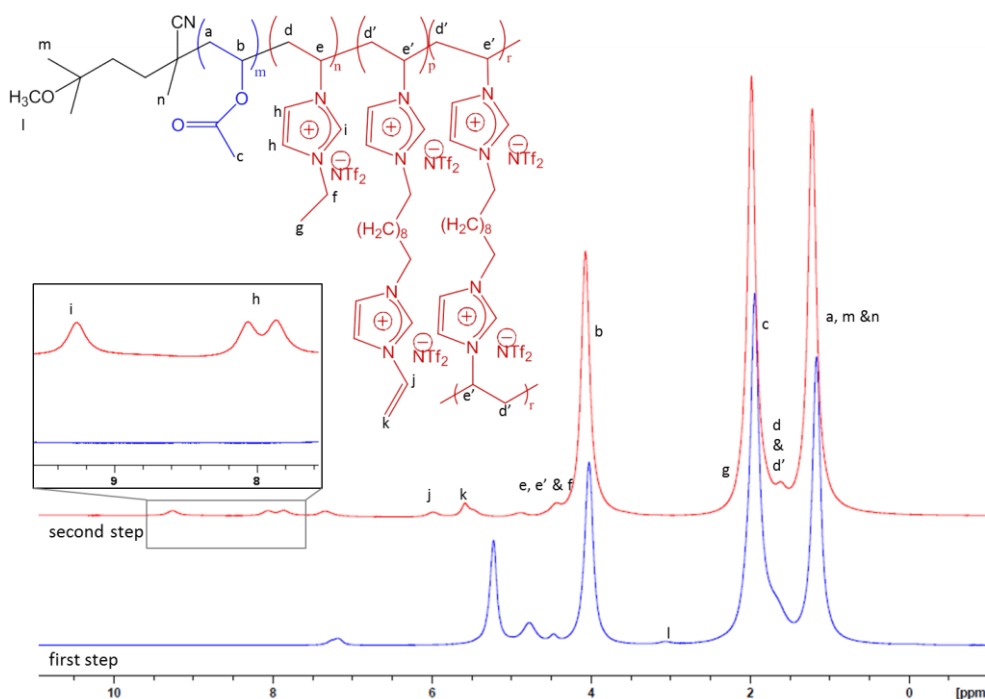


Figure IV-7. NMR spectra of the copolymer resulting from the two step synthesis after the first step (blue curve) and after the second step (red curve), in CDCl_3 .

Conclusions

In this chapter, the use of CMRCcP of a neutral and an ionic liquid vinyl/divinyl system for nanogel synthesis is implemented. The reactivity of the cross-linker is supposed to be very different from the reactivity of the vinyl monomer. The selected mono- and divinyl co-monomer pairs are as follows: VEtImBr and DVA, in the one hand, and VAc and DVImBr, on the other hand.

We have developed a single-step synthetic strategy to form poly(VEtImBr-*co*-DVA 8.1 mol.%) nanogel in DMF by CMRCcP at 30 °C with a monomer concentration [VEtImBr] of 0.493M. Such copolymers are water-soluble, and SEC traces are characteristic of a cross-linked architecture.

However, the attempted single-step synthesis of poly(VAc-*co*-DVImBr) in the presence of alkyl(III) adduct is unsuccessful, as the monomer conversion remains very low.

To circumvent the latter issue, the formation of star-like polymer *via* an arm-first two-step process can be contemplated. To keep the same solvent for both steps, copolymerization is preformed in ethyl acetate. The IL co-monomers used during the second step of the process thus consists of a hydrophobic bis(trifluoromethanesulfonyl)imide (NTf₂⁻) counter-anion. This two-step synthetic pathway allows achieving a core-shell structure constituted of a cross-linked PIL-based core and external poly(vinyl acetate) branches, which cannot be achieved *via* a one-step synthetic approach.

References

1. A. Hirao, R. Goseki and T. Ishizone, *Macromolecules*, 2014, **47**, 1883-1905.
2. H. Eschwey and W. Burchard, *Polymer*, 1975, **16**, 180-184.
3. P. Polanowski, J. K. Jeszka and K. Matyjaszewski, *Polymer*, 2014, **55**, 2552-2561.
4. P. Polanowski, J. K. Jeszka and K. Matyjaszewski, *Polymer (United Kingdom)*, 2013, **54**, 1979-1986.
5. H. Gao and K. Matyjaszewski, *Progress in Polymer Science (Oxford)*, 2009, **34**, 317-350.
6. D. Kuckling and A. Wycisk, *Journal of Polymer Science, Part A: Polymer Chemistry*, 2013, **51**, 2980-2994.
7. K. Matyjaszewski and N. V. Tsarevsky, *Journal of the American Chemical Society*, 2014, **136**, 6513-6533.
8. K. Matyjaszewski, *Macromolecules*, 2012, **45**, 4015-4039.
9. A. E. Smith, X. Xu and C. L. McCormick, *Progress in Polymer Science (Oxford)*, 2010, **35**, 45-93.
10. J. Nicolas, Y. Guillaneuf, C. Lefay, D. Bertin, D. Gigmes and B. Charleux, *Prog. Polym. Sci.*, 2013, **38**, 63.
11. Y. Amamoto, M. Kikuchi, H. Otsuka and A. Takahara, *Polymer Journal*, 2010, **42**, 860-867.
12. A. Debuigne, R. Poli, C. Jérôme, R. Jérôme and C. Detrembleur, *Progress in Polymer Science (Oxford)*, 2009, **34**, 211-239.
13. M. Hurtgen, C. Detrembleur, C. Jerome and A. Debuigne, *Polymer Reviews*, 2011, **51**, 188-213.

14. C. Detrembleur, A. Debuigne, M. Hurtgen, C. Jérôme, J. Pinaud, M. Fèvre, P. Coupillaud, J. Vignolle and D. Taton, *Macromolecules*, 2011, **44**, 6397-6404.
15. P. Coupillaud, M. Fèvre, A. L. Wirocius, K. Aissou, G. Fleury, A. Debuigne, C. Detrembleur, D. Mecerreyes, J. Vignolle and D. Taton, *Macromolecular Rapid Communications*, 2014, **35**, 422-430.
16. D. Cordella, A. Kermagoret, A. Debuigne, R. Riva, I. German, M. Isik, C. Jérôme, D. Mecerreyes, D. Taton and C. Detrembleur, *ACS Macro Letters*, 2014, **3**, 1276-1280.
17. R. Marcilla, M. Sanchez-Paniagua, B. Lopez-Ruiz, E. Lopez-Cabarcos, E. Ochoteco, H. Grande and D. Mecerreyes, *Journal of Polymer Science, Part A: Polymer Chemistry*, 2006, **44**, 3958-3965.
18. T. Das, T. K. Paira, M. Biswas and T. K. Mandal, *The Journal of Physical Chemistry C*, 2015, **119**, 4324-4332.
19. Y. Xiong, J. Liu, Y. Wang, H. Wang and R. Wang, *Angewandte Chemie - International Edition*, 2012, **51**, 9114-9118.
20. M. J. Muldoon and C. M. Gordon, *Journal of Polymer Science, Part A: Polymer Chemistry*, 2004, **42**, 3865-3869.
21. Y. Zuo, N. Guo, Z. Jiao, P. Song, X. Liu, R. Wang and Y. Xiong, *Journal of Polymer Science, Part A: Polymer Chemistry*, 2015, **54**, 169-178.
22. S. Park, H. Y. Cho, K. B. Wegner, J. Burdynska, A. J. D. Magenau, H. J. Paik, S. Jurga and K. Matyjaszewski, *Macromolecules*, 2013, **46**, 5856-5860.
23. W. Li, Y. Yu, M. Lamson, M. S. Silverstein, R. D. Tilton and K. Matyjaszewski, *Macromolecules*, 2012, **45**, 9419-9426.
24. L. A. Connal, P. A. Gurr, G. G. Qiao and D. H. Solomon, *Journal of Materials Chemistry*, 2005, **15**, 1286-1292.
25. Q. Chen, Y. Xu, X. Cao, L. Qin and Z. An, *Polymer Chemistry*, 2014, **5**, 175-185.
26. P. Polanowski, J. K. Jeszka and K. Matyjaszewski, *Polymer*, 2014, **55**, 2552-2561.
27. A. Blencowe, J. F. Tan, T. K. Goh and G. G. Qiao, *Polymer*, 2009, **50**, 5-32.
28. T. G. McKenzie, E. H. H. Wong, Q. Fu, S. J. Lam, D. E. Dunstan and G. G. Qiao, *Macromolecules*, 2014, **47**, 7869-7877.
29. T. Öztürk, M. Göktas and B. Hazer, *Journal of Applied Polymer Science*, 2010, **117**, 1638-1645.
30. J. Poly, D. J. Wilson, M. Destarac and D. Taton, *Journal of Polymer Science Part A: Polymer Chemistry*, 2009, **47**, 5313-5327.

31. Y. Piette, A. Debuigne, C. Jerome, V. Bodart, R. Poli and C. Detrembleur, *Polymer Chemistry*, 2012, **3**, 2880-2891.
32. R. Marcilla, J. A. Blazquez, J. Rodriguez, J. A. Pomposo and D. Mecerreyes, *Journal of Polymer Science, Part A: Polymer Chemistry*, 2004, **42**, 208-212.
33. H. He, M. Zhong, B. Adzima, D. Luebke, H. Nulwala and K. Matyjaszewski, *Journal of the American Chemical Society*, 2013, **135**, 4227-4230.
34. M. R. Fineman, S.D., *J. Polym. Sci.*, 1950, **5**, 259-262.
35. M. Hurtgen, A. Debuigne, C. A. Fustin, C. Jérôme and C. Detrembleur, *Macromolecules*, 2011, **44**, 4623-4631.

Chapter V

Synthesis of Hydrophobic Poly(ionic liquids)-based Nanogels *via* Cobalt-Mediated Radical Cross-linking Copolymerization (CMRCcP) and Their Use for Patterning Surfaces.

Abstract.

Cobalt-mediated radical cross-linking copolymerization (CMRCcP) has been proven a useful way to form nanogels under mild conditions. Chapter II reported the formation of hydrophilic PIL-based nanogels, emphasizing the possibility of chain extension reactions due to dormant C-Co chain ends. Chapter III described the CMRCcP of neutral and IL comonomer in a two-step process, yielding a core-shell structure with a poly(vinyl acetate) shell, and hydrophobic PIL-based core.

In this chapter, we report the copolymerization of *N*-vinyl-3-ethyl imidazolium bis(trifluoromethanesulfonyl)imide (VEtImNTf₂) with 1,13-divinyl-3-decyl diimidazolium bis(trifluoromethanesulfonyl)imide (DVImNTf₂) as cross-linker, leading to the formation of hydrophobic poly(ionic liquid)-based nanogels, *via* CMRCcP in solution in ethyl acetate, at 30 or 40 °C. Various parameters of copolymerization, including the amount of cross-linker, the temperature and the concentration, were investigated. Reactivation of the dormant chain ends was demonstrated by chain extension experiments. The thermal behavior of the resulting nanogels was studied too. The poly(VEtImNTf₂-*co*-DVImNTf₂) nanogels of first- and second-generation were also coated onto mica surface and analyzed by atomic force microscopy (AFM). Different patterns referred to as ‘breath figures’, but also ordered aggregates or interconnected pores were observed, depending on the cross-linking density of the nanogels, their concentration and the solvent used (THF/H₂O 98/2 v/v or THF). Finally, the ionic conductivity from a thin film made of the second-generation nanogel was equal to $1.9 \cdot 10^{-5}$ S/cm at 80 °C, which is higher than that of the first-generation poly(VEtImNTf₂-*co*-DVImNTf₂ 8 mol.%) at the same temperature.

Introduction

According to IUPAc's definition, nanogels are cross-linked soluble polymeric network with a dimension under 100nm¹. Their three-dimensional network results from both inter- and intra-molecular cross-linking. The cross-linked structure of nanogel makes an impact of their overall properties: as such, their viscosities - lower than that of their linear counterparts of similar molar mass – make nanogels excellent candidates in coatings at high solid contents, or as additives for organic binders. Usual synthetic pathways to nanogels include the post-polymerization cross-linking of preformed primary chains^{2, 3}, or the free-radical cross-linking copolymerization (FRCcP) of vinyl/divinyl (co)monomers in dispersed media, or FRCcP in highly dilute solution^{4, 5}.

As predicted by the works of Flory⁶ and Stockmayer⁷, such copolymerization in rather high concentrated solutions, or containing high amount of cross-linker (more than one cross-linker per primary chains) leads to macrogelation of the polymer network⁸. As previously discussed (see Chapter II), FRCcP provides little control over the internal network structure: the heterogeneity of the kinetic chain length and the distribution of cross-linking points within the final network are usually ascribed to i) a very fast chain growth; and ii) extensive intramolecular cross-linking (cyclization) forming nano/microgels⁸.

Controlled radical cross-linking polymerization (CRCcP) methods have been anticipated to lead to a more homogeneous distribution of cross-linking points within (nano)gels⁹⁻¹³. Indeed, in a CRCcP, not only do much more primary chains start growing simultaneously from the early stage of the process, but chain growth is also much slower, which favors chain relaxation and translational diffusion¹⁴, hence enhancing the probability of intermolecular cross-linking reactions.

While differences between FRCcP and CRCcP methods have been supported by experimental findings (*e.g. via* elastic or swelling analyses, light scattering measurements)¹²,

¹⁵ as previously described in Chapter II, section II-3, recent reports¹⁶ have questioned the 'better' homogeneity of CRCcP-mediated gels, as opposed to FRCcP-derived ones. According to Oppermann *et al.*¹⁶, gels obtained by CRCcP appear to be more homogeneous only because they are much less densely cross-linked (reduced cross-linking efficiency) as compared to FRCcP¹⁶. Eventually, at the same effective network density, CRCcP-derived gels would not necessarily exhibit a more even distribution of cross-linking bridges.

The use of a controlling agent in CRCcP yet provides a better control of the kinetic chain length. It also enables the gel point to be postponed and to introduce larger amounts of cross-linker¹⁷⁻²¹. Last but not least, dormant chain-ends can be reactivated in gels prepared by CRCcP, allowing for chain extension reactions and synthesis of core-shell structures²²⁻²⁴. CRCcP process can be implemented by nitroxide-mediated polymerization (NMP)^{8, 25}, reversible addition-fragmentation chain transfer (RAFT)²⁶⁻²⁸ and atom transfer radical polymerization (ATRP)^{3, 21, 29, 30}.

In Chapter III, the use of cobalt-mediated radical cross-linking copolymerization (CMRCcP) to form cross-linked structures has been established. In this way, synthesis of PVAc- and hydrophilic poly(ionic liquid) (PIL)-based nanogels has been evidenced. CMRCcP experiments reported in Chapter III have been conducted on a monovinyl monomer and a divinyl cross-linker of similar structure. Control over the kinetic chain length of the primary chains of the nanogels has been demonstrated. On the other hand, chain extension reactions from the parent (first-generation) PIL- and PVAc-based nanogels have also shown that dormant carbon-cobalt chain ends can be reactivated. In addition, the hydrophilicity of these PIL-based nanogels could be tuned by subsequent anion exchange (= metathesis reaction).

In the present chapter, the CMRCcP method has been applied to achieve hydrophobic PIL-based nanogels, in the latter circumstances, based on poly(*N*-vinyl-3-ethyl imidazolium)

featuring hydrophobic bis(trifluoromethanesulfonyl)imide counter anions. PILs are polymeric versions of ionic liquids (ILs), representing a new class of polyelectrolytes of tunable solubility, showing a rather high ionic conductivity, and a broad range of glass transition temperatures. Owing to their combined properties emanating from IL units and their polymeric nature, PILs find potential applications in areas, such as analytical chemistry³¹, biotechnology, gas separation³², dispersants, solid ionic conductors for energy, catalysis³³, etc³⁴. As was previously discussed in Chapter III, changing the counter-anion of poly(ionic liquids) (PILs) can tune or completely turn over their properties, such as their solubility, their glass transition temperature, their hydrophilicity, or even the kinetics of their polymerization³⁵⁻³⁸. Here, we tried to directly achieve hydrophobic nanogels. Hydrophobic PILs in general have gained an increasing interest in specific applications^{37, 39}. For instance, PIL-based (co)polymers have been extensively studied as potential materials for thin layer conductivity⁴⁰.

Here, we wish to describe the synthesis of hydrophobic PIL nanogels based on *N*-vinyl-3-ethyl imidazolium bis(trifluoromethanesulfonyl)imide VEtImNTf₂ monomer *via* CMRCcP. To this end, we resorted to 1,13-divinyl-3-decyl diimidazolium bis(trifluoromethanesulfonyl)imide (DVImNTf₂) as a cross-linker, whose double bonds supposedly exhibit a similar reactivity to that of VEtImNTf₂. The bis(trifluoromethanesulfonyl)imide counter anion, denoting as NTf₂⁻, is known to form a highly delocalized ion pair with imidazolium moieties³⁷ (structure of NTf₂⁻ on Scheme V-1). To the best of our knowledge, the formation of hydrophobic PIL-based nanogels by a controlled radical pathway has never been reported before.

CMRCcP of VEtImNTf₂ and DVImNTf₂ was performed in ethyl acetate solution, in presence of a pre-synthesized alkyl-cobalt(III) complex (R-Co(acac)₂, **1**) as a single-

component initiator/mediating agent. The capacity to further extend these nanogels was also explored, either *via* coupling reactions or *via* chain extending experiments.

Some of CMRCcP-derived nanogels of poly(VETImNTf₂-*co*-DVImNTf₂) were then investigated as coatings for structured surfaces, referred to as ‘breath figures’⁴¹. Given the hydrophobic nature of the nanogels, and the reported ionic conductivity of linear NTf₂-containing copolymers^{42, 43}, samples of first- and second-generation nanogels were also assessed in ionic conductivity measurements.

Experimental section

Materials

Ethyl acetate was dried over CaH₂ and cryo-distilled. 2,2,6,6-Tetramethylpiperidine 1-oxo (TEMPO) (98%, Aldrich) was used as received. The alkyl-cobalt(III) initiator (R-Co(acac)₂/mediating agent (**1**)) was synthesized as already reported⁴⁴. The ionic liquid (IL) monovalent monomer, *N*-vinyl-3-ethyl imidazolium bromide (VETImBr), was synthesized as reported in the literature⁴⁵. 1,13-Divinyl-3-decyl diimidazolium bromide (DVImBr) was synthesized following the same strategy, using dibromodecane. The reaction mixture was left to stir for 3 days. Both VETImBr and DVImBr then underwent an anion exchange, from bromide to bis(trifluoromethanesulfonyl)imide NTf₂⁻³¹. They were first solubilized in deionized water, and 2 equivalents of LiNTf₂ were added under stirring to the aqueous solution. The resulting DVImNTf₂ is a solid, while VETImNTf₂ is a viscous liquid.

Syntheses of first-generation nanogels

Copolymerization of N-vinyl-3-ethyl imidazolium bis(trifluoromethanesulfonyl)imide (VEtImNTf₂) with 5 mol.% of 1,13-divinyl-3-decyl diimidazolium bis(trifluoromethanesulfonyl)imide (DVIImNTf₂) in ethyl acetate.

In a typical procedure, VEtImNTf₂ (2 g, 5.10⁻³ mol) and DVIImNTf₂ (0.06 g, 2.5 10⁻⁴ mol, 5 mol.%) was introduced in a previously flamed Schlenk tube, dried under vacuum overnight and degassed by three vacuum/Argon cycles. Degassed ethyl acetate (10 mL) was then added to the monomer, and the mixture was stirred at 30 °C. A solution of R-Co(acac)₂ **1** (0.40 mL, 7.4 10⁻⁵ mol, solution at 1.18 M) in CH₂Cl₂ was then introduced in the medium under Argon. Aliquots were regularly withdrawn both for the conversion by ¹H NMR, and for SEC analysis. Samples for SEC were quenched by TEMPO. Results are shown in Tables V-1 and V-2.

Syntheses of second-generation nanogels

Isoprene-coupling.

In a typical procedure, after 24h of copolymerization –see above, first-generation nanogel synthesis- the reaction medium was separated into three portions *a*, *b* and *c*. Part *a* was used for analysis of the first-generation nanogel, *b* was diluted by ethyl acetate by a factor 2, and then 0.5 mL of isoprene (5.10⁻³ mol) were added to the diluted solution. Part *c* was not diluted, and 0.5 mL of isoprene were added. The two solutions were then left for stirring overnight.

Chain extension reaction on a first-generation nanogel leading to a hairy nanogel (no cross-linker in the extensions).

In a typical procedure, VEtImNTf₂ (0.5 g, 1.25 · 10⁻³ mol) was introduced in a previously flamed Schlenk tube, and dried under vacuum overnight. Ethyl acetate (2.5 mL) was then added to the medium, and the mixture is stirred. 2.5 mL of the first-generation copolymerization medium is then transferred to the Schlenk tube. Aliquots are taken out for conversion and SEC analysis. Results are summarized in Figure V-7.

Characterizations

Conversions were determined by ¹H NMR spectroscopy in acetone-d₆ on a Bruker AC-400 Spectrometer. According to the procedure reported by Matyjaszewski *et al.*³¹, macromolecular parameters of PILs (M_n, M_w/M_n) were determined by size exclusion chromatography (SEC), with a SFD S5200 autosampler liquid chromatograph equipped with a SFD refractometer index detector 2000, carried out in tetrahydrofuran (THF) containing 10 mM LiTf₂N (flow rate: 1 mL·min⁻¹) at 35 °C according to a previously reported procedure.³⁷ A PSS SDV analytical linear S 5 µm column (molar mass range: 100–150 000 Da), protected by a PL gel 5 µm guard column, was calibrated with PS standards.

Differential scanning calorimetry (DSC) measurements were carried out using a Q1000 apparatus from TA Instruments. DSC experiments were performed with aluminum sealed pans. A constant rate of heating/cooling of 10 °C/min was used for all experiments.

Transmission electron microscopy (TEM) images were recorded on a Hitachi H7650 microscope working at 80 kV equipped with a GATAN Orius 11 Megapixel camera. Samples were prepared *via* deposition of a drop of polymeric solution on a TEM grid, and subsequent absorption of solution excess.

Atomic force microscopy (AFM) images were recorded in air with a Nanoscope IIIa microscope operating in tapping mode. The probes were commercially available silicon tips with a spring constant of 42 N/m, a resonance frequency of 285 Hz and a typical radius of curvature in the 8-10 nm range. Freshly cleaved mica was used as substrate. For the preparation of porous surfaces, sample solutions in THF/water (98/2 v/v %) at a concentration of 10.0 mg/mL (respectively in THF at concentrations of 1.0 and 0.1 mg/mL) were deposited on the substrate (20 μ L) and immediately spin-coated (duration: 60 s, rate: 1500 to 2000 rpm).

Coatings for conductivity measurements were realized *via* spin-coating on indium titanium oxide (ITO) surface of a polymer solution in THF (respectively in a THF/PGMEA 9/1 v/v mixture). The surface was then annealed 5 minutes at 130 °C to eliminate any remaining traces of the solvent. AFM imaging was used to assess the durability of the coating after annealing. A top aluminium electrode was then placed on top of the polymer film. In order to remove traces of moisture, the samples were annealed again at 100 °C before ionic conductivity was measured. The impedance is fitted by means of a Voigt's equivalent electrical circuit. The equivalent circuit was composed of the electrode resistance R_c in series with two high-frequency capacitances in parallel with the resistances. One loop of the circuit represents the material, and the second one represents the electrolyte (the PIL nanogel). Finally, the ionic conductivity is calculated as follow:

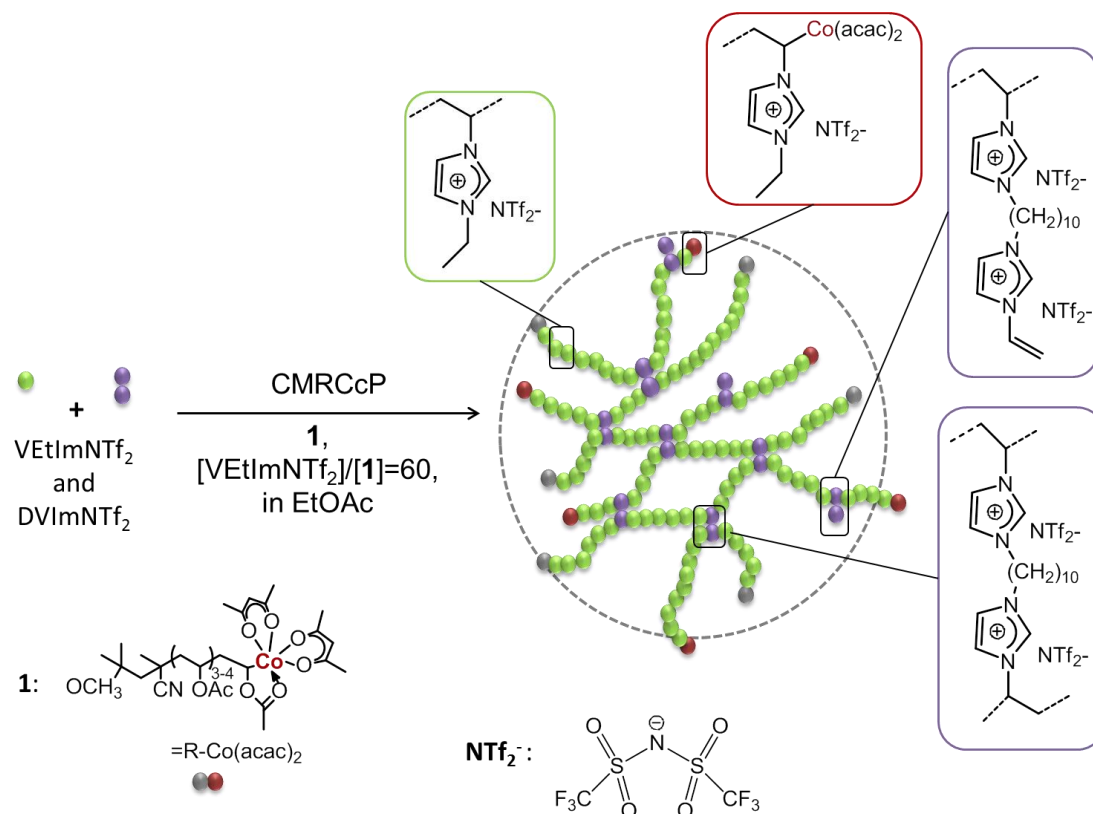
$$\sigma = \frac{1}{R_{electrolyte}} * \frac{t}{S}$$

with t the thickness of the electrolyte layer (cm), S the electrode contact surface (cm²) and $R_{electrolyte}$ extracted from Nyquist plot of impedance spectroscopy.

Results and discussion

CMRCcP of the hydrophobic IL-type monomer, namely, *N*-vinyl-3-ethyl imidazolium bis(trifluoromethanesulfonyl)imide (VETImNTf₂) in presence of 1,13-divinyl-3-decyl

diimidazolium bis(trifluoromethanesulfonyl)imide (DVIImNTf₂) as cross-linker, was carried out using the preformed alkyl-cobalt(III) adduct (R-Co(acac)₂ denoted as **1**) as mediating agent (see Scheme V-1). Ethyl acetate was selected as the solvent for these copolymerizations, on the basis of recent works by Cordella *et al.*⁴⁶ on CMRP-derived hydrophobic PILs and related all PIL-based block copolymers. The initial ratio of monomer over **1** was kept constant and at the same value than for the hydrophilic PIL-based nanogel reported in Chapter II, *i.e.* [VEtImNTf₂]/[**1**] = 60. The amount of cross-linker, the effect of the temperature and the dilution were also investigated (see Table V-1).



Scheme V-1. Cobalt-mediated radical cross-linking copolymerization of VEtImNTf₂ and DVIImNTf₂ mediated by **1** in ethyl acetate; conditions of dilution and temperature vary depending on the reaction considered (see Table V-1).

Table V-1. Synthesis of first-generation nanogels by CMRCcP of VEtImNTf₂ and DVImNTf₂, and molecular characteristics of the copolymers after 8 hours of reaction.

Entry	[VEtImNTf ₂] (mol/L)	T (°C)	DVImNTf ₂ (mol.%)	Conversion (%) ^a	M _n (g/mol) ^b	M _p (g/mol) ^c	M _w /M _n ^b
1	0.493	30	3	80	3700	3900	1.14
2	0.493	30	5	64	7800	9700	1.29
3	0.493	30	8	90	9800	13200	1.59
4	0.493	30	15	65	10900	14500	1.60
5	0.493	30	20	46	4700	8400	1.40
6	2.465	30	5	68	6400	10000	1.88
7	0.493	40	15	67	15000	28600	2.22

^a Determined by ¹H NMR in acetone-d₆. ^b Molar masses and dispersities were determined by SEC in THF with 10mM LiNTf₂. ^c M_p represents the molar mass of the maximum of the peak, and was determined by SEC in THF with 10mM LiNTf₂. Conditions: CMRCcP in ethyl acetate, [VEtImNTf₂]/[**1**] = 60, 8h of copolymerization.

CMRCcP's of VEtImNTf₂ and DVImNTf₂

CMRCcP's of VEtImNTf₂ and DVImNTf₂ in ethyl acetate were monitored *via* ¹H NMR and SEC analysis, following the conversion of all vinyl groups. It was not possible to distinguish the conversion of VEtImNTf₂ to that of DVImNTf₂, due to their strong similarities in structure and their peaks overlapping in ¹H NMR spectroscopy. The crosslinks not being cleavable, degradation of the resulting nanogels to access their primary chain lengths (see Chapter III) was not feasible either here.

The influence of the concentration of cross-linker on the final copolymer was investigated by a series of syntheses in ethyl acetate, at a concentration of 0.493 M, at 30 °C (Table V-2, and Figure S V-1). Under such conditions, syntheses containing high amounts of cross-linker led to a high conversion (90% of conversion for 8 mol.% of DVImNTf₂, Table V-1, entry 3, as determined by ¹H NMR) without macrogelation. This might be ascribed to a

high probability of cyclization. Yet, gelation was observed for CMRCcP containing 20 mol.% of divinyl imidazolium. The low dispersities found for the first hours of copolymerization ($M_w/M_n < 1.1$) was likely indicative of the pending double bonds of the cross-linkers reacting at latter stages of the process. Figure S V-2 (in Supporting Information) shows the ^1H NMR of the copolymer, denoted as poly(VEtImNTf₂-*co*-DVImNTf₂ 8 mol.%). The effect of temperature (Figure V-2) and of dilution (Figure V-3 and V-4) was also investigated (see further).

Table V-2. Kinetics of CMRCcP's of *N*-vinyl-3-ethyl imidazolium bis(trifluoromethanesulfonyl)imide (VEtImNTf₂) and 1,13-divinyl-3-decyl diimidazolium bis(trifluoromethanesulfonyl)imide (DVImNTf₂) using **1**.

Entry	DVImNTf ₂ (mol.%)	Time (h)	Conv. (%) ^a	M _n (g/mol) ^b	M _p (g/mol) ^c	M _w /M _n ^b
1	3	0.5	20	2300	2300	1.03
		1	32	2500	2700	1.04
		4	66	3500	3500	1.07
		8	80	3900	3700	1.14
		24	98	4900	4300	1.21
2	5	0.5	22	3100	3000	1.01
		1	27	3700	3700	1.02
		4	50	5900	5500	1.13
		8	64	7800	9700	1.29
		24	-	9400	13100	1.31
3	8	0.5	22	3500	3600	1.01
		1	34	4400	4200	1.06
		4	58	7300	8700	1.28
		8	90	9800	13200	1.59
		24	-	11000	14300	1.56
4	15	0.5	16	3900	4000	1.01
		1	30	4900	4700	1.06
		4	54	8600	9900	1.34
		8	65	10900	14500	1.60
		24	-	14100	22100	1.80

Table V-2 following p.155

5	20	0.5	3			
		1	6	2000	2000	1.03
		4	17	3500	3400	1.13
		8	46	5700	8300	1.4
		24	macrogel	-	-	-

^a Conversion of double bonds was determined by ¹H NMR in acetone-d₆. ^b Molar masses and dispersities were calculated *via* SEC (eluent: THF with 10mM LiNTf₂). ^c M_p represents the molar mass at the maximum of the peak, and was determined by SEC in THF with 10mM LiNTf₂. Conditions: all polymerizations occur at 30 °C, with a ratio [VEtImNTf₂]/[**1**]=60, in dried ethyl acetate ([VEtImNTf₂]₀=0.493mol.L⁻¹).

Effect of the concentration of cross-linker

Expectedly, molar masses of nanogels increase by increasing the concentration of DVImNTf₂ (Tables V-2 and Figure V-1), for a fixed concentration in monomer VEtImNTf₂ and in the mediating agent **1** (kinetic monitoring *via* SEC traces can be found in Supporting Information, Figure S V-1). Multimodal SEC traces of poly(VEtImNTf₂-*co*-DVImNTf₂) are characteristic of cross-linked architectures, and are clearly shifted towards higher molar masses when the concentration in cross-linker is increased (Figure V-1a). For same comonomers concentrations, molar masses increase with the conversion of the comonomers, in line with a controlled process (Table V-2 and Figure S V-1). Figure V-1b shows the semi-logarithmic plot of Ln([VEtImNTf₂]₀/[VEtImNTf₂]) *vs.* time for these CMRCcP's. The comparison shows that no significant difference in conversion rate is observed during the first stages of the process. It is noteworthy that following a similar procedure, aqueous CMRCcP of hydrophilic VEtImBr and DVImBr led to macroscopic gel for a cross-linker content superior to 4.8 mol.% (see Chapter III).

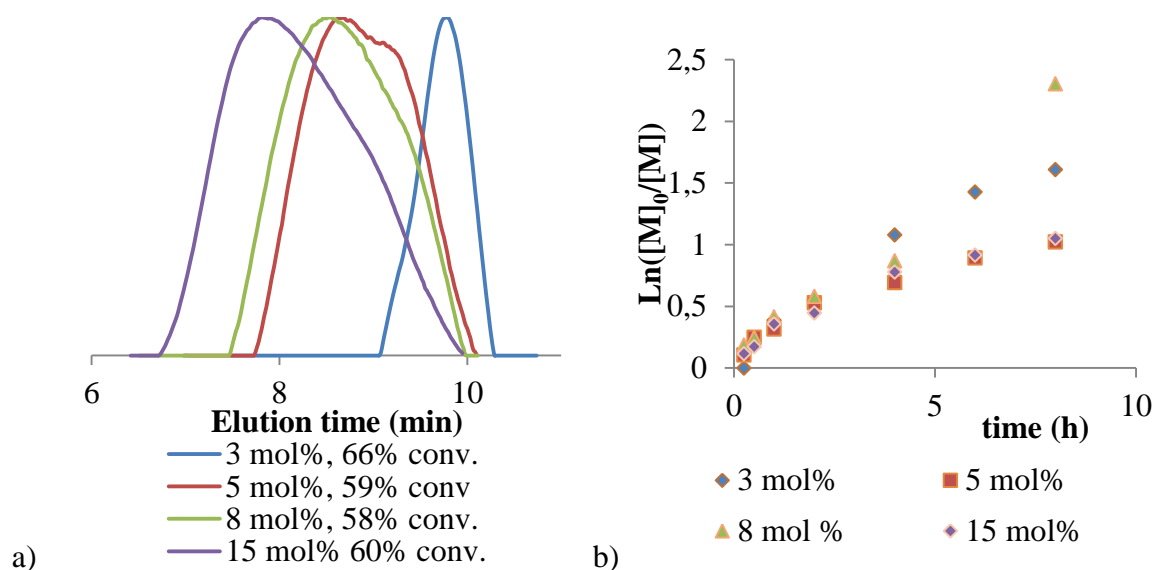


Figure V-1. a) SEC analysis in THF containing 10mM LiNTf₂ of poly(VEtImNTf₂-co-DVImNTf₂) nanogels prepared after 8h of polymerization, in ethyl acetate ([VEtImNTf₂]=0.493M) in presence of **1** ([VEtImNTf₂]/[**1**]=60), and b) $\ln([M]_0/[M])$ vs. time for each CMRCcP, M representing VEtImNTf₂ + DVImNTf₂.

Effect of temperature

Cobalt-mediated radical polymerization (CMRP) has been proven to be more thermally sensitive than other CRCCP⁴⁷. In the present work, CMRCcP was also effective at a slightly higher temperature (40 °C instead of 30 °C in the previous series). This is shown in the SEC traces in Figure V-2. The evolution of the vinyl conversion –monitored by ¹H NMR– did not vary significantly either. However, SEC traces of the two copolymerizations showed an increase of both molar mass and dispersity as the temperature increased, as observed at 8 hours of copolymerization in Figure V-2 (SEC traces of the copolymerization occurring at 40 °C can be found in Annexes in Figure S V-3). This might be correlated to a higher probability of intermolecular cross-linking reactions over cyclization ones.

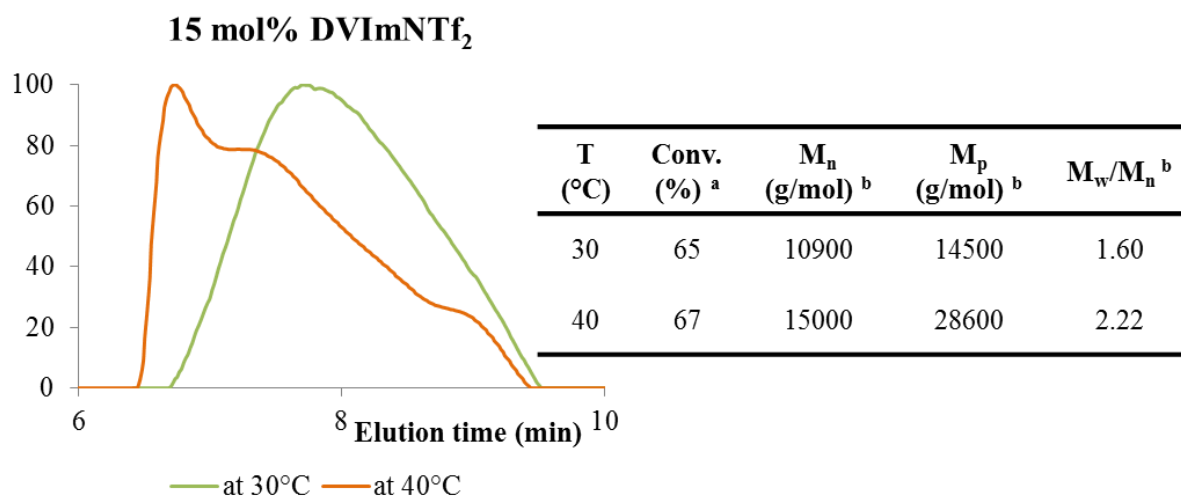


Figure V-2. SEC analysis in THF containing 10mM LiNTf₂ of the CMRCcP of VEtImNTf₂ and DVImNTf₂ at 15 mol.% of cross-linker, respectively, at 30 °C (green curve) and at 40 °C (orange curve), at 8 hours of copolymerization. ^a Conversion is determined by ¹H NMR in acetone-d₆. ^b Molar masses and dispersities are calculated *via* THF SEC.

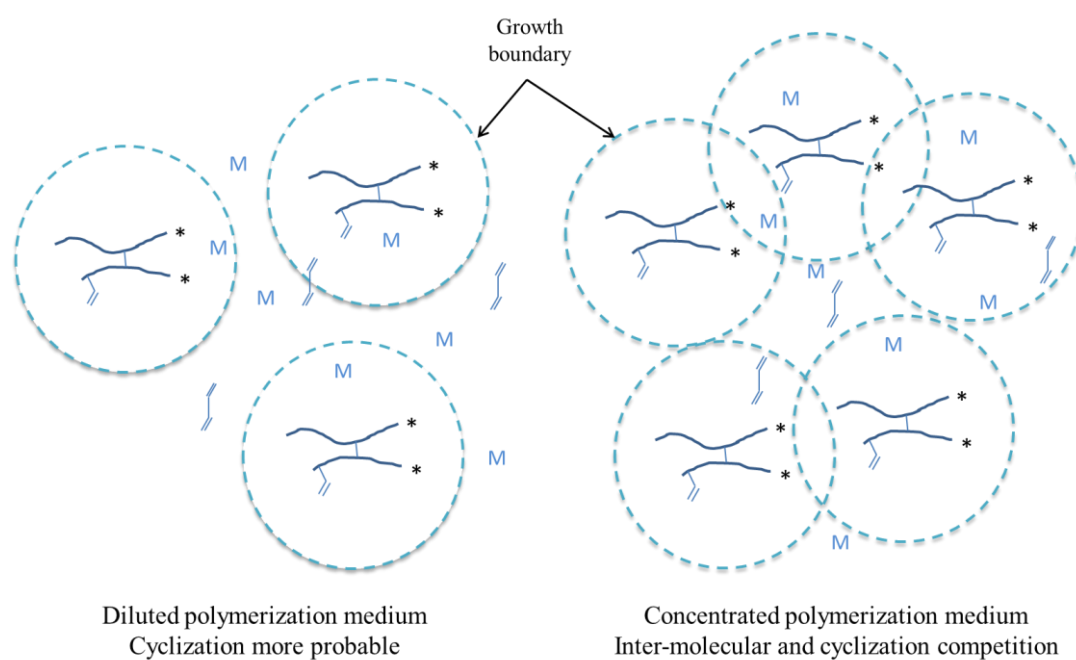
Effect of dilution

Armes *et al.* have shown that the initial concentration of monomer plays a crucial role in the competition between cyclization and inter-molecular cross-linking⁴⁸. The authors have defined an intermediate concentration, *c*^{*}, between the domain of diluted media (in which cyclization is more likely) and the domain of concentrated media (in which inter-molecular cross-linking is more likely). While the exact value of *c*^{*} depends on each system, the authors acknowledge that *c*^{*} is usually around 10 wt.% of monomer.

Here, the same VEtImNTf₂/DVImNTf₂ mixture was polymerized in ethyl acetate at 30 °C, in presence of **1**, using two different concentrations *i.e.* either at 0.493M, or at 2.465M.

The conversion, as determined by ¹H NMR, proved independent of the dilution of the medium (Figure V-3b). However, related SEC traces showed some differences (Figure V-3a and V-4). This might be the reflect of higher probability of inter-molecular branchings for a more concentrated copolymerization medium (Scheme V-2), leading to a nanogel with a

higher molar mass (28 600 g/mol at 40 °C vs. 14 500 g/mol at 30 °C), and broader dispersity (2.22 at 40 °C vs. 1.60 at 30 °C). Note that the SEC peak observed at high molar mass on Figure V-3a for sample prepared at 2.465M, was beyond the exclusion limit of the SEC column. The separation range of the SEC columns being between 100 and 150000 g/mol, the absolute molar mass of the nanogel should therefore be much higher than 150000 g/mol.



Scheme V-2. The importance of dilution in the competition between inter-molecular cross-linking and cyclization (inspired by Armes *et al.*⁴⁸).

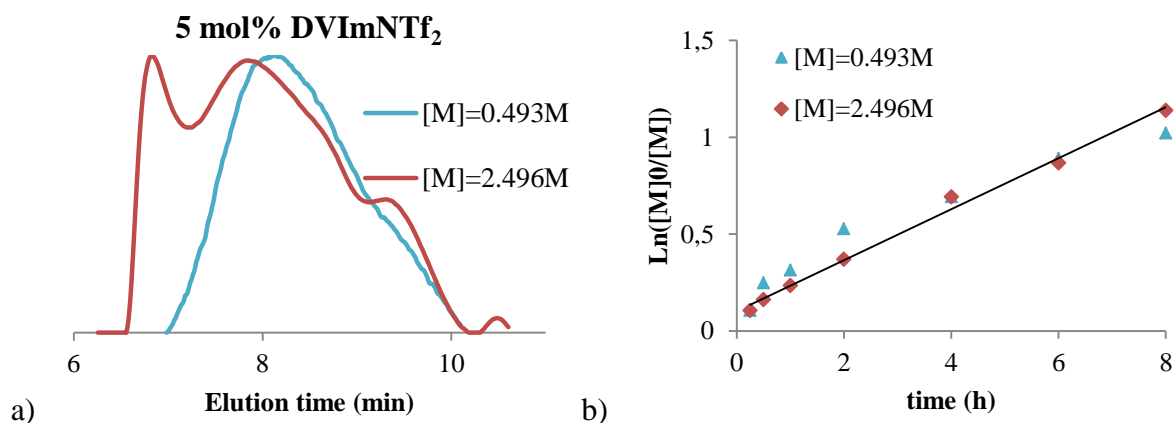


Figure V-3. a) SEC traces of CMRCcPs of VEImNTf₂ and DVImNTf₂, at 0.493M (in blue) or 2.465M (in red); b) Ln([M]₀/[M]) vs. time, M representing VEImNTf₂ + DVImNTf₂. Conditions: CMRCcP in ethyl acetate at 30 °C, in presence of **1** ([VEImNTf₂]/[**1**] = 60), with 5 mol.% of DVImNTf₂.

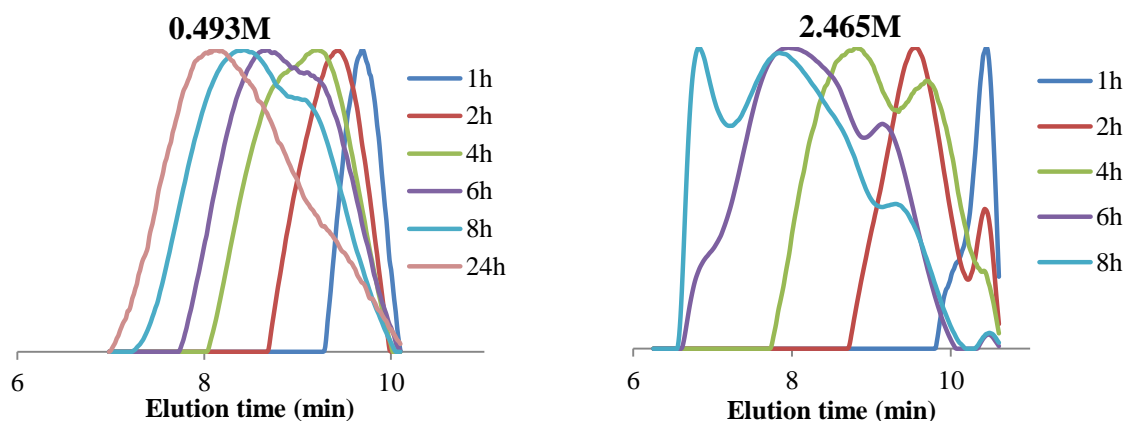


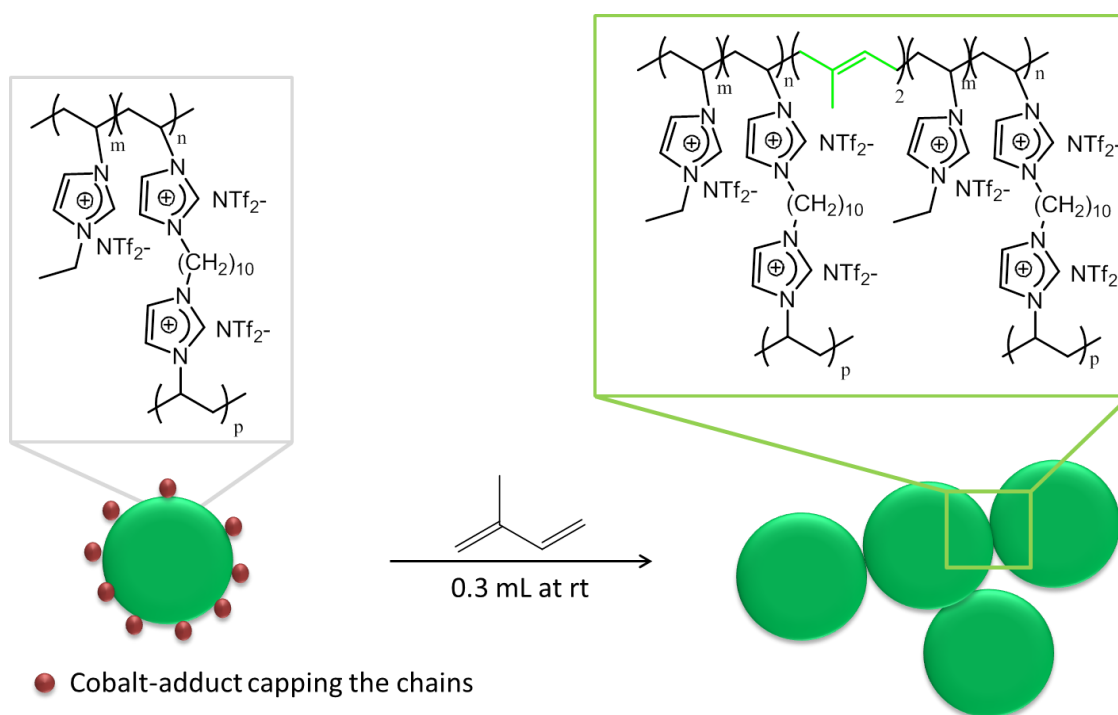
Figure V-4. SEC traces in THF containing LiNTf₂ 10 mM of CMRCcPs of VEImNTf₂ and DVImNTf₂ at (a) 0.493M and (b) 2.465M in ethyl acetate at 30 °C, at different times of polymerization.

2nd-generation nanogels by isoprene coupling or by chain extension reactions

Chain extension reactions and coupling reactions on a preformed “first-generation” nanogel are expected to lead to a “second-generation nanogel”, which also establishes that dormant cobalt-carbon (C-Co) bond at the chain end can be reactivated.

Another way of reactivating the dormant chain ends grown by CMRP is through isoprene coupling⁴⁹. Addition of isoprene has indeed been reported to induce a fast and quantitative coupling reaction, called cobalt-mediated radical coupling (CMRC), when introduced onto polymer chains end-capped by $\text{Co}(\text{acac})_2$ ^{50, 51}.

The isoprene coupling of the nanogels is schematized in Scheme V-3. Isoprene was either directly introduced to the copolymerization medium, or after the medium was diluted by a factor 2. In the first case, macrogel was achieved after stirring overnight (Figure V-5a), after addition of isoprene. In contrast, under diluted conditions, no macrogelation was noted.



Scheme V-3. Expected coupling of CMRCcP-derived poly(VEtImNTf₂-co-DVImNTf₂) nanogels by adding isoprene.

Compared to hydrophilic PIL-based nanogels, the analysis *via* dynamic light scattering (DLS) of corresponding hydrophobic nanogels was easier, as hydrophobic PIL-based nanogels were not expected to aggregate as much. The copolymers before and after isoprene

coupling were thus analyzed by DLS in THF. Surprisingly, the correlation chart gave a monodisperse population after CMRC, which would mean that inter-molecular coupling between the nanogels by isoprene would stabilize the solution. However, aggregates were observed again after three minutes of sonication (in Supporting Information Figure S V-4) and most of the gel was precipitated.

TEM imaging of the results of isoprene coupling in dilute medium are shown in Figure V-6. Resulting coupled nanostructures seem to correspond to either aggregates of a few nanogels with diameters comprised between 50 and 100 nm (Figure V-6a), or to more complex structures (Figure V-6b).

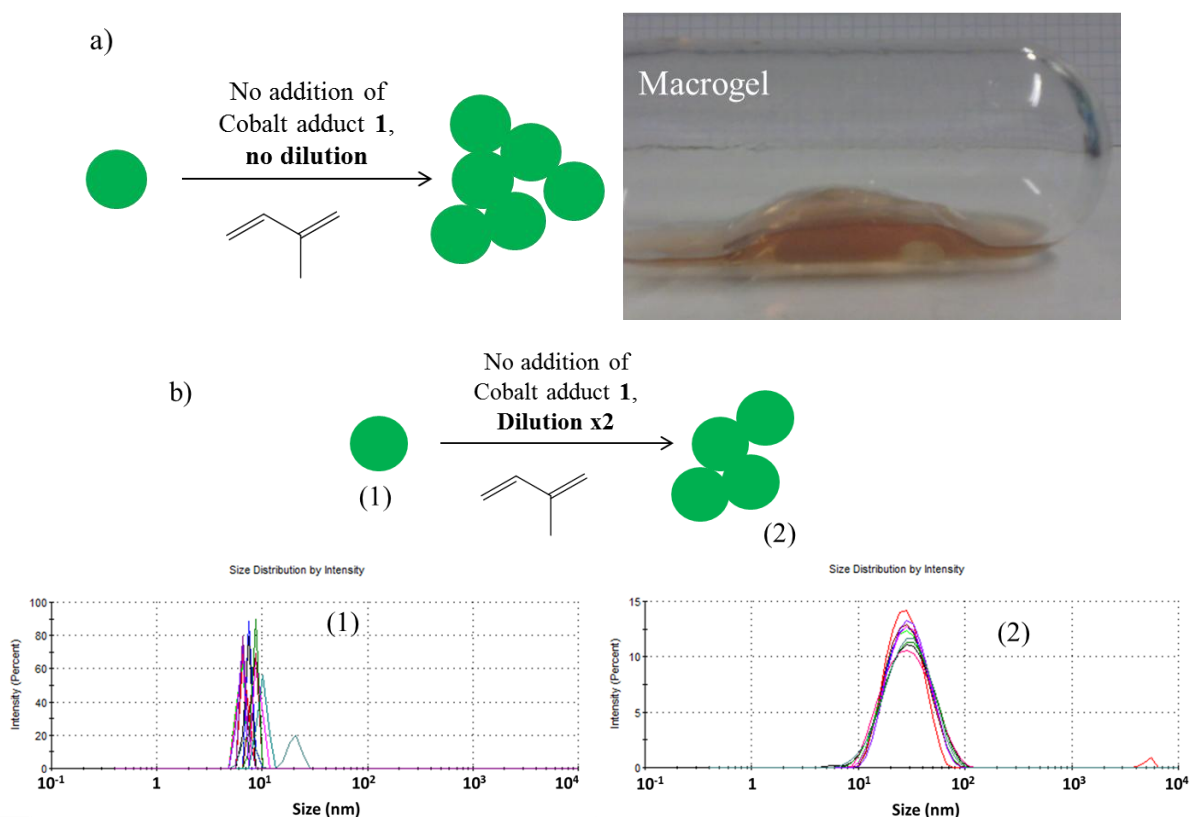


Figure V-5. a) Copolymer resulting from a coupling reaction of the first-generation poly(VEtImNTf₂-co-DVImNTf₂ 5 mol.%) with isoprene, without any dilution of the medium ([VEtImNTf₂]=0.493M); b) schematic representation and DLS results of the copolymers after reaction of poly(VEtImNTf₂-co-DVImNTf₂ 5 mol.%) with isoprene, after dilution of the

medium ($[\text{VEtImNTf}_2]=0.246\text{M}$. Conditions: all DLS measurements are performed on solutions of THF with a nanogel concentration of 1wt.%.

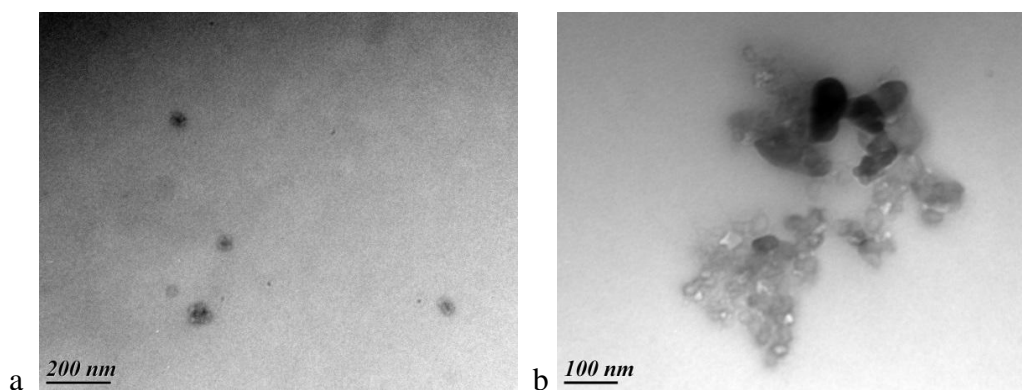
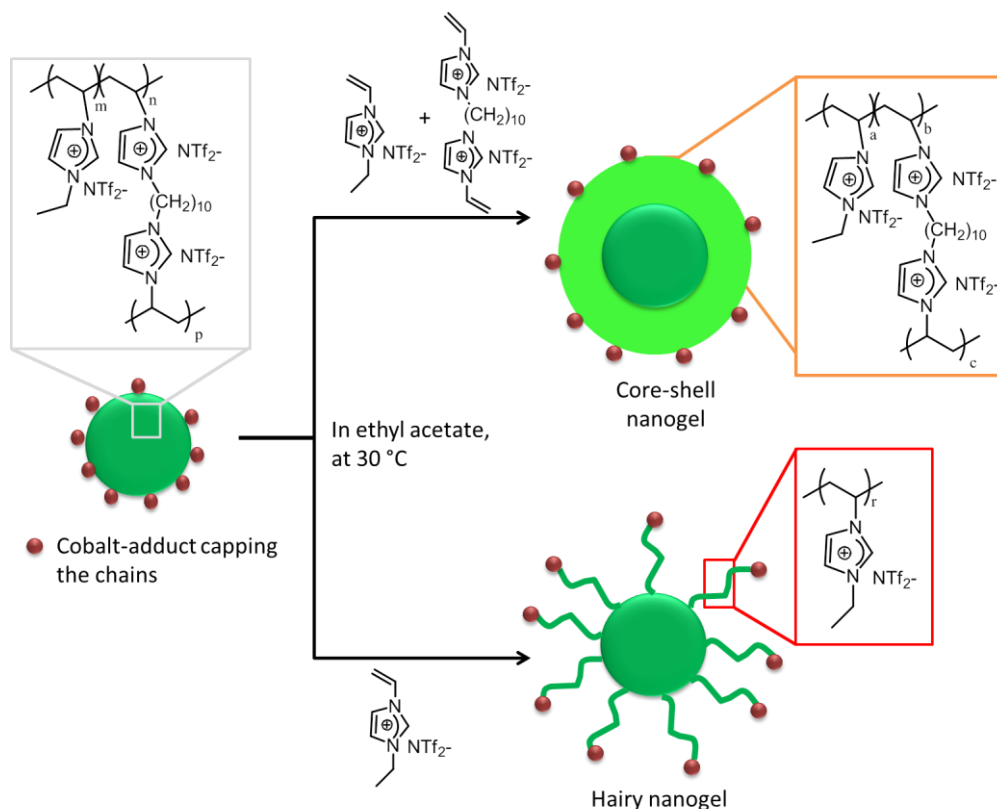


Figure V-6. TEM imaging of the isoprene-coupled nanogels resulting from the diluted isoprene coupling. No sonication step is realized prior to the TEM analysis.

Chain extension reactions were next performed on a 1st-generation nanogel of poly(VEtImNTf_2 -*co*- DVImNTf_2 5 mol.%) synthesized in ethyl acetate at 30 °C (with $[\text{VEtImNTf}_2]=0.493\text{M}$, conversion = 73 % after 9 hours of polymerization). The reaction medium was then added to a new load of VEtImNTf_2 monomer (0.5 g, $1.25 \cdot 10^{-3}$ mol.) or a mixture of VEtImNTf_2 (0.5 g, $1.25 \cdot 10^{-3}$ mol.) and DVImNTf_2 (0.015 g, 5 mol.%) (Scheme V-4) previously degassed under dynamic vacuum, so that $[\text{VEtImNTf}_2]/\mathbf{1} = 60$. The 2nd-generation polymerization was stirred at 30 °C for 24 hours in EtOAc.



Scheme V-4. Schematic representation of chain extension reactions on PIL-based nanogels with: a) a mixture of VEtImNTf₂ and DVImNTf₂; b) VEtImNTf₂ only.

Table in Figure V-7c shows the conversion of the vinyl double bond of monomers (56% of conversion on 24 hours for the “hairy nanogel”, and 48% of conversion for the core-shell nanogel). Unfortunately, SEC traces did not show any polymer. Though 1st-generation nanogels could be eluted by SEC in THF with an eluent containing 10 mM of LiNTf₂, the “2nd-generation” samples (the 2nd feed of monomer containing either 0 or 5 mol.% of cross-linker) could not be eluted, most likely because of a filtration over the 0.2 μm filter prior to the SEC analysis. TEM population of spherical objects with a diameter under 100 nm; on the other hand, TEM of the 2nd-generation nanogel with cross-linked extensions showed mainly aggregates, with a size higher than 200 nm.

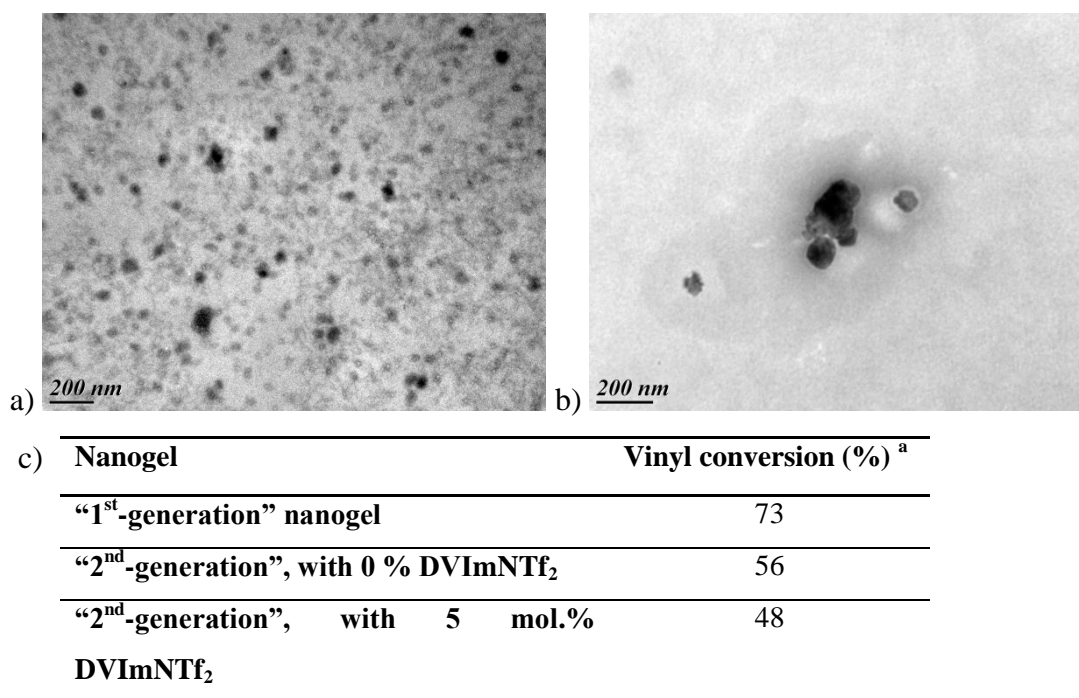


Figure V-7. TEM imaging of: a) 1st-generation nanogel containing 5 mol.% of DVImNTf₂; b) 2nd-generation nanogel containing the same amount of DVImNTf₂; c) conversion of first-generation nanogel and two second-generation samples. ^aConversion determined by ¹H NMR in acetone-d₆ after 24h of reaction.

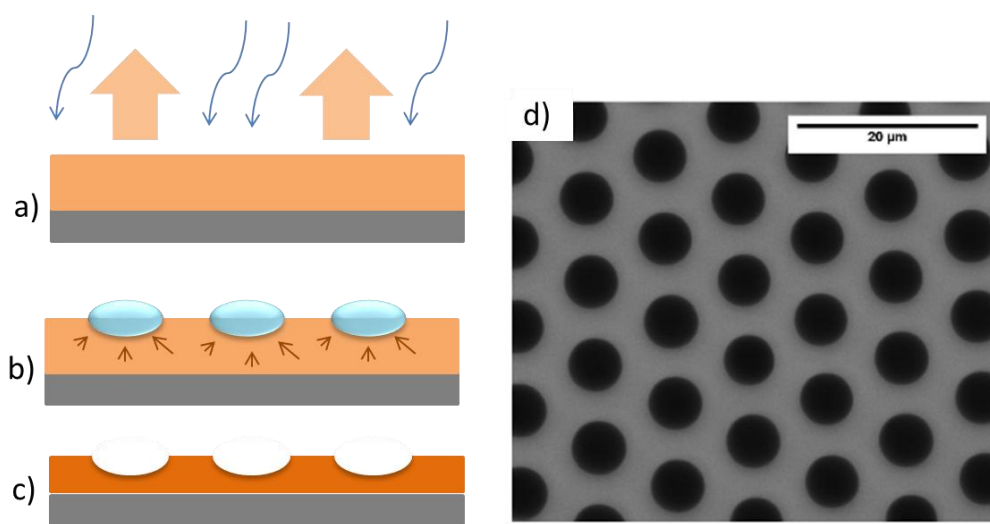
A series of hydrophobic cross-linked PIL-based nanogels was thus achieved for the first time by CMRCcP.

AFM imaging of PILs nanogel films

These hydrophobic PIL nanogels were expected to form structured coatings different from those observed with their hydrophilic counterparts (see Chapter III). Several studies have indeed reported that hydrophobic polymeric materials can spontaneously form nanostructured porous surfaces, referred to as ‘breath figures’⁴¹. The structuration of films made of the hydrophobic PIL-based nanogels described above was thus studied by AFM.

The spontaneous formation of ‘breath figures’⁵² has first been reported by François *et al.* in 1994. As illustrated in Scheme V-5, upon casting a polymeric solution on a substrate,

the solvent slowly evaporates. Thus, evaporation being endothermic, it causes the spontaneous condensation of water droplets on the surface under a humid atmosphere (relative humidity > to 50%). The polymer precipitates around those water droplets, stabilizing them and (ideally) avoiding their coalescence by forming a ‘protective layer’ around them⁴¹. In the case of polymeric nanoparticles, this is achieved *via* a so-called Pickering stabilization. The ensuing evaporation of water droplets leaves behind a porous polymeric surface, called breath figure. Under optimal conditions, *i.e.* depending on molar mass of the polymer, deposition conditions, solvent volatility, humidity, etc.), the porous coating resembles a highly ordered honeycomb structure^{53, 54}.



Scheme V-5. Formation of breath figures: a) a polymeric solution is cast upon a surface, causing the evaporation of the solvent, and the subsequent condensation of water on the surface; b) the polymer stabilizes the water droplet; c) after evaporation of the water droplet, the polymeric coating maintains its porous patterned surface; d) SEM of a honeycomb structured surface by spin-coating of PS⁵⁵ Copyright ACS Publications.

Several studies have shown that, not only the way of casting the polymer coating has a strong impact on the final surface, but also the nature of the polymer itself. For instance, while

PS star-like polymers show a porous structure when cast upon a surface in humid conditions⁵⁶, coatings of PS homopolymers do not display such ordered pattern.

Block copolymers have also been repeatedly studied^{57, 58}. Poly *et al.*⁵⁹ have reported that nanogels of poly(vinyl acetate) (PVAc) can form better arranged porous coatings than their linear PVAc counterparts. PVAc nanogels can achieve a porous patterned surface, for which the number and the size of the pores depend on their cross-linking density. Over the past few years, other types of polymeric architectures generating ‘breath figures’ have been investigated: they include grafted copolymers⁶⁰, dendritic⁶¹ and star-like polymers⁵⁶, just to cite a few. Recently, Billon *et al.*⁶² have shown the influence of a cationic (respectively anionic) chain-end on a linear PS ordered surface.

To investigate the possible formation of patterned porous surfaces from our hydrophobic NTf₂-containing PIL nanogels, the study was conducted simultaneously with linear hydrophobic PILs and related nanogels containing 3, 5, 8 and 15 mol.% of DVImNTf₂ (Table V-3). A freshly cleaved negatively charged mica surfaces was selected as substrate for AFM imaging. It was indeed expected that polycationic nanogels could easily adhere on such a surface.

AFM cantilever was used in tapping mode to prevent any deterioration of the polymeric surface. Polymeric solutions were prepared in THF, owing to the volatility of this solvent.

Table V-3. (Co)polymers used for AFM imaging of polymer-coated mica surface.

Entry	Nanogel	M_n (g/mol) ^b	M_p (g/mol) ^c	M_w/M_n ^b
1	Linear PVetImNTf ₂	14800	20000	1.25
2	poly(VetImNTf ₂ - <i>co</i> -DVImNTf ₂ 3 mol.%)	4900	4300	1.21
3	poly(VetImNTf ₂ - <i>co</i> -DVImNTf ₂ 5 mol.%)	9400	13100	1.41
4	poly(VetImNTf ₂ - <i>co</i> -DVImNTf ₂ 8 mol.%)	11000	14300	1.56
5	poly(VetImNTf ₂ - <i>co</i> -DVImNTf ₂ 15 mol.%)	14200	22100	1.70
6	poly(VetImNTf ₂ - <i>co</i> -DVImNTf ₂ 5 mol.%) with linear extensions	-	-	-
7	poly(VetImNTf ₂ - <i>co</i> -DVImNTf ₂ 5 mol.%) with cross-linked extensions	-	-	-

^a Determined by ¹H NMR in acetone-d₆. ^b Molar masses and dispersities were determined by SEC in THF with 10mM LiNTf₂. ^c M_p represents the molar mass of the maximum of the peak, and was determined by SEC in THF with 10mM LiNTf₂. Conditions: CMRCcP in ethyl acetate, ([VetImNTf₂]/[**1**] = 60), 8h of copolymerization.

1st-generation nanogels at 10 mg/mL

The PIL-based nanogels have been dissolved in two different solvents at 10 mg/mL: i) THF/H₂O 98/2 (v/v), and ii) THF. For a same concentration, a porous surface was observed on mica surfaces for the homopolymer and for each nanogel of PILs-NTf₂ (Figure V-8 below), except for nanogel **5** (poly(VetImNTf₂-*co*-DVImNTf₂ 15 mol.%) which could not be spin-coated on mica at 10 mg/mL. During deposition, the evaporation of THF caused the condensation of water droplets. A honeycomb structure was eventually detected after the water was evaporated. At 10 mg/mL, we observed a porous patterned surface whatever the solvent used.

When water was added in the solution before spin coating (first row), the different samples gave irregular packed pores, resulting from water droplet coalescence, due to poor stabilization of the droplets. Cross-linking density seemed to improve the Pickering stabilization: increasing the cross-linking of the nanogels increased the number of pores and decreased the pores' diameter, *i.e.* less coalescence of the water droplets, providing a better stabilization.

By using THF as solvent (second row, Figure V-8), the porous patterned surfaces showed a better Pickering stabilization of the condensed water droplets, than in the THF/H₂O mixture. These observations differed from what was described by Poly *et al.*⁵⁹, where coatings of poly(VAc-*co*-DVA) nanogels were better defined when water was added to the solution. This difference might be ascribed to the ionic liquid nature of our nanogels.

The coating made from the homopolymer showed interconnected pores from both solvents, though the size of pattern varied. Less interconnected pores, and better long-range orders were noted on related surfaces irrespective of the cross-linking density of the nanogels.

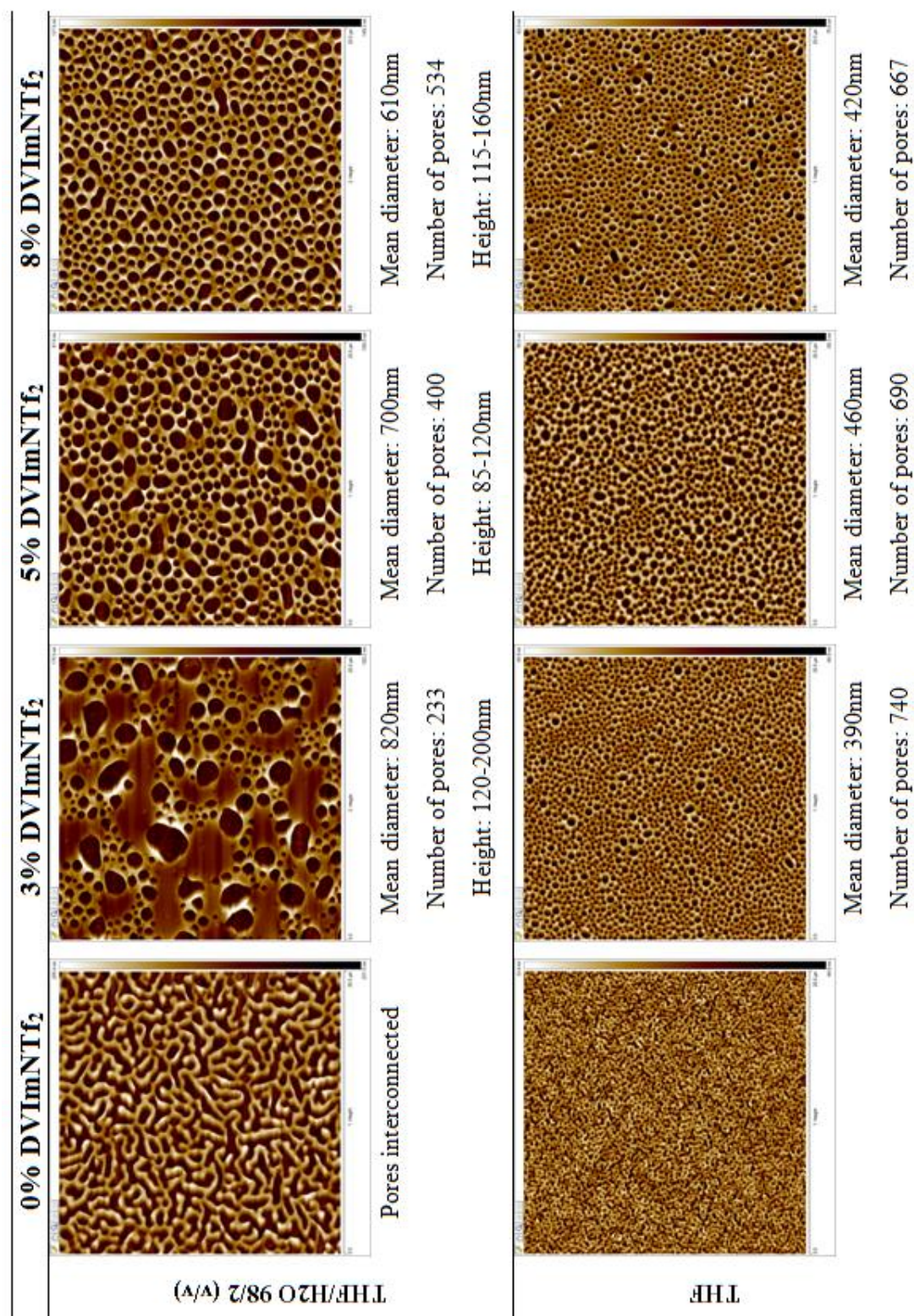
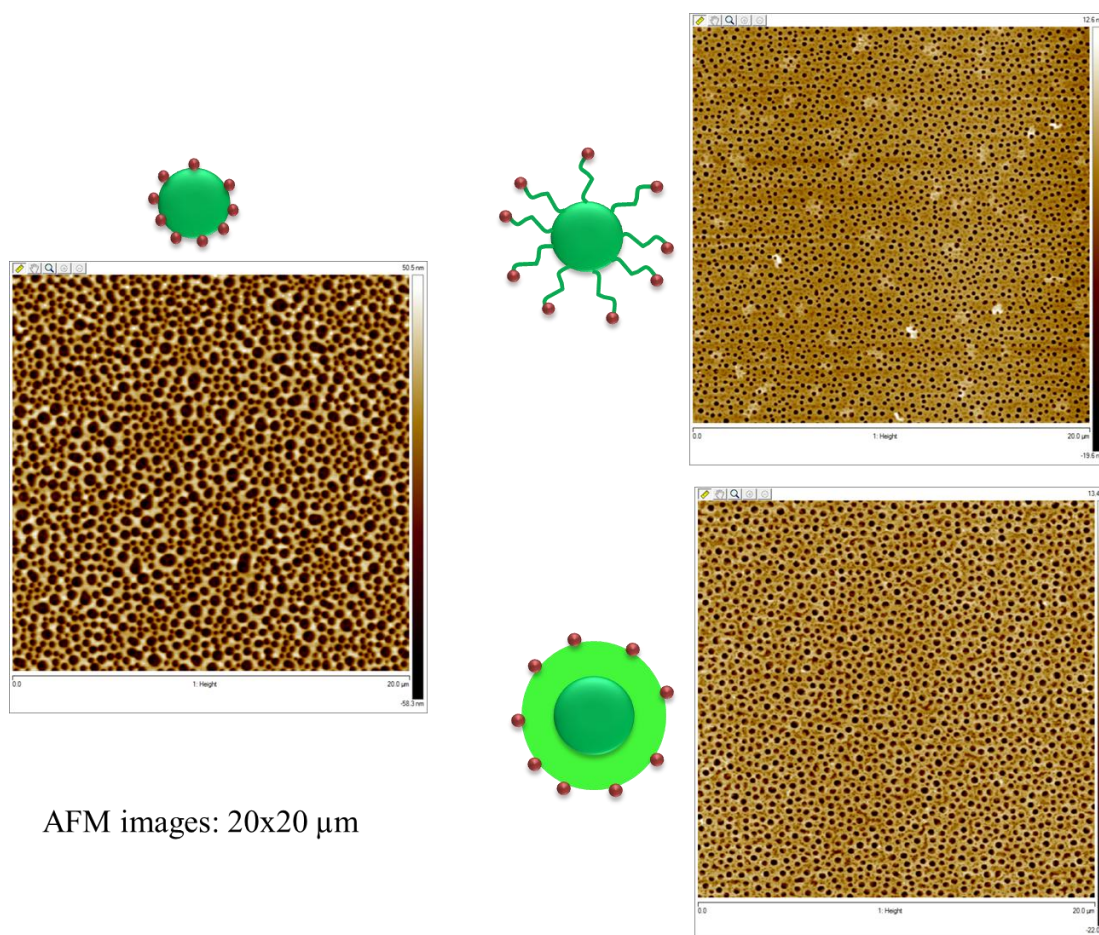


Figure V-8. AFM images (20x20 μm) of the solution of homopolymers (0% DVImNTf₂) and of nanogels 2, 3 and 4 (from left to right). Conditions: solutions of 10 mg/mL, spin-coated on a freshly cleaved mica surface, in either THF/H₂O 98/2 (v/v), or THF.

Comparison of 1st- and 2nd-generation nanogels at 10 mg/mL

The first-generation nanogel, poly(V_{Et}ImNTf₂-*co*-DVImNTf₂ 5 mol.%) was spin-coated from a THF solution, and compared to the two second-generation nanogels (the second feed of monomer containing either 0 or 5 mol.% of cross-linker, respectively nanogels **6** and **7** in Table V-3). While all samples exhibited porous patterned surfaces (Figure V-9), the surface of the parent nanogel showed interconnected pores, reflecting the direct effect of the incomplete Pickering stabilization of water droplets. On the other hand, after both chain extensions, interconnected pores were not observed and the pore sizes were smaller than before, indicating a better stabilization of the droplet. Both chain extensions reactions thus exhibited a significantly improved stabilization.

The 2nd-generation nanogel with *linear* extended chains (nanogel **6**) gave the smaller pore size, with a mean diameter of 290 nm *vs.* either 460 for the 1st generation nanogel or 330 nm for the 2nd generation with crosslinked extensions (nanogel **7**). As for the 2nd-generation nanogel with *cross-linked* extended chains (nanogel **7**), it showed a better ordered long-range surface, giving rise to better defined honeycomb nanostructure (Figures V-10 and V-11). Considering that the solvent and concentration were the same for these three nanogels, these changes could only be ascribed to the overall architecture of each type of nanogel.



AFM images: 20x20 μm

Nanogel		Pores
1st-generation		Mean diameter: 460 nm Number of pores: 690 Height: 70-80 nm
2nd-generation with linear extensions		Mean diameter: 290 nm Number of pores: 1090 Height: 20-25 nm
2nd-generation extensions	with cross-linked extensions	Mean diameter: 330 nm Number of pores: 1000 Height: 25-30 nm

Figure V-9. AFM imaging (20x20 μm) of the first-generation nanogel (VETImNTf₂-co-DVImNTf₂ 5 mol.%) on the left, and the second-generation nanogels after chain extensions containing either VETImNTf₂ only or VETImNTf₂ with DVImNTf₂ (see also Scheme V-4).

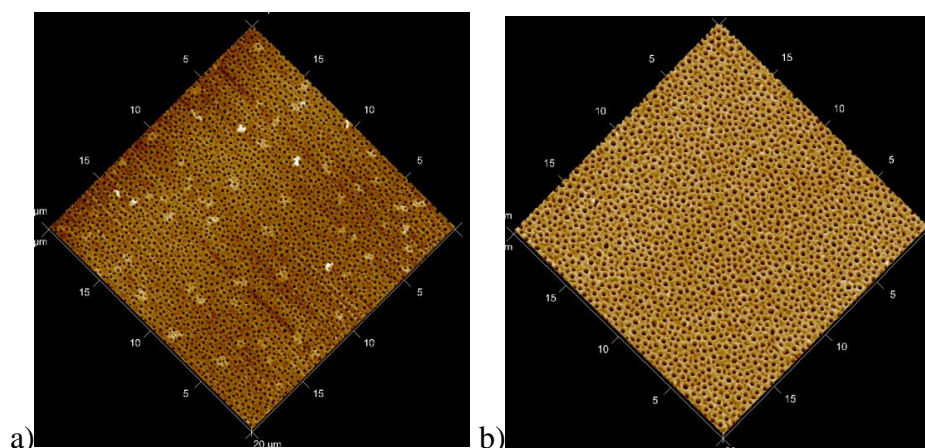


Figure V-10. 3D images of the coating made from 2nd-generation nanogels: a) with linear extensions; b) with cross-linked extensions (see Scheme V-4).

Nanogels in solution in THF at 1 mg/mL

The AFM images of the three 1st-generation nanogels (nanogels **2**, **3** and **4** in Table V-3), at a concentration of 1mg/mL in THF, showed significant differences compared to the same nanogels deposited at a higher concentration (10 mg/mL). Instead of porous surfaces observed from nanogel solutions at 10mg/mL (Figure V-8), a pattern of ‘volcano-like’ rings was observed at 1mg/mL (Figure V-11 and V-12). The interior of each ring was found to contain pores and aggregates of polymers (Figure V-11c), with at least one comparatively big aggregate. The size distribution and the number of motives seemed dependent on the internal structure of the nanogels: the higher the cross-linking density was, the smaller the diameter and the more structure they were.

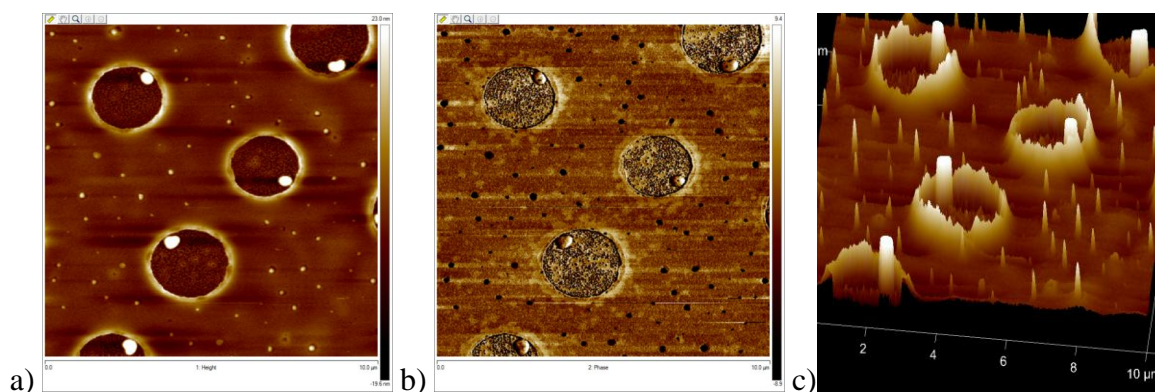


Figure V-11. AFM imaging: a) in height; b) in phase, of the surface of the nanogel poly(V_EtImNTf₂-*co*-DVImNTf₂ 5 mol.%) at 1 mg/mL in THF, spin-coated on a freshly cleaved mica substrate (AFM: 10x10 μm); c) 3D representation of the same image.

In addition, the dewetting phenomenon outside of the rings was less pronounced as the cross-linking density increased. The count rate increased with the cross-linking as well, and the size of the pattern decreased. At 15 mol.% of DVImNTf₂ (nanogel **5** in Table V-3), the pattern was no longer a hollow circle, but gave pseudo-regular aggregates of nanogels. The mean height of these aggregates was found around 120 nm.

The aforementioned dewetting phenomenon outside of the ‘rings’ was in fact similar to observations by Lee *et al.* on a PNIPAM-SDS thin film⁶³. Several publications have described the formation of ‘nano-rings’ when polymeric solutions are eventually too diluted to self organize into honeycomb-like surfaces. These nano-rings have been explained either by a Pickering emulsion stabilization mechanism⁶⁴, or by the self-aggregation of nanogels (what Boneberg *et al.* coined colloidal adhesion⁶⁵). Structures observed in our case were however much larger (1 to 3 μm) than values reported in the literature^{64,65}. This self-assembly of ‘porosity’ and aggregates inside the pattern might thus be considered as indicative of a dewetting. Weiss *et al.*⁶⁶ have shown a similar pattern for PS films on silica surface, that undergo dewetting after annealing.

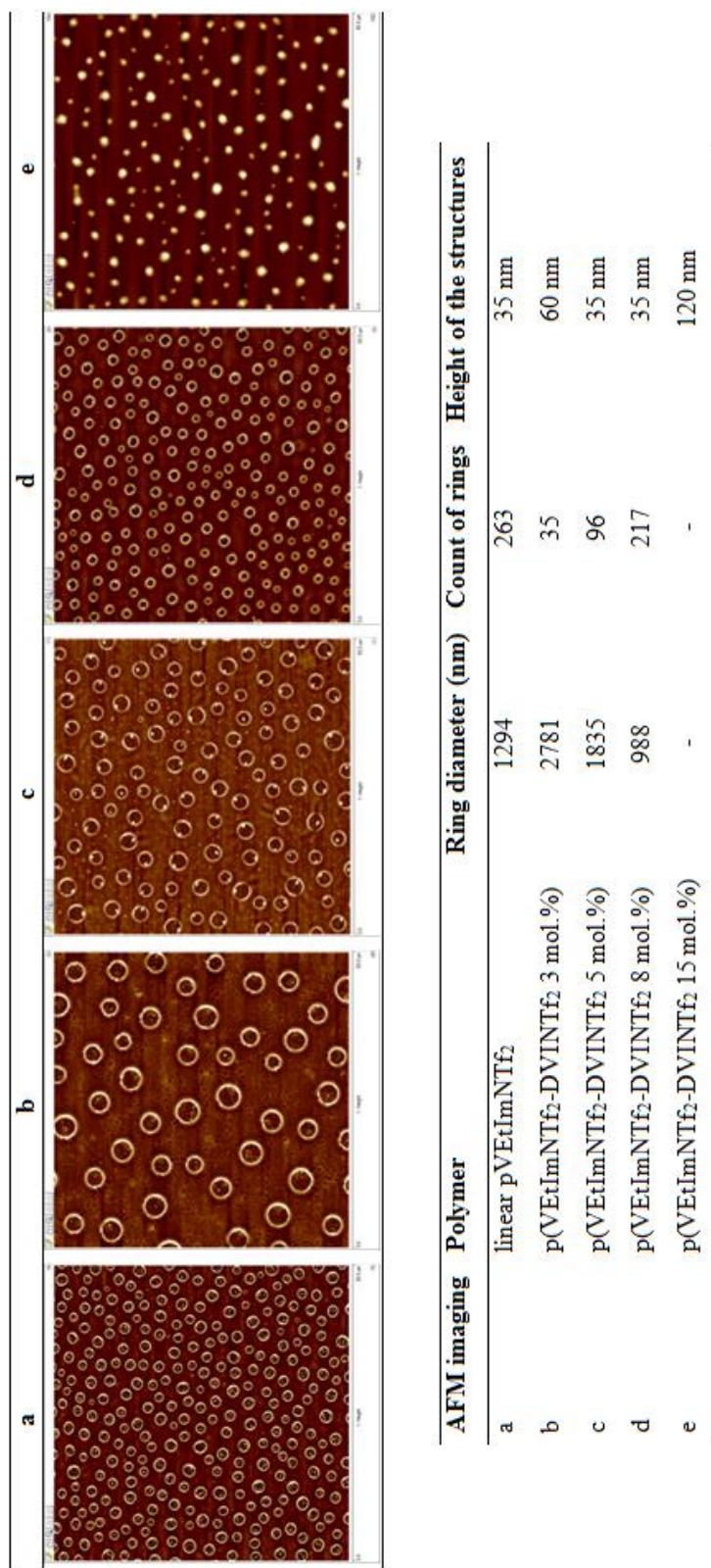


Figure V-12. AFM images (50x50 μ m) of the solution of linear pVEtImNTf₂ (a) and nanogels 2, 3, 4 and 5 (b, c, d, e, respectively). Conditions: solutions of 1 mg/mL in THF, spin-coated on a freshly cleaved mica surface.

Given the evolution of the patterned coatings from nanogels **2**, **3** and **4**, we expected the coatings from the nanogel **5** to contain volcano-like rings of even smaller diameters: however, this was not the case. A “forest” of aggregates of nanogels was observed, that were separated across the mica surface. The clear separation could occur as a ‘colloidal adhesion’ dewetting phenomenon. Interestingly, Weiss *et al.* have observed a similar pattern which they have called “polymer drops”⁶⁶. While we observed such aggregates for a higher degree of cross-linking, these authors have however reported such ‘polymer drops’ for smaller polymer chains (with a molar mass of 4000 g/mol).

Thermal analysis and conductivity measurements

Thermal analysis

The thermal analysis of some of these nanogels of first and second-generation was achieved by TGA and DSC. The thermal degradation profiles of compounds are provided in Figure V-13. The two blue curves represent the hydrophilic nanogel containing a bromide counter-anion. The dark blue curve shows the weight loss ratio as determined by TGA, while the light blue curve has been re-calculated, by assuming that the first weight loss up to 150 °C is due to water removal. The derivative of the function weight loss=f(T) was used to remove the complete first weight loss.

Interestingly, the hydrophobic nanogels proved more thermally stable than hydrophilic ones. Both the nanogel achieved after anion exchange, and copolymers directly synthesized with NTf₂ as the counter anion, began to degrade at roughly 400 °C, compared to 300 °C for the hydrophilic bromide-containing nanogels (Figure V-13).

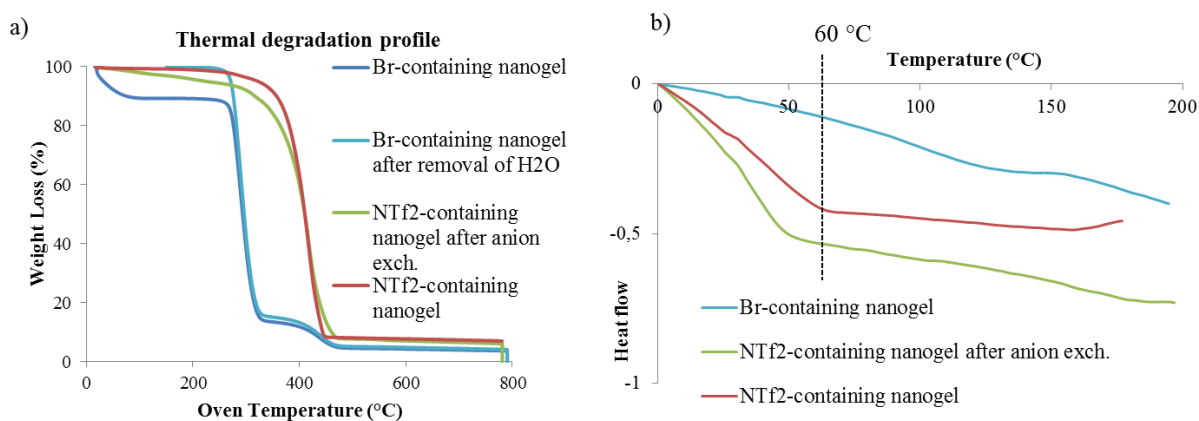


Figure V-13. a) Thermal degradation of nanogels with a bromide counter anion before (dark blue) and after (light blue) removal of water percentage in the calculations, the same nanogel after anion exchange with NTf_2^- (green), and a hydrophobic nanogel polymerized directly with a counter anion NTf_2^- (red); b) DSC curves of nanogels containing either Br^- (light blue) or NTf_2^- (red curve for the polymerization of VETImNTf_2 , and green for the anion exchange on the nanogel) as counter-anions.

While the degradation profile of the two hydrophobic NTf_2^- -containing samples (green and red curves) appeared similar, the nanogel prepared after anion exchange from a parent hydrophilic compound seemed less thermally stable than the nanogel directly synthesized in ethyl acetate. This might be explained by a partial anion exchange reaction.

No glass transition temperature, T_g , could be found for these PIL nanogels (Figure V-13), irrespective of the counter-anion. The T_g of their linear counterparts have been reported to be equal to 60 °C for NTf_2^- -containing PIL, and to 235 °C for Br-containing polymer³⁷.

Ionic conductivity tests

PIL-based copolymers were next considered as solid copolymer electrolytes^{37, 40}. A lot of research has been carried out in the field of polymers as solid electrolytes pertaining to polyether-alkali-metal salts⁶⁷⁻⁶⁹; poly(ethylene)glycol is a trademark polymer for this application. However, the efficiency of these polymeric materials is hindered by the PEO

tendency to crystallize⁷⁰. An alternative pathway to these materials is the direct incorporation of ionic liquid groups in the main-chain or side-chain of polymers. In this context, PILs have been extensively studied³⁷. For instance, Mecerreyes *et al.* have established that exchanging the counter anion of a PIL dramatically changes its ionic conductivity⁷¹.

In more recent years, using more complex polymer architecture, such as block copolymers, has been investigated as a way to combine a rather high ionic conductivity and good mechanical properties^{72, 73}. In contrast, only a few branched architectures have been investigated^{74, 75}. One recent example of by Xie *et al.* has assessed the ionic conductivity of hyperbranched poly(triazolium)s⁷⁴. External parameters, such as humidity, the use of exogenous ions, or the temperature, have a strong influence on the ionic conductivity. For comparison purposes, Ohno *et al.* have reported the values for the VEtImNTf₂ monomer and its homopolymer of 10⁻² and 10⁻⁵ S/cm, respectively⁴², using a bulk method: the polyelectrolyte is deposited between two plates, thus avoiding the possibility of dewetting.

PILs, in general, exhibit a much higher ionic conductivity when associated with a bis(trifluoromethanesulfonyl)imide counter anion (NTf₂⁻), compared to a bromide one⁷¹. This is due to the non-coordinating and highly delocalized character of the NTf₂ counter anion favoring its mobility. In the case of ethyl imidazolium monomeric unit, the glass transition temperature of NTf₂-containing polymer (≈ 60 °C) is much lower than that of Br-containing polymer (≈ 235 °C), which increases the mobility of the anion.

The potential of the poly(VEtImNTf₂-*co*-DVImNTf₂ 3 mol.%), and poly(VEtImNTf₂-*co*-DVImNTf₂ 8 mol.%) nanogels (**2** and **4** in Table V-3), as single-ion conductors at the solid state, were thus considered in this work. Our poly(VEtImNTf₂-*co*-DVImNTf₂ 5 mol.%) and its 2nd-generation “hairy nanogel” (respectively nanogels **3** and **6** in Table V-3) were also assessed.

These measurements were realized at LCPO in collaboration with Dr. Karim Aïssou using electronic impedance spectroscopy (EIS). We provide here the results of our preliminary study, without a thorough optimization. Indeed, parameters such as the relative humidity, the temperature or the use of exogenous ILs can influence the ionic conductivity measurements, and these were not studied in a systematic manner.

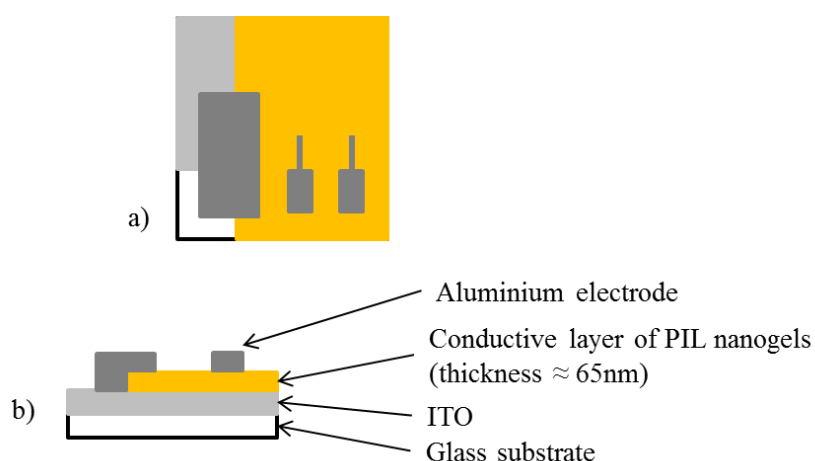


Figure V-14. Illustration of the cell stacking for the PIL nanogels ionic conductivity measurements.

In this work, each nanogel was spin-coated on an indium titanium oxide (ITO) glass substrate, and annealed for 5 min at 80 °C. When the coating was stable (with no sign of dewetting) after this first annealing, another step (130 °C for 10 minutes) allowed removing remaining traces of solvent. The durability of the nanogel coating was then assessed by AFM after annealing. Since the ionic conductivity is affected by the contact surface between the polymer electrolyte and the top electrode, a change in the topology of the surface would influence the conductivity.

AFM results show that the layer of poly(VETImNTf₂-co-DVImNTf₂ 3 mol.%) was subjected to dewetting when annealed at 80 °C, as observed in Figure S V-5 and in Table V-4. Another solvent was then tried: a THF/PGMEA 9/1 v/v mixture (PGMEA: propylene glycol

methyl ether acetate, which is characterized by a high boiling point = 145 °C). It was hypothesized that the slower evaporation of PGMEA might result in a more stable PIL-based nanogel coating. However, after annealing at 80 °C for 5 minutes, a dewetting phenomenon was still observed (Figure S V-5, second row, and Table V-4).

As for the poly(V_{Et}ImNTf₂-*co*-DVImNTf₂ 8 mol.%) nanogel solubilized in THF/PGMEA 9/1 v/v at 10 mg/mL, no dewetting was noted after annealing at 80 °C (Figure S V-5), but dewetting occurred after annealing at 130 °C for 10 minutes (Figure V-15a). To circumvent that issue, the poly(V_{Et}ImNTf₂-*co*-DVImNTf₂ 8 mol.%) nanogel was solubilized in THF/PGMEA 9/1 (v/v) at 20 mg/mL: under such conditions, the surface showed no sign of dewetting after annealing treatment at 130 °C (Figure V-15b). These solution conditions were then implemented for nanogels **3** and **6**.

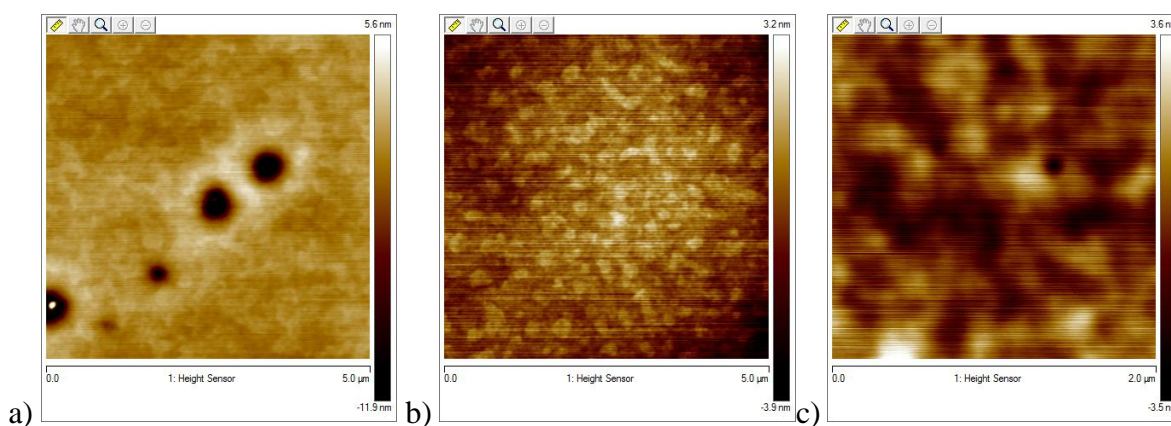


Figure V-15. AFM imaging of the a) spin-coated (on ITO substrate) nanogel **5** in THF/PGMEA 9/1 (v/v) at 10 mg/mL and b) the same at 20 mg/mL, and annealing at 130 °C for 10 minutes at 4000 rpm; spin-coated nanogel **6**, in THF/PGMEA 9/1 (v/v) at 20 mg/mL.

Table V-4. Summary of the annealing experiments and results, depending on the nanogel used, the solvent and concentration of the initial copolymer solution.

Nanogel	Solvent	Concentration	Results
Nanogel 2	THF	10 mg/mL	dewetting at 80 °C
Nanogel 2	THF/PGMEA 9/1 v/v	10 mg/mL	dewetting at 80 °C
Nanogel 4	THF	10 mg/mL	dewetting at 80 °C
Nanogel 4	THF/PGMEA 9/1 v/v	10 mg/mL	stable at 80°C dewetting at 130 °C
Nanogel 4	THF/PGMEA 9/1 v/v	20 mg/mL	stable at 130 °C
Nanogel 3	THF/PGMEA 9/1 v/v	20 mg/mL	polymer not completely soluble at this concentration
Nanogel 6	THF/PGMEA 9/1 v/v	20 mg/mL	stable at 130 °C

The nanogel **3** could not be solubilized in the THF/PGMEA mixture at 20 mg/mL, and thus, could not be spin-coated on ITO surface. In contrast, the 2nd-generation nanogel **6** was easily spin-coated, and showed no sign of dewetting after annealing at 130 °C (Figure V-15c). Thus, the ionic conductivity could be determined on the two surfaces derived from the nanogels **4** and **6**, at 20 mg/mL in THF/PGMEA 9/1 (v/v) mixture. Results are presented in Table V-5.

After being spin-coated into a thin conductive layer (thickness $t \approx 65$ nm *via* reflectometry) on an ITO surface, the coating was annealed at 130 °C for 10 minutes, to evaporate any traces of solvent. Controlling the surface state after annealing is especially important since the ionic conductivity depends directly on the contact surface between the polyelectrolyte and the top electrode.

An aluminium thick top electrode with a 2 mm² active area was placed on top of the film, as illustrated in Figure V-14. In order to eliminate traces of moisture, samples were annealed at 100 °C, and ionic conductivity was measured (Figure V-16).

Voigt's equivalent electrical circuit, used here to fit the data, is represented in Figure V-16. The equivalent circuit was composed of the electrode resistance R_c in series with two high-frequency capacitances in parallel with the resistances. One loop of the circuit represents the material, and the second one represents the electrolyte (the PIL nanogel). The ionic conductivity was calculated as follows:

$$\sigma = \frac{1}{R_{electrolyte}} * \frac{t}{S}$$

with the thickness of the electrolyte layer, t (in cm), S the electrode contact surface (cm²) and $R_{electrolyte}$ extracted from Nyquist plot of impedance spectroscopy.

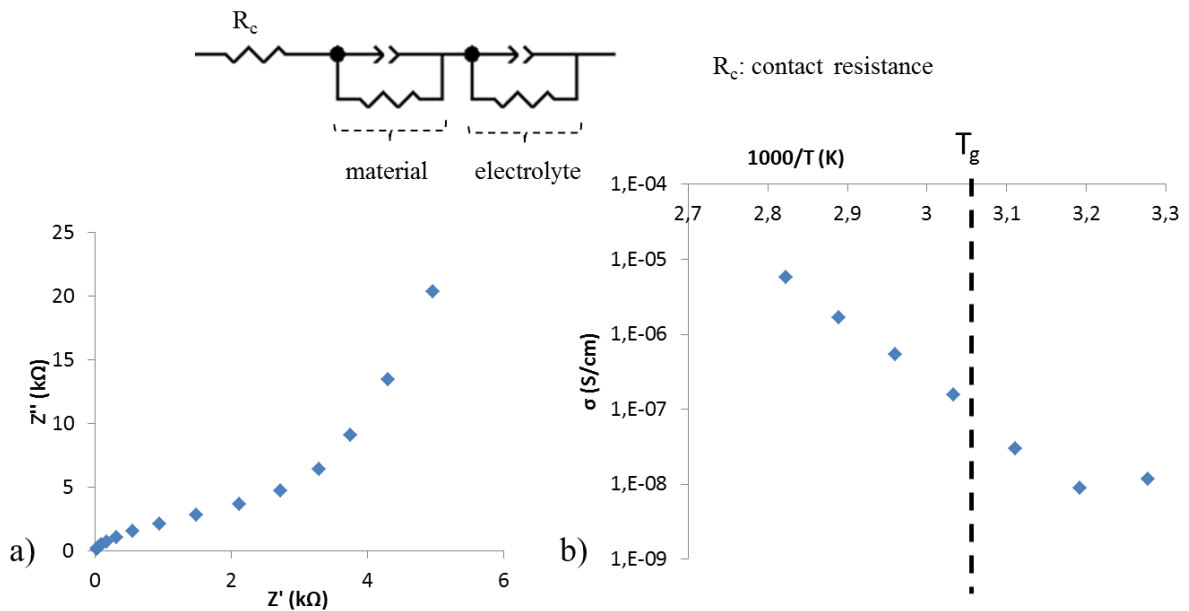


Figure V-16. a) Imaginary impedance vs. real impedance at 100 °C for poly(VETImNTf₂-co-DVImNTf₂ 8 mol.%) nanogel; b) conductivity vs. inverse temperature for poly(VETImNTf₂-co-DVImNTf₂ 8 mol.%) nanogel. Schematic: Voigt's equivalent circuit used to fit data. The

glass transition temperature (T_g) reported on the graph is 60 °C, the literature data for PVeImNTf₂ homopolymer.

Table V-5. Ionic conductivity of the PIL-based nanogel at 40 °C (below T_g) and 80 °C.

Sample	Coating thickness (nm) ^a	σ (S/cm) at 30 °C	σ (S/cm) at 80 °C
poly(VeImNTf ₂ - <i>co</i> -DVIImNTf ₂ 8mol.%)	65	1.2 10 ⁻⁸ S/cm	5.7 10 ⁻⁶ S/cm
poly(VeImNTf ₂ - <i>co</i> -DVIImNTf ₂ 5mol.%) after linear extension	45	5.4 10 ⁻⁹ S/cm	1.9 10 ⁻⁵ S/cm

^a Coating thickness is measured by reflectometry.

At 80 °C, the anhydrous ionic conductivity was found equal to $\sigma_{\text{nanogel}} \approx 5.10^{-6}$ S/cm (Figure V-16) for nanogel **4**. Under the same conditions, Dr. Aïssou at LCPO measured an ionic conductivity of 3.10⁻⁵ S/cm for a block copolymer PVAc-*b*-PVeImNTf₂ (Table S V-1 in Supporting Information)⁷⁶. The ionic conductivity of our nanogels was yet lower than that of a linear polymer homologue (5.7 10⁻⁶ S/cm for the nanogel vs. 3.10⁻⁵ S/cm for the linear block copolymer).

Remarkably, the ionic conductivity of the ‘hairy nanogel’(**6**) was found higher than that of the nanogel **4** at 80 °C (1.9 10⁻⁵ S/cm vs. 5.7 10⁻⁶ S/cm). The difference between linear and cross-linked NTf₂-containing PILs can be explained by a loss of chain mobility in the nanogel. The internal structure of the two nanogels might thus partly explain the difference in ionic conductivity: the ‘hairy nanogel’ architecture might allow more chain mobility than the 1st-generation nanogel. Figure S V-6 compares the ionic conductivity of several PIL-based architectures at 80 °C, and seems to indicate that both nanogels **4** and **6** possess a higher ionic conductivity than other PIL-based architecture already reported. However, it is important to emphasize that most of the ionic conductivity measurements reported in the literature were

carried out in bulk (a layer of polymer between two electrodes, thus dewetting is not possible), while measurements described in this work involve polymers thin films.

Conclusions.

Hydrophobic positively charged nanogels, namely, poly(*N*-vinyl-3-ethyl imidazolium bis(trifluoromethanesulfonyl)imide-*co*-1,13-divinyl-3-decyl diimidazolium bis(trifluoromethanesulfonyl)imide), were directly prepared by one-step cobalt-mediated radical crosslinking copolymerization (CMRCcP) in ethyl acetate at 30 °C. The pre-synthesized alkyl-cobalt(III) mediating agent **1** enabled to introduce rather large amounts of cross-linker without the occurrence of macrogelation. The effect of temperature and dilution on the copolymerization was investigated, as well as the concentration of cross-linker. The extent of cyclization tended to increase with dilution, and seemingly decreased at higher temperatures.

Dormant carbon-cobalt(III) chain-end could be reactivated, enabling the synthesis of core-shell structures or macrogels. To the best of our knowledge, CRCcP-derived hydrophobic PIL-based nanogels have never been described before.

The coating properties of these nanogels were investigated *via* AFM after spin-coating, and porous patterned surfaces were achieved. The structure of the nanogels was found to have a dramatic impact on the surfaces observed. Thus, porous patterned surfaces were better ordered in absence of water in the polymeric solution, prior to spin-coating. Coatings resembling the most to a honeycomb pattern were achieved from “second-generation” nanogels generated after linear chain extensions.

Ionic conductivity measurements on such second-generation nanogels gave the best results with a value of $1.9 \cdot 10^{-5}$ S/cm at 80 °C compared to $5.7 \cdot 10^{-6}$ S/cm for the first-generation poly(VEtImNTf₂-*co*-DVIImNTf₂ 8 mol.%). An ionic conductivity assessment on a

more complete array of NTf₂-containing nanogels could be interesting: for instance, an arm-first nanogel with longer arms, or a PIL nanogel containing a spacer group, such as poly(4-vinylbenzyl ethyl imidazolium-NTf₂) nanogel for instance.

These hydrophobic PIL-based nanogels could also be considered for other applications, including, for instance, antibacterial surfaces since hydrophobic coating should not be subjected to re-solubilization once immersed in water.

Supporting Information.

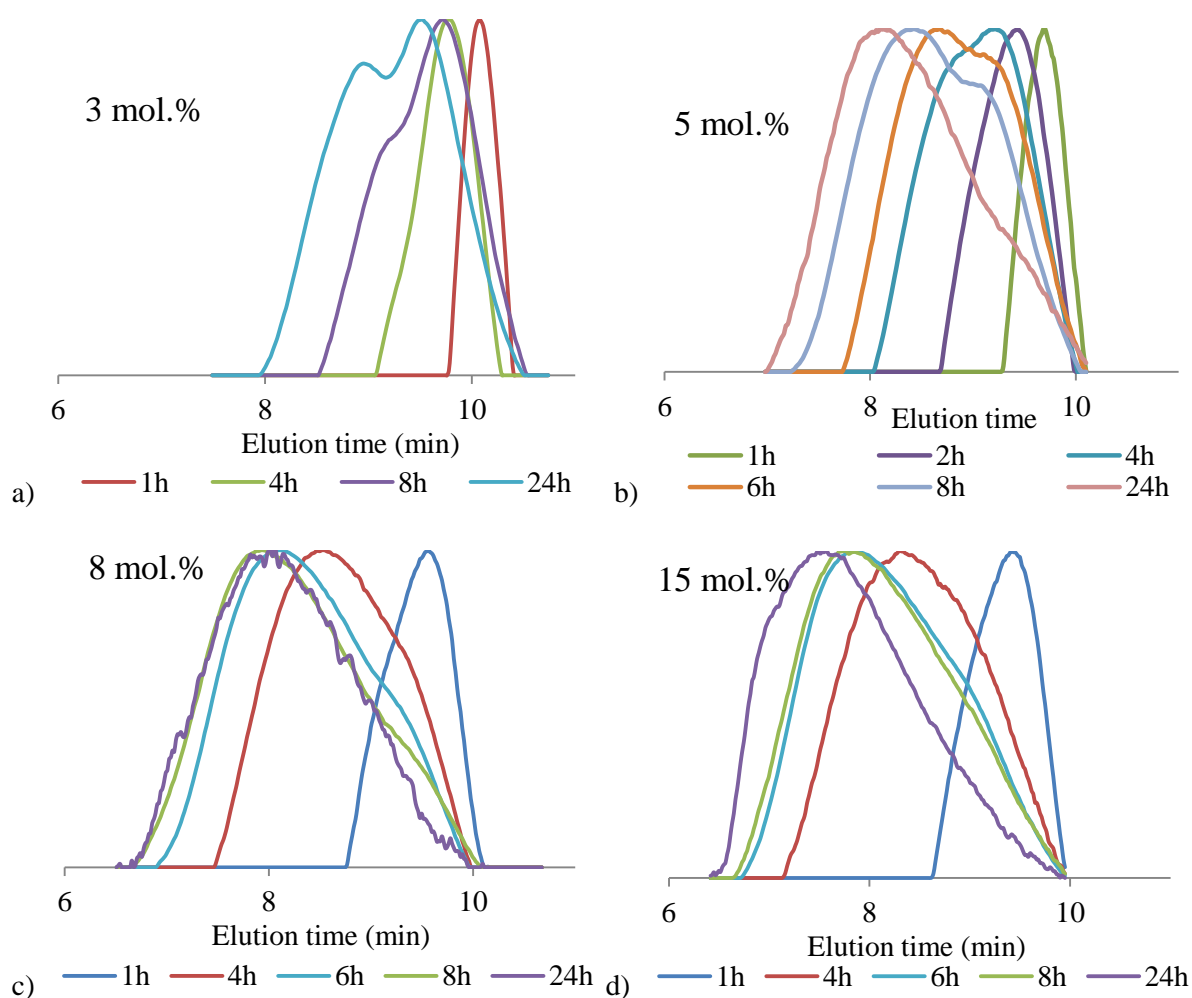


Figure S V-1. SEC traces at different times of the copolymerizations of VEtImNTf₂ with a) 3 mol.% of DVImNTf₂; b) 5 mol.% of DVImNTf₂; c) 8 mol.% of DVImNTf₂; d) 15 mol.% of DVImNTf₂. Conditions: [VEtImNTf₂]/[1]=60, [VEtImNTf₂]= 0.403M in ethyl acetate, 30 °C.

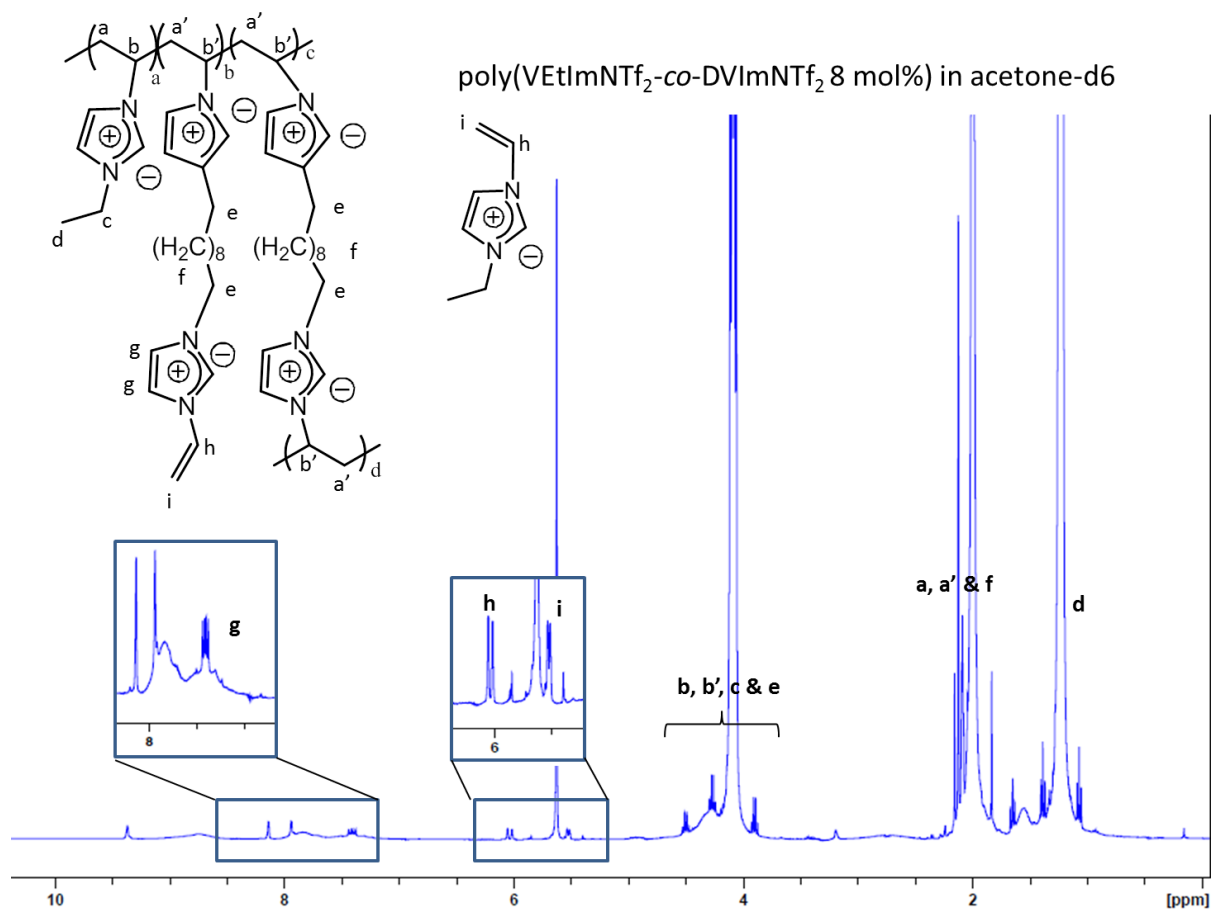


Figure S V-2. NMR spectrum of the final copolymer poly(VETImNTf₂-co-DVImNTf₂ 8 mol.%) in acetone-d₆. Some residual monomer may account for the very visible C=C peaks.

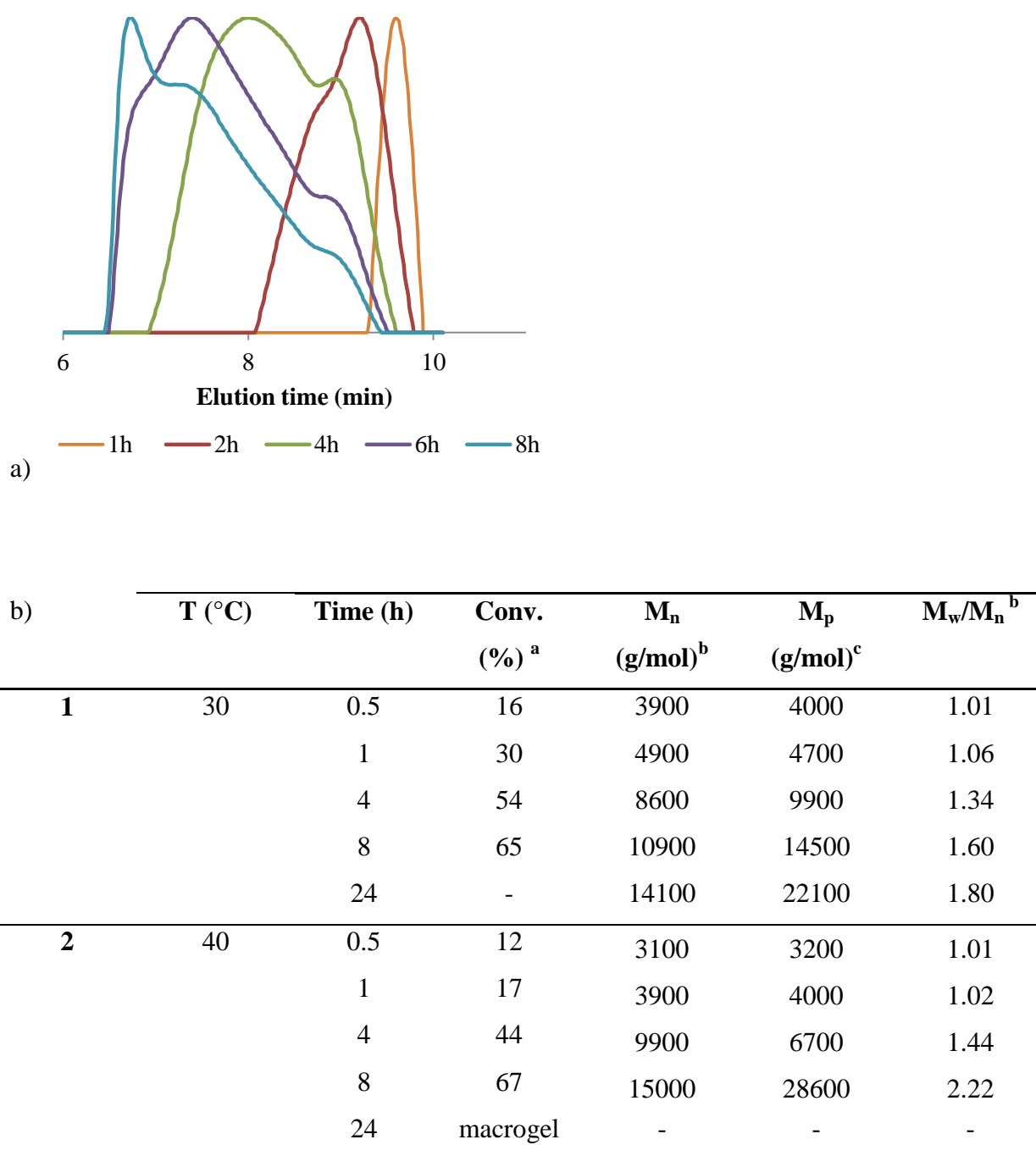


Figure S V-3. a) SEC traces of the copolymerization of VETImNTf₂ with 15 mol.% of DVImNTf₂, at 40 °C; b) corresponding molecular characteristics of the poly(VETImNTf₂-co-DVImNTf₂ 15 mol.%) nanogels during the CMRCcPs at 30 °C and 40 °C. Conditions: [VETImNTf₂]/[**1**]=60, [VETImNTf₂]= 0.403M in ethyl acetate.

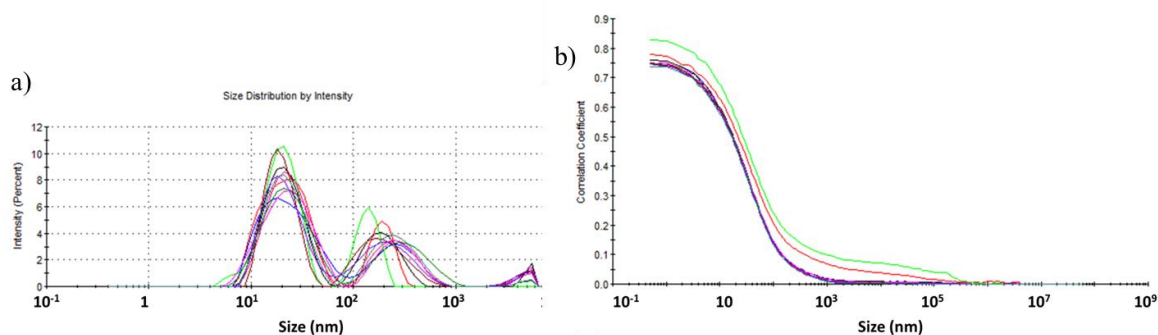


Figure S V-4. DLS analysis of the coupled nanogels (isoprene coupling in diluted conditions, followed by 3 minutes of sonication): a) size distribution by intensity; b) correlation chart.

Conditions: all DLS measurements are performed on solutions of THF with a nanogel concentration of 1wt.%, and repeated 10 times.

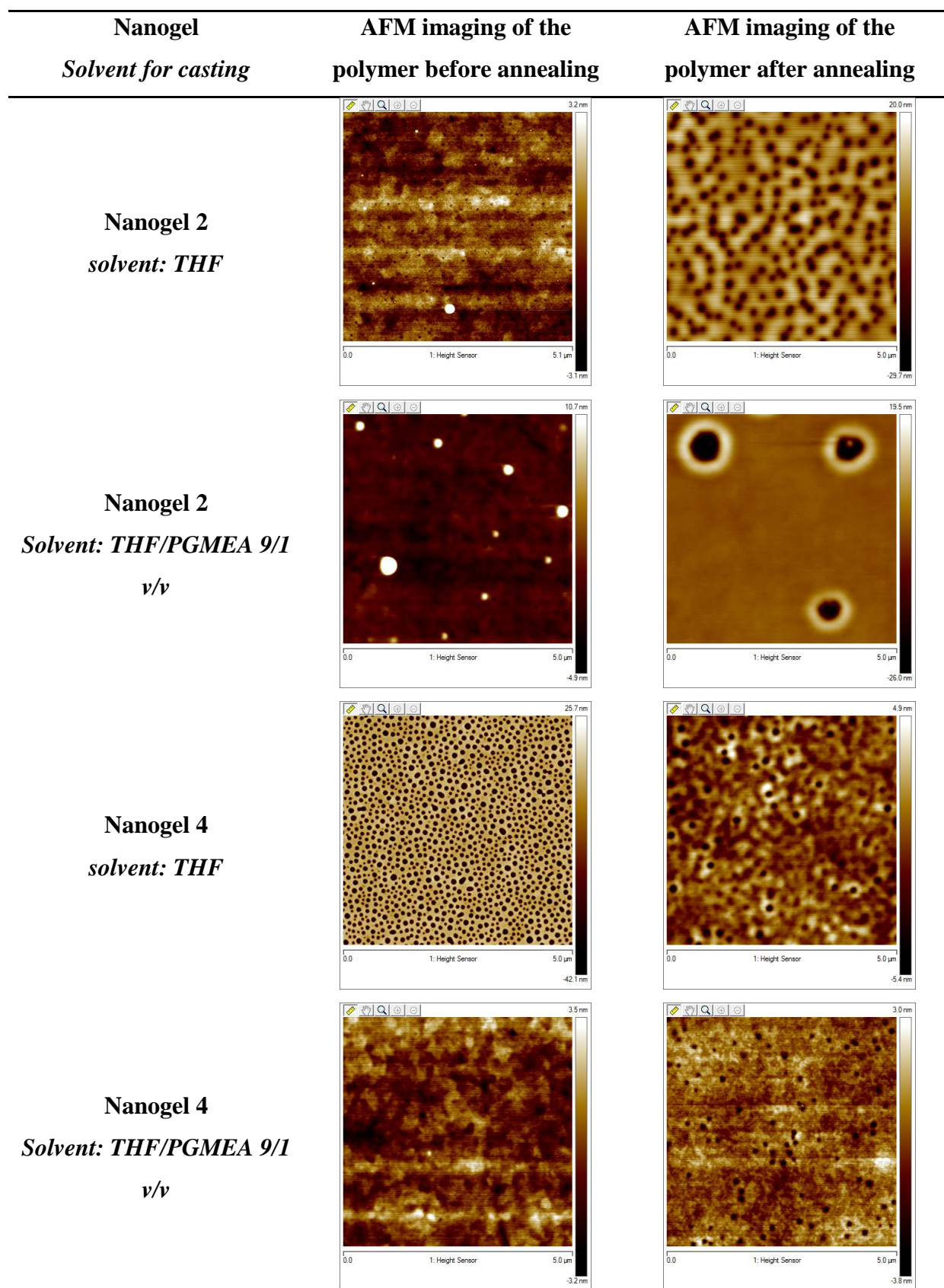


Figure S V-5. AFM imaging (height) of poly(VETImNTf₂-co-DVImNTf₂ 3 mol.%) spin-coated thin layer on ITO substrate before and after annealing at 80 °C. Conditions: nanogels

solubilized either in THF or in a mix THF/PGMEA 9/1 prior to casting at 10 mg/mL (PGMEA: propylene glycol methyl ether acetate).

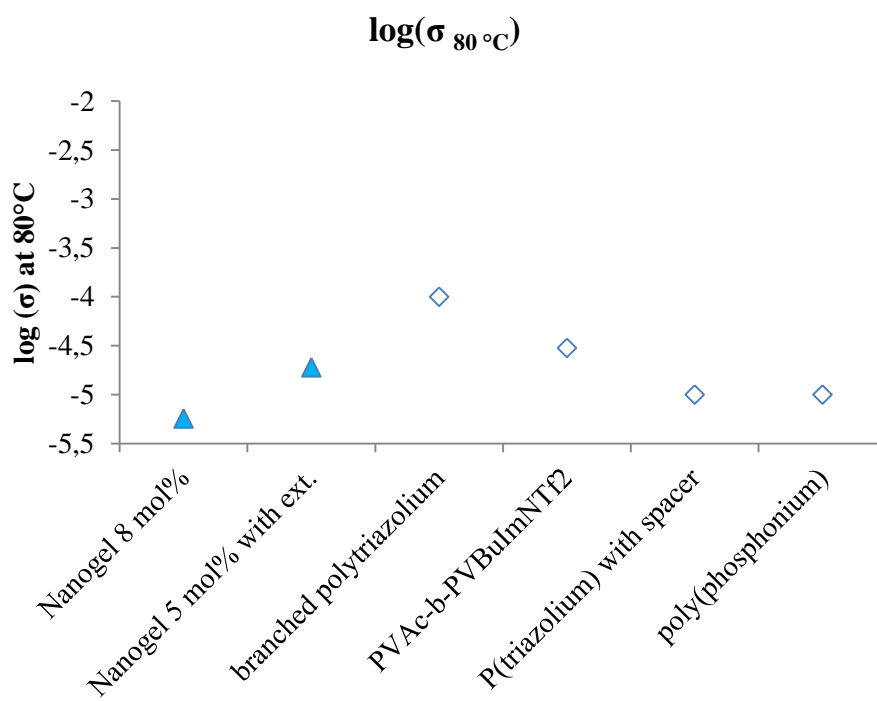


Figure S V-6. Comparison of the ionic conductivity of an array of PIL-based architectures from the literature.

Table S V-1. Comparison of the ionic conductivity values and methods of measurement in literature.

Polymers	Method	Conductivity	groups
poly(VETImNTf ₂ -co-DVImNTf ₂ 8 mol.%) nanogel	<i>Thin film</i>	1.2 10 ⁻⁸ S/cm at 30 °C 5.7 10 ⁻⁶ S/cm at 80 °C	<i>LCPO</i>
2 nd -generation “hairy nanogel”	<i>Thin film</i>	5.4 10 ⁻⁹ S/cm at 30 °C 1.9 10 ⁻⁵ S/cm at 80 °C	<i>LCPO</i>

Hyperbranched poly(triazolium)	Polymer in bulk	10^{-6} S/cm at 30 °C 10^{-4} S/cm at 80 °C	Xie, Sung <i>et al.</i> , <i>Polym Chem</i> 2015 , DOI: 10.1039
Block copolymer PVAc-b-PVBuImNTf ₂	<i>Thin film</i>	3.10^{-8} S/cm at 30 °C 3.10^{-5} S/cm at 80 °C	LCPO (Paul)
	Polymer in bulk	10^{-4} S/cm at 30 °C 10^{-2} S/cm at 80 °C	(Paul), mesures effectuées par E. Drockenmuller
Poly(triazolium) linear with spacer	Polymer in bulk	$8. 10^{-10}$ S/cm at 30 °C 10^{-5} S/cm at 80 °C	Drockenmuller <i>et al.</i> , <i>J. Polym. Sci. Part A: Polym. Chem.</i> 2013 , 51, 34–38
PVEtImNTf ₂	Polymer in bulk	10^{-6} S/cm at 30 °C No measure at 80 °C	Ohno, <i>Macromol. Symp.</i> 2007 , 249–250, 551–556
Monomer VEtImNTf ₂	Polymer in bulk	$\approx 3. 10^{-2}$ S/cm at 30 °C No measure at 80 °C	
Poly(phosphonium) NTf ₂	Polymer in bulk	10^{-7} S/cm at 30 °C 10^{-5} S/cm at 80 °C	Gin, Noble <i>et al.</i> , <i>Journal of Membrane Science</i> 2016 , 498, 408–413

References

1. IUPAC, *Pure Appl. Chem.*, 2007, **79**, 1801-1829.
2. C. Legros, M. C. De Pauw-Gillet, K. C. Tam, S. Lecommandoux and D. Taton, *European Polymer Journal*, 2014, **62**, 322-330.
3. H. Gao and K. Matyjaszewski, *Progress in Polymer Science (Oxford)*, 2009, **34**, 317-350.
4. Y. Xiong, J. Liu, Y. Wang, H. Wang and R. Wang, *Angewandte Chemie - International Edition*, 2012, **51**, 9114-9118.

5. M. J. Muldoon and C. M. Gordon, *Journal of Polymer Science, Part A: Polymer Chemistry*, 2004, **42**, 3865-3869.
6. P. J. Flory, *Journal of Physical Chemistry*, 1942, **46**, 132-140.
7. W. H. Stockmayer, *The Journal of Chemical Physics*, 1943, **11**, 45-55.
8. N. Ide and T. Fukuda, *Macromolecules*, 1998, **32**, 95-99.
9. J. Poly, D. J. Wilson, M. Destarac and D. Taton, *Macromolecular Rapid Communications*, 2008, **29**, 1965-1972.
10. J. K. Oh, S. A. Bencherif and K. Matyjaszewski, *Polymer*, 2009, **50**, 4407-4423.
11. K. Matyjaszewski and N. V. Tsarevsky, *Nature Chemistry*, 2009, **1**, 276-288.
12. J. A. Yoon, C. Gayathri, R. R. Gil, T. Kowalewski and K. Matyjaszewski, *Macromolecules*, 2010, **43**, 4791-4797.
13. Q. Yu, Y. Zhu, Y. Ding and S. Zhu, *Macromolecular Chemistry and Physics*, 2008, **209**, 551-556.
14. W. A. Braunecker and K. Matyjaszewski, *Progress in Polymer Science (Oxford)*, 2007, **32**, 93-146.
15. R. Wang, Y. Luo, B.-G. Li and S. Zhu, *Macromolecules*, 2008, **42**, 85-94.
16. R. Scherf, L. S. Müller, D. Grosch, E. G. Hübner and W. Oppermann, *Polymer (United Kingdom)*, 2015, **58**, 36-42.
17. H. Gao, P. Polanowski and K. Matyjaszewski, *Macromolecules*, 2009, **42**, 5925-5932.
18. D. Konkolewicz, S. Sosnowski, D. R. D'Hooge, R. Szymanski, M. F. Reyniers, G. B. Marin and K. Matyjaszewski, *Macromolecules*, 2011, **44**, 8361-8373.
19. P. Polanowski, J. K. Jeszka, W. Li and K. Matyjaszewski, *Polymer*, 2011, **52**, 5092-5101.
20. P. Polanowski, J. K. Jeszka and K. Matyjaszewski, *Polymer*, 2010, **51**, 6084-6092.
21. J. Rosselgong and S. P. Armes, *Macromolecules*, 2012, **45**, 2731-2737.
22. J. Poly, D. James Wilson, M. Destarac and D. Taton, *Macromolecular Rapid Communications*, 2008, **29**, 1965-1972.
23. H. Kawaguchi, *Polymer International*, 2014, **63**, 925-932.
24. S. Quan, Y. Wang, A. Zhou, P. Kumar and R. Narain, *Biomacromolecules*, 2015, **16**, 1978-1986.
25. N. Ide and T. Fukuda, *Macromolecules*, 1997, **30**, 4268-4271.
26. G. Moad, *Polymer International*, 2015, **64**, 15-24.
27. M. Achilleos, T. Krasia-Christoforou and C. S. Patrickios, *Macromolecules*, 2007, **40**, 5575-5581.

28. A. Gregory and M. H. Stenzel, *Progress in Polymer Science*, 2012, **37**, 38-105.
29. D. J. Siegwart, J. K. Oh and K. Matyjaszewski, *Progress in Polymer Science (Oxford)*, 2012, **37**, 18-37.
30. T. Terashima, S. Nishioka, Y. Koda, M. Takenaka and M. Sawamoto, *Journal of the American Chemical Society*, 2014, **136**, 10254-10257.
31. H. He, M. Zhong, B. Adzima, D. Luebke, H. Nulwala and K. Matyjaszewski, *Journal of the American Chemical Society*, 2013, **135**, 4227-4230.
32. B. J. Adzima, S. R. Venna, S. S. Klara, H. He, M. Zhong, D. R. Luebke, M. S. Mauter, K. Matyjaszewski and H. B. Nulwala, *Journal of Materials Chemistry A*, 2014, **2**, 7967-7972.
33. P. Coupillaud, J. Pinaud, N. Guidolin, J. Vignolle, M. Fèvre, E. Veaudecenne, D. Mecerreyes and D. Taton, *Journal of Polymer Science, Part A: Polymer Chemistry*, 2013, **51**, 4530-4540.
34. J. Lu, F. Yan and J. Texter, *Progress in Polymer Science (Oxford)*, 2009, **34**, 431-448.
35. K. Vijayakrishna, D. Mecerreyes, Y. Gnanou and D. Taton, *Macromolecules*, 2009, **42**, 5167-5174.
36. L. C. Tomé, M. A. Aboudzadeh, L. P. N. Rebelo, C. S. R. Freire, D. Mecerreyes and I. M. Marrucho, *Journal of Materials Chemistry A*, 2013, **1**, 10403-10411.
37. D. Mecerreyes, *Progress in Polymer Science (Oxford)*, 2011, **36**, 1629-1648.
38. H. He, M. Zhong, D. Luebke, H. Nulwala and K. Matyjaszewski, *Journal of Polymer Science, Part A: Polymer Chemistry*, 2014, **52**, 2175-2184.
39. J. Yuan, D. Mecerreyes and M. Antonietti, *Progress in Polymer Science*, 2013, **38**, 1009-1036.
40. P. C. Marr and A. C. Marr, *Green Chemistry*, 2016.
41. A. Zhang, H. Bai and L. Li, *Chemical Reviews*, 2015, **115**, 9801-9868.
42. H. Ohno, *Macromolecular Symposia*, 2007, **249-250**, 551-556.
43. M. G. Cowan, M. Masuda, W. M. McDanel, Y. Kohno, D. L. Gin and R. D. Noble, *Journal of Membrane Science*, 2016, **498**, 408-413.
44. A. Debuigne, Y. Champouret, R. Jérôme, R. Poli and C. Detrembleur, *Chemistry - A European Journal*, 2008, **14**, 4046-4059.
45. R. Marcilla, J. A. Blazquez, J. Rodriguez, J. A. Pomposo and D. Mecerreyes, *Journal of Polymer Science, Part A: Polymer Chemistry*, 2004, **42**, 208-212.
46. D. Cordella, A. Kermagoret, A. Debuigne, C. Jérôme, D. Mecerreyes, M. Isik, D. Taton and C. Detrembleur, *Macromolecules*, 2015, **48**, 5230-5243.

47. M. Hurtgen, A. Debuigne, C. A. Fustin, C. Jérôme and C. Detrembleur, *Macromolecules*, 2011, **44**, 4623-4631.
48. J. Rosselgong, S. P. Armes, W. R. S. Barton and D. Price, *Macromolecules*, 2010, **43**, 2145-2156.
49. C. Detrembleur, A. Debuigne, M. Hurtgen, C. Jérôme, J. Pinaud, M. Fèvre, P. Coupillaud, J. Vignolle and D. Taton, *Macromolecules*, 2011, **44**, 6397-6404.
50. A. Debuigne, R. Poli, J. De Winter, P. Laurent, P. Gerbaux, P. Dubois, J. P. Wathelet, C. Jérôme and C. Detrembleur, *Chemistry - A European Journal*, 2010, **16**, 1799-1811.
51. A. Debuigne, C. Jérôme and C. Detrembleur, *Angewandte Chemie - International Edition*, 2009, **48**, 1422-1424.
52. G. Widawski, M. Rawiso and B. François, *Nature*, 1994, **369**, 387-389.
53. M. Hernandez-Guerrero and M. H. Stenzel, *Polymer Chemistry*, 2012, **3**, 563-577.
54. A. Muñoz-Bonilla, M. Fernández-García and J. Rodríguez-Hernández, *Progress in Polymer Science*, 2014, **39**, 510-554.
55. E. Ferrari, P. Fabbri and F. Pilati, *Langmuir*, 2011, **27**, 1874-1881.
56. L.-W. Zhu, W. Yang, L.-S. Wan and Z.-K. Xu, *Polymer Chemistry*, 2014, **5**, 5175-5182.
57. M. Hernández-Guerrero, T. P. Davis, C. Barner-Kowollik and M. H. Stenzel, *European Polymer Journal*, 2005, **41**, 2264-2277.
58. A. Muñoz-Bonilla, E. Ibarboure, E. Papon and J. Rodriguez-Hernandez, *Langmuir*, 2009, **25**, 6493-6499.
59. J. Poly, E. Ibarboure, J. F. Le Meins, J. Rodriguez-Hernandez, D. Taton and E. Papon, *Langmuir*, 2011, **27**, 4290-4295.
60. L. Pessoni, S. Lacombe, L. Billon, R. Brown and M. Save, *Langmuir*, 2013, **29**, 10264-10271.
61. A. S. De León, S. Malhotra, M. Molina, R. Haag, M. Calderón, J. Rodríguez-Hernández and A. Muñoz-Bonilla, *Journal of Colloid and Interface Science*, 2015, **440**, 263-271.
62. S. Chen, M. H. Alves, M. Save and L. Billon, *Polymer Chemistry*, 2014, **5**, 5310-5319.
63. L.-T. Lee, M. d. C. V. da Silva and F. Galembeck, *Langmuir*, 2003, **19**, 6717-6722.
64. Y. Liu, T. Murao, Y. Nakano, M. Naito and M. Fujiki, *Soft Matter*, 2008, **4**, 2396-2401.

65. J. Boneberg, F. Burmeister, C. Schäfle, P. Leiderer, D. Reim, A. Fery and S. Herminghaus, *Langmuir*, 1997, **13**, 7080-7084.
66. X. Zhai and R. A. Weiss, *Langmuir*, 2008, **24**, 12928-12935.
67. X. G. Sun and J. B. Kerr, *Macromolecules*, 2006, **39**, 362-372.
68. S. Seki, M. A. B. H. Susan, T. Kaneko, H. Tokuda, A. Noda and M. Watanabe, *Journal of Physical Chemistry B*, 2005, **109**, 3886-3892.
69. K. Timachova, H. Watanabe and N. P. Balsara, *Macromolecules*, 2015, **48**, 7882-7888.
70. M. Yoshizawa and H. Ohno, *Chemistry Letters*, 1999, **9**, 889-890.
71. R. Marcilla, F. Alcaide, H. Sardon, J. A. Pomposo, C. Pozo-Gonzalo and D. Mecerreyes, *Electrochemistry Communications*, 2006, **8**, 482-488.
72. P. Coupillaud and D. Taton, in *Applications of Ionic Liquids in Polymer Science and Technology*, Springer Berlin Heidelberg, 2015, pp. 69-102.
73. K. M. Meek and Y. A. Elabd, *Journal of Materials Chemistry A*, 2015, **3**, 24187-24194.
74. M. Xie, J. Wu, R. Sun, X. Liao, J. Chen and J. Wang, *Polymer Chemistry*, 2015.
75. Y. Men, D. Kuzmicz and J. Yuan, *Current Opinion in Colloid and Interface Science*, 2014, **19**, 76-83.
76. P. Coupillaud, M. Fèvre, A. L. Wirotius, K. Aissou, G. Fleury, A. Debuigne, C. Detrembleur, D. Mecerreyes, J. Vignolle and D. Taton, *Macromolecular Rapid Communications*, 2014, **35**, 422-430.

Chapter VI

Coating and Antibacterial Properties of Poly(ionic liquid)-based Nanogels Synthesized by Cobalt-Mediated Radical Cross-linking Copolymerization (CMRCcP).

Abstract.

In chapters III and IV were discussed the synthesis of hydrophilic poly(ionic liquid)-based nanogels by cobalt-mediated radical cross-linking copolymerization.

In this chapter are examined the coating properties and antibacterial activities both in solution and on a surface of the different (co)polymers previously described in Chapters III through IV. The presentation is made by differentiating these (co)polymers according to their overall architecture: linear homopolymers and cross-linked nanogels. Nanogels tested include hydrophilic compounds consisting of *N*-vinyl-3-ethylimidazolium bromide (VEtImBr) units with different counter anions (namely divinyl adipate or 1,13-divinyl-3-decyl diimidazolium bromide).

The adherence of the coatings is evaluated *via* QCM-D and contact angle measurements, and their durability is assessed through immersion tests. Antibacterial activity of the hydrophilic copolymers is tested in solution against Gram-positive and Gram-negative bacteria, *via* the 'shake-flask' method. Minimum inhibitory concentrations (MIC) of the more promising nanostructures are finally assessed. An effect of the architecture is observed, as the PIL-based nanogels exhibit a lower MIC than the linear counterpart of their primary chains.

Introduction

Due to its resistance to chemicals and corrosion, stainless steel has found its way in our daily life. However, without particular precaution, stainless steel is unable to prevent the proliferation of bacteria on its surface, leading to the formation of biofilms when the material is ageing. On a solid surface, bacteria form colonies, and subsequent biofouling, which can lead to further infections. Therefore, developing antibacterial coatings is of prime importance.

As described in the introduction of this work (Chapter I), there are two main categories of polymeric coatings¹, which are defined by the actions they undertake to fight the invasion of bacteria on the surface² leading to bio-fouling (*i.e.* the adhesion and film formation of bacteria on a surface). In the one hand, passive coatings prevent bacteria from anchoring themselves on a surface, usually *via* steric hindrance (*e.g.* PEG brushes) or electrostatic repulsion. On the other hand, active antibacterial polymers actually show intrinsic bactericide properties. In the latter case, different possibilities can be considered: either the polymer itself or the monomeric unit is biocidal³, or the polymer can be loaded with bactericidal nanoparticles or molecules, as has been amply demonstrated with silver nanoparticles⁴⁻⁶. Polymer coatings releasing silver nanoparticles have been studied in depth, especially given the excellent antibacterial properties of the released silver⁷. However, some reports have questioned the effect of silver nanoparticles on health and environment⁸. Therefore, an increasing attention has been paid to develop surfaces that could inherently show antibacterial properties, without the release of any biocides⁹ (more detailed explanations can be found in chapter I). The advantage of this type of surfaces is twofold: i) they do not release any toxic nanoparticles; ii) they do not require any reloading after usage.

Cationically charged polymers represent a viable alternative of antibacterial coatings, as they can interact with the negatively-charged walls of the bacteria cells. Thus, quaternary ammonium polymer compounds have been established to interact with the negatively-charged

Chapter VI: *Coating and antibacterial properties of PIL-based nanogels...*

outer membrane of Gram-negative bacteria (respectively the cell membrane of Gram-positive bacteria). The damage to the outer membrane (respectively cell membrane) enables the leakage of cytoplasmic content, which eventually causes the cell death.

Chitosan has been extensively studied for its very wide antibacterial properties, but its main drawback remains its poor solubility at pH above 6.5 (see Chapter I)^{10, 11}. Poly(ionic liquid)s (PILs) have been recently proposed as possible antibacterial materials.

PILs represent a special class of polyelectrolytes with properties originating from their ionic liquid (IL) units (such as thermal and chemical stabilities, high ion conductivity) combined with their intrinsic polymeric nature (*e.g.* film forming ability)¹²⁻¹⁵. Interestingly, changing their counter-anion is a simple way to further tune their properties¹⁶. ILs have long been known as solvents for the preparation of polymer¹⁷, and previous studies have shown that cationic ILs can possess antibacterial activity¹⁸, depending on their counter-anion and alkyl chain length¹⁹⁻²¹. Gilmore *et al.* have especially showed that for 1-alkyl 3-methyl imidazolium chloride with an alkyl chain of 6 carbons or more was sufficient to observe antibacterial activity of the ionic liquid³. Finally, Cameron *et al.* have recently established that PIL brushes grafted onto hydroxyethyl cellulose exhibit an excellent antibacterial activity²².

More generally speaking, some polymers have been abundantly reported for their antibacterial applications²³, including chitosan²⁴, poly(ethylene imine)²⁵ or linear quaternary ammonium polymers^{26, 27}, by themselves or loaded with nanoparticles^{5, 6, 28} (silver) or a hybrid of both. Architectures other than “simple” linear polymers have also been considered for this application. For instance, Detrembleur *et al.* have developed polyelectrolyte micelles²⁹ or nanogels³⁰ for coatings with an antibacterial character. Main methods of polymer deposition on a surface include dip-coating and spin-coating of a preformed polymer, and grafting from or grafting onto a selected surface. Grafting PIL-chains onto a surface has been reported either by surface-initiated ring opening metathesis to prevent biofouling on those surfaces³¹, or by

Chapter VI: Coating and antibacterial properties of PIL-based nanogels...

click chemistry³². While covalently bond coatings exhibit good antibacterial activity (see Chapter I), they require multi-step processes to activate the pristine surface.

In the present chapter, we have turned our attention to the antibacterial activity in solution of the various PIL-based nanogels described in the previous chapters, surfaced their coating abilities. All antibacterial tests in solution are carried out with (co)polymers synthesized *via* cobalt-mediated radical cross-linking copolymerization (CMRCcP). We have thus investigated the antibacterial activity in solution of a homopolymer of VEtImBr compared to that of several nanogels based on the same monomer units. The final aim is to evaluate whether such cross-linked structures can exhibit specific -and better- antibacterial activity than linear polymer homologues, and thus provide long-lasting antibacterial activity when coated on stainless steel surface. Preliminary investigations of the deposition of the nanogel on stainless steel are also described.

Experimental section

Materials

Dimethylformamide (DMF, Aldrich, 99.8%) and methanol (MeOH, HPLC grade) were dried over molecular sieves and degassed by bubbling Argon during 15 minutes. Milli-Q water and acetone were degassed by bubbling Argon during 30 minutes. 2,2,6,6-Tetramethylpiperidine 1-oxy (TEMPO) (98%, Aldrich) was used as received. The alkyl-cobalt(III) (R-Co(acac)₂) was synthesized as already reported³³. *N*-Vinyl-3-ethyl imidazolium bromide (VEtImBr) was synthesized as reported in the literature¹⁶. 1,13-Divinyl-3-decyl diimidazolium bromide (DVIImBr) was synthesized following the same strategy. Vinyl acetate (VAc) was dried on calcium hydride to eliminate water, and cryo-distilled prior to use. Divinyl adipate (DVA, Aldrich, >99%) was employed as received.

Chapter VI: Coating and antibacterial properties of PIL-based nanogels...

Characterization

Molar masses and dispersities of hydrophilic polymers (*i.e.* of poly(*N*-vinyl-3-ethyl imidazolium bromide) (PVEtImBr) were determined by aqueous size exclusion chromatography (SEC), in an eluent containing NaCl (0.1M) and trifluoroacetic acid (TFA, 0.1% vol), at 30 °C (pressure: 540 PSI; flow rate: 1mL/min), with a SEC equipped with a pre-column (PSS NOVEMA Max analytical 10 micron, 8.0×50 mm) and a linear column (PSS NOVEMA Max analytical linear S micron 8.0×300 mm).

¹H NMR spectra of the reaction medium and final product were recorded at 25 °C with a Bruker spectrometer (400 MHz), in DMSO-d₆.

Syntheses

Typical copolymerization of N-vinyl-3-ethyl imidazolium bromide (VEtImBr) with 1,13-divinyl-3-decyl diimidazolium bromide (DVImBr) via CMRCcP in organic solvent

VEtImBr (1 g, 6.2 10⁻³ mol.), and divinylimidazolium DVImBr (0.1 g, 4.8 mol.%) were introduced in a Schlenk tube and degassed by 3 vacuum-argon cycles, and 12 mL of dry, degassed solvent were added. The solvent was either dimethylformamide (DMF) or a mixture of DMF and methanol (MeOH) (8/4) (v/v). The flask was thermostated at 30 °C and a solution of alkyl-cobalt(III) initiator (0.40 mL, 7.4 10⁻⁵ mol., solution at 1.18M) in CH₂Cl₂ was then added. The reaction medium was stirred. Aliquots were regularly removed for determining the conversion by ¹H NMR. Samples for SEC H₂O were quenched by TEMPO and DMF is removed by dialysis before SEC H₂O. Samples for SEC in THF undergo an anion exchange before SEC THF.

Chapter VI: Coating and antibacterial properties of PIL-based nanogels...

Aqueous copolymerization of N-vinyl-3-ethyl imidazolium bromide (VEtImBr) and 1,13-divinyl-3-decyl diimidazolium bromide (DVImBr) via CMRCcP

A solution of alkyl-cobalt(III) initiator (0.40 mL, $7.4 \cdot 10^{-5}$ mol., solution at 1.18 M) in CH_2Cl_2 was introduced in a Schlenk tube already degassed by 3 vacuum-argon cycles. The CH_2Cl_2 was then evaporated under vacuum. The Schlenk tube was put under argon again, and the alkyl-cobalt(III) adduct was solubilized in 0.5 mL of previously degassed acetone. VEtImBr (1g, $6.2 \cdot 10^{-3}$ mol.), and divinylimidazolium DVImBr (0.1 g, 4.8 mol.%) were introduced in another Schlenk tube and degassed by 3 vacuum-Argon cycles, and 12 mL of milli-Q water were added. The second Schlenk tube was degassed by bubbling Argon during 30 minutes, and the solution of ionic liquid monomer in water was added to the first Schlenk tube, containing the solution of alkyl-cobalt(III) adduct. The reaction medium was stirred at 30 °C. Aliquots were regularly withdrawn for determining the conversion by ^1H NMR. Samples for SECs were quenched by TEMPO, and samples for THF SEC were submitted to an anion exchange before injection.

Copolymerization of N-vinyl-3-ethyl imidazolium bromide (VEtImBr) and DVA in solution, in presence of the alkyl-cobalt(III) adduct

In a typical procedure, VEtImBr (1 g, $6.2 \cdot 10^{-3}$ mol.), and divinyl adipate (8.1 mol.%, 0.1g) were introduced in a Schlenck tube and degassed by 3 vacuum-argon cycles, and 12 mL of dry, degassed mixture of DMF and methanol (8/4, v/v) were added. The flask was thermostated at 30 °C and a solution of alkyl-cobalt(III) (0.25 mL, $7.4 \cdot 10^{-5}$ mol., solution at 1.18M) in CH_2Cl_2 was added. The reaction medium was stirred. Aliquots were regularly taken out for the conversion by ^1H NMR. Samples for SEC H_2O were quenched by TEMPO and dialyzed against water to remove DMF before SEC H_2O .

Table VI-1. Variations of the conditions of polymerization, and characterization of the nanogels by aqueous SEC.

Entry	Polymerization solvent	Architecture	M _n (g/mol)	M _w (g/mol)	M _w /M _n
1	DMF	homopolymer	9000	10600	1.43
2	DMF	2.9 mol.% DVImBr ^a	9800	10200	2.18
3	DMF	4.8 mol.% DVImBr ^a	- ^b	- ^b	- ^b
4	H ₂ O	2.9 mol.% DVImBr ^a	21600	41200	2.7
5	H ₂ O	4.8 mol.% DVImBr ^a	17800	18500	3.45
6	DMF	8.1 mol.% DVA ^a	14000	13400	4.60

^a Nanogel of poly(*N*-vinyl-3-ethyl imidazolium bromide) with the indicated amount of cross-linker. ^b Not determined.

Antibacterial assessment in solution: “Shake Flask” Method

The screening of the compounds for antibacterial activity was done using *Escherichia Coli* and *S. Epidermidis* via a viable cell counting method, since they represent both Gram-negative and Gram-positive type bacteria. A schematic representation of the process is represented in Figure VI-1.

Typically, a freeze-dried ampoule of *Escherichia Coli* (DH5α) was opened and the culture was picked up with a micropipette and placed in 2 mL of nutrient broth (composition for 1 L of nutrient broth (Luria Bertani): 10 g bactotryptone, 5 g of extract of yeast, sodium chloride) which was then incubated at 37 °C overnight. Then, 200 μL of the culture was placed in 100 mL of nutrient broth and the bacterial culture was incubated at 37 °C for 4 hours. At this stage, the culture of *Escherichia Coli* contained ca. 10⁸ cells/mL (absorbance at 600 nm equal to 0.6) and was used for the test. Upon appropriate dilution with sterilized 0.9 % saline water, a culture of about 10⁵ cells/mL was prepared and used for antibacterial testing. The polymers (previously sterilized by UV) were each dispersed in 9 mL of sterile 0.9 %

Chapter VI: Coating and antibacterial properties of PIL-based nanogels...

saline water (the solution was sterilized at 121 °C for 20 minutes). 1mL of the bacterial culture was then added to each polymer solutions, which reach 2, 5 or 10 mg/mL of polymer. At the same time, 1mL of bacterial culture was added to another flask containing 9 mL of sterile saline water: this would be the positive control of the antibacterial test. Decimal dilutions were prepared, and the starting cell concentration was determined by the spread drop method: this method (spread of three 10 μ L drops on a Petri box containing LB Agar) allows us to triplicate each measure, ensuring the repeatability of the experiment. At different contact times, 0.1 mL portions were picked up, and decimal serial dilutions (10^1 until 10^5) were prepared by mixing 100 μ L with 900 μ L of sterile saline water. From these dilutions, the surviving bacteria were counted by the spread drop method. The Petri dishes were incubated at 37 °C overnight. After incubation, the colonies of bacteria were counted.

The same protocol was carried out for the antibacterial assessment of the polymers in solution against Gram-positive bacteria, *i.e.* *S. Epidermidis*. Results are shown in Figure VI-2.

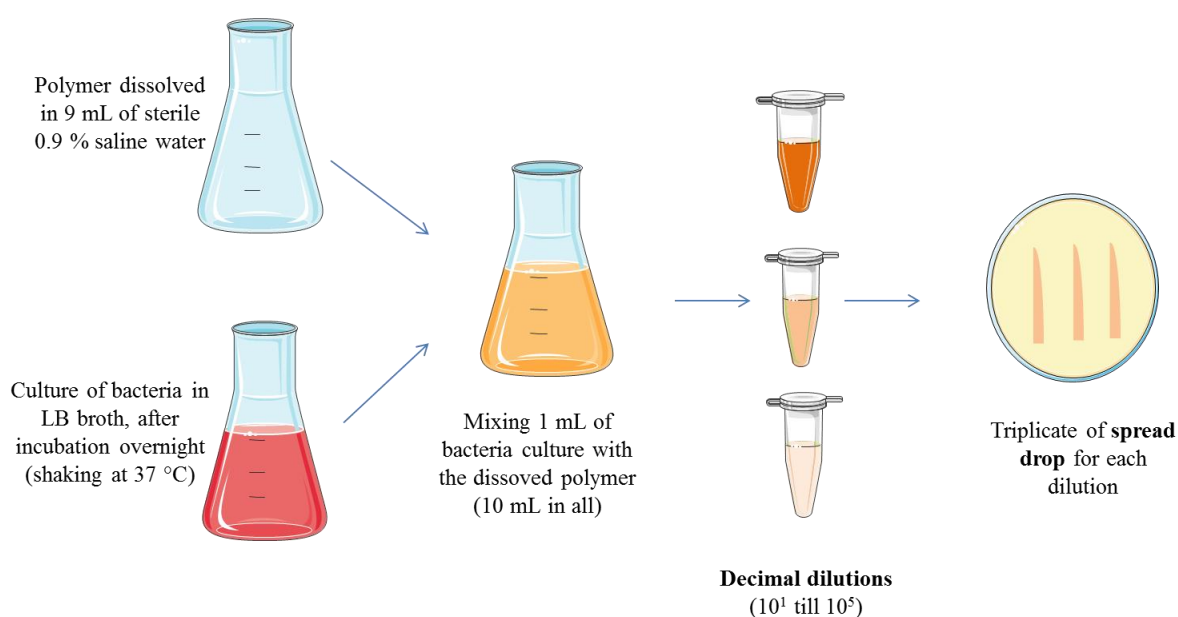


Figure VI-1. Antibacterial assessment in solution: “shake-flask” process.

Chapter VI: Coating and antibacterial properties of PIL-based nanogels...

MIC determination

MIC determinations were conducted according to Andrews *et al*³⁴. Dilutions of 10 mg/mL of polymers in LB broth were realized, and 11 two-fold dilutions were prepared in the same solvent. The inoculum was prepared from a colony incubated overnight (37 °C) in LB broth. This inoculum was then diluted 10-fold. Then, 50 µL of polymer dilution was mixed with 50 µL of inoculum. The solutions were incubated at 37 °C overnight, and the bacterial colonies were counted by optical density (absorbance at 600 nm).

QCM-D protocol: Film growth in aqueous media

Film growth was followed in real time using Quartz Crystal Microbalance coupled with Dissipation technique (QCM-D). A Q-Sense E4 was used in this study. The stainless steel-coated AT-cut resonator (fundamental frequency: 5MHz) was first put under ozonolysis before being installed in the cell. First, distilled water was introduced in the cell and the circulation was maintained until obtaining a stable baseline. Polymer deposition was then initiated by switching the liquid exposed to the crystal from distilled water to a polymer solution with a concentration of 2.5 g/L. Polymer was allowed to adsorb onto the substrate for 10 minutes before being rinsed by distilled water to get a uniform positive coating on the resonator.

QCM-D protocol: durability of the film after drying

Film growth was followed in real time using Quartz Crystal Microbalance coupled with Dissipation technique (QCM-D). A Q-Sense E4 was used in this study. The stainless steel-coated AT-cut resonator (fundamental frequency: 5 MHz) was first put under ozonolysis before being installed in the cell. First, distilled water was introduced in the cell and the circulation was maintained until obtaining of a stable baseline. Polymer deposition was then

Chapter VI: *Coating and antibacterial properties of PIL-based nanogels...*

initiated by switching the liquid exposed to the crystal from distilled water to a polymer solution with a concentration of 2.5 g/L. The experiment was then stopped, and the crystal was removed from the cell and dried by compressed air. After drying, the crystal was then placed in the cell again, the fundamental frequencies calculated again. The rinsing step took place afterwards, until obtaining a stable baseline. The crystal was dried again, and the fundamental frequencies were re-calculated.

Stainless steel surfaces preparation

Stainless steel 304 2B (SS) surfaces (2 cm x 2 cm), supplied by CRM Group AC&CS (Belgium), were cleaned with acetone and ethanol (scrubbing was realized with an optical tissue) and dried under argon. The polymer was then deposited by spin-coating an aqueous solution of 2.5 g/L at 2500 rpm for 1 minutes, and 3500 for 5 minutes.

Contact angle determination

The stainless steel and polymer-coated stainless steel prepared as stated above were then used to determine the contact angle of the surfaces.

Results and discussion

Assessment of antibacterial properties in solution

The dynamic shake flask method was used to assess the ability of the (co)polymers in solution to kill gram-positive and gram-negative bacteria, namely, *S. Epidermis* and *E. Coli.*, respectively. For these experiments, different concentrations were reached for each of the polymers, shaken with 10 mL of bacteria suspension (the bacterial concentration was evaluated through the control solution) at 37 °C for 18 hours. Aliquots were withdrawn at 30,

Chapter VI: Coating and antibacterial properties of PIL-based nanogels...

60, 120, 180 minutes, and overnight (18 hours). The number of viable cells in the suspension was counted after decimal dilutions and overnight incubation on Agar plates. Each Agar plate counted a triplicate of wide –spread droplets (spreading of 10 μ L drops for each sample). The MIC of the more promising copolymers were then determined.

Tested at different weight concentrations of polymers, all *S. Epidermis* (Gram-positive) bacteria were killed within the first half hour of exposure. No bacterial growth was observed after 18 hours of exposure.

The graphs below represent the average of each triplicate against *E. Coli* (Figure VI-2). At a concentration of 10 mg/mL, all PIL-based nanogels showed antibacterial activity against *E. Coli* (Figure VI-2a). This established that both the homopolymer and the nanogels based on poly(vinyl imidazolium) exhibit antibacterial properties.

Of particular interest, the only polymers that were found to kill all *E. Coli* bacteria within 2 hours of exposure were the nanogel derivatives. Both nanogels containing 4.8 mol.% of DVImBr as cross-linker and the ‘mixed’ nanogel, denoted as poly(VEtImBr-co-DVA 8.1 mol.%), proved 100 % effective under two hours. In contrast, after 2 hours of exposure of the homopolymer, 6.5 % of *E. Coli* bacteria remained alive. The cross-linked architecture thus seemed to improve the antibacterial activity of the PILs, in particular for a rather high cross-linking density.

While the exact time needed to eliminate all bacteria differed from one sample to another, exposure to the PIL-based homopolymers or nanogels killed all bacterial cells overnight.

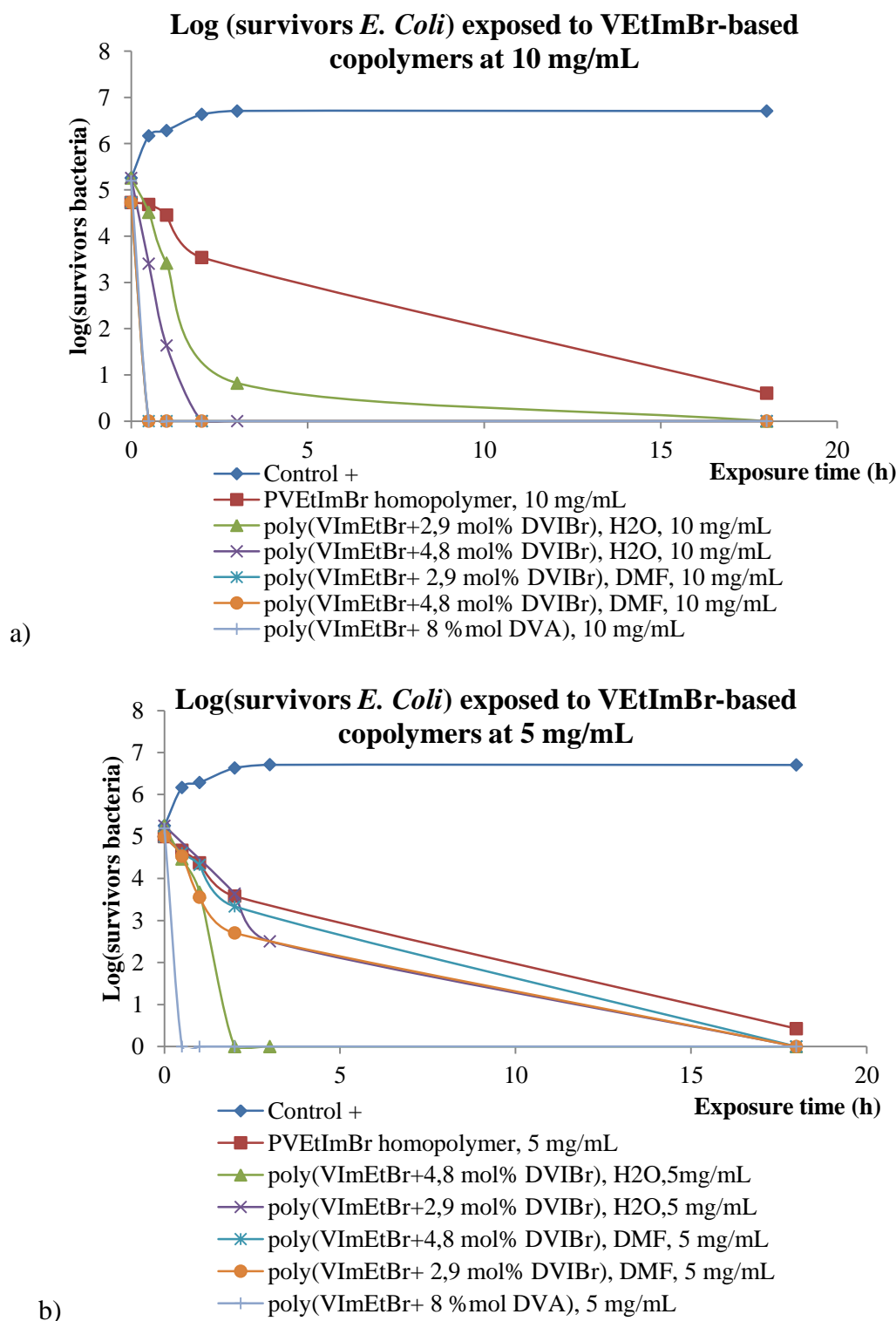


Figure VI-2. Evolution of the population of *E. Coli* in contact with the (co)polymers: a) at a polymer concentration of 10 mg/mL; b) at a polymer concentration of 5 mg/mL. Conditions of the assesment: “flask-shake” method, with broth-dilution and wide-spread droplets (triplicating the spreading of 10 μ L drops for each sample).

Chapter VI: Coating and antibacterial properties of PIL-based nanogels...

The same nanogels were then tested at a lower concentration (5 mg/mL). Again, in the case of the poly(VEtImBr-co-DVImBr) prepared with 4.8 mol.% in H₂O and of the DVA-containing nanogel, all bacteria cells were killed within 120 minutes of exposure (Figure VI-2b). This confirms that PVEtImBr-based nanogels exhibit antibacterial properties against both *S. Epidermidis* (Gram-positive) and *E. Coli* (Gram-negative). Since the most promising and sustainable nanogels are those synthesized in water, the minimum inhibitory concentration (MIC) of the two nanogels (containing respectively 2.9 and 4.8 mol.% of cross-linker) was assessed (Table VI-2).

Interestingly, although NMR and SEC data showed that the two hydrophilic PIL-based nanogels possessed different architectures (see Table VI-1, differences of molar masses and dispersity), their MICs were found identical against Gram-positive and Gram-negative bacteria, as can be observed in Table VI-2.

The MICs of the two nanogels were similar. Two homopolymer analogues, *i.e.* with the same *N*-vinyl ethyl imidazolium bromide repeating unit as that of the nanogels, but having a different molar mass (degree of polymerization (DP) of 40 and 1250) were also analyzed. The molar mass of the short PVEtImBr sample was found in the same range as that of the primary chains of the nanogel (DP of 40 for the linear homopolymer *vs.* 60 for the primary chains of the nanogels). Interestingly, the MIC of the nanogels was lower than the MIC of the smaller homopolymer, but higher than that of the longer homopolymer, for both *S. Epidermidis* and *E. Coli*.

An effect of architecture has also been noted for poly(ethylene imine)- and chitosan-based particles (see Chapter I, section III). For instance, antibacterial activity of PEI-based physically cross-linked nanogels is 3-5 times better than the best modified PEI in literature³⁵. Such a difference has been ascribed to the 'nanogel' structure, which allows more effective

Chapter VI: Coating and antibacterial properties of PIL-based nanogels...

damages done to bacterial cell wall than the unmodified polymer counterpart. To the best of our knowledge, such architecture has not been investigated for PIL-based copolymers yet.

Table VI-2. Minimum inhibitory concentration (MIC) of the PIL-based nanogels, compared with homopolymers.

Copolymers	MIC against <i>S. Epidermidis</i> ($\mu\text{g/mL}$)	MIC against <i>E.Coli</i> ($\mu\text{g/mL}$)
PVEtImBr (DP = 40)	312	1250
Poly(VEtImBr-co-DVImBr 2.9mol.%) synthesized in water	39	78
Poly(VEtImBr-co-DVImBr 4.8mol.%) synthesized in water	39	78
PVEtImBr (DP = 1250)	19.5	39

Assessment of the coating properties

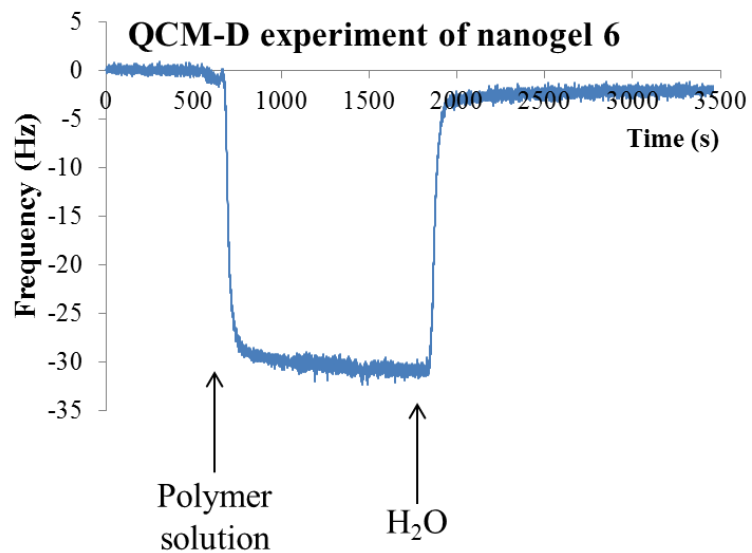
As emphasized in Chapter I, polymeric coatings can be physically or chemically anchored to surfaces. Here, we wish to avoid multistep processes -necessary for activating stainless steel surface and covalently grafting the nanogels- thus, the nanogels would have to be physically anchored (by dip- or spin-coating) to the surface. A major issue of such process would be the long-lasting character of the coating, for instance when immersed in water. Once deposited on a surface, it was hypothesized that the cross-linked architecture of the nanogels, along with their high molar mass, would prevent their possible re-solubilization. This hypothesis was further tested by QCM-D analyses.

Deposition via QCM-D

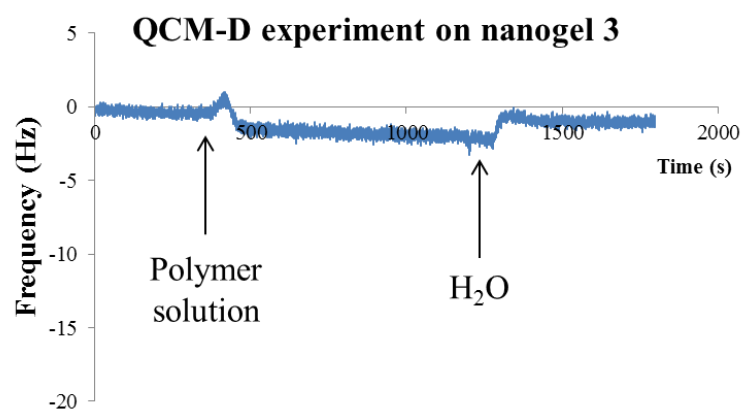
Quartz Crystal Microbalance coupled with Dissipation (QCM-D) was used to follow the film growth in real time on stainless steel coated sensors under flow, by measuring the

Chapter VI: Coating and antibacterial properties of PIL-based nanogels...

variation of the resonant frequency vs. time. The process models a dip-coating deposition, followed by a rinsing step. A decrease in frequency was indicative of the deposition of the polymer. Aqueous solutions of 2.5 wt.% of polymer **1** (homopolymer), **3** and **6** were used for these experiments. Resulting frequency variations can be seen on Figure VI-3.



a)



b)

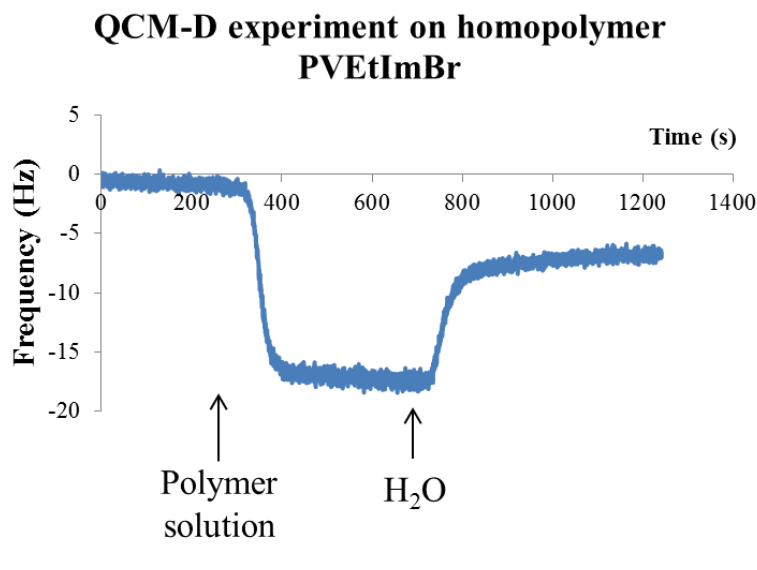


Figure VI-3. Frequency variation during a QCM-D measurement on a 2.5 wt.% aqueous solution of: a) nanogel **6**; b) nanogel **3**; c) homopolymer PVEtImBr.

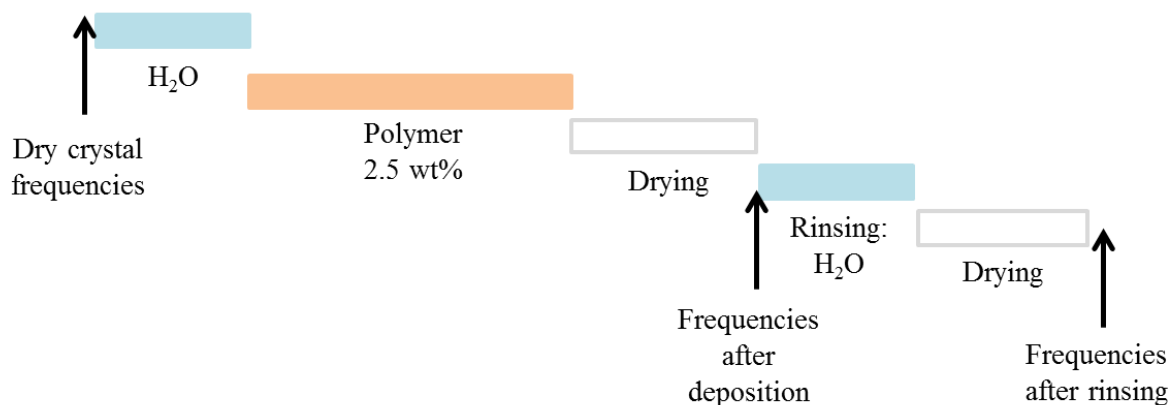
Directly after depositing the polymer, and obtaining a flat baseline (meaning that the deposition is over), the surface was rinsed with water without any surface drying between the deposition and the rinsing steps. The goal was to observe whether the polymer was strongly interacting with the surface or not.

The DVA-containing nanogel (polymer **6**, Figure VI-3a) could be deposited quite efficiently during the QCM-D process, as compared to the all PIL-based nanogel (polymer **3**, Figure VI-3b). However, after rinsing the coated surface with water, both nanogels (Figure VI-3a and c) were removed, as indicated by the final frequency that was closed to the original one. On the contrary, the PVEtImBr homopolymer was shown to deposit more quickly, with a deposition step lasting 400 seconds, as opposed to the 1400 seconds necessary for the deposition of nanogel **6**, the coating remaining stuck to the surface after rinsing.

These experiments highlight that, while PIL-based nanogels spontaneously deposit on stainless steel, they are removed from the surface when rinsing with water. It can be hypothesized that drying the coating before the rinsing step may stop the nanogels from re-

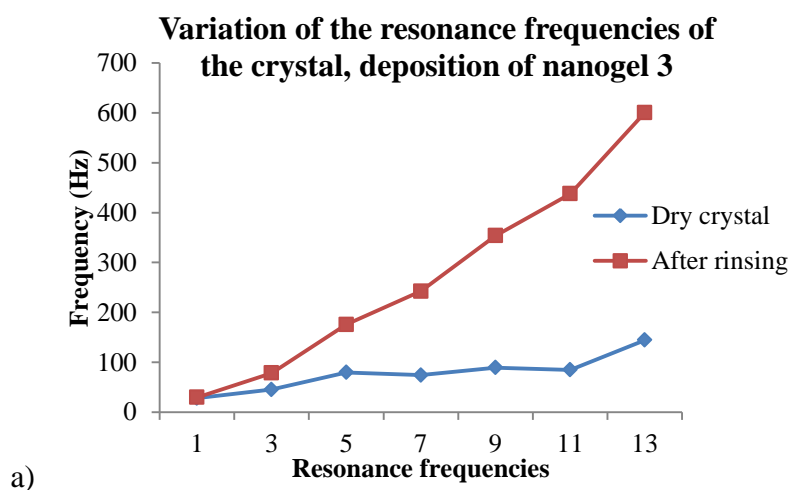
Chapter VI: Coating and antibacterial properties of PIL-based nanogels...

solubilizing in water as easily. Thus, another method was set up (Scheme VI-1). A 5-minute drying step was inserted after polymer deposition, and after rinsing with water.



Scheme VI-1. QCM-D methods, using a drying step between the deposition of the polymer and the rinsing.

This method was used on nanogels **3**, **5** and **6**, *i.e.* the three nanogels exhibiting the best antibacterial activity in solution (Figure VI-2). The necessity to stop the QCM-D twice for drying the stainless steel makes it impossible to obtain graphical results as the ones in Figure VI-3. What we compare here are the resonance frequencies of the crystal at the beginning of the experiment, after the deposition and drying step, and after the rinsing and drying step.



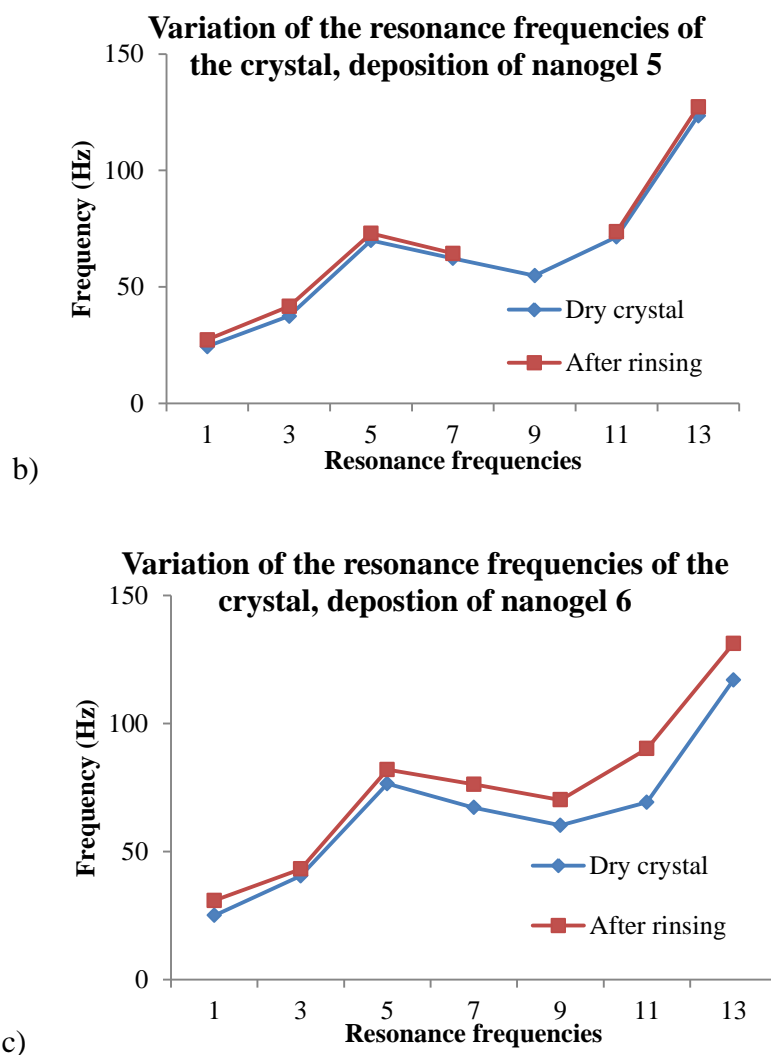


Figure VI-4. Variations of the resonance frequencies of the dried crystal before deposition (in blue), and after the process described in Scheme VI-1 (in red): a) for the nanogel **3**; b) for the nanogel **5**; c) for the nanogel **6**.

On the one hand, the nanogel **3** that was synthesized in DMF seemed less prone to re-solubilization during rinsing, if the coating had been dried beforehand. The deposition of nanogel **6** (DVA-containing) showed a slight difference between the resonance frequencies of the crystal at the beginning and at the end of the process. On the other hand, the nanogel **5** (synthesized in H₂O) did not appear to stay on the stainless steel during the rinsing step. Furthermore, the comparison of the resonance frequencies after the deposition and after the

Chapter VI: Coating and antibacterial properties of PIL-based nanogels...

rinsing (Supporting Information Figure S VI-1) showed that a large portion of nanogels was still lost in the rinsing process, for all three nanogels tested.

Thus, the deposition of nanogels on stainless steel under continuous flow (as is the case in QCM-D measurements) did not exhibit long-lasting properties.

Contact angle and immersion test

It was hypothesized that nanogels might be more easily coated on stainless steel if the process did not occur under continuous flow. To verify this, 2x2 cm square bare stainless steel surfaces were coated *via* either a dip-coating process (5 minutes in an aqueous solution of nanogel 2.5 wt.%, and a rinsing step of 1 minute in water), or a spin-coating process (same polymer solution, 1 minute at 2500 rpm followed by 5 minutes at 3500 rpm). After 48 hours of drying under air current, their contact angles were measured as a way of proving the deposition of hydrophilic polymers. Bare stainless steel surface is hydrophobic (contact angle above 90°), while hydrophilic-coated surface would exhibit a lower contact angle (below 90°).

Poly(VEtImBr-*co*-DVImBr 4.8 mol.%) synthesized in DMF (nanogel **3**) was deposited on a bare stainless steel surface by a dip-coating process. Once the surface was dried, (under air flow for 10 minutes, then 48 hours at air), The coating was very inhomogeneous. The contact angle of the coated stainless steel was measured nonetheless.

Water droplets used to measure the contact angle of the surface left a perfectly visible trace on the coating after drying, showing that this polymer coating was not permanent at all when in contact with water (Figure VI-5).

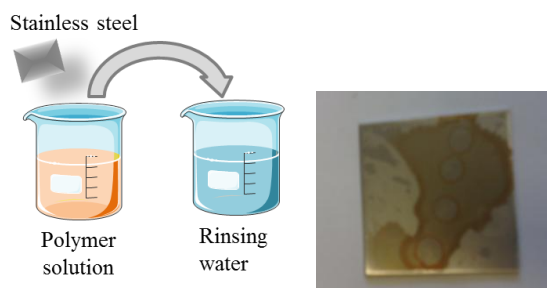


Figure V-5. Dip-coating method and resulting coated surface for a nanogel.

For this reason, we decided to use a spin-coating process on the bare stainless steel surfaces (all hydrophilic PIL-based polymers were solubilized in water at 2.5 wt.%, and spin-coated on stainless steel surfaces (2500 rpm for one minute, and 3500 rpm for 5 minutes). The coated stainless steel surfaces were then left to dry overnight. In Table VI-3 below are the resulting contact angle measurements for several nanogels for which the antibacterial activities were previously assessed. To evaluate the durability of the coating, nanogel-coated stainless steel was immersed overnight (18 hours) in water. Then, the polymer-coated stainless steel surfaces were dried and contact angles were measured again (results are in Table VI-3).

Contact angle is a quantitative measurement of the wetting of a surface by a liquid, water in our case. The contact angle is given when the drop of water is deposited, and 30'' after deposition, to show whether the droplet shape changed or not. Measuring the contact angle is a simple but efficient way to observe whether the polymer deposited on the stainless steel coupon remained on the surface after 18 hours of immersion in water. Bare stainless steel is hydrophobic (with a contact angle of more than 90°). After spin-coating an aqueous solution of the nanogel on the surface, the contact angle dropped (see Figure VI-6), showing that the coated-surface was more hydrophilic than before, in line with the deposition of the hydrophilic nanogel. The contact angle of the nanogels cross-linked with 4.8 mol.% of DVImBr showed no notable difference whether were prepared in water or in DMF: both

Chapter VI: Coating and antibacterial properties of PIL-based nanogels...

nanogels exhibited similar behavior, with a contact angle around 20° after spin-coating, and around 50° after 18 hours of immersion in milli-Q water.

After immersion in water overnight, the contact angles of the polymer-coated surfaces were measured again: they were in the range of 40° to 60°. Most of the surfaces' contact angle had then increased (the surfaces were more hydrophobic after immersion in water than right after the coatings deposition), indicating that part of the polymers might have re-dissolved in water. Interestingly, the poly(V_{EtImBr-co-DVImBr} 2.9 mol.%) nanogel synthesized in water observed the inverse trend: after immersion in water, the coated surface was more hydrophilic than before (75° ± 3 vs. 52° ± 5). One possible explanation would be that this nanogel being more loosely cross-linked than the other three tested, its structure allowed for more mobility of its hydrophilic primary chains.

Table VI-3. Contact angle for the stainless steel surfaces spin-coated with 2.5 wt.% of aqueous polymer solutions, before and after immersion in water.

	Before immersion		After immersion	
	0s	30s	0s	30s
Bare stainless steel	98 +/-1	92 +/-1		
V_{EtImBr} + 4.8mol.% DV_{ImBr}, in DMF	25 +/- 1	19 +/- 2	47 +/- 1	43 +/- 1
V_{EtImBr} + 2.9 mol.% DV_{ImBr}, in H₂O	78 +/- 3	75 +/- 3	57 +/- 6	52 +/- 5
V_{EtImBr} + 4.8 mol.% DV_{ImBr}, in H₂O	20 +/- 1	14 +/- 1	54 +/- 0	53 +/- 0
V_{EtImBr} + 8 mol.% DVA	22 +/- 2	21 +/- 3	65 +/- 2	62 +/- 1

Conditions: contact angle are measured directly after deposition (0s) and 30s after deposition in each case. Each measurement is replicated between 4 and 6 times, and an average value is calculated.

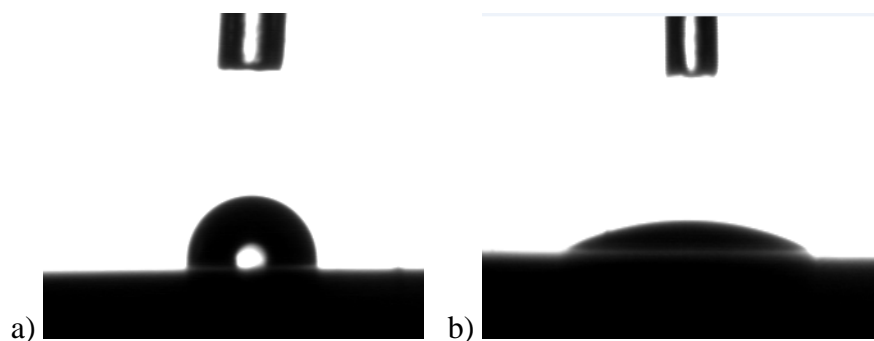


Figure VI-6. Photograph of the drops used to determine the contact angle of each surface: a is the stainless steel surface, and b) is the polymer coated stainless steel (entry 5 in the table).

Conclusion

Antibacterial activities of hydrophilic PIL-type architectures were assessed against both Gram-positive (*Bacillus*) and Gram-negative (*E. Coli*) bacteria in solution. Both linear and nanogels of poly (*N*-vinyl-3-ethyl imidazolium bromide) were found antibacterial in solution. The MIC of nanogels synthesized in water were further assessed against *S. Epidermidis* (39 $\mu\text{g/mL}$) and *E. Coli* (78 $\mu\text{g/mL}$) against both Gram-positive and Gram-negative bacteria. The MIC of these nanogels proved lower than that of a linear counterpart of lower molar mass (DP = 40), but higher than the MIC value of a linear counterpart of very high molar mass (DP = 1250).

Deposition tests were then realized on stainless steel surface *via* spin-coating, and contact angle showed the change in hydrophobicity of the surface (from hydrophobic surfaces to hydrophilic ones). After immersion, the contact angles of the coated stainless steel surfaces show less hydrophilicity (from 30° to 40°-50°), showing that part of the hydrophilic coating is solubilized in water, but not enough to let the surfaces completely hydrophobic again. Interestingly, it seems that the nanogels synthesized in water are solubilized more easily during the immersion tests than the copolymers synthesized in DMF. Such difference might be ascribed to their differences in structure (nanogels with 4.8 mol.% cross-linker synthesized

Chapter VI: Coating and antibacterial properties of PIL-based nanogels...

in water could be dried during purification, and re-solublized for SEC measurements, while nanogels synthesized in DMF did not solubilize again in SEC eluent).

Supporting Information

Table S VI-1. Variations of the frequencies of the QCM-D crystal before the measurement, and after depositing the polymer, rinsing and drying the crystal, of the polymers **3**, **6**.

Polymers	Crystal frequencies	Dried bare crystal	After rinsing and drying
3	1	28	30
	3	45	78
	5	80	176
	7	74	242
	9	89	354
	11	85	438
	13	144	601
6	1	25	31
	3	41	43
	5	77	82
	7	67	76
	9	60	70
	11	69	90
	13	117	131

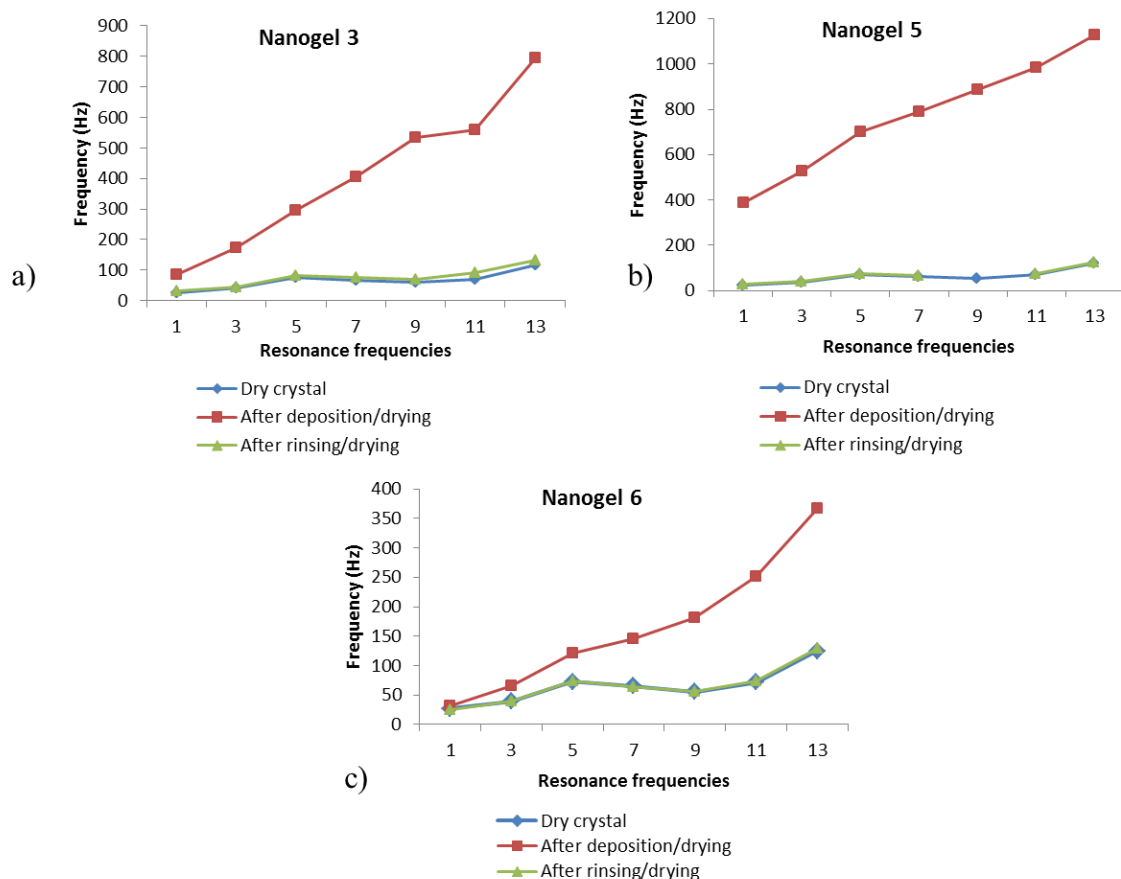


Figure S VI-1. Resonance frequencies resulting from the QCM-D experiments with drying steps: a) for nanogel 3, b) for nanogel 5; c) for nanogel 6.

References

1. K. Glinel, P. Thebault, V. Humblot, C. M. Pradier and T. Jouenne, *Acta Biomaterialia*, 2012, **8**, 1670-1684.
2. F. Siedenbiedel and J. C. Tiller, *Polymers*, 2012, **4**, 46-71.
3. L. Carson, P. K. W. Chau, M. J. Earle, M. A. Gilea, B. F. Gilmore, S. P. Gorman, M. T. McCann and K. R. Seddon, *Green Chemistry*, 2009, **11**, 492-497.
4. E. Faure, C. Falentin-Daudré, C. Jérôme, J. Lyskawa, D. Fournier, P. Woisel and C. Detrembleur, *Progress in Polymer Science*, 2013, **38**, 236-270.
5. S. Taheri, A. Cavallaro, S. N. Christo, L. E. Smith, P. Majewski, M. Barton, J. D. Hayball and K. Vasilev, *Biomaterials*, 2014, **35**, 4601-4609.
6. W. Lee, K.-J. Kim and D. Lee, *Biometals*, 2014, 1-11.

Chapter VI: Coating and antibacterial properties of PIL-based nanogels...

7. C. You, C. Han, X. Wang, Y. Zheng, Q. Li, X. Hu and H. Sun, *Mol Biol Rep*, 2012, **39**, 9193-9201.
8. C. Marambio-Jones and E. M. V. Hoek, *Journal of Nanoparticle Research*, 2010, **12**, 1531-1551.
9. A. M. Carmona-Ribeiro and L. D. de Melo Carrasco, *International Journal of Molecular Sciences*, 2013, **14**, 9906-9946.
10. M. Kong, X. G. Chen, K. Xing and H. J. Park, *International Journal of Food Microbiology*, 2010, **144**, 51-63.
11. J. Duan, X. Liang, Y. Cao, S. Wang and L. Zhang, *Macromolecules*, 2015, **48**, 2706-2714.
12. Y. Kohno, S. Saita, Y. Men, J. Yuan and H. Ohno, *Polymer Chemistry*, 2015, **6**, 2163-2178.
13. Y. Men, D. Kuzmicz and J. Yuan, *Current Opinion in Colloid and Interface Science*, 2014, **19**, 76-83.
14. J. Yuan, D. Mecerreyes and M. Antonietti, *Progress in Polymer Science*, 2013, **38**, 1009-1036.
15. P. Coupillaud and D. Taton, in *Applications of Ionic Liquids in Polymer Science and Technology*, Springer Berlin Heidelberg, 2015, pp. 69-102.
16. R. Marcilla, J. A. Blazquez, J. Rodriguez, J. A. Pomposo and D. Mecerreyes, *Journal of Polymer Science, Part A: Polymer Chemistry*, 2004, **42**, 208-212.
17. M. Isik, H. Sardon and D. Mecerreyes, *International Journal of Molecular Sciences*, 2014, **15**, 11922-11940.
18. S. N. Riduan and Y. Zhang, *Chemical Society Reviews*, 2013, **42**, 9055-9070.
19. S. Y. Choi, H. Rodriguez, H. Q. N. Gunaratne, A. V. Puga, D. Gilpin, S. McGrath, J. S. Vyle, M. M. Tunney, R. D. Rogers and T. McNally, *RSC Advances*, 2014, **4**, 8567-8581.
20. G. Liu, R. Zhong, R. Hu and F. Zhang, *Biophysical Reviews and Letters*, 2012, **7**, 121-134.
21. J. Guo, Q. Xu, Z. Zheng, S. Zhou, H. Mao, B. Wang and F. Yan, *ACS Macro Letters*, 2015, 1094-1098.
22. F. Joubert, R. P. Yeo, G. J. Sharples, O. M. Musa, D. R. W. Hodgson and N. R. Cameron, *Biomacromolecules*, 2015, **16**, 3970-3979.
23. K. N. Kalinov, M. G. Ignatova, N. Manolova, N. Markova, D. Karashanova and I. Rashkov, *RSC Advances*, 2015.

Chapter VI: Coating and antibacterial properties of PIL-based nanogels...

24. M. Z. Elsabee and E. S. Abdou, *Materials Science and Engineering C*, 2013, **33**, 1819-1841.
25. W. Cheng, C. Yang, X. Ding, A. C. Engler, J. L. Hedrick and Y. Y. Yang, *Biomacromolecules*, 2015.
26. M. G. Cowan, M. Masuda, W. M. McDanel, Y. Kohno, D. L. Gin and R. D. Noble, *Journal of Membrane Science*, 2016, **498**, 408-413.
27. R. Tejero, D. Lopez, F. Lopez-Fabal, J. L. Gomez-Garces and M. Fernandez-Garcia, *Polymer Chemistry*, 2015.
28. C. García-Astrain, C. Chen, M. Burón, T. Palomares, A. Eceiza, L. Fruk, M. Á. Corcuera and N. Gabilondo, *Biomacromolecules*, 2015.
29. C. Falentin-Daudré, E. Faure, T. Svaldo-Lanero, F. Farina, C. Jérôme, C. Van De Weerd, J. Martial, A. S. Duwez and C. Detrembleur, *Langmuir*, 2012, **28**, 7233-7241.
30. E. Faure, C. Falentin-Daudré, T. S. Lanero, C. Vreuls, G. Zocchi, C. Van De Weerd, J. Martial, C. Jérôme, A. S. Duwez and C. Detrembleur, *Advanced Functional Materials*, 2012, **22**, 5271-5282.
31. Q. Ye, T. Gao, F. Wan, B. Yu, X. Pei, F. Zhou and Q. Xue, *Journal of Materials Chemistry*, 2012, **22**, 13123-13131.
32. H. He, S. Averick, E. Roth, D. Luebke, H. Nulwala and K. Matyjaszewski, *Polymer (United Kingdom)*, 2014, **55**, 3330-3338.
33. A. Debuigne, Y. Champouret, R. Jérôme, R. Poli and C. Detrembleur, *Chemistry - A European Journal*, 2008, **14**, 4046-4059.
34. J. M. Andrews, *Journal of Antimicrobial Chemotherapy*, 2001, **48**, 5-16.
35. S. Chattopadhyay, E. Heine, A. Mourran, W. Richtering, H. Keul and M. Möller, *Polymer Chemistry*, 2016, **7**, 364-369.

General Conclusions and Perspectives

The main objective of this work was to develop a straightforward and novel synthetic strategy to positively charged branched (co)polymers that could be suitable as coatings with long-lasting antibacterial (AB) properties for stainless steel. The targeted copolymers were made of cationic polymeric ionic liquids –referred to as poly(ionic liquid)s (PILs). We hypothesized that PILs of high molar mass arranged in the form of nanogels might be useful to impart long-term AB activity to stainless steel. Moreover, the variation of the counter-anion (*e.g.* using Br⁻ or N(SO₂CF₃)₂ = NTf₂⁻) was expected to be a simple means to tune the overall properties of these PIL-based nanogels, in particular, both their AB activity and coating durability.

To this end, we expanded previous works on cobalt-mediated radical polymerization (CMRP) of *N*-vinyl-imidazolium type monomers (see Scheme 1). The first objective was to achieve different cross-linked architectures named nanogels, *via* the cobalt-mediated radical cross-linking copolymerization (CMRCcP). This was achieved using a vinyl monomer and a divinyl cross-linker either of similar (Chapters II and IV) or of completely dissimilar structure (Chapter III). CMRCcP was thus implemented on either hydrophilic (bromide-containing) or hydrophobic (NTf₂-containing) ionic liquid monomers.

We firstly validated the principle of the CMRCcP process to the synthesis of poly(vinyl acetate) (PVAc)-based nanogels, using in this case, vinyl acetate and divinyl adipate (DVA) as co-monomers, in presence of an organocobalt(III) complex acting both as initiator and controlling agent. Formation of poly(vinyl acetate-*co*-divinyl adipate) (PVAc-*co*-DVA) nanogels, and subsequent cleavage of the cross-linker emanating from DVA, showed the kinetic chain length of primary chains was well controlled by the organocobalt(III) complex. CMRCcP was performed under mild conditions, *i.e.* at 40 °C, in ethyl acetate with 10 wt.% of monomer. Chain extension experiments demonstrated that PVAC chain ends could be reactivated. This was achieved either by adding a new load of VAc and DVA, or a

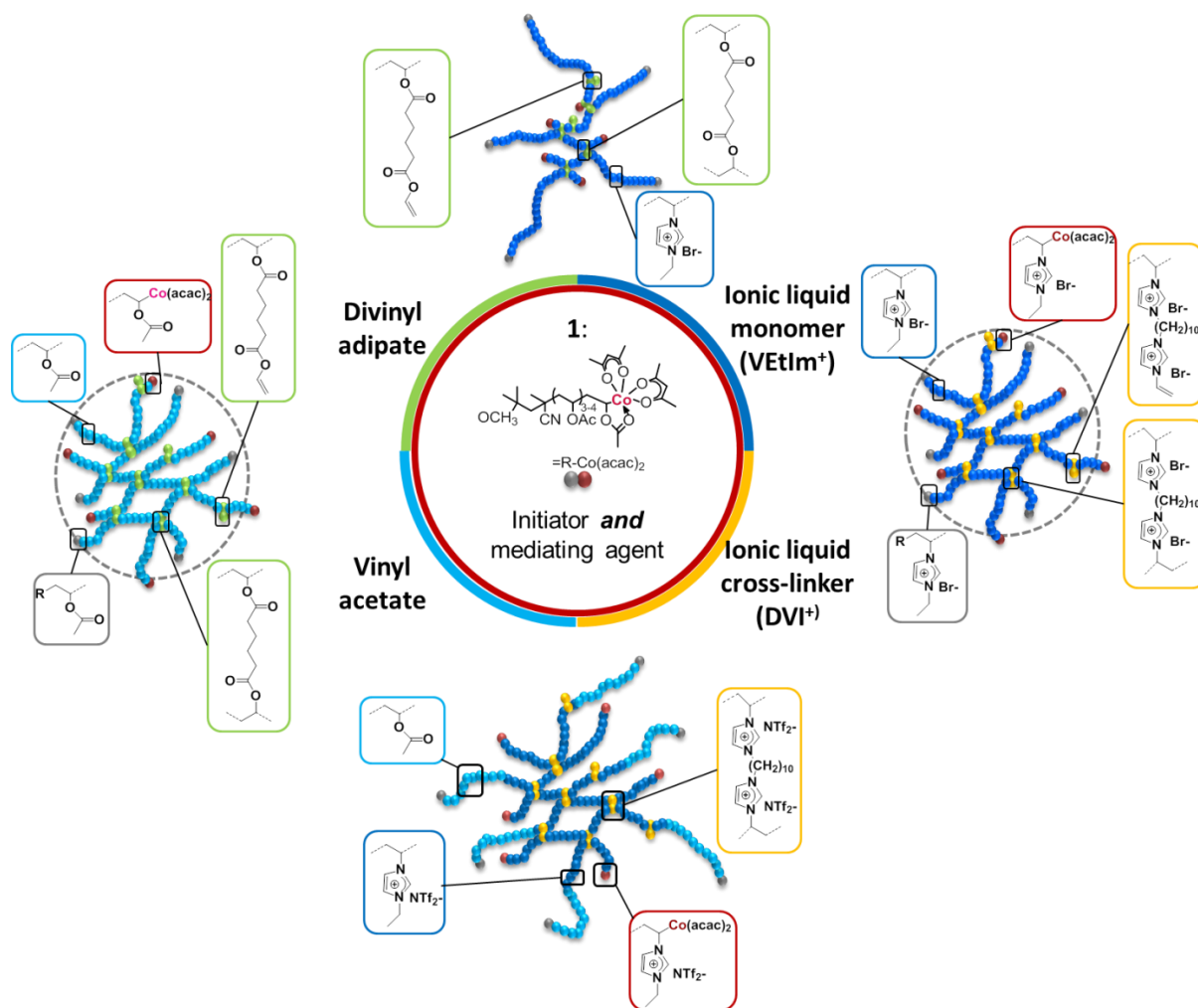
General Conclusions and Perspectives

hydrophobic ionic liquid monomer, namely, *N*-vinyl-3-ethyl imidazolium bis(trifluoromethanesulfonyl)imide (VETImNTf₂).

CMRCcP of *N*-vinyl-3-ethyl imidazolium bromide (VETImBr) and 1,13-divinyl-3-decyl diimidazolium bromide (DVImBr) cross-linker was then achieved at 30 °C either in organic or aqueous solution, forming hydrophilic PIL-based nanogels. Up to 5 mol.% of DVImBr cross-linker could be incorporated without macrogelation occurring, witnessing the occurrence of intramolecular crosslinking (= cyclization) during CMRCcP. Chain extensions could be conducted directly in water as a means to derive core-shell PIL-based structures thanks to the presence of carbon-cobalt bond at the PIL chain ends, CMRCcP involving a mono- and a divinyl co-monomers of similar structure thus led to the formation of globular nanogels.

When applied to a mixture of co-monomers of very dissimilar structure, CMRCcP led to a different architecture only in one case. Copolymerizing VAc with DVImBr indeed met with limited success, due to too unfavorable reactivity ratios. In order to achieve a cross-linked architecture consisting of a PIL core and PVAc chains in the shell, hence to circumvent the reactivity issue, another two-step arm-first pathway was thus implemented. PVAc arms were first grown by CMRP, which was followed by addition of a mixture of VETImNTf₂ with DVImNTf₂ to the reaction medium. In this way, synthesis of “hybrid” star-like compounds made of a PIL nanogel core surrounded by PVAc arms could be achieved by CMRCcP (Scheme 1).

General Conclusions and Perspectives



Scheme 1. Copolymerizations achieved by CMRCcP of neutral and ionic liquid-type monomers, and the variations in architecture.

The direct synthesis of hydrophobic PIL nanogels, *i.e.* based on VEImNTf₂ units was then accomplished by CMRCcP using DVImNTf₂ as cross-linker. Second-generation nanogels consisting of either linear extended chains after addition of a second feed of VEImNTf₂, or of cross-linked shell – in the latter case, the second feed comprised VEImNTf₂ and DVImNTf₂ were also synthesized. An array of those hydrophobic nanogels were then investigated as coatings for porous patterned surfaces. Both second-generation hydrophobic PIL-based nanogels gave better-organized honeycomb structures, compared to any of the first-generation nanogels tested. The second-generation nanogels with the linear

General Conclusions and Perspectives

extended chains showed smaller pore size and dispersity while the second-generation with cross-linked extensions exhibited the structure resembling the most to a honeycomb pattern.

Thin films of some of the NTF₂-containing nanogels were also evaluated in ionic conductivity tests. The highest ionic conductivity ($1.9 \cdot 10^{-5}$ S/cm at 80 °C) was obtained with the second-generation nanogel with linear extensions, the nanogel structure showing a better resistance to annealing than poly(vinyl imidazolium) homopolymer homologue.

Finally, the hydrophilic PIL-based nanogels were assessed for antibacterial activity in aqueous solution, against Gram-positive and Gram-negative bacteria. The minimum inhibitory concentration, or MICs, of the more promising compounds were found equal to 39 µg/mL against *S. Epidermidis* and 78 µg/mL against *E. Coli*. For the sake of comparison, linear PILs with a degree of polymerization (DP) of 40, *i.e.* similar to the DP of the primary chains of the nanogels, gave a MIC value of 312 µg/mL against *S. Epidermidis* and 1250 µg/mL against *E. Coli*. High DP homopolymers gave much lower MIC values: 19.5 µg/mL against *S. Epidermidis* and 39 µg/mL against *E. Coli*. The hydrophilic nanogel structure thus proved beneficial for developing AB activity, in comparison to PIL equivalent homopolymer. However, while coating properties on stainless steel surface were assessed *via* contact angle method, AB tests on PIL-based nanogels coatings should be realized.

Overall, this PhD work demonstrates that CMRCcP is a powerful tool to access PIL-based nanogels of tunable properties, not only in organic solvent, but also in water, under mild experimental conditions. Potential applications are multiple, including as antibacterial coatings or as solid ionic conductors, due to both the ionic liquid nature of the polymer, and the cross-linked architecture inherent to nanogels. Reactivation of dormant chain-ends also allows for the synthesis of core-shell structures. The combination of the cross-linked structure

General Conclusions and Perspectives

with the properties of PIL-based polymers show the potential of these nanogels as coatings for different applications.